Frontispiece:

Helicopter at the fluence of the Roaring Lion and Beautiful
Rivers during a reconnaissance survey of molybdenum prospects
in West Nelson, October 1977.

*"Some sort of pattern of molybdenum occurrences in association
with granitic rocks in western Nelson is now emerging.
....this region is an area of, at least, mild molybdenum
metallogeny.
If he is to limit reasonably the range of his expensive helicopter-
borne operations in this difficult country, the prospecting
geologist would hope to have some guidelines both in relation
to the geology and to the adaptibility of such techniques as
geochemistry...."*

G. J. Williams (1974)
Economic Geology of New Zealand.

ALAN JOHN EGGERS

GEOLOGY AND MINERALIZATION OF THE

BALD HILL MOLYBDENUM OCCURRENCE,

BULLER DISTRICT, WEST NELSON,

NEW ZEALAND.

Submitted for the degree of

Master of Science in Geology

at the Victoria University of Wellington.

July 1978.

ABSTRACT

Molybdenite mineralization occurs within the Bald Hill Prospect (West Nelson) in brecciated and hornfelsed Greenland Group slates and metagreywackes and associated quartz trondhjemite porphyry minor intrusions (Lyell Porphyry).

Potassium argon (K-Ar) ages of the Lyell Porphyry, several granites forming part of the adjacent Karamea Granite batholith (Bald Hill Granites) and mineralized hornfelsic country rocks fall in the range 102-120 Ma (mid-Cretaceous). Adjacent lower Ordovician Greenland Group slates yielded four K-Ar ages in the range 112-226 Ma indicating partial argon outgassing of these older meta-sediments.

The Bald Hill Granites and the Lyell Porphyry granitic rocks belong to separate petrogenic provinces. Bald Hill Granites forming the western margin of the Karamea Granite batholith occur as a suite of foliated, medium-grained, muscovite-bearing leucogranites, pink microgranites and biotite-granites. Chemically these rocks are peraluminous-potash granites with 72-75% SiO_2, $MgO < 1\%$, $CaO < 1\%$, $K_2O > Na_2O$ with $Rb > Sr$ and always contain more than 30% normative quartz and 3% normative corundum. In contrast, the Lyell Porphyry rocks intruding both Greenland Group and Bald Hill Granite country rocks, form a series of small, high-level plutons and cross-cutting dykes of quartz trondhjemite, granodiorite, quartz diorite,

lamprophyre and quartz-bearing gabbroporphyry. Chemically
the Lyell Porphyry intrusive rocks are soda-rich calc-
alkaline granitoids containing 46-70% SiO_2, >1% MgO,
>2.2% CaO, with Na_2O > K_2O and Sr > Rb with less than 28%
normative quartz and less than 2% normative corundum.

From their studies of granite batholiths in southeastern
Australia, Chappell and White (1974) recognise two contrasting
granitoid types called I-type and S-type granites. The
Lyell Porphyry and several other intrusive stocks associated
with molybdenum mineralization in West Nelson and North
Westland are shown to correspond to I-type granites, in
contrast to the Karamea batholith granites (including Bald
Hill Granites) which conform to S-type granites.

Sulphur isotopic analyses of mineralization for ten
molybdenum prospects in West Nelson indicate uniformly high
temperatures of mineralization in the range 400° to 500°C,
with a probable magmatic source for sulphur.

The Bald Hill and other S-type granites forming the
Karamea batholith were probably formed by the ultrametamor-
phism of crustal sedimentary material. The Lyell Porphyry
and other molybdenum-bearing calc-alkaline intrusive stocks
represent melt phases of deeper origin intruding the overlying
granites and sediments. The emplacement of these stocks
appears to equate with north-south lineaments and large
scale circular features in the granite terranes of West
Nelson.

The geological setting, age, petrological characteristics
and molybdenite mineralization of the Lyell Porphyry and

Bald Hill Granites are similar to that of other West Nelson occurrences. All are associated with mid-Cretaceous minor granitic porphyry intrusions, emplaced in Paleozoic metasediments, close to the margins of the Karamea and Separation Point batholiths.

CONTENTS

List of Tables

List of Figures

INTRODUCTION

Molybdenum mineralization associated with granites and Paleozoic sediments in West Nelson has been known since the earliest geological survey work and exploration by gold prospectors (eg: Webb, 1910; Ongley and MacPherson, 1923; Williams and Sanderson, 1959). In recent years several of these molybdenum localities have been re-examined in detail as part of mineral exploration programmes for molybdenum-copper-lead-zinc and silver-gold deposits. Williams (1974) has compiled and summarised geological information for many of these molybdenum occurrences and was the first to record a possible general association with Cretaceous igneous rocks within Paleozoic metasediments. This compilation plus recent 'open file' Mines Department reports and published geochronological and geological studies indicate most, if not all, of these molybdenum localities to have many structural, age, petrographic and petrochemical similarities (see Fig. 2-4 for names and locations of molybdenum occurrences in West Nelson).

A new molybdenum occurrence (known as Bald Hill) has recently been found in the headwaters of the Lyell Stream. The Lyell Stream drains the western slopes of Bald Hill (S35/556776 alt. 1380 m), which forms the southern part of the Lyell Range. Molybdenum-copper with minor bismuth mineralization is associated with a series of calc-alkaline intrusive porphyry stocks and dykes

intruding and cross-cutting metasediments and gneissic granite country rocks.

The purpose of this study was to map in detail the Bald Hill occurrence, to examine the structure, age, petrography and geochemistry of the area, particularly of the plutonic rocks, and to compare this data with previous work on other West Nelson molybdenum prospects. With the exceptions of 1) Knuckle Hill, where no molybdenum mineralization has been located in outcrop (Bates, pers. comm.) and 2) Burgoo Stream where mineralized samples were supplied by T. E. Bates, all of the molybdenum occurrences have been briefly visited and mineralized samples collected for a sulphur isotope study.

Twenty-five new potassium argon ages of the mineralized zones, country rocks and several granite phases are presented. New major element rock analyses of the Greenland Group metasediments (25), hornfelsed metasediments (25) and plutonic rocks (50) from Bald Hill are given and, in addition, most of these rocks were analysed for Ba, Cu, Ni, Zn, Pb, Mo, S, Sr, Rb, Zr, Th, and Y. New sulphur isotope data for co-existing sulphides from ten of the West Nelson molybdenum occurrences are also presented.

CHAPTER ONE

GENERAL GEOLOGY, STRUCTURE AND

REGIONAL GEOCHEMISTRY

I. Geology and Structure:

The Bald Hill molybdenum-copper-bismuth mineralization

of West Nelson occurs within brecciated and hornfelsed

metagreywackes and argillites of the lower Ordovician

Greenland Group and Cretaceous intrusive porphyries within,

and close to the western margin of the Karamea Granite

batholith. A detailed geological map of the Bald Hill

area is given in Fig. 1-1a (Geological Legend, Fig. 1-1b)

and diagrammatic cross sections in Fig. 1-2. (Rock

sample numbers, locations and V.U.W. Geology Department

numbers given in Appendix I).

Structurally the Bald Hill area is extensively faulted,

with major faults (eg: Lyell Fault; Bowen, 1964) generally

trending north-south and steeply dipping to the west. An

elongate zone of porphyries and hornfels containing quartz-

pyrite-molybdenite-chalcopyrite-bismuth-bismuthinite

mineralization approximately 2.5 km long and 0.7 km wide,

also strikes north-south, subparallel to the regional strike

of the Greenland Group metasediments. This zone may extend

northwards into the headwaters of the south branch of the

Mokihinui River and as far south as Englishmans Creek,

where reconnaissance mapping and geochemical sampling

LYELL STREAM BALD HILL AREA

GEOLOGY

Faults.	
Dip and strike.	
Streams.	
② Camp sites.	

NB: See seperate sheet for geological legend.

SCALE 1:10000   0   100   200   300 metres.
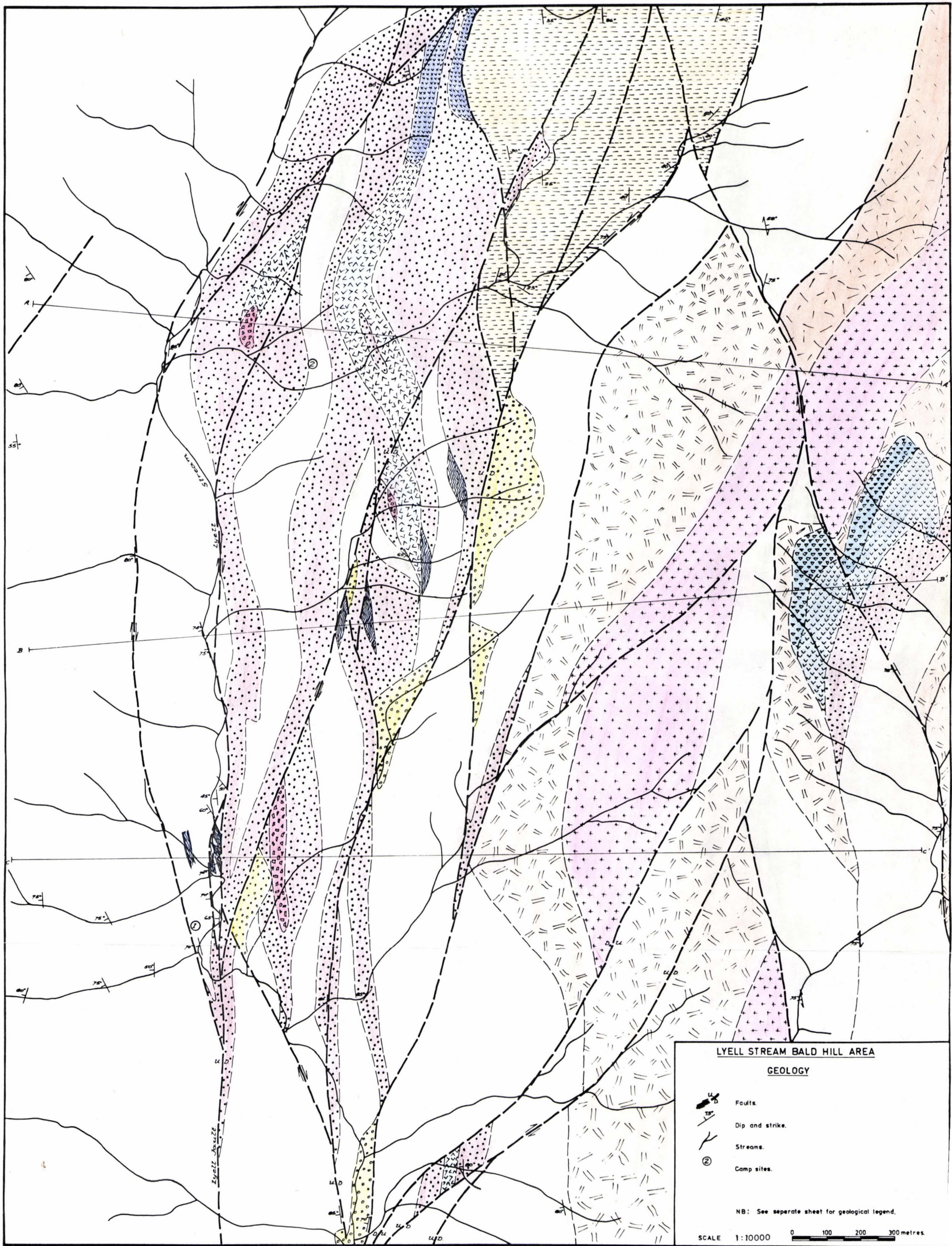
Fig. 1-1a: Detailed geological map of the Bald Hill
molybdenum prospect.

GEOLOGICAL MAP LEGEND
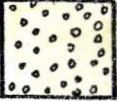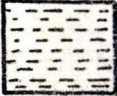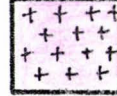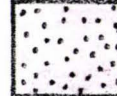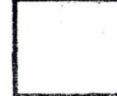
POORLY SORTED FAN AND RIVER GRAVELS	HAWERA SERIES		TERTIARY
BEDDED SILTSTONES, MUDSTONES, BASAL QUARTZ GRITS AND COAL MEASURES	BRUNNER-MANGLES FM.		
QUARTZ-OLIGOCLASE TRONDHJEMITE PORPHYRY MINERALIZED			
MEDIUM TO FINE GRAINED GRANODIORITE WITH GREEN BIOTITE. WEAKLY MINERALIZED.			
HORNBLENDE BEARING DIORITE WITH ANDESINE PLAGIOCLASE. WEAKLY MINERALIZED	LYELL PORPHYRY		CRETACEOUS
PORPHYRITIC LAMPROPHYRE DYKES. SOME LATE? K-FELDSPAR PHENOCRYSTS. WEAKLY MINERALIZED.			
COARSE GRAINED OLIVINE AND PYROXENE BEARING GABBRO-PORPHYRY. MINERALIZED			
WEAKLY FOLIATED MEDIUM GRAINED MUSCOVITE-ALBITE LEUCOGRANITE.			
ALBITE BEARING PINK MICRO-GRANITE WITH ABUNDANT 'CLOTS' OF MICACEOUS MINERALS.	BALD HILL GRANITES		*CRETACEOUS? (TUHUAN?)
WEAKLY FOLIATED ALKALI BIOTITE-GRANITE. XENOCRYSTS OF MICACEOUS MINERALS.			
PURPLISH BIOTITE-HORNFELS WITH FRACTURE AND JOINT QUARTZ-SULPHIDE VEINING	ALTERED GREENLAND GROUP		*ORDOVICIAN?
SILICIFIED AND BRECCIATED HORNFELS CONTAINING PYRITIC VUGS			
GREY-GREEN STEEPLY DIPPING GREYWACKE AND ARGILLITE METASEDIMENTS.	GREENLAND GROUP		ORDOVICIAN

Fig. 1-1b: Legend for geological map (Fig. 1-1a) and diagrammatic cross sections (Fig. 1-2).

*Cretaceous K-Ar ages; See text, chapter 2.
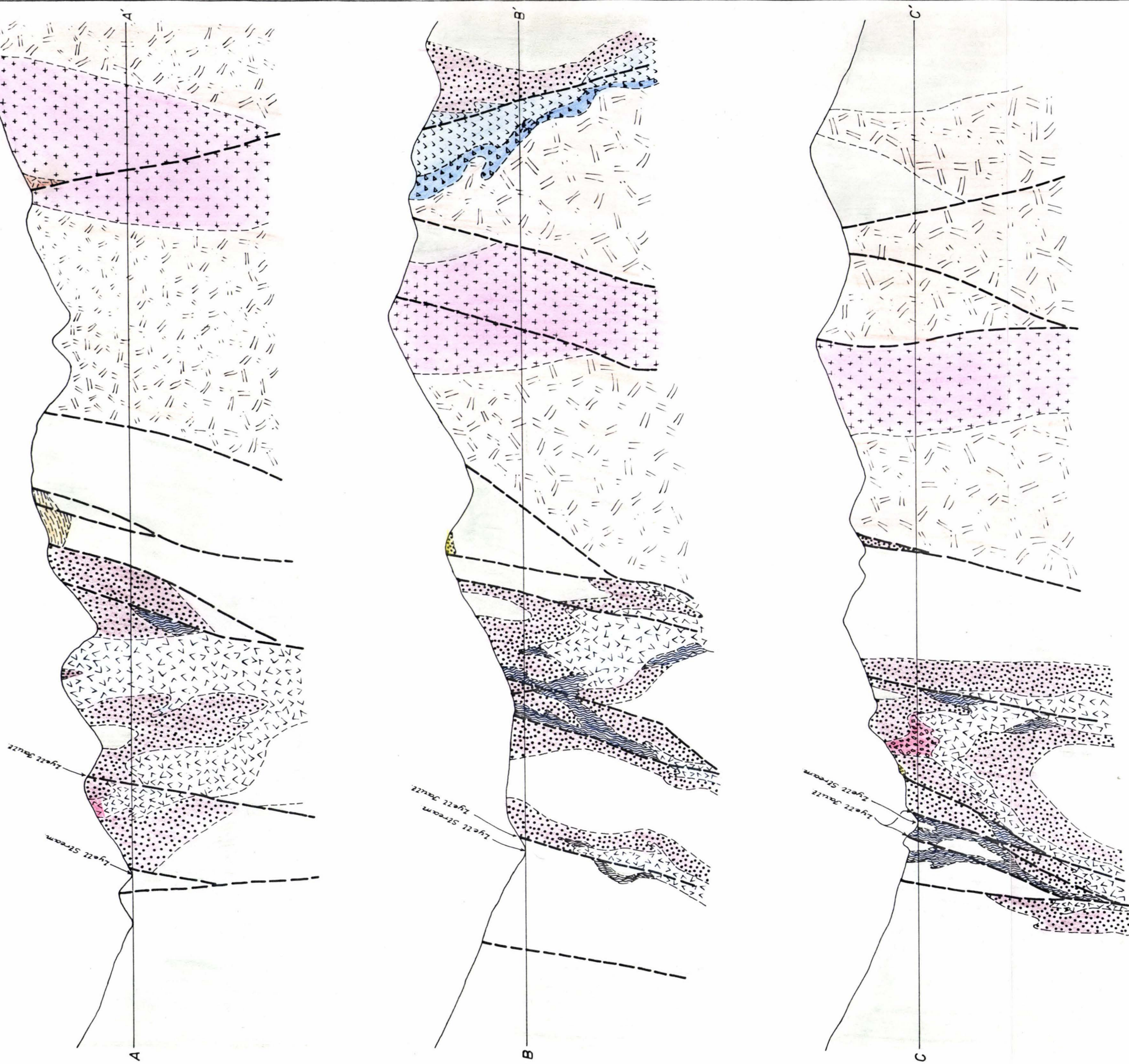
DIAGRAMMATIC CROSS SECTIONS
LYELL STREAM BALD HILL AREA

SCALE 1:10000

0   100   200   300   400   500 metres

N.B. Location of cross sections A-A', B-B', and C-C' are shown on geological map.
For geological legend see separate sheet.

Fig. 1-2: Diagrammatic cross sections for the Lyell Stream-
Bald Hill area. For location of sections A-A',
B-B' and C-C' see Fig. 1-1a.

have indicated similar hornfelsic sediments and
mineralization. The sulphides in the mineralized zone
are mainly associated with fracture-controlled quartz
veins in the porphyries and hornfels. However, signi-
ficant amounts of sulphide are also related to metasomatic
alteration in the sediments and as disseminated mineralization
within the Lyell Porphyry. The quartz veins, generally
1-2 cm thick, have no regular orientation and form a stock-
work type of deposit.

The Greenland Group sediments (Cooper, 1975) are
represented by monotonous sequences of indurated, greenish-
grey metagreywacke and argillite, regionally metamorphosed
to prehnite-pumpellyite or greenschist facies which dip
steeply to the west. Locally they have been thermally
metamorphosed to purplish biotite-hornfels (and sometimes
brecciated) where associated with the younger porphyries
and mineralization.

The Bald Hill Granites (informal name) of the Bald
Hill area immediately to the east of the main mineralized
zone, form the western margin of the Karamea Granite
batholith, and where seen, appear to be in fault contact
with the Greenland Group sediments. These muscovite-
bearing granites are medium to coarse grained gneissic
alkali-rich leucogranites, pink microgranites and biotite-
granites. Clots of biotite and foliated textures seen in
both hand specimen and thin section, gneissic textures,
occasional occurrence of pumpellyite and prehnite minerals,
strain features in quartz, bent cleavage in micas and twins

in feldspars, all suggest the Bald Hill Granites have been affected by regional metamorphic events.

A series of minor intrusives, collectively termed the Lyell Porphyry (informal name), intrude both the Greenland Group and the Bald Hill Granite country rocks. The Lyell Porphyry forms a series of small high-level plutons and cross-cutting dykes of quartz trondhjemite porphyry, granodiorites, quartz diorites, lamprophyre and quartz-bearing gabbroporphyry. The porphyries contain fresh quartz, strongly zoned sodic plagioclase phenocrysts, biotite and abundant sulphides. The plagioclase is often highly altered and the rocks extensively metasomatised (especially the more basic rocks), but they do not show the regional metamorphism apparent in the country rocks. Characteristic biotite thermal alteration envelopes surround the quartz trondhjemite and gabbroporphyry where they intrude the Greenland country rocks.

Mudstones, siltstones and sandstones of the Mangles Formation (Bowen, 1964), and basal coal measures and quartz grits of the Brunner Coal Measures (Bowen, 1964) unconformably overlying the metasedimentary and plutonic rocks are the youngest rocks in the area. These lower Tertiary (Eocene-Miocene) sediments form a downfaulted syncline in the northeast of Fig. 1-1a.

II. Regional Geochemistry

Initial reconnaissance of the Bald Hill area during December 1976 and January 1977 consisted of regional
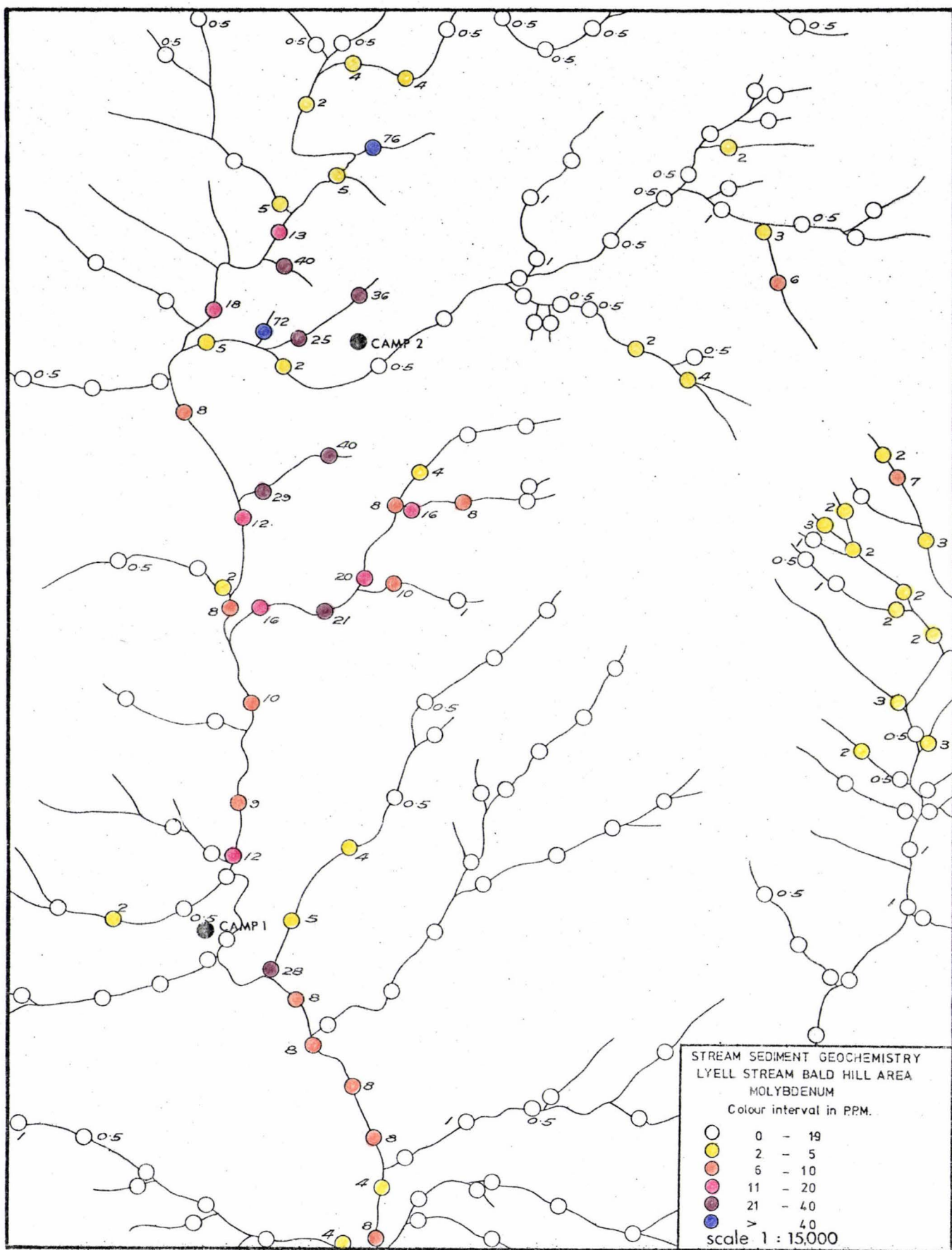
Fig. 1-3: Molybdenum stream sediment geochemistry for the Lyell Stream-Bald Hill area.
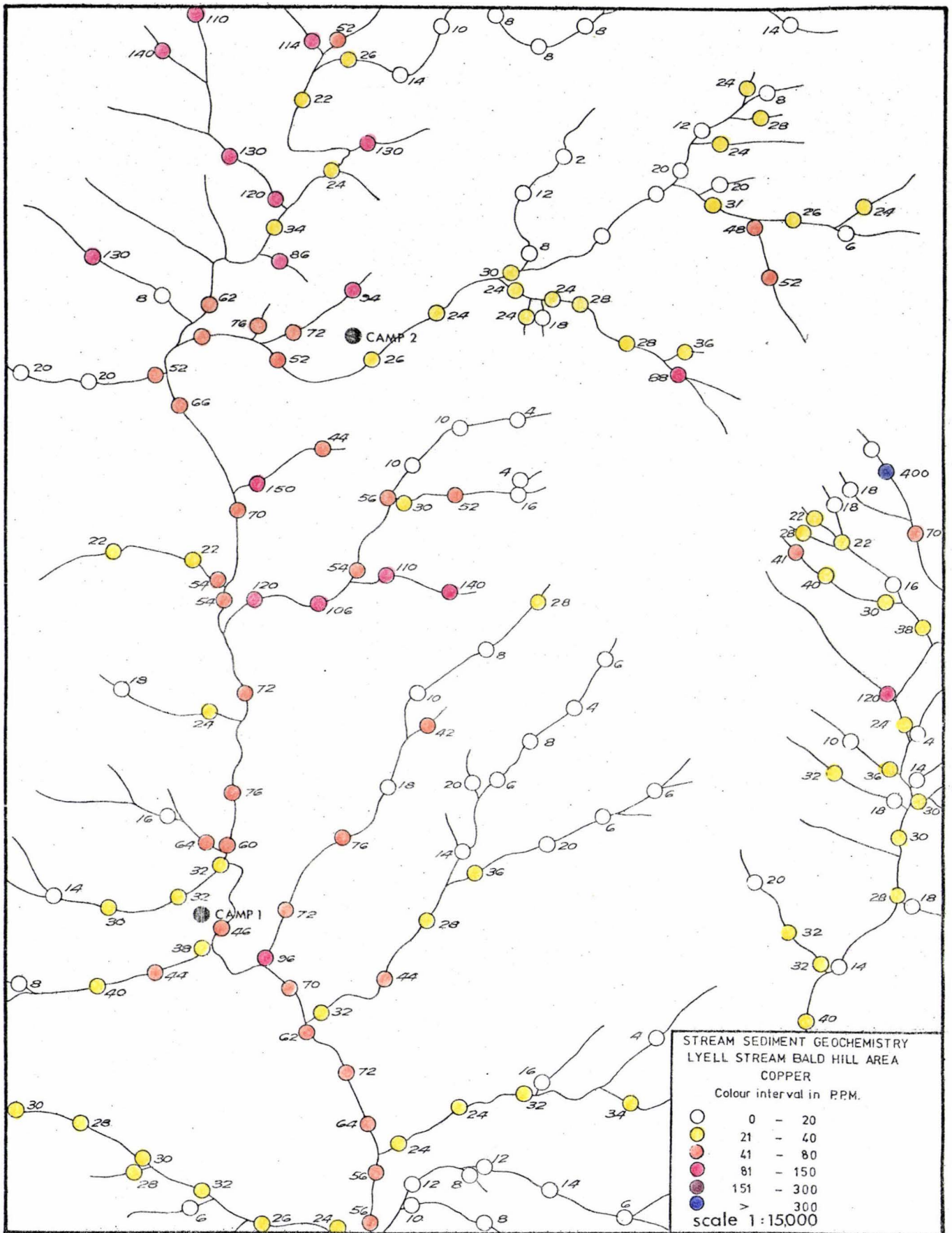
Fig. 1-4: Copper stream sediment geochemistry for the Lyell
Stream-Bald Hill area.

SOIL SAMPLE GEOCHEMISTRY
LYELL STREAM BALD HILL AREA
MOLYBDENUM
Contour interval in P.P.M.

1	0	— 1·9
2	2	— 5
3	6	— 10
4	11	— 20
5	21	— 40
6	>	40

scale 1 : 15,000
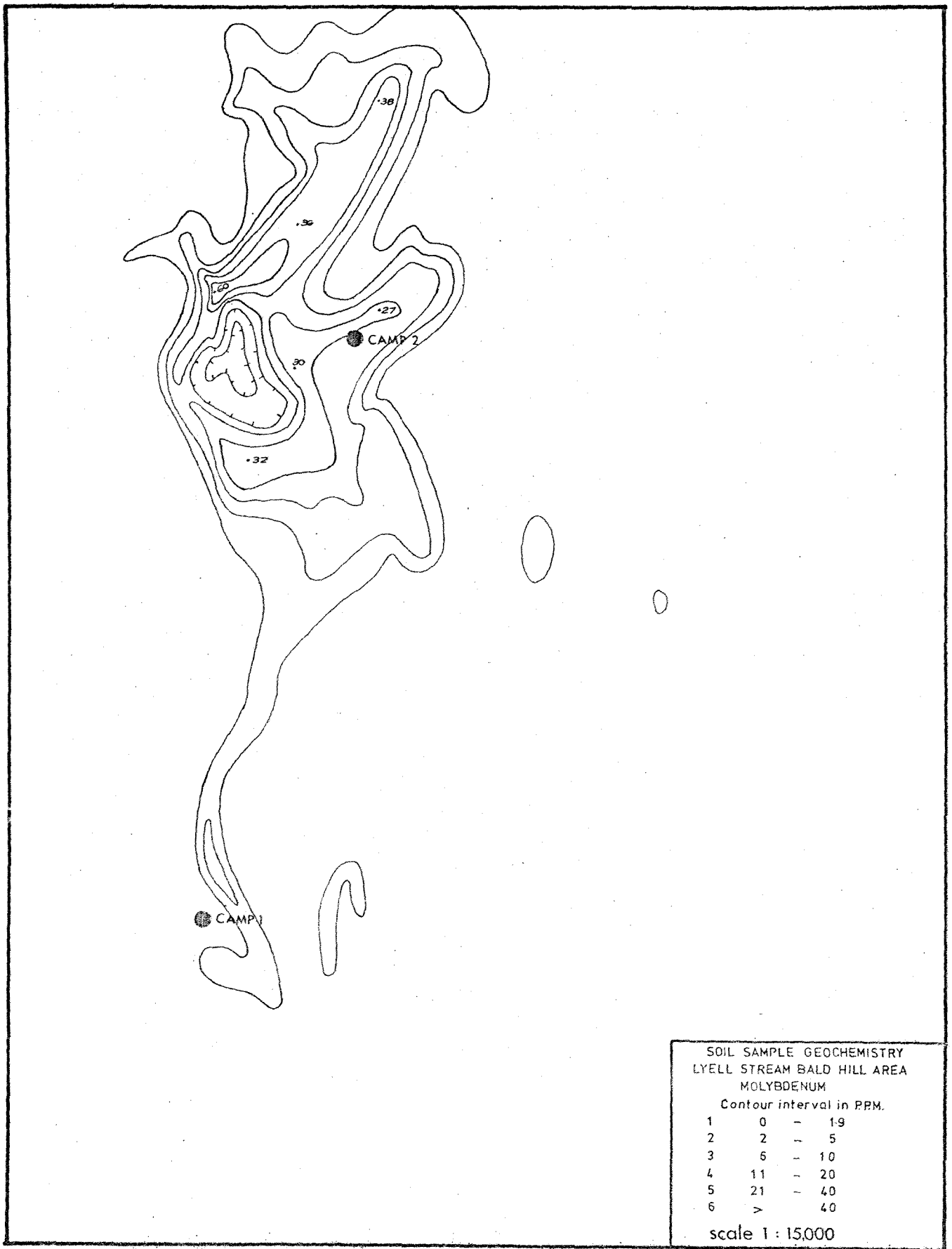
Fig. 1-5: Molybdenum soil geochemistry for the Lyell Stream-
Bald Hill area.
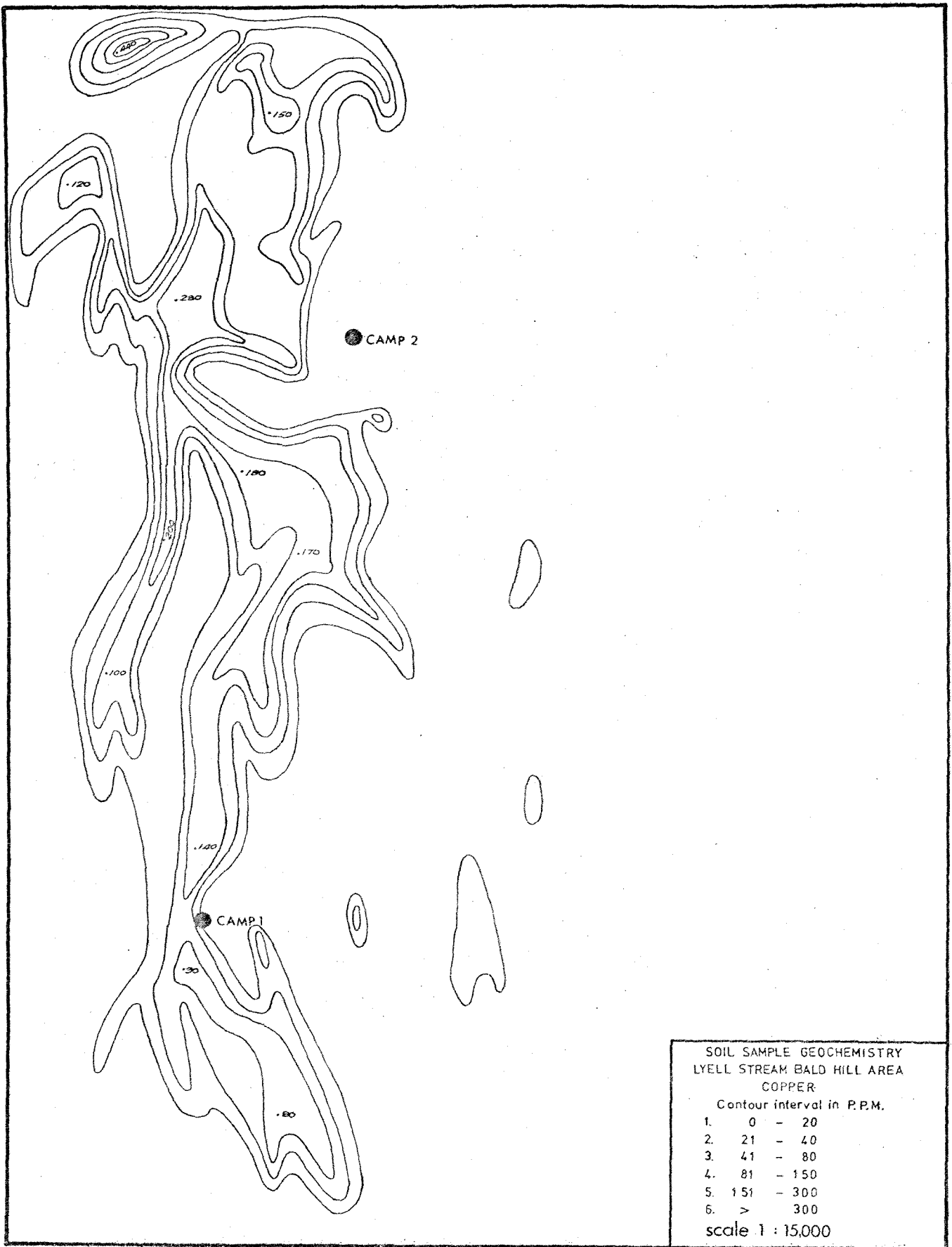
Fig. 1-6:   Copper soil geochemistry for the Lyell Stream-Bald
            Hill area.

Fig. 1-7: Photograph showing remnant fan and outwash gravels
           (arrowed) overlying hornfelsed Greenland Group
           metasediments.

mapping and stream sediment sampling to outline areas of

interest and any geochemically anomalous zones. Sieved

stream sediments were collected at 200 m intervals and

analysed for Ag, Pb, Zn, Cu and Mo. Stream sediment

results for molybdenum and copper are presented in

Fig. 1-3 and Fig. 1-4 respectively. The weakly anomalous

area for molybdenum (max. 76 ppm) is closely coincident

with anomalous copper values (max. 400 ppm). Regional

mapping and stream sediment sampling was followed by

ridge and spur soil sampling and detailed mapping of

the zone of interest. Soil geochemistry indicated a

narrow anomalous zone of molybdenum (max. 60 ppm) and
copper (max. 440 ppm) values, subparallel to the regional
geology (Figs. 1-5 and 1-6) and spatially coincident with
the highest stream sediment values. However, owing to
the capping of many spurs with fan and outwash gravels,
(Fig. 1-7) soil sampling results were of little use in
further systematically defining any anomalous zones.

CHAPTER TWO

GEOCHRONOLOGY

Introduction:

Potassium argon (K-Ar) ages have been determined for the Greenland Group metasediments, Bald Hill Granites, Lyell Porphyries and alteration associated with the mineralization within and surrounding the molybdenite-pyrite mineralization at Bald Hill.

K-Ar dating to establish both the relative and absolute ages of this suite of rocks was undertaken firstly, to establish a possible genetic relationship between molybdenum mineralization, the hornfels, the intrusive porphyries and spatially associated granites (i.e. metallogenesis) and secondly, to compare the absolute age of the Bald Hill mineralization with other molybdenum bearing deposits associated with minor intrusives within and marginal to the Karamea and Separation Point Granite batholiths in West Nelson (i.e. petrogenesis).

The mineral separations, rock sample preparation and potassium argon determinations were all completed at the Institute of Nuclear Sciences, Lower Hutt.

Analytical Techniques:

Samples of Greenland Group slates (4), biotite hornfels (3), Lyell Porphyry (3) and Bald Hill Granites (9) were selected for K-Ar dating. The slates and hornfels were

analysed as total rock samples, being carefully crushed in a stainless steel mortar and sieved to 200-400 μm mesh size, thus avoiding finer fractions that might lose argon during the crushing process. Where possible, biotite and muscovite were separated from the granites and porphyry at the 200-400 μm size, using a magnetic separator, for mineral age determinations of the plutonic rocks.

Experimental methods in use for K-Ar dating at the Institute of Nuclear Sciences have been described by Adams (1974), and the theory is briefly outlined in Appendix II. Experimental methods are hence briefly described. Potassium is determined by rock digestion in hydrofluoric and nitric acid, followed by separation on cation exchange columns and measurement on a modified flame spectrophotometer using potassium hydrogen phthalate standards. Argon is extracted from the samples by RF induction heating of the sample to 1400 to 1500°C, in a stainless steel ultra-high vacuum (UHV) system. The obtained gases are then purified by a 3A molecular sieve to remove water vapour and by titanium sublimation of other reactive gases. Argon quantities are then assessed by ^{38}Ar isotope dilution procedures on an on-line AEI-MS10 mass spectrometer.

Errors of individual age determinations are assessed by combining component errors in ^{40}Ar/^{38}Ar and ^{36}Ar/^{38}Ar ratio measurement, ^{38}Ar tracer calibration, mass discrimination and potassium analysis. The accuracy of the techniques was checked by several analyses of international rock and mineral standards listed in Table 2-1.

Table 2-1: Analyses of international potassium argon rock and mineral standards

Name	Origin	K wt %	^{40}Ar (radiogenic) nl/gm	% total	Age* Ma	Ref.**
P-207 Muscovite	U.S. Geological Survey	8.626	28.17	91.4	80.3±0.6	
		(8.593)	(28.22)	(90)	(81.0)	1
Arvonia Slate[1] A-7	Florida State University	3.364	41.44	98.6	286±2	
		(3.36)	(43.5)	(90)	(300)	2
GL-0 Glauconite	A.R.N.L., Paris	6.642	24.95	85.7	92.0±0.7	
		(6.59)	(24.82)	(7-20)	(-)	3

1: total rock (200-400 μm)

*: Decay constants, ^{40}K: $\lambda_\beta = 0.472 \times 10^{-9}$ yr^{-1}, $\lambda_e = 0.584 \times 10^{-10}$ yr^{-1}

K/K = 0.0119 atomic %

Errors are one standard deviation

**: 1 = Lanphere and Dalrymple (1965, 1967)
2 = Harper et al. (1973)
3 = Odin (1976)

Preferred analytical averages are listed in brackets.

Results:

Twenty-five K-Ar total rock, muscovite and biotite ages have been determined for the Bald Hill suite of rocks and results plotted on the Cretaceous time scale (Fig. 2-1). Sample locations and ages are shown on a generalized geological map in figure 2-2. Sample details, analytical data and ages are listed in Table 2-2.

Owing to the fine-grained nature of the Greenland Group argillites and hornfels, total rock rather than component mineral ages were determined. Ages for the argillites range widely from 112-226 million years (Ma) but the biotite-hornfels ages form a closer grouping of 103-120 Ma. In contrast the biotite mineral ages of the Lyell Porphyry, 112-116 Ma, and the muscovite-biotite mineral pair ages of the Bald Hill Granites occupy very limited ranges which are comparable with the experimental errors of individual age determinations. The ages of co-existing muscovite and biotite in the Bald Hill pink microgranite and biotite-granite are concordant in every case and the ages for the three Bald Hill Granite types cannot be considered significantly different.

Discussion:

I. Bald Hill Area

Greenland Group slates and phyllites to the south of the Buller District in North and South Westland have been previously dated, using K-Ar method, yielding total rock ages
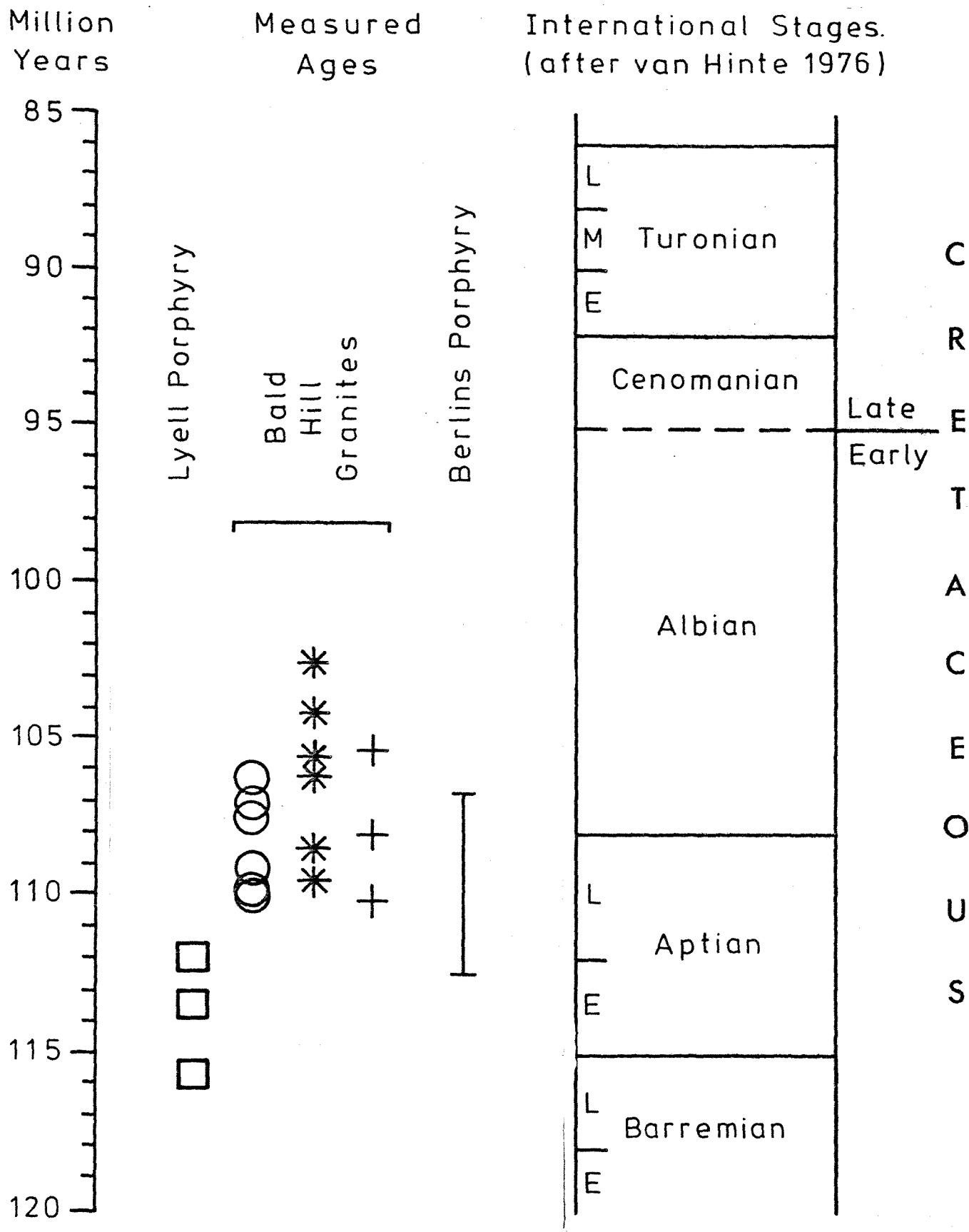
Fig. 2-1: Cretaceous time scale showing ages of samples listed in
Table 2-2. International stages are those of van Hinte
(1976) with minor modifications discussed in a similar
diagram in Adams and Nathan (1978). Squares show
trondhjemite porphyry ages, circles pink microgranite
ages, asterisks biotite-granite ages and crosses
leucogranite ages.
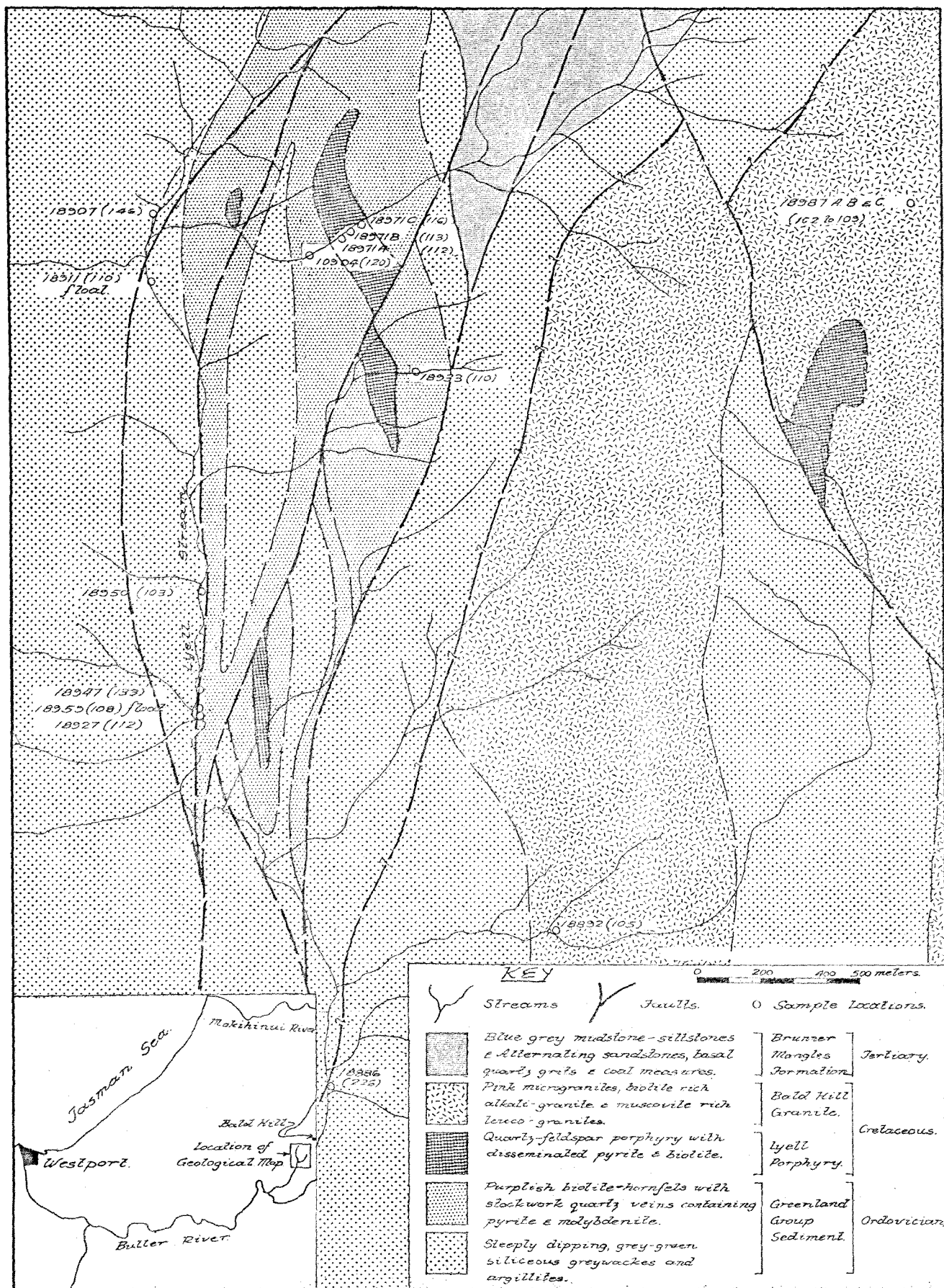
Fig. 2-2: Generalized geological sketch map of the Bald Hill area,
showing sample locations (except 18988A-C) and measured
ages in brackets.

Table 2-2: Potassium argon ages of granites and country rocks at Bald Hill, Buller district, South Island, New Zealand

Sample No.	INS R* No.	Rock Description	Grid ref. NZMS 1	K wt %	^{40}Ar (radiogenic) nl/gm	% total	Age** Ma
1) GREENLAND GROUP							
18886	6245TR	Fissile argillite	S25/538707	3.285	30.77	96.8	226±2
18907	6244TR	" "	S25/534743	3.662	21.57	96.1	146±1
18927	6246TR	" "	S25/535725	3.023	13.59	96.7	112±1
18947	6247TR	" "	S25/536729	4.221	22.64	98.6	133±1
18904	6252TR	Biotite-hornfels	S25/540741	2.690	12.95	93.2	120±1
18933	6254TR	" "	S25/542737	3.437	15.10	91.9	110±1
18950	6253TR	" "	S25/535733	0.964	3.99	85.1	103±1
2) LYELL PORPHYRY							
18971A	6250bi	Quartz trondhjemite porphyry	S25/524743	5.514	24.76	94.5	112±1
18971B	6262bi	" " "	S25/524743	5.232	23.83	95.7	113±1
18971C	6263bi	" " "	S25/524743	5.056	23.52	93.7	116±1
3) BALD HILL GRANITES							
18988A	6248mu	Pink microgranite	S25/565816	7.170	31.56	95.5	110±1
"	6248bi	" "	"	6.987	29.89	95.7	107±1
18988B	6258mu	" "	S25/565816	7.142	30.31	95.6	106±1
"	6258bi	" "	"	6.918	29.74	96.0	107±1
18988C	6259mu	" "	S25/565816	7.564	33.32	95.2	110±1
"	6259bi	" "	"	6.830	29.86	96.4	109±1
18987A	6249mu	Biotite-granite	S25/559751	6.151	25.18	93.8	102±1
"	6249bi	" "	"	6.643	29.20	94.6	106±1
18987B	6260mu	" "	S25/559751	7.702	32.47	92.2	105±1
"	6260bi	" "	"	6.673	29.00	95.8	108±1
18987C	6261mu	" "	S25/559751	7.582	31.56	94.4	104±1
"	6261bi	" "	"	6.548	28.72	25.0	109±1

Table 2-2 (ctd)

Sample No.	INS R* No.	Rock description	Grid ref. NZMS 1	K wt %	^{40}Ar (radiogenic) nl/gm	% total	Age** Ma
18892	6255mu	Muscovite-leucogranite	S25/551719	7.803	32.87	33.0	105±1
18911	6256mu	" "	S25/534740	7.751	34.22	82.5	110±1
18959	6257mu	" "	S25/536729	8.343	36.11	93.3	108±1

* TR = total rock (200-400 μm), bi = biotite, mu = muscovite

** Decay constants, ^{40}K: $\lambda_\beta = 0.4962 \times 10^{-9}$ yr^{-1}, $\lambda_e = 0.581 \times 10^{-10}$ yr^{-1}

^{40}K/K = 0.01167 atomic % (Steiger and Jager, 1977).

Errors are one standard deviation.

in the range 298-438 Ma (Adams et al., 1975). The range
is thought to be a consequence of the thermal events
associated with Tuhuan (or earlier) metamorphic and plutonic
events. Cooper (1974) also considered these metasediments
to be of Ordovician age on the basis of graptolite fossil
occurrences in the Reefton area. The scattered ages of the
Greenland Group argillites from the Lyell Stream area, 226,
146, 133 and 112 Ma are thus unusual. However when considered
with the hornfels and granite ages nearby, (less than 1 km
away), of 103-120 Ma, it is clear that the pattern indicates
partial argon loss within a thermal aureole around the
mineralized area for which petrographic effects are not
otherwise discernible. The maximum age of 226 Ma therefore
provides only a minimum value for the metamorphisms of the
Greenland Group in this area.

Hornfelsisation and mineralization of the Greenland
Group, intrusion and mineralization of the Lyell Porphyry
are all clearly related, with the 112-166 Ma ages of the
Lyell Porphyry dating the high level intrusion and cooling
of the small porphyry plutons. Mineralization occurs as
both disseminated molybdenite and pyrite and quartz-pyrite-
molybdenum veins in the Lyell Porphyry and as quartz-
pyrite-molybdenite (with minor chalcopyrite and bismuth)
bearing veins in the biotite-hornfels. The biotite-hornfels
is in turn spatially related to the mineralized Lyell
Porphyry (see Figs. 1-1a and 2-2). Total rock ages of
103-120 Ma for the biotite-hornfels then reflect the time
of hydrothermal alteration and mineralization of the

Greenland Group metasediments.

The K-Ar ages of the Bald Hill Granites, 102-110 Ma forming the western margin of the Karamea Granite batholith are almost certainly a consequence of the youngest plutonic event, the nearby intrusion of mineralized minor granitic rocks and probable regional tectonic activity accompanying the intrusion. Petrographical and petrochemical evidence of the Bald Hill Granites (presented in chapters 3 and 4 respectively) indicate these granites are of the same petrogenic province as the 'main phase' Karamea Granite batholith and not the minor, molybdenum-bearing granitic phases. Karamea batholith granites have been dated using the Rb/Sr technique by Aronson (1965; 1968) and are shown to be of Tuhuan age (280-320 Ma). It is well known that granite rocks constitute isotopically open systems (eg: Adams et al., 1975) and therefore may be isotopically 'reset' by later thermal events. Hence it is impossible to indicate by K-Ar or Rb/Sr mineral ages alone whether a granite is an older rock, which has undergone cooling and regional uplift following orogenic activity or whether it has formed at that time by granitic plutonism accompanying orogeny.

There are, however, several lines of evidence to suggest that the 'Tuhuan' ages for the Karamea batholith granites are real ages:

1) Aronson's Rb/Sr mineral ages previously mentioned above.

2) K-Ar biotite age of 295±8 Ma from the main Karamea batholith granite 2 km west of Questa Creek at Karamea Bend reported by Smale (1976).

3) The scatter of K-Ar ages for Greenland Group meta-
   sediments, 112 Ma to 226 Ma, within 1 km of Cretaceous
   porphyry intrusives at Bald Hill.

4) Total rock K-Ar ages of calcareous basic and pelitic
   schists of 200-203 Ma adjacent to mid-Cretaceous
   intrusives reported by Wodzicki (1972) from Copperstain
   Creek.

The mid-Cretaceous ages for the minor intrusives are also
real, viz:

1) Aronson (1968) has Rb/Sr dated a biotite from the
   Berlins Porphyry at 113-117 Ma.

2) Mid-Cretaceous Rb/Sr isochron ages for intrusive granitic
   rocks in the Victoria Range near Reefton (Adams, 1978;
   pers. comm.).

3) The mid-Cretaceous K-Ar dates for minor molybdenum-
   bearing intrusives reported by Hulston and McCabe (1972),
   Wodzicki (1972), Smale (1976), Rabone (1977), Tullock
   (1977), Adams and Nathan (1978) and the Lyell Porphyry
   K-Ar ages presented in this study.

In summary, at Bald Hill, the mineralization and
plutonic activity are too close together in the field to
escape the possible thermal effect of one upon the other
and so, the muscovites and biotites of the Bald Hill Granites
have been 'isotopically reset' by a combination of later
minor intrusive activity and regional tectonic activity
accompanying intrusion (Rangitata Orogeny). The K-Ar ages
of the Lyell Porphyry, 112-116 Ma (Albian to Aptian), can

be considered close to the time of intrusion and
mineralization as these rocks form small high level
intrusions which rapidly cooled. However, the Bald Hill
Granites, of probable Tuhuan age, K-Ar ages of 102-110 Ma,
form more deeply seated masses which subsequently cooled
more slowly, more likely reflect the time of uplift,
erosion and cooling rather than intrusion.

II. Other West Nelson Molybdenum Prospects

Recent 'open file' Mines Department reports from
various mining and mineral exploration companies (see
Appendix V), data compiled by Williams (1974), Eggers
and Adams (1978) and published geochronological and
geological studies indicate several molybdenum occurrences
in West Nelson and North Westland are associated with
young acidic porphyries and satellite stocks which have
many petrographic and petrochemical similarities. These
stocks intrude the Karamea (Tuhuan) and Separation Point
Granite batholiths and associated lower Paleozoic low-grade
metasediments. Many of these minor molybdenum-bearing
granitic rocks have been K-Ar dated and this data is
summarised in Fig. 2-3. Names and location of these
deposits are shown in Fig. 2-4. All previously published
and unpublished K-Ar ages have been recalculated using new
K-Ar decay constants of Steiger and Jager (1977).

At Cascade Creek, 25 km to the west of Bald Hill and
20 km east of Westport, Bailey (1973) describes copper-
molybdenum mineralization associated with the Berlins
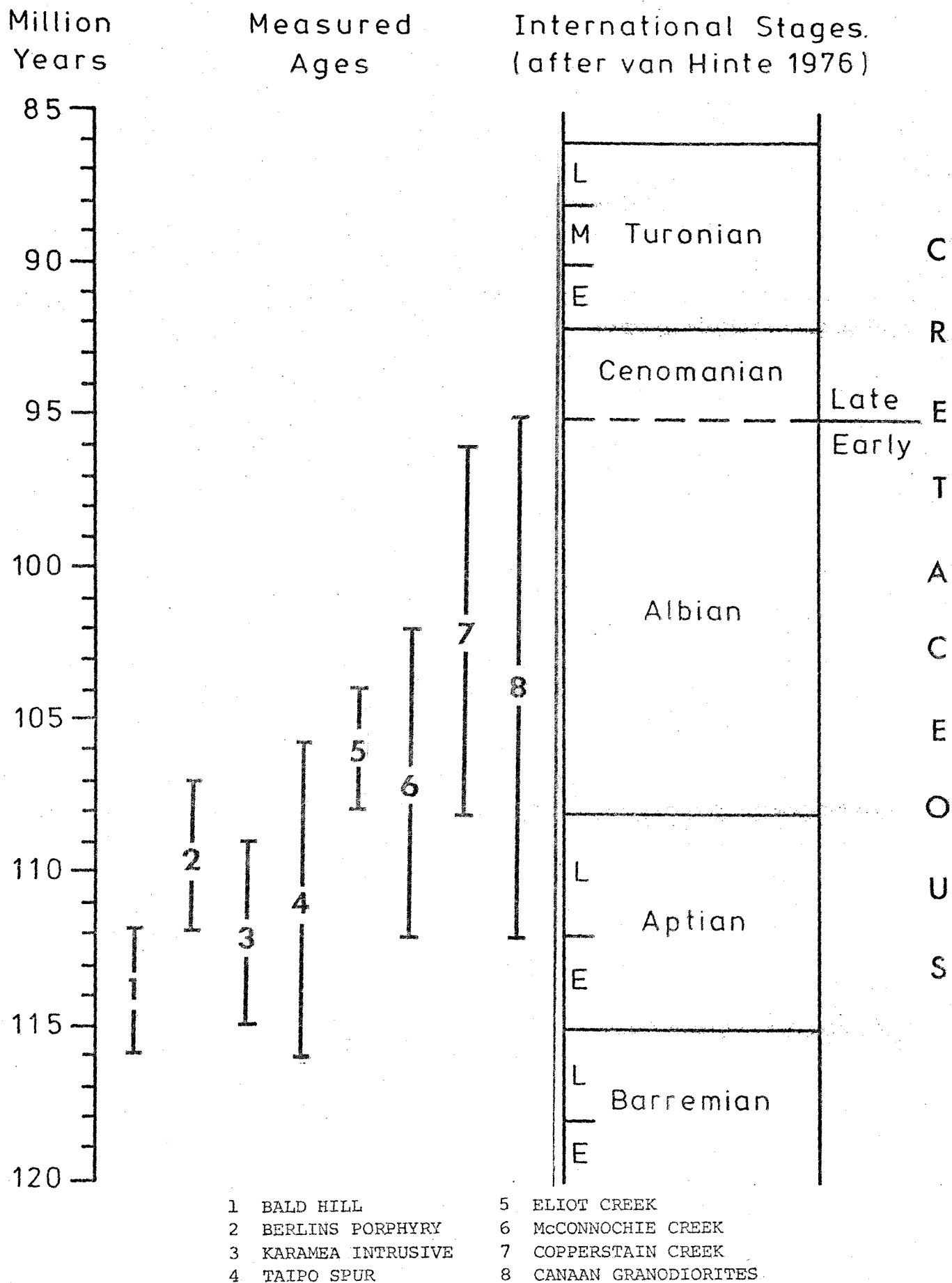
Fig. 2-3: Cretaceous time scale showing age data for molybdenum-bearing granitic intrusives from Bald Hill and seven other molybdenum prospects in West Nelson and North Westland, South Island, N.Z.
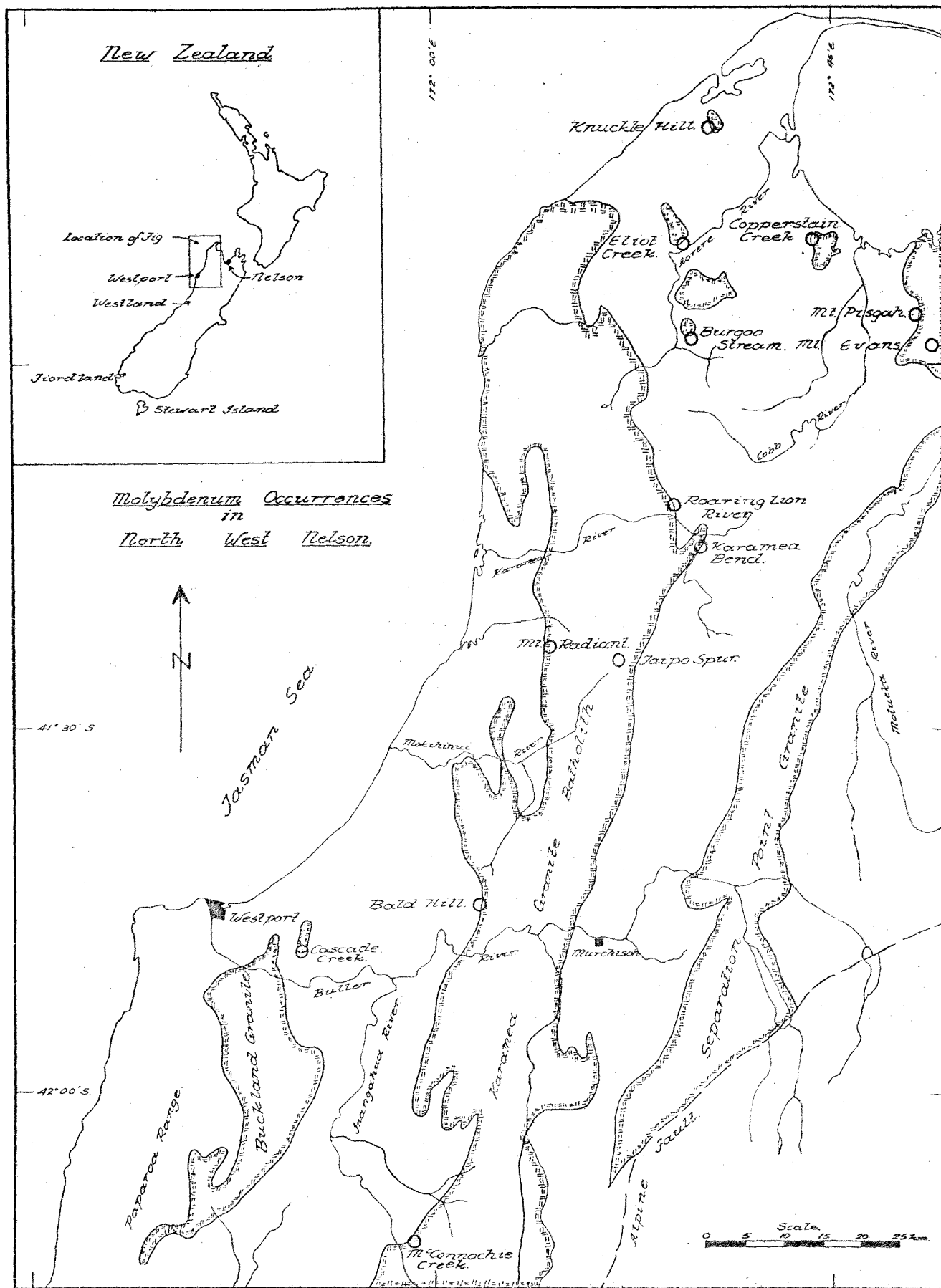
Fig. 2-4: Map of West Nelson and North Westland showing Karamea
and Separation Point granite batholiths and location
of molybdenum prospects.

Porphyry (Nathan, 1974). This hypabyssal quartz porphyry which intrudes an Upper Mesozoic granodiorite stock associated with Ordovician Greenland Group metasediments, is a porphyritic granodiorite-hyalodacite hypabyssal suite and can be indirectly related to subaerial acidic volcanism of the Stitts Tuff member of the Hawks Crag Breccia (Albian). K-Ar ages of the Berlins Porphyry, 105-110 Ma (Adams and Nathan, 1978), are considered close to the time of intrusion since these rocks are rapidly cooled, high level intrusions (cf. Lyell Porphyry). The Buckland Granite, which yielded ages of 97-102 Ma, is intruded by the Berlins Porphyry (Adams and Nathan, 1978). This rock is a much coarser grained, deeper seated granite than the porphyry and as with the Bald Hill Granites, is considered by Adams and Nathan more likely to reflect the time of uplift and cooling rather than intrusion.

At Taipo Spur, 40 km northeast of Bald Hill, the 'Tuhuan' Luna Granite has been intruded by the more acidic Taipo Granite, consisting of porphyritic microgranites, aplite dykes and rare pegmatitic lenses. The Taipo Granite is associated with molybdenum, base metal and rare bismuth mineralization and has been described by Henderson (1975), Rabone (1977) and others (see Appendix V). Unpublished age data (Rabone, 1977) indicate that granitic and pegmatitic intrusion and probable associated molybdenite mineralization occurred at 106-116 Ma, very similar to the age patterns established elsewhere.

At Big Bend, in the Karamea River, about 70 km northeast of Bald Hill, Smale (1976), Rabone (1977) and others in Mines Department reports (Appendix V) have described molybdenum-quartz vein mineralization and hydrothermal alteration associated with small stocks of porphyritic microgranodiorites, micromonzonites and microdiorites intruding Ordovician metasediments and Upper Carboniferous Karamea granites. These porphyritic intrusives have yielded two biotite ages of 112±3 Ma. These ages contrast strongly with the 295±8 Ma biotite age from the main Karamea batholith 2 km to the west.

In the Aorere Valley, 20 km southwest of Collingwood, small biotite-adamellite stocks intrude lower Paleozoic sandstones and pelitic schists at Eliot Creek. Molybdenum-bismuth-base metal sulphide mineralization and hydrothermal alteration occurs in and adjacent to these Eliot Creek stocks (Rabone, 1977). Biotite from the hornfelsed country rocks and muscovite from the greisen-granite with disseminated molybdenite yield ages of 104 to 107 Ma (Adams pers. comm.), again emphasising the association of Cretaceous plutonic rocks with molybdenite occurrences.

In the Separation Point Granite batholith, east of the Karamea batholith, molybdenite-base metal mineralization is recorded from Copperstain Creek and Mount Pisgah (Canaan). The Copperstain Creek mineralization is associated with a satellite stock of Separation Point Granite 18 km west of the western margin of the main Separation Point Granite.

The geology of Copperstain Creek was first described by
Bell and others (1907) and a detailed study was made by
Wodzicki (1972). Wodzicki reported a maximum K-Ar biotite
age of 108 Ma for a granodiorite intrusive carrying
disseminated molybdenite and intruding regionally meta-
morphosed and calcareous basic and pelitic schists which
gave two maximum K-Ar total rock ages of 200 and 203 Ma.
Some further, younger ages, 89-100 Ma, appear to reflect
a thermal overprint of the adjacent Onahau Granite, a
younger satellite stock of the main Separation Point batholith.
The Canaan molybdenite-base metal-scheelite quartz reefs
have not been directly dated, but lie within the Separation
Point Granite, on its western margin along the contact between
the granites and the older Rameka intrusives. The
Separation Point Granite nearby has yielded K-Ar dates,
mostly on biotites and hornblendes, in the range 78-127 Ma,
with a slight concentration in the range 95-112 Ma (Hulston
and McCabe, 1972; Aronson, 1965, 1968).

On the eastern side of the Karamea Granite batholith
in the Roaring Lion River watershed and Burgoo stream,
between Big Bend and Eliot Creek, molybdenite mineralization
is associated with stocks and dykes of quartz porphyritic
granodiorite and granite or quartz vein stockworks in
Ordovician metasediments (see mining company reports,
Appendix V). To the west, molybdenite is known from the
Mount Radiant area, including the Anaconda Reef (Webb, 1910;
Reed, 1958; Williams and Sanderson, 1959; Wodzicki, 1960;
Bailey, 1972), immediately south of the Little Wanganui

River. Quartz lodes containing molybdenite, pyrite,
chalcopyrite, bornite and tetrahedrite are concentrated
at a contact of biotite-granites and adamellites with
hornfelsed and schistose metasediments of probable
Ordovician age. The porphyritic granite also intrudes
coarser grained, main phase Karamea batholith granites.

At the southern end on the western margin of the
Karamea batholith at McConnochie Creek, in the Victoria
Ranges southeast of Reefton, Henderson (1917) reported
molybdenite from a reef close to the granites of the Victoria
Range and from pegmatite boulders in rivers immediately to
the north. These granites include several small stocks of
quartz-porphyry which yield biotite and muscovite K-Ar
ages in the range 102-112 Ma (Tullock, pers. comm.).

All the above molybdenite occurrences, including the
Bald Hill data presented, emphasise the consistent association
of molybdenite mineralization with mid-Cretaceous minor
granitoid plutonism close to the contacts of the major
western Nelson granite batholiths with early Paleozoic
country rocks. The minor granitoid intrusives are of mid-
Cretaceous age (100-115 Ma) and distinctly younger than the
Tuhuan phase of major plutonism (280-370 Ma).

The mineral age data discussed in this study, and
also the data reported by Aronson and others, are minimum
ages only and all indicate that uplift, cooling and
substantial erosion of the granites was coeval with the
Rangitata Orogeny (100-120 Ma). However as shown by this
study, and as Aronson also considered, extensive plutonic

activity occurred in the Westland foreland province
associated with the New Zealand Geosyncline in Cretaceous
times.

CHAPTER THREE

PETROGRAPHY

Introduction:

Metasedimentary and plutonic rocks from Bald Hill
have been examined petrographically to determine their bulk
mineralogical and textural characteristics for classification
and to describe alteration mineralogy. Greywackes and
argillites are classified using grain size and confirmed by
geochemical characteristics (Chapter 4). The thermally
altered hornfels are classified using alteration mineral
assemblages. Plutonic rocks have been classified modally
(Table 3-1; Fig. 3-1) and supported by textural and geo-
chemical evidence (classification and nomenclature after
Travis, 1955; and Streckeisen, 1967, 1973). The tonalite
has been termed a quartz trondjemite as it contains >30%
quartz, >40% oligoclase feldspar and approximately 10%
ferromagnesium minerals (Streckeisen, 1973).

I. Greenland Group Metasediments:

Country rocks, into which the Bald Hill Granites and
Lyell Porphyry plutonic rocks have intruded, are well
indurated green-grey metagreywackes and argillites of the
Greenland Group. The greywackes comprise medium to fine-
grained subrounded to subangular quartz grains with relatively
rare sodic plagioclase (andesine?) and rock fragments in a
silt sized quartz-sericite-clay matrix (Fig. 3-2). Fine

Fig. 3-1: QAP modal classification of the Bald Hill plutonic
rocks after Streckeisen (1967, 1973). Average
modal composition of each rock type plotted.

Table 3-1: Modal composition of the Bald Hill plutonic rocks
(in volume %)

	BHG (1)			LP (2)				
	LG	PM	BG	TP	GD	DI	LD	GP
Quartz	45	43	41	36	25	15	10	7
Orthoclase	8	7	7	-	10	-	-	-
Microcline	14	13	14	-	6	-	-	-
Albite	21	21	19	-	-	-	-	-
Oligoclase	-	-	-	44	40	-	-	-
Andesine	-	-	-	-	-	48	-	-
Labradorite	-	-	-	-	-	-	53	44
Muscovite	11	9	8	2	-	-	-	-
Biotite	-	6	9	12	14	11	-	-
Pyroxene	-	-	-	-	2	4	12	6
Amphibole	-	-	-	-	-	19	15	26
Olivine	-	-	-	-	-	-	5	4
Accessories (3)	1	1	2	6	3	3	5	13

(1) Bald Hill Granites: LG: Leucogranite
                          PM: Pink microgranite
                          BG: Biotite-granite

(2) Lyell Porphyries: TP: Trondhjemite porphyry
                          GD: Granodiorite
                          DI: Quartz diorite
                          LD: Lamprophyre dykes
                          GP: Gabbroporphyry

(3) includes apatite, sphene, zircons, beryl, calcite, oxide
     and sulphide minerals.

pleochroic pumpellyite, abundant chlorite, very fine sphene
or rutile, and prehnite(?) along with minor opaques indicate
the greywackes to be partially reconstituted by widespread
regional metamorphism to prehnite-pumpellyite metamorphic
grade. Greywackes grade petrographically and chemically into
the less siliceous argillitic slates which consist of fine
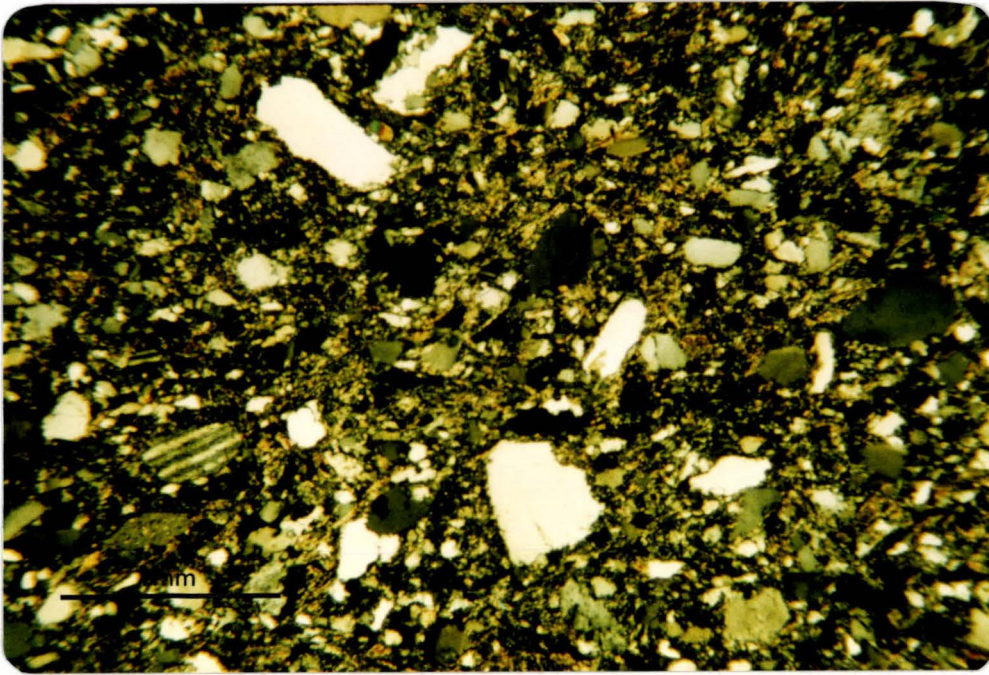
Fig. 3-2: Subangular quartz grains with rare sodic plagioclase grains in 18888. Greywacke, Greenland Group metasediment (XP).
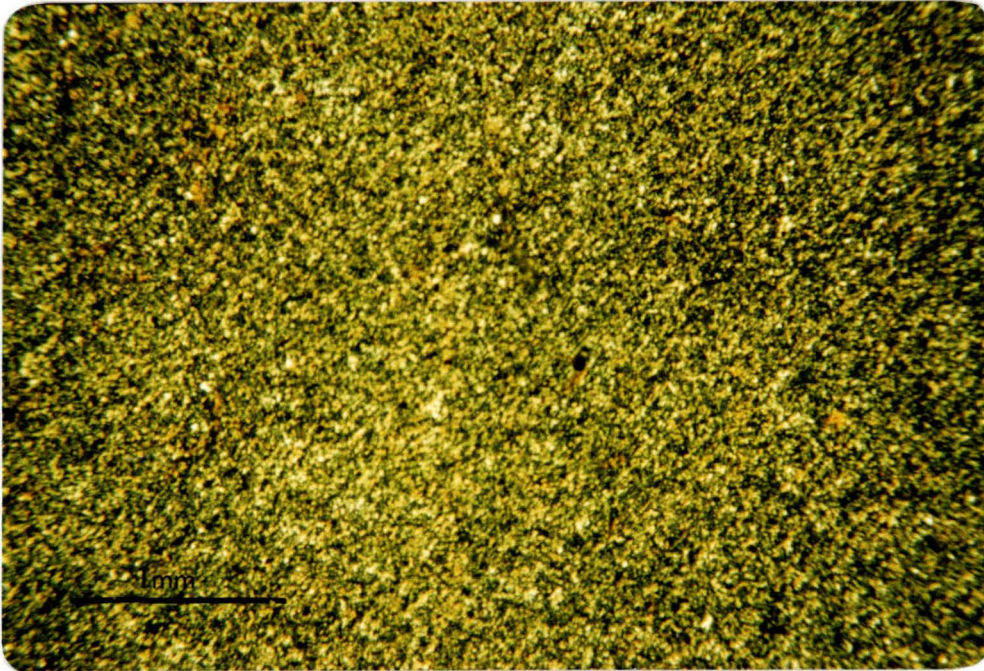
Fig. 3-3: Photomicrograph showing fine-grained quartz and quartz-biotite-sericite-chlorite matrix in 18927. Argillite, Greenland Group metasediment (XP).

grained quartz and quartz-biotite-sericite-chlorite matrix containing minor sphene(?) (Fig. 3-3). Argillites often have a "spotted" appearance due to some recrystallization and formation of muscovite rich layers.

Locally the metasediments have been completely recrystallized to high grade, coarser grained quartz-muscovite-biotite-hornfels schist containing accessory zircon and minor apatite (Fig. 3-4). The schists are probably part of a remnant metamorphic aureole associated with the intrusion of the Bald Hill batholith granites. Outcrop of these schists is very rare and as such could not be systematically mapped. Later(?) intense thermal alteration accompanying intrusion of the Lyell Porphyries has affected the metasediments and hornfels schists for distances up to 150 metres from intrusive contacts, obliterating both relict sedimentary and high grade metamorphic textures and mineral assemblages. Owing to the quartz-rich, subaluminous nature of the metasediments, thermal alteration mineralogy is simple. Three zones of increasing propylitic alteration can be recognised in the field and microscopically:

Zone I

Development of schistosity and cleavage in hand specimen and introduction of pyrite-muscovite±biotite and/or quartz and calcite veins is characteristic of initial thermal alteration of the metasediments (Fig. 3-5). This initial propylitization forms a peripheral zone to more intensely
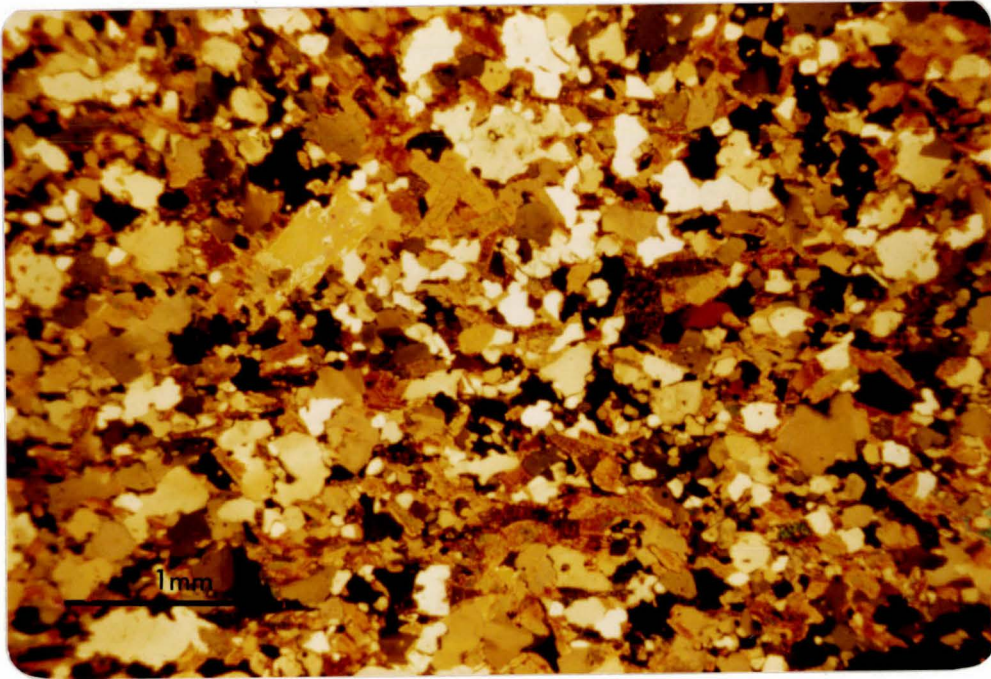
Fig. 3-4: Completely recrystallized quartz-muscovite-biotite
           hornfels schist, 18849. Metamorphosed Greenland
           Group (PL).
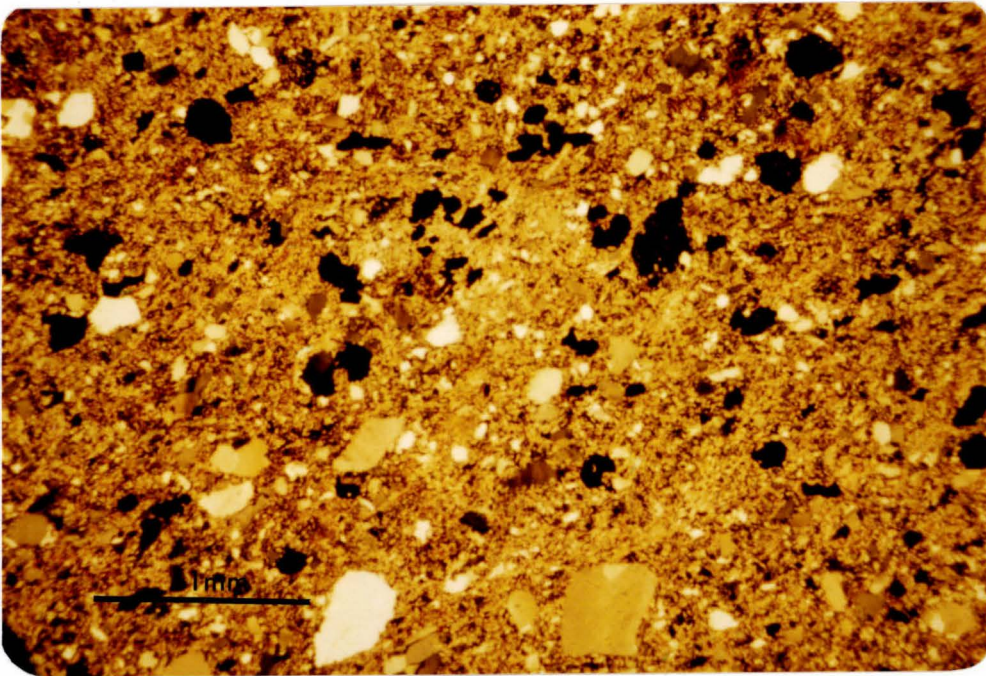
Fig. 3-5: Disseminated pyrite in greywacke of zone I hornfels,
           18897. Altered Greenland Group (PL).

altered (zone II) metasediments, and can often be recognised petrographically only by the presence of finely disseminated pyrite. Minor fracture and joint controlled quartz-sulphide veining occurs within zone I hornfels.

Zone II

Zone II hornfels are noticeably coarser grained and purplish from the abundance of biotite and often contain quartz-sulphide bearing veins. Microscopically the biotite — hornfels have a completely recrystallized matrix of pleochroic brown-red biotite, muscovite, zircon(?) with disseminated pyrite and infilled fractures of quartz and opaque sulphides (pyrite) (Fig. 3-6). Zone II alteration forms "envelopes" surrounding intrusive porphyry stocks and silicified breccia (zone III hornfels) and also occurs along fault zones where thermal alteration intensity generally increases.

Zone III

The metasediments have been pervasively altered and recrystallized to a fine-grained quartz-muscovite mosaic, impregnated with pyrite similar to zone I. The rock is often brecciated and cemented by coarse-grained quartz veins with pyritic vugs and some molybdenite mineralization (Fig. 3-7). Hematite and magnetite also occur, especially in the quartz veins. Zone III type alteration is of limited extent, being associated with breccia pipes(?) and immediately surrounding stockwork quartz-sulphide veins (ie: on sub-microscopic
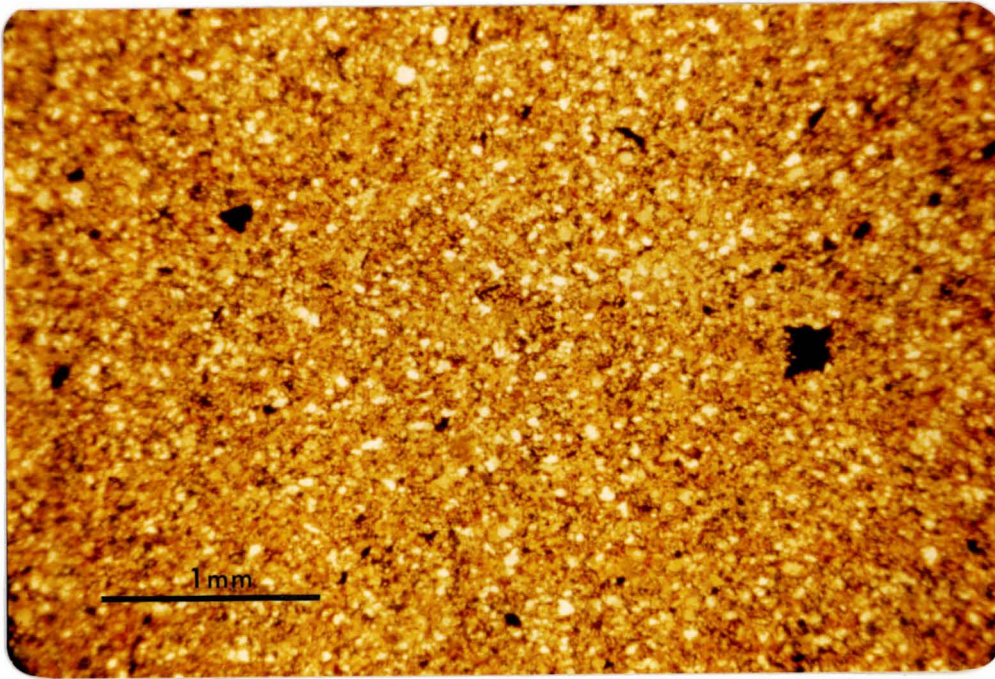
Fig. 3-6:   Fine-grained biotite and disseminated pyrite in zone II
            hornfels, 18939. Altered Greenland Group (PL).
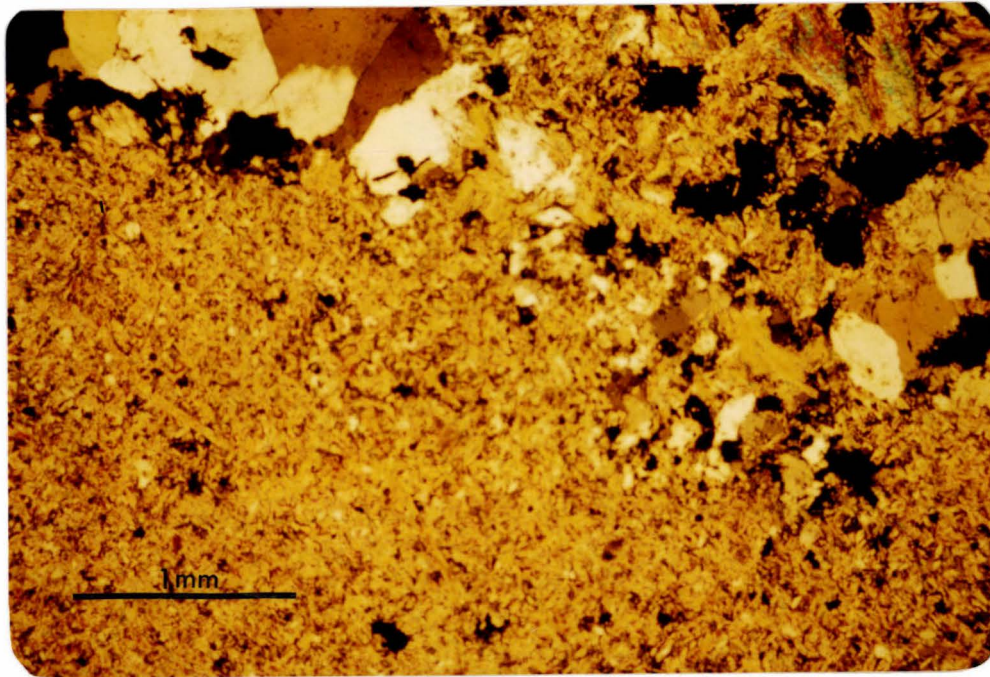
Fig. 3-7:   Pervasively altered metasediment with muscovite bearing
            quartz-sulphide veins, 18882.   Zone III hornfels.
            Altered Greenland Group (PL).

scale) within zone II hornfels. Within zone III any
original metasedimentary textures are totally obliterated
with complete recrystallization and replacement of the
original matrix.

II. Plutonic Rocks:

(a) Bald Hill Granites

Bald Hill Granites form the western margin of the
Karamea Granite batholith, which intrudes Ordovician
Greenland metasediments. These granites are, in turn,
intruded by the Cretaceous Lyell Porphyry. The granites
are a suite of medium to coarse grained muscovite-bearing
quartz rich alkali granites. Three main petrographic types
in the Bald Hill area are shown to have close mineralogical
and textural affinities.

Leucogranite

The leucogranites are medium to coarse grained rocks
(1-4 mm), texturally showing a foliation of quartz, feldspars
and micas. The rocks contain a greater proportion of
muscovite (with an absence of biotite), than the other Bald
Hill Granites, but texturally and mineralogically are similar
to the pink microgranite and the biotite-granite. The
leucogranites contain highly strained quartz, micrographic
orthoclase and albite containing quartz and muscovite
inclusions, microcline and coarse muscovite (Fig. 3-8).
Foliation and microgranulation of quartz with a lineation
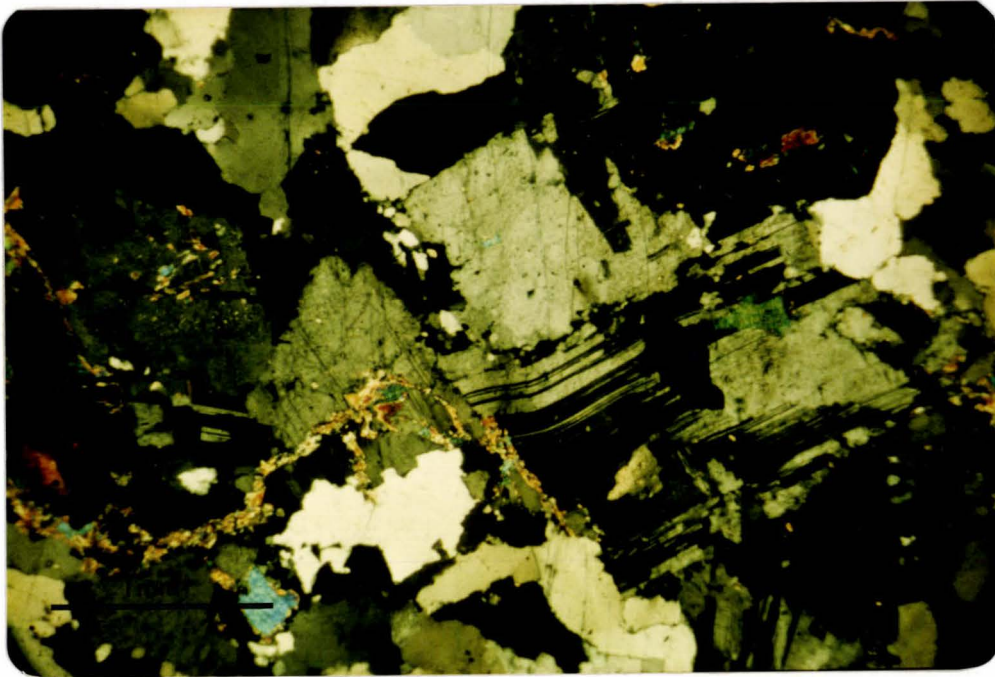
Fig. 3-8: Albite with kinked twins, micrographic orthoclase with
a weakly foliated texture in 18959. Leucogranite,
Bald Hill Granite (XP).
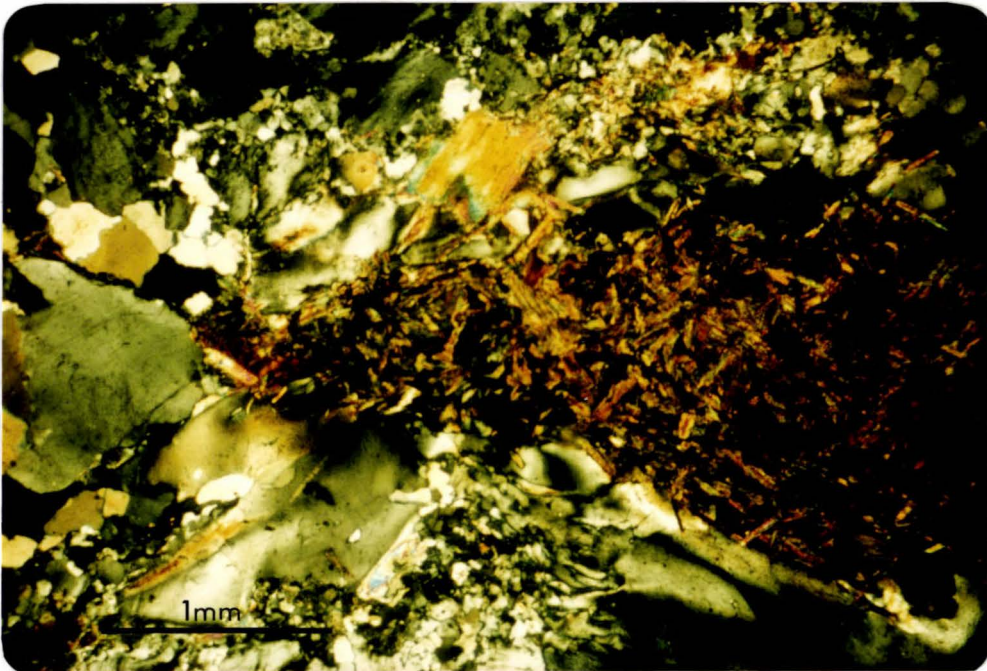
Fig. 3-9: 'Xenocrystic clot' of biotite, strained and micro-
granulated quartz in 18901. Pink microgranite,
Bald Hill Granite (XP).

of muscovites and some larger feldspar crystals give the granite a gneissic texture. Kinked twins in the sodic plagioclases (albite, $2V_\gamma$ 80°, An_{5-10}) and bent cleavage planes in muscovites are common. Accessory prismatic apatite (uniaxial negative), chlorite and minor opaques occur with very fine grained tabular prehnite.

Pink microgranite

The pink microgranites have a mottled, pink appearance in hand specimen, the biotite and muscovite forming "clots" and potash feldspars producing the characteristic pink colouration. Mineralogically the rocks are very similar to the biotite-granite, although biotite is always subordinate to muscovite and texturally the pink microgranites tend to be finer grained (<1-2 mm), with more micrographic inter-growths of quartz and sodic feldspars. Graphic intergrowths of quartz and orthoclase occur. Microscopically (Fig. 3-9), quartz is strained and granulated similar to the quartz in other Bald Hill Granites along with kinked twins in albite crystals and bent cleavage planes in muscovites and biotites. The micaceous minerals usually have a preferred orientation or form elongate "xenocrystic clots" (see Fig. 3-9). The rocks contain orthoclase and microcline, the orthoclase often having a micrographic texture, or being completely recrystallized to quartz-muscovite mosaic. Accessory colourless prismatic apatite, greenish fine grained prehnite and pale green beryl (high relief, grey-yellow interference colours, uniaxial negative) occur with minor disseminated sulphides.

Biotite-granite

The biotite-granites show a weak alignment of alkali feldspars and micas in hand specimen. Microscopically (Fig. 3-10) the coarse grained, granular rocks (1-5 mm) have a foliation of quartz and feldspar minerals with a lineation of biotites and muscovites. They have similar mineralogies and textures to other Bald Hill Granites (i.e. granulated and strained quartz, orthoclase, microcline, albite (An_{6-10}) with kinked twins, muscovite and biotite with bent cleavage planes, accessory prismatic apatite, zircons, prehnite and pale green beryl), although muscovite is always subordinate to biotite. The albite often has micrographic intergrowths of quartz and muscovite with minor sericitic alteration. Micaceous minerals frequently occur as elongate xenocrysts similar to the xenocrysts in the pink microgranite (see Fig. 3-9).

(b) Lyell Porphyries

These rocks occur as a series of small cross-cutting stocks and dykes, generally elongate in shape, intruding Greenland metasediments and Bald Hill Granites. They are a series of calc-alkaline quartz trondhjemites, granodiorites and quartz diorites. Lamprophyre dykes and gabbroic rocks also occur, although these more basic rocks tend to be highly metasomatised and may predate the intrusion of the more acid porphyries. Both the acid and the more basic rocks are, however, petrographically distinct from the Bald Hill Granites, not having been affected by the metamorphic
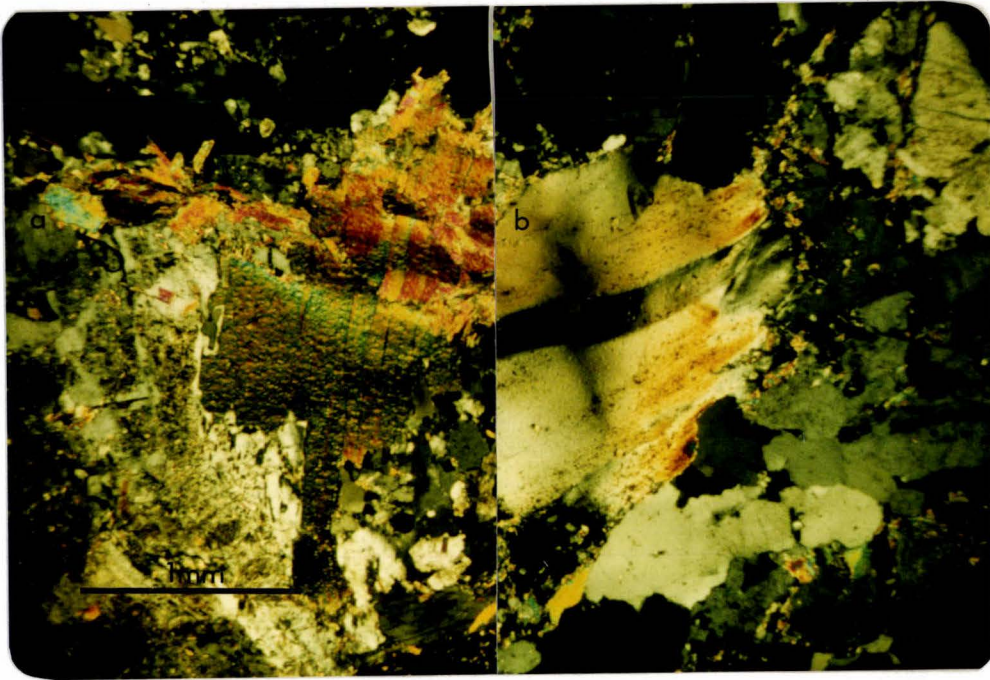
Fig. 3-10a and b: Bent cleavage planes in coarse muscovite and
                    strained quartz features in 18987.   Biotite-
                    granite, Bald Hill Granite (XP).
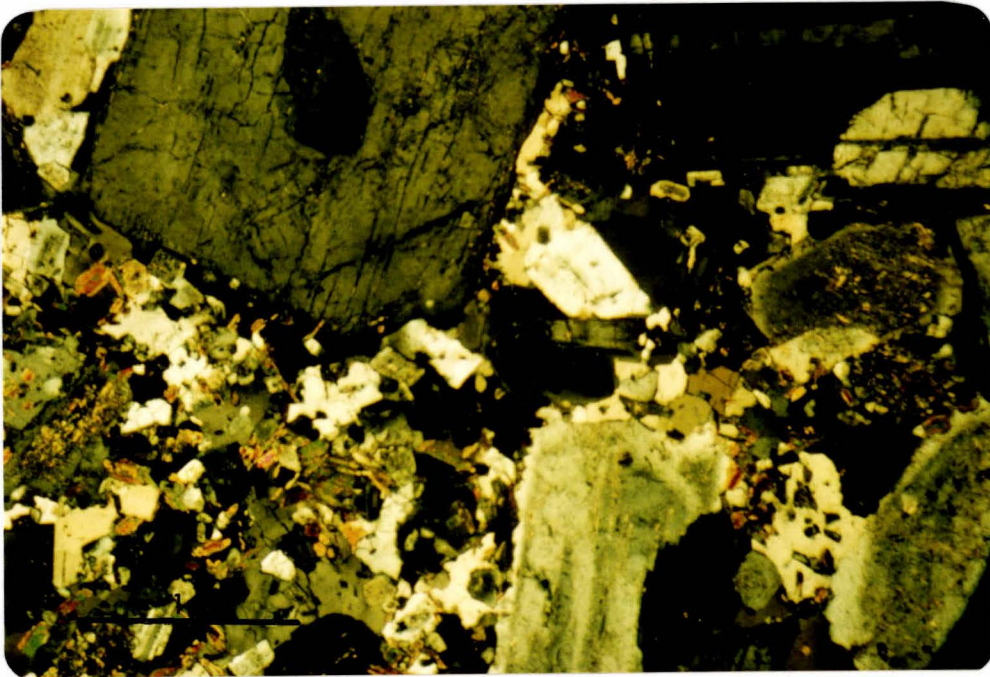
Fig. 3-11:   Zoned oligoclase phenocrysts in finer quartz, feldspar
             and biotite groundmass, 18960.   Quartz trondhjemite
             porphyry.   Lyell Porphyry (XP).

processes which have strained and weakly foliated the alkali granites. There are distinct mineralogical, compositional and textural variations between stocks. Composition ranges from granitic to gabbroic with textural changes from porphyritic quartz trondhjemite, hypidiomorphic granodiorites and quartz diorites, near subvolcanic-trachytic textures of the lamprophyre dykes to doleritic-gabbroic textures in the most basic rocks (ie: gabbroporphyry).

Quartz trondhjemite porphyry

Porphyritic quartz bearing trondhjemites have large subhedral (2-6 mm) plagioclase phenocrysts in a finer grained granular groundmass of quartz, feldspars and ferromagnesium minerals. The trondhjemite is distinguished from other Lyell Porphyry rocks by its high proportion of quartz (up to 40%), lack of potash feldspars, content of up to 45% oligoclase, and absence of pyroxenes or amphibole mineral phases. Oligoclase phenocrysts ($2V_\gamma$ 85°, An_{12-24}) with albitic twinning are complexly zoned (Fig. 3-11). The groundmass contains fresh quartz, normally zoned oligoclase and pleochroic biotites (α light tan, β brown orange, γ dark brown). Biotites often contain well developed, needle-like inclusions of rutile(?) (Fig. 3-12). Minor muscovite, prismatic apatite, opaque euhedral sulphide minerals (pyrite magnetite) are present with accessory calcite associated with the pyrite. The quartz trondhjemites are generally fresh and show little, if any, alteration of feldspars and ferromagnesium minerals. However, one highly altered sample (18842) shows complete
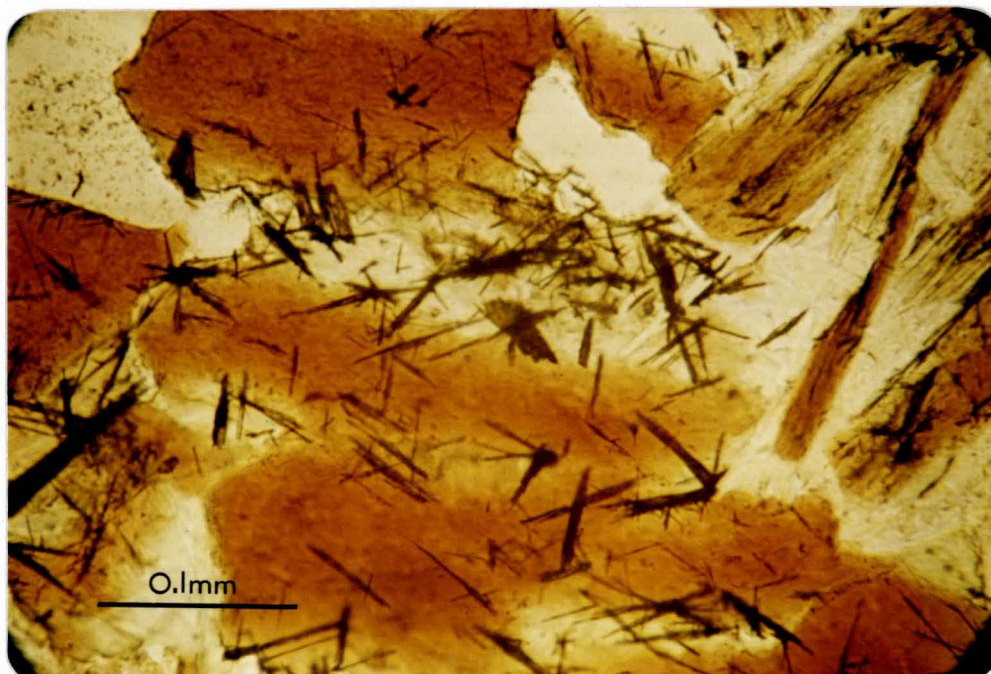
Fig. 3-12: Photomicrograph of biotites in 18840 with needle-like inclusions of rutile(?) (PL).
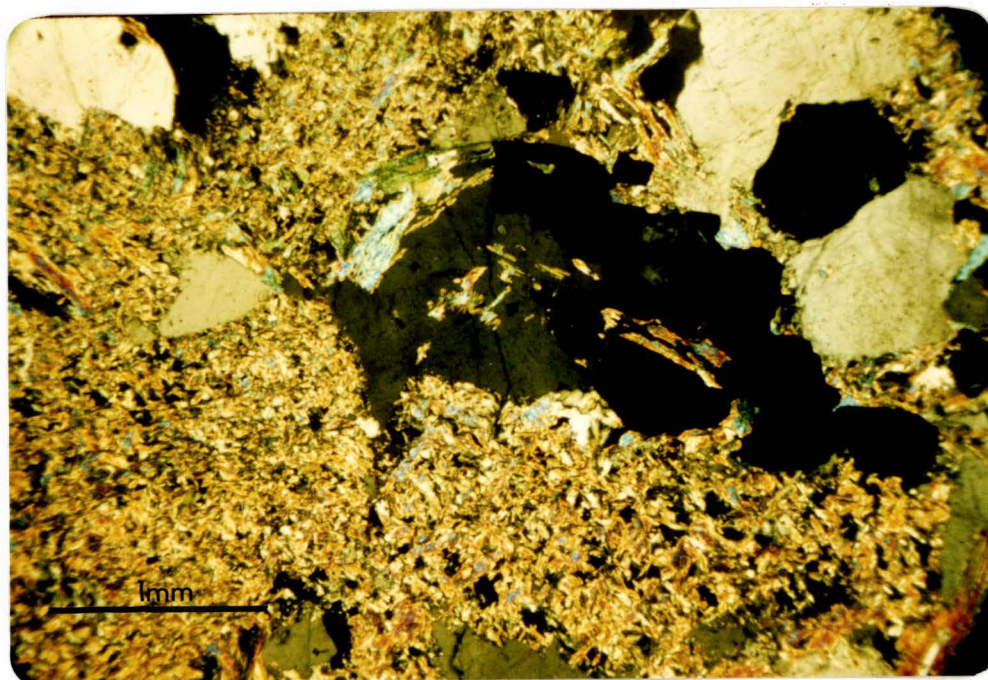
Fig. 3-13: Quartz trondhjemite showing complete replacement of plagioclase and biotite minerals to a quartz-sericite-pyrite assemblage, 18842. Altered Lyell Porphyry (XP).

alteration and replacement of feldspars and biotite minerals
to a quartz-sericite-pyrite assemblage (Fig. 3-13).

Granodiorite

The granodiorites are medium grained (<1-2 mm) rocks
with a hypidiomorphic-granular texture (Fig. 3-14). However
occasional zoned plagioclases are slightly coarser grained
(up to 4 mm), producing a weakly porphyritic texture in some
rocks. The rock is composed of quartz, orthoclase, microcline,
calcic oligoclase, and biotite with accessory pyroxenes,
apatite, zircons and opaque sulphide minerals. The grano-
diorites have less quartz (up to 28%), and more potash-bearing
feldspars than the trondhjemites. Microcline, which composes
3-5% of the rocks, is usually intergranular and occasionally
perthitic. Subhedral oligoclase ($2V_\gamma$ 80°, An_{20-30}) tends to
be slightly more calcic than the oligoclase in the more acid
trondhjemites. Pleochroic biotite (α pale tan-grey,
β greenish-grey-brown, γ dark olive green-grey) often shows
alteration to pale green chlorite. Pale green pyroxene,
possibly hypersthene(?) ($2V_\gamma$ 85°, weakly pleochroic mineral)
is present as a fine, anhedral-granular mineral in close
association with other ferromagnesium phases. Fine grained
opaque minerals occur as inclusions in biotite crystals and
larger euhedral, cubic crystals (pyrite). Prismatic apatite
forms inclusions in plagioclase feldspars and biotites. A
rare, brown, weakly pleochroic mineral with high relief and
straight extinction is probably zircon.
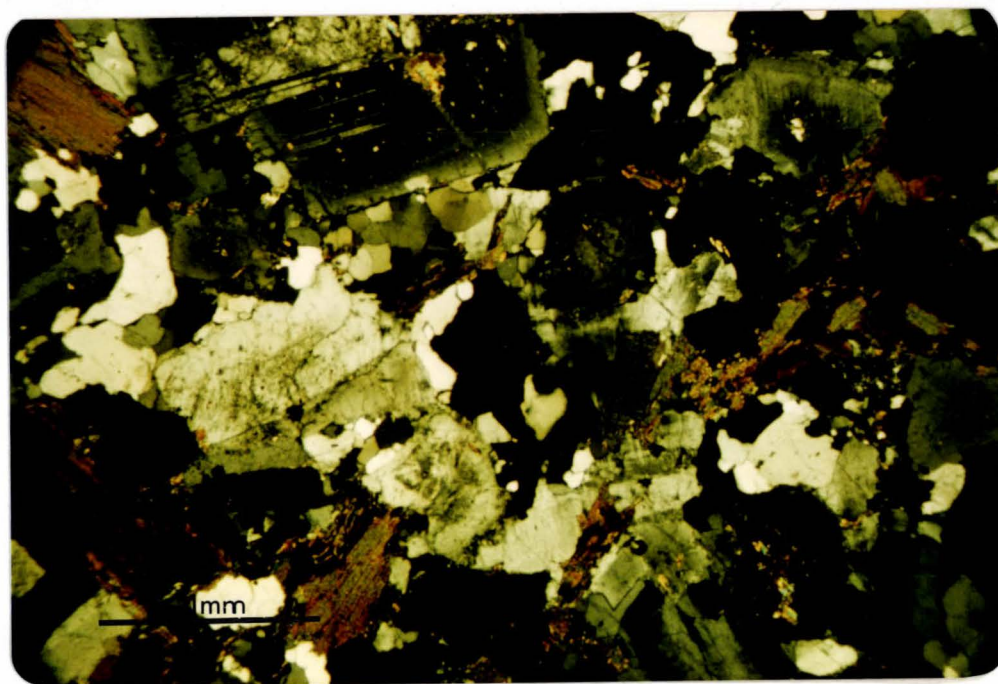
Fig. 3-14:   Zoned oligoclase and tabular greenish biotite in
             18963.   Granodiorite, Lyell Porphyry (XP).
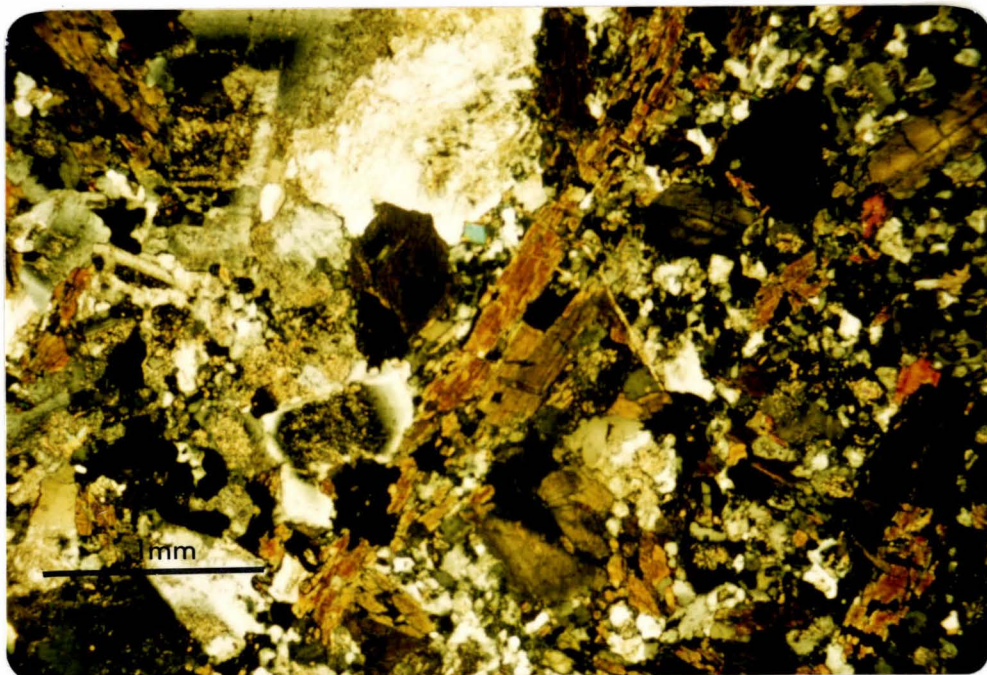
Fig. 3-15:   Zoned andesine plagioclase, brown hornblende and
             opaque minerals in 18980.   Quartz diorite, Lyell
             Porphyry (XP).

Quartz diorite

Medium grained diorites have hypidiomorphic-granular textures and are composed of quartz, andesine, brown biotite, sodic amphiboles, minor hypersthene with accessory apatite, sphene, calcite and opaque sulphide minerals (Fig. 3-15). The plagioclase composition, presence of minor pyroxene (up to 5%) and greater abundance of amphiboles (up to 20%) distinguish the quartz diorites from the more acidic trondhjemites and granodiorites, and the more basic olivine bearing lamprophyre and gabbroic rocks. Subhedral andesine ($2V_\gamma$ 80°, An_{34-44}) crystals are normally zoned and generally larger than surrounding quartz and ferromagnesium minerals. Hornblende is strongly pleochroic ($2V_\gamma$ 80°, α deep greenish-blue, β bluish green, γ yellow-green: riebeckite ?). Brown-green biotite is occasionally pseudomorphed by, and altered to, pale green chlorite. Pale green fine subhedral pyroxene (hypersthene ?) is closely associated with other ferromagnesium and opaque minerals. Accessory prismatic apatite, euhedral opaques (modally up to 4%) and rare sphene(?) are present.

Lamprophyre dykes

These dyke rocks have a strongly porphyritic texture with relict olivine, pyroxene and feldspar phenocrysts (up to 5 mm) in a finer-grained trachytic groundmass. The groundmass is composed of lathe-like plagioclases with very fine granular, high relief olivine, and probably pyroxene (augite ?), quartz, amphiboles and opaque sulphide minerals.
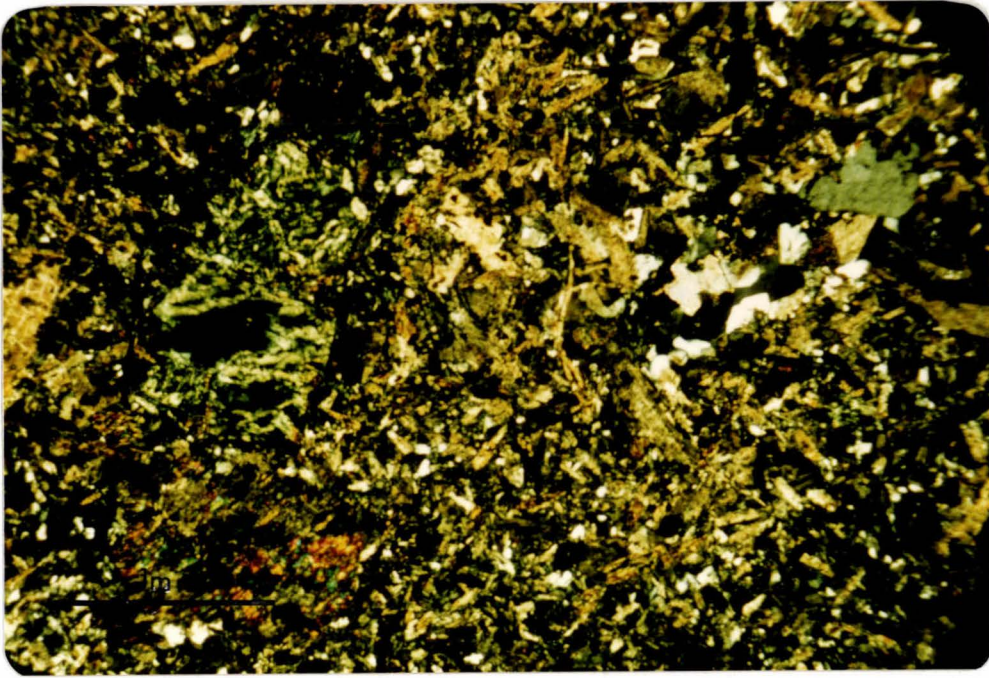
Fig. 3-16: Metasomatically replaced phenocrysts in finer,
            trachytic groundmass in 18929. Lamprophyre dyke
            rock, Lyell Porphyry (XP).
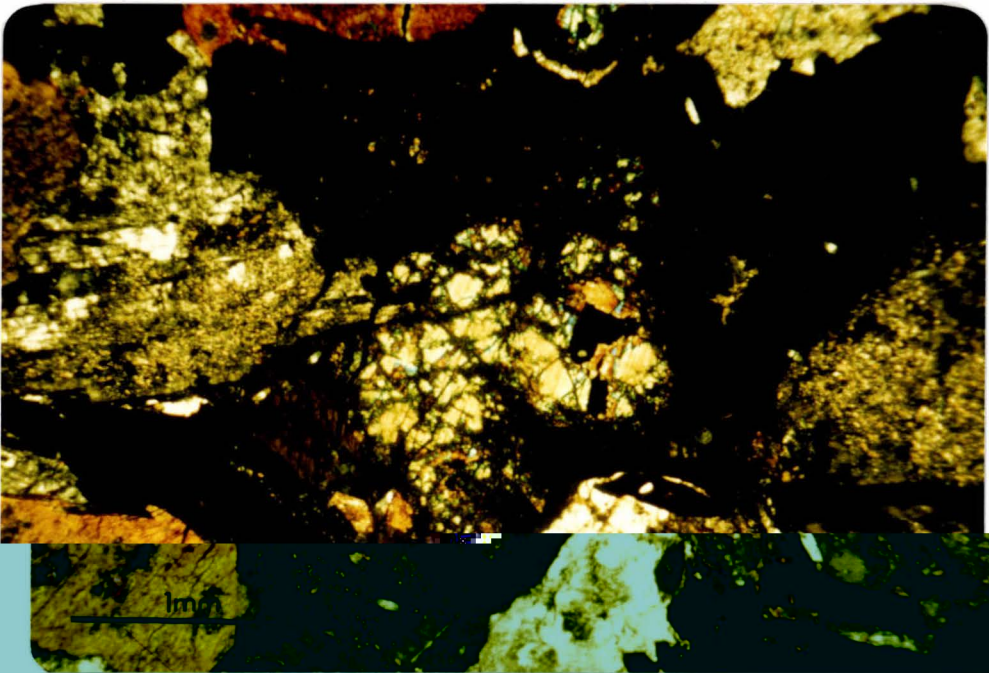
Fig. 3-17: Olivines and clinopyroxenes being replaced by
            secondary amphiboles, quartz and opaque minerals
            in 18908. Gabbroporphyry, Lyell Porphyry (XP).

Considerable metasomatic alteration has occurred in these lamprophyres. Plagioclases are, mainly, zoned calcic labradorites (An_{62-72}) with possible minor bytownite occurring in the finer groundmass. Plagioclases compose up to 60% of the mode. Olivine phenocrysts are usually pseudomorphed by serpentine alteration showing characteristic mesh structure (Fig. 3-16). Pyroxenes ($2V_\gamma$ 65°, wavy extinction, augite ?) have, in turn, been replaced by pale green uralitic tremolite ($2V_\gamma$ 80°, high birefringence, 10° extinction) along crystal margins and cracks or joints. Abundant chlorite is closely associated with the serpentine and amphibole alteration minerals. Calcite, needle-like apatite and abundant opaque sulphide minerals form accessories.

Gabbroporphyry

The most mafic rocks, the gabbroic rocks, have a coarse doleritic-gabbroic texture being originally composed of coarse grained plagioclases and clinopyroxenes with minor olivine. However, metasomatic alteration has produced abundant secondary amphiboles, quartz, chlorite and sulphide minerals (Fig. 3-17). The plagioclases (labradorite, $2V_\gamma$ 70°, An_{58-66}) are zoned with albite twins and are usually highly sericitic. Remnant pyroxene cores ($2V_\gamma$ 60°, oblique extinction) are pseudomorphed by pale green uralitic amphiboles ($2V_\gamma$ 80°, tremolite-actinolite ?) and chlorite alteration, often completely replacing the clinopyroxenes. Olivines occur as fine granular remnants, often being completely pseudomorphed by
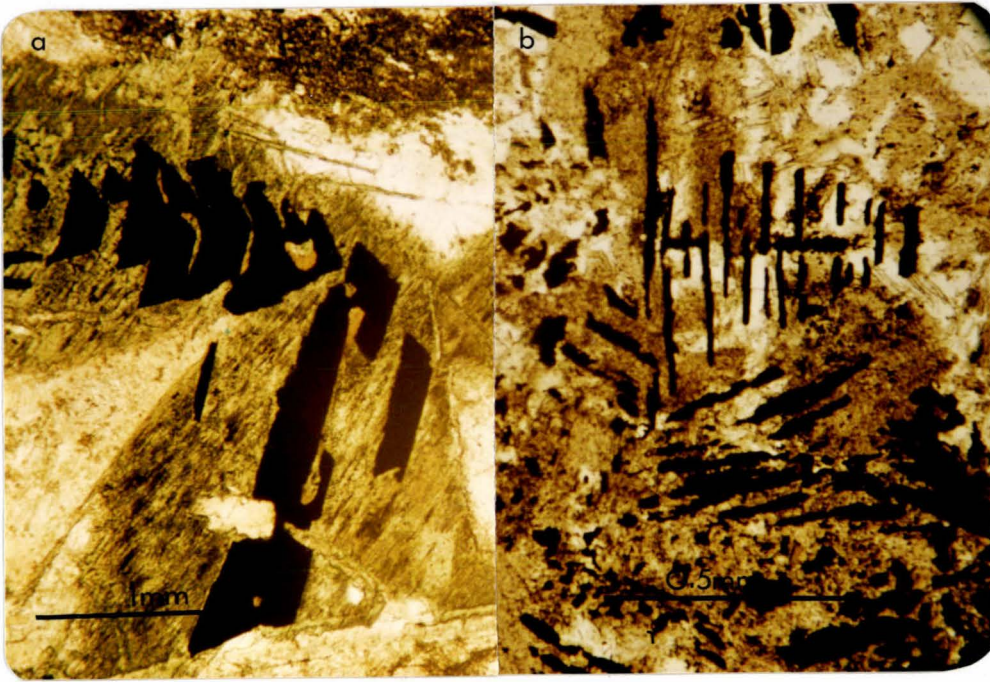
Fig. 3-18a and b: Photomicrographs of sulphide replacement
textures in the gabbroporphyry (a, 18908; b, 18812).

serpentine, micas and chlorite. Abundant euhedral cubic

and needle-like opaque minerals (ilmenite, magnetite and

rutile, see chapter 5) are present. The opaque minerals

have exsolved and replaced pyroxene minerals during

alteration to produce unusual replacement textures

(dendritic ?) (Fig. 3-18a and b). Opaque minerals have

an average grain size of about 1 mm and make up to 15% of

the mode. Accessory needle-like apatite (up to 1 mm) and

secondary anhedral quartz occur throughout the gabbroic

rocks.

CHAPTER FOUR

GEOCHEMISTRY

Introduction:

Major and trace element analyses were determined for Greenland Group metasediments, biotite-hornfels, silicified breccia, Bald Hill Granites and the Lyell Porphyry suite of rocks. CIPW norms were calculated for the Bald Hill and Lyell Porphyry granites. All previously published and unpublished major element analyses available for molybdenum-bearing intrusive granitic rocks and 'Karamea phase' granites in West Nelson are given for comparison and CIPW norms calculated.

Major and trace element analyses of rocks were determined by X-Ray Fluorescence spectrometry (XRF). The methods used, machine settings, accuracy and precision for the data are given in Appendix III.

Bulk chemistry of the siliceous Greenland greywackes and argillites shows a transition from regionally metamorphosed metasediments through thermal hornfels zone I, biotite-hornfels zone II, to silicified hornfels zone III. Greywackes can be distinguished from argillites by major element variation plots.

The Bald Hill Granites and the Lyell Porphyry granitic rocks are shown by major and trace element data to belong to separate petrogenic provinces. The Bald Hill Granites are peraluminous potash-rich gneissic granites of sedimentary origin, the Lyell Porphyry being a consanguinous series of soda-rich calc-alkaline granitic rocks of igneous origin.

Greenland Group metasediments, or geochemically similar
sedimentary material, are considered as possible source
rocks for the 'Karamea batholith' granites in West Nelson,
the molybdenum bearing calc-alkaline minor intrusives being
generated at greater depths, intruding the overlying granites
and sedimentary material.

In the following discussion of geochemistry, each of
the rock suites is treated in turn and a possible model
for the petrogenesis of the granites discussed.

Greenland Group Metasediments:

Major and trace element chemistry of representative
metasediments of the Greenland Group are given in Table 4-1.
Analyses of zone I and zone II of the hornfelsed sediments
and the silicified sediments of zone III are given in
Tables 4-2, 4-3 and 4-4 respectively. Averages are listed
in Table 4-5.

The metasediments in the Bald Hill area were examined
to:

1) Compare their geochemical characteristics with published
   data for Greenland Group metasediments (Nathan, 1972).

2) Compare the chemistry of these Ordovician metasediments
   with the other Ordovician metasedimentary sequences in
   West Nelson area and Southeastern Australia which are
   associated with molybdenum bearing granitic intrusives.

3) Outline geochemical changes that took place in these
   metasediments during hydrothermal alteration and mineral-
   ization accompanying the emplacement of the granitic
   intrusive rocks.

Table 4-1: Major and trace element analyses of the Greenland Group metagreywackes and argillites

	18885	18886	18887	18887/2	18888	18888/2	18890	18893	18907	18915	18918	18922
Type*	G	A	G	G	G	G	G	G	A	A	G	G
SiO_2	71.53	62.20	78.36	77.98	73.66	72.91	77.06	74.06	61.05	67.01	74.72	72.53
TiO_2	0.71	0.74	0.61	0.61	0.59	0.58	0.52	0.67	0.81	0.74	0.85	0.67
Al_2O_3	13.81	17.70	9.12	9.03	11.76	11.69	10.11	12.13	18.08	14.61	11.78	12.27
Fe_2O_3	1.17	0.87	0.32	0.24	0.38	0.35	0.00	0.49	0.19	0.32	0.10	0.19
FeO	3.60	5.40	2.88	2.88	3.52	3.52	3.08	3.56	6.12	5.12	3.48	4.08
MnO	0.04	0.07	0.02	0.01	0.03	0.03	0.03	0.03	0.04	0.04	0.01	0.04
MgO	2.20	3.38	1.52	1.49	2.06	2.03	1.66	2.06	3.58	2.84	1.97	2.20
CaO	0.26	0.30	0.42	0.43	0.45	0.46	0.21	0.31	0.22	0.21	0.46	0.28
Na_2O	1.16	1.49	1.26	1.24	2.07	2.02	1.54	1.58	1.30	1.47	1.32	1.60
K_2O	2.93	4.37	1.79	1.76	2.13	2.13	1.95	2.52	4.38	3.20	2.64	2.43
P_2O_5	0.19	0.16	0.15	0.16	0.13	0.13	0.14	0.18	0.17	0.15	0.26	0.19
L.O.I.[†]	2.75	3.60	2.08	2.08	2.36	2.36	1.85	2.20	3.60	3.19	1.77	2.36
Total	99.71	100.28	98.52	98.10	99.14	98.22	99.31	99.80	99.55	98.90	99.36	98.84
Fe_2O_3[1]	5.17	6.87	3.52	3.44	4.29	4.26	2.41	4.45	7.00	6.01	3.97	4.72
Ba	413	704	377		332		381		681			
Cu	11	29	15		15		16		27			
Ni	30	44	22		28		28		44			
Zn	242	110	57		78		72		105			
Pb	9	73	3		13		13		9			
Mo	4	1	2		2		2		1			
S	636	118	118		190		104		142			
Sr	37	21	58		69		65		23			
Rb	126	205	78		103		116		213			
Zr	230	124	351		131		265		142			
Th	14	16	11		11		14		19			
Y	34	32	26		40		32		41			
K/Rb	193	177	190		172		180		171			

* G: greywacke, A: argillite

† Loss on ignition

1 Total iron expressed as Fe_2O_3

Table 4-1: continued

	18925	18926	18926/2	18927	18927/2	18928	18942	18947	18949	18979	18991	18991/2
Type*	G	G	G	A	A	G	G	A	A	A	G	G
SiO_2	73.16	71.82	72.09	64.03	64.30	73.50	75.15	58.43	65.47	57.26	76.48	77.96
TiO_2	0.71	0.69	0.69	0.75	0.77	0.65	0.64	0.71	0.77	0.72	0.56	0.56
Al_2O_3	12.19	12.50	12.41	16.35	16.48	11.21	11.72	19.49	15.45	20.19	10.26	10.43
Fe_2O_3	0.00	0.12	0.18	1.34	1.08	0.80	0.72	1.16	0.93	0.92	0.00	0.00
FeO	4.32	4.08	4.08	4.76	4.76	3.16	3.04	5.52	4.60	5.72	3.48	3.48
MnO	0.04	0.04	0.03	0.04	0.04	0.04	0.01	0.06	0.06	0.06	0.03	0.02
MgO	2.13	2.19	2.17	3.23	3.23	1.88	2.09	3.73	2.87	3.67	1.83	1.81
CaO	0.32	0.28	0.29	0.23	0.26	0.28	0.24	0.20	0.20	0.27	0.30	0.30
Na_2O	1.66	1.61	1.62	1.52	1.58	1.62	1.34	1.05	2.13	1.66	1.31	1.30
K_2O	2.39	2.50	2.49	3.82	3.78	2.25	2.84	5.16	3.41	5.08	2.19	2.24
P_2O_5	0.22	0.19	0.18	0.14	0.15	0.18	0.16	0.12	0.20	0.11	0.14	0.15
L.O.I.[†]	2.40	2.29	2.29	3.03	3.03	2.01	1.19	3.58	2.41	3.26	2.01	2.01
Total	99.54	98.32	98.51	99.29	99.46	97.55	99.86	99.21	99.30	98.92	98.59	100.25
Fe_2O_3[1]	4.50	4.65	4.71	6.63	6.35	4.31	4.10	7.29	6.04	7.28	3.71	3.70
Ba		391		593		374		741				
Cu		22		29		25		29				
Ni		24		41		27		45				
Zn		77		113		73		130				
Pb		11		10		4		22				
Mo		2		-		3		-				
S		187		81		327		127				
Sr		41		33		38		35				
Rb		113		182		95		268				
Zr		247		125		251		93				
Th		16		14		14		17				
Y		34		32		28		35				
K/Rb		184		174		197		159				

* G: greywacke, A: argillite

† Loss on ignition

1 Total iron expressed as Fe_2O_3

Table 4-2: Major and trace element analyses of zone I hornfelsed
            metasediments

	18895	18897	18897/2	18916	18916/2	18919	18920	18952	18982	18982/2
Type*	A	G	G	G	G	A	G	A	G	G
SiO_2	64.10	75.07	75.35	71.84	72.17	59.68	70.90	57.56	72.18	72.68
TiO_2	0.83	0.64	0.64	0.73	0.73	0.73	0.70	0.77	0.80	0.70
Al_2O_3	16.54	11.55	11.74	12.89	12.98	19.18	12.83	20.20	12.57	12.68
Fe_2O_3	1.12	1.26	1.32	0.59	0.51	1.26	1.37	1.65	0.00	0.00
FeO	4.36	2.27	2.27	3.80	3.80	5.40	3.48	5.04	4.00	4.00
MnO	0.02	0.03	0.03	0.03	0.03	0.05	0.02	0.04	0.04	0.03
MgO	3.22	2.00	2.06	2.41	2.31	3.40	1.88	3.96	2.14	2.22
CaO	0.39	0.29	0.29	0.28	0.28	0.23	0.26	0.12	0.41	0.45
Na_2O	1.35	1.79	1.56	1.08	0.90	0.87	0.88	0.81	2.14	1.39
K_2O	4.51	2.72	2.74	3.18	2.64	5.22	3.35	5.69	3.17	3.07
P_2O_5	0.19	0.19	0.19	0.20	0.19	0.12	0.20	0.12	0.19	0.19
L.O.I.[†]	2.90	2.10	2.10	2.28	2.28	2.69	3.32	3.61	1.92	1.92
Total	99.54	99.92	100.29	99.31	99.35	98.84	99.20	99.57	99.45	99.33
Fe_2O_3[1]	5.96	3.78	3.82	4.70	4.73	7.26	5.24	7.25	4.41	4.43
Ba	582	353		477		757	480	900	451	
Cu	44	44		13		29	28	46	17	
Ni	28	24		25		47	24	27	29	
Zn	53	38		62		135	40	114	55	
Pb	11	12		9		17	10	34	6	
Mo	6	6		10		–	1	–	–	
S	2140	787		121		397	8000	490	236	
Sr	59	28		28		61	34	27	45	
Rb	220	126		145		278	163	287	149	
Zr	193	236		283		96	230	96	223	
Th	14	12		16		21	17	15	15	
Y	48	41		42		37	47	39	40	
K/Rb	170	179		182		156	171	164	177	

* G: greywacke, A: argillite

† Loss on ignition

1 Total iron expressed as Fe_2O_3

Table 4-3: Major and trace element analyses of biotite-hornfels metasediments (zone II)

	18896	18896/2	18903	18931	18931/2	18939	18978	18984
Type*	A	A	A	A	A	A	A	A
SiO_2	68.76	68.66	66.03	57.71	58.57	56.03	60.00	69.43
TiO_2	0.79	0.78	0.70	0.77	0.80	0.75	0.79	0.66
Al_2O_3	15.19	15.25	16.11	20.41	20.74	19.98	18.92	15.20
Fe_2O_3	1.46	1.44	1.48	2.78	2.66	2.65	2.04	2.12
FeO	3.48	3.48	3.48	3.32	3.32	4.60	3.80	3.20
MnO	0.02	0.04	0.04	0.04	0.04	0.05	0.05	0.03
MgO	2.51	2.59	2.91	3.83	3.77	3.57	3.34	2.65
CaO	0.26	0.26	0.28	0.38	0.41	0.26	0.10	0.29
Na_2O	0.96	1.41	0.79	2.27	1.92	1.34	0.78	1.15
K_2O	4.24	4.19	4.61	6.10	6.21	5.23	4.93	4.38
P_2O_5	0.17	0.16	0.12	0.13	0.14	0.12	0.13	0.12
L.O.I.[†]	3.06	3.06	2.40	3.21	3.21	4.12	4.11	3.12
Total	100.90	101.31	98.96	100.96	101.77	98.69	98.87	102.26
Fe_2O_3 [1]	5.33	5.31	5.35	6.47	6.35	7.76	5.97	5.67
Ba	551		793	909		843	782	689
Cu	46		106	112		158	27	75
Ni	27		34	32		35	24	25
Zn	44		36	48		68	113	38
Pb	15		9	8		10	24	8
Mo	5		2	4		1	-	957
S	2390		1670	6330		6240	92	8100
Sr	38		37	55		45	21	32
Rb	168		186	237		212	248	169
Zr	206		103	96		85	106	100
Th	15		14	18		15	19	13
Y	33		22	18		35	23	27
K/Rb	209		206	214		205	165	215

* G: greywacke, A: argillite

† Loss on ignition

1 Total iron expressed as Fe_2O_3

Table 4-4: Major and trace element analyses of silicified metasediments (zone III)

	18894	18905	18905/2	18906	18932	18945	18976
SiO_2	72.79	76.30	76.28	72.77	80.16	79.54	75.76
TiO_2	0.79	0.75	0.74	0.67	0.27	0.62	0.58
Al_2O_3	14.19	10.81	10.96	12.09	8.53	9.15	11.07
Fe_2O_3	3.04	2.95	2.90	4.21	2.00	2.21	3.30
FeO	0.88	0.64	0.64	1.24	0.56	1.12	1.12
MnO	0.00	0.01	0.01	0.00	0.00	0.00	0.00
MgO	1.32	1.10	1.22	1.21	0.42	0.86	1.29
CaO	0.02	0.04	0.04	0.11	0.64	0.02	0.19
Na_2O	0.07	0.48	0.23	0.99	1.15	0.11	0.71
K_2O	4.73	3.50	3.48	3.12	1.99	3.08	3.41
P_2O_5	0.06	0.07	0.07	0.17	0.07	0.06	0.13
L.O.I.[†]	2.95	2.92	2.92	3.49	2.48	2.37	3.23
Total	100.83	99.58	99.49	100.08	98.24	99.15	100.80
Fe_2O_3[1]	4.01	3.66	3.61	5.58	2.26	3.45	4.54
Ba	972	551		441	199	495	550
Cu	69	28		40	8	22	1645
Ni	9	15		22	4	6	13
Zn	11	9		27	16	10	42
Pb	0	7		6	2	8	12
Mo	15	2		20	1	11	-
S	4550	8600		4680	6020	4630	12000
Sr	13	9		25	45	4	6
Rb	79	142		195	87	107	121
Zr	216	414		218	51	284	197
Th	15	17		14	3	13	36
Y	17	35		27	4	26	33
K/Rb	497	205		247	190	242	234

† Loss on ignition
1 Total iron expressed as Fe_2O_3

Table 4-5: Representative bulk chemical analyses of hornfels
alteration sequence

	(1)	(2)	(3)	(4)
SiO_2	62.84	60.44	63.59	76.30
TiO_2	0.75	0.78	0.75	0.64
Al_2O_3	17.12	18.64	17.55	10.95
Fe_2O_3	0.87	1.34	2.08	2.88
FeO	5.28	4.93	3.55	0.85
MnO	0.05	0.03	0.04	0.01
MgO	3.33	3.53	3.11	1.02
CaO	0.24	0.25	0.30	0.14
Na_2O	1.40	1.01	1.41	0.50
K_2O	4.11	5.14	4.99	3.32
P_2O_5	0.15	0.14	0.14	0.08
FeO/Fe_2O_3	6.10	3.60	1.70	0.30
Ba	680	746	757	573
Cu	28	40	99	33
Ni	43	34	24	11
Zn	114	100	47	14
Pb	13	21	10	4
Mo	0	2	4	10
S	117	1000	4950	5700
Sr	28	49	42	19
Rb	217	262	194	104
Zr	121	128	118	237
Th	16	16	15	12
Y	35	41	27	22
K/Rb	157	163	213	265

(1) Average Greenland argillite.

(2) Average Zone I argillite.

(3) Average Zone II argillite.

(4) Average Zone III argillite.

Major element variations of the low grade regionally

metamorphosed Greenland Group samples are illustrated in

Fig. 4-1 where weight percent oxides are plotted against

weight percent SiO_2. The diagrams show a clear division

between greywacke and argillite. The range of composition

for greywacke is 71 to 79% SiO_2, <14% Al_2O_3, <6% total iron,

<2.5% MgO and <3% K_2O, whereas, the argillites are less

siliceous (57 to 67% SiO_2) and always contain more alumina,

iron, magnesium and potassium than the greywackes. Al_2O_3,

MgO, total iron and K_2O all show a pronounced linear decrease

with increasing silica content in both greywackes and

argillites. The metasediments contain <1% CaO, and the

ratio of K_2O/Na_2O is invariably >1, being generally higher

in the argillites (K_2O/Na_2O = 3 to 5). The alkali diagram

(Fig. 4-2) shows that there is a clear separation between

older Greenland Group metasediments and the Torlesse

greywackes of Mesozoic age, the Greenland metasediments

being consistently less sodic.

In both molecular alkali-calcium iron (ACF) and

molecular alkali-iron-magnesium (AFM) plots the Greenland

Group rocks (Figs. 4-3a and b) occupy a field quite distinct

from other Torlesse greywackes. On the ACF diagram the samples

plot within the Greenland Group field as defined by Nathan

(1976). The AFM diagram shows the Greenland samples to be

generally higher in magnesium and iron than equivalent

Torlesse facies rocks (probably reflecting the lack of

feldspars and volcanic rock fragments in the Greenland suite).
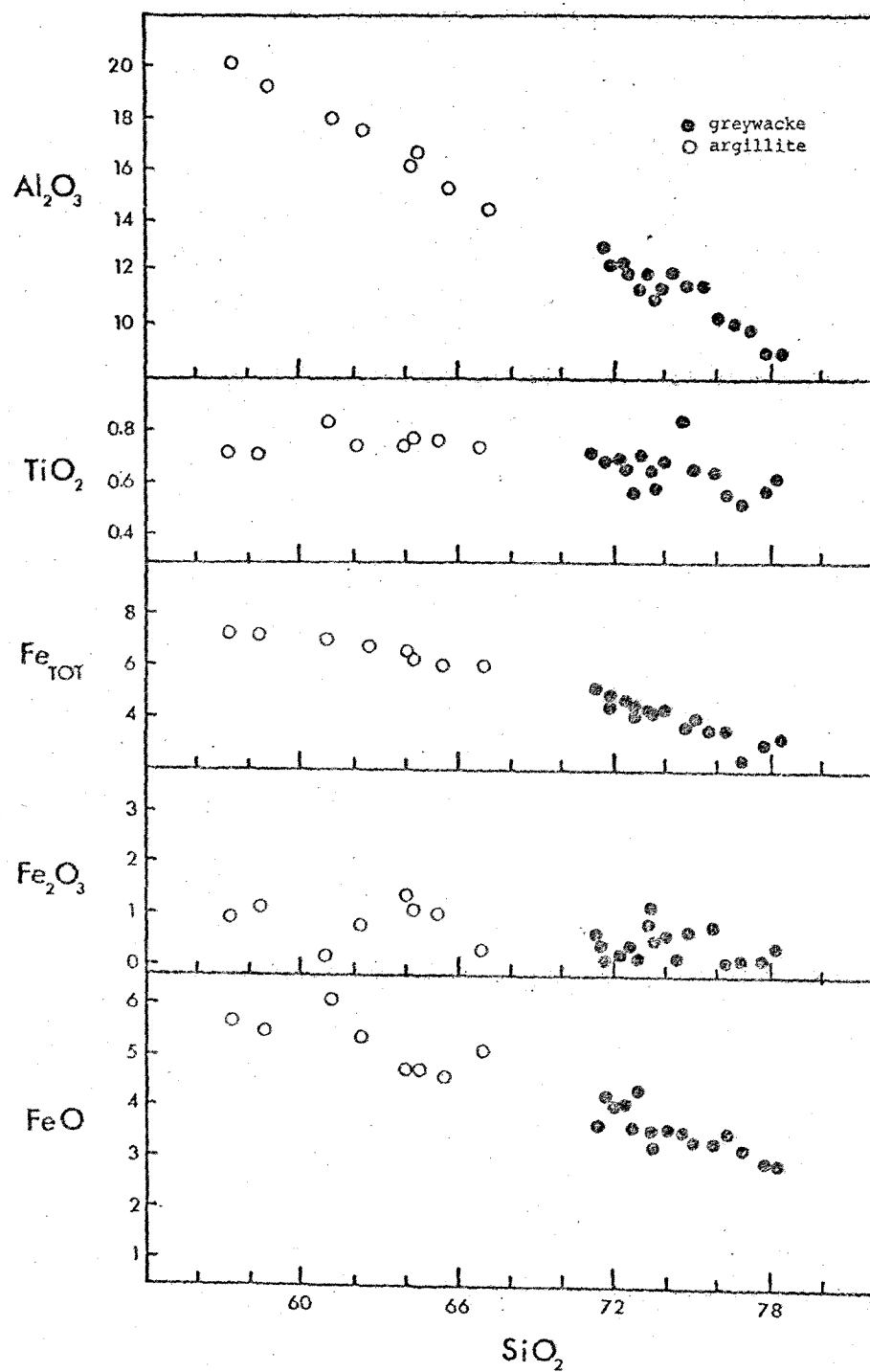
Fig. 4-1: Variation diagrams for the Greenland Group metasediments.
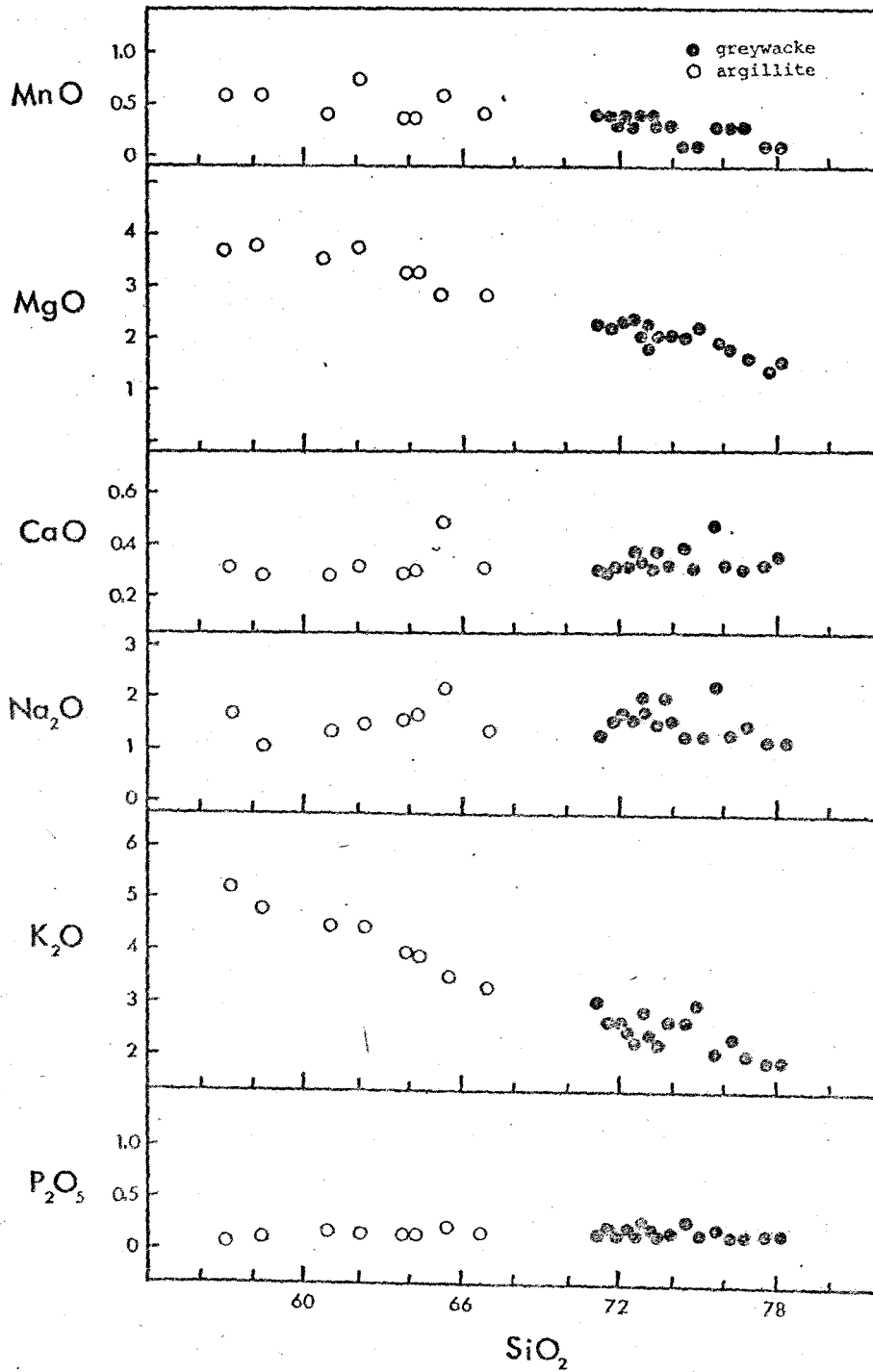
Fig. 4-1:   Variation diagrams for the Greenland Group metasediments.
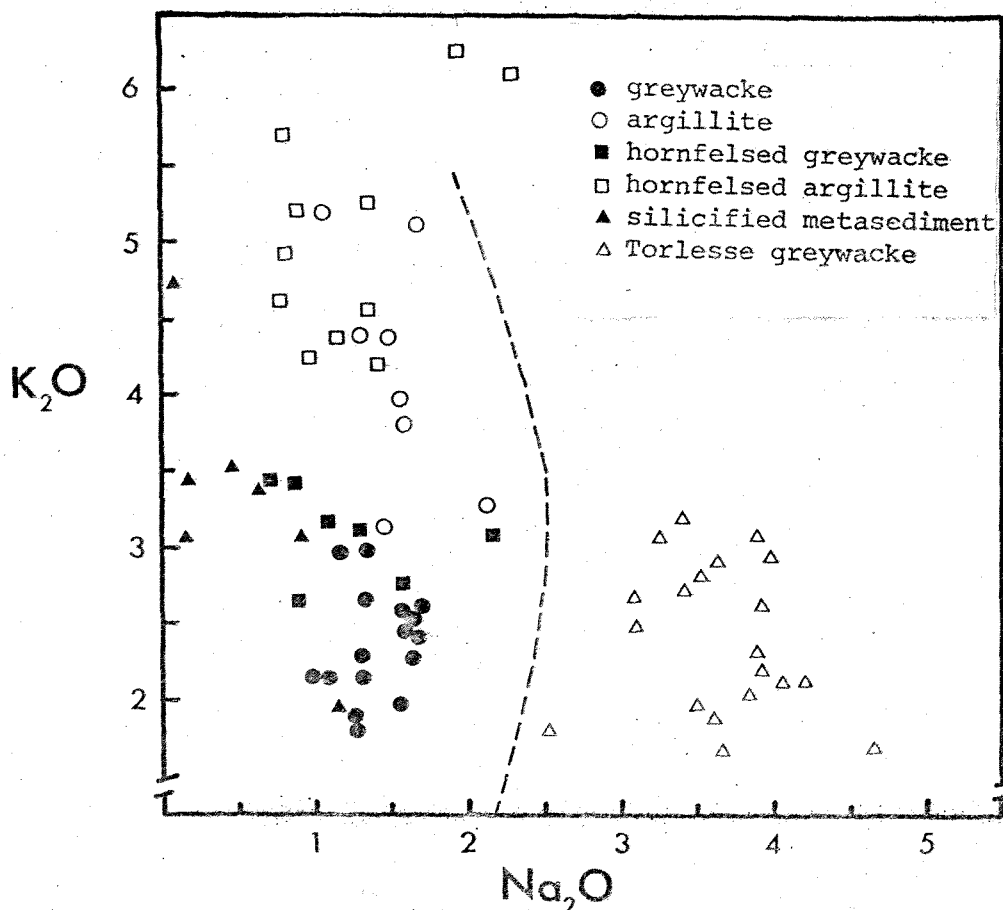
Fig. 4-2:   Alkali diagram (K$_2$O vs. Na$_2$O) for Greenland Group
             metasediments.
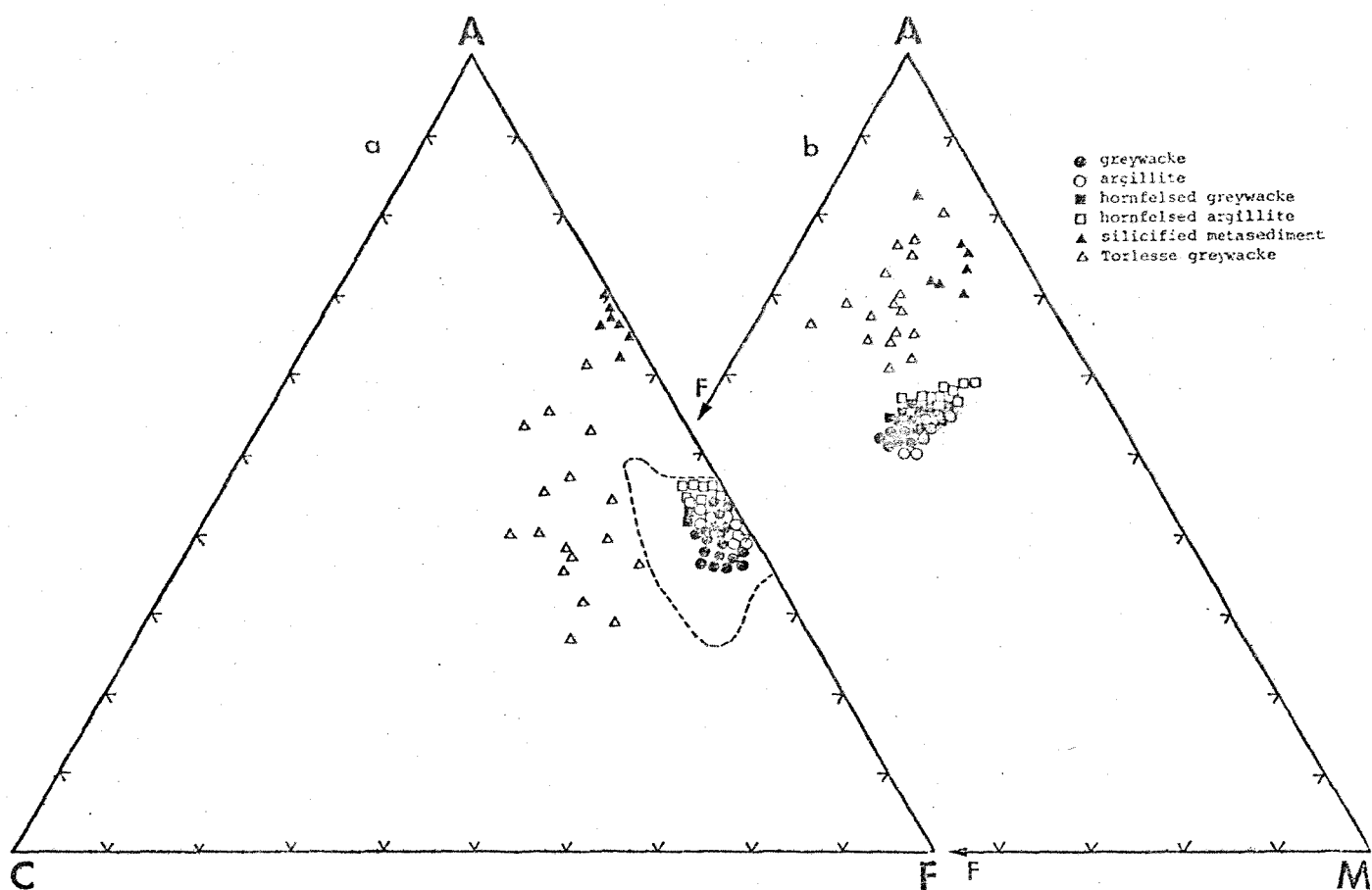
Fig. 4-3a and b: ACF and AFM diagrams for major element analyses
                   of the Greenland Group metasediments.

Major element abundances of rocks from the hornfels zones I and II are not significantly different from the non-hornfelsed sediments and display similar trends on the variation diagrams in Fig. 4-4. The hornfels are slightly enriched in ferric iron, potassium and magnesium oxides and contain less ferrous iron (probably due to weak potassic alteration of the matrix), in general having higher K_2O/Na_2O ratios than equivalent Greenland metasediments (see Fig. 4-2). The hornfels plot within the Greenland Group field on ACF and AFM diagrams (Fig. 4-3).

In the argillites, the FeO/Fe_2O_3 ratios (Fig. 4-5) decline from an average of approximately 6 in the Greenland argillites to 3.6 in hornfels zone I, 1.7 in zone II and 0.3 in zone III. FeO/Fe_2O_3 ratios in the greywackes do not appear to show the same decrease. This is probably due to a lack of matrix in the greywackes, with the result that hydrothermal alteration has had less effect than in the argillites, and the ferric iron content of the greywackes has remained uniformly low.

The more intensely altered, zone III, metasediments show a continuation of major element trends indicated by initial hornfelsing, with potassium, ferric iron and magnesium components increasing while sodium and ferrous iron oxides show corresponding decreases on the variation plot (Fig. 4-4). The high silica content (72 to 80%) and lower soda, magnesia and ferrous iron indicate virtual complete hydrothermal replacement of the original greywacke/
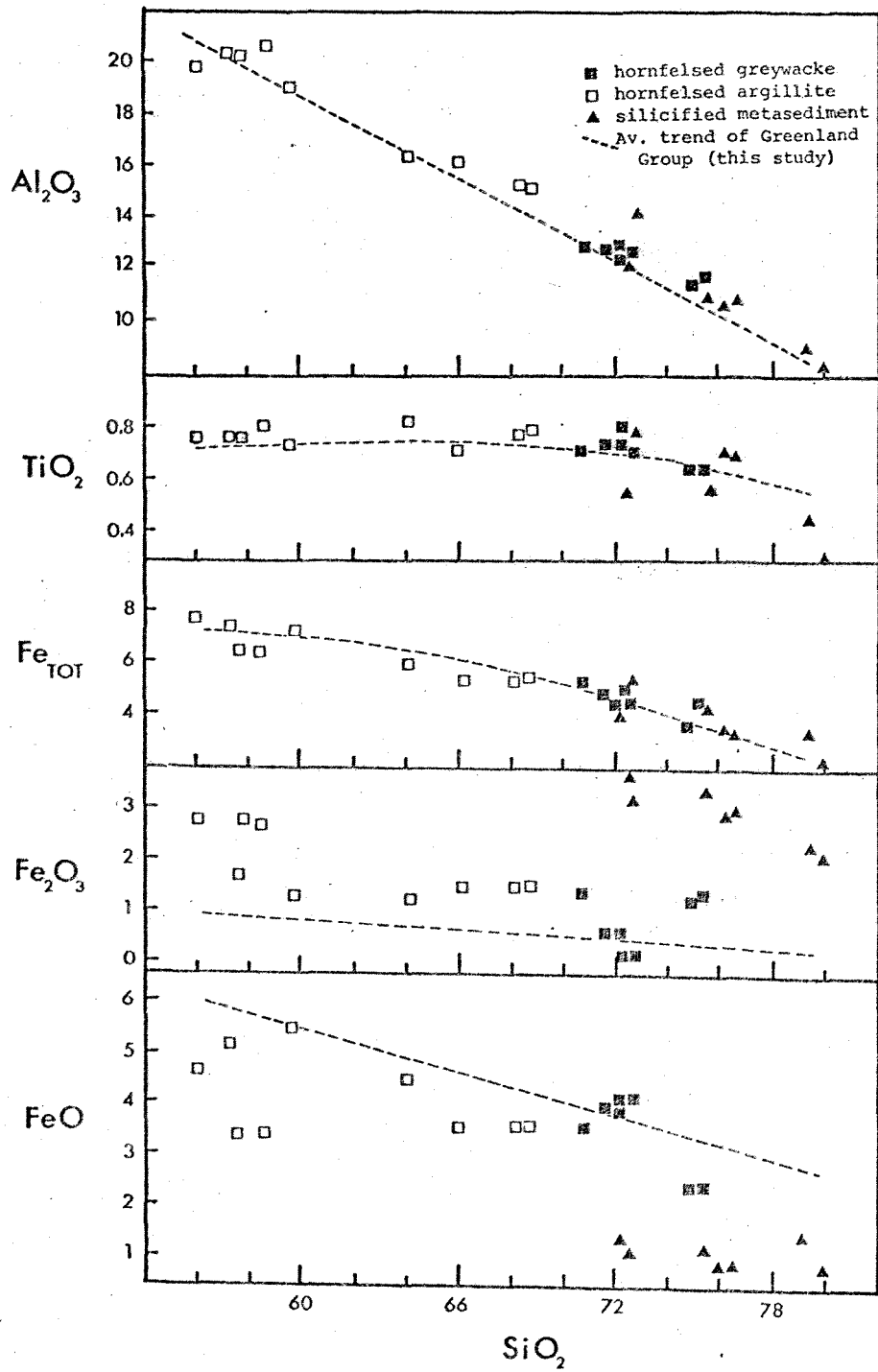
Fig. 4-4: Variation diagrams for analyses of hornfels zones I, II and III.
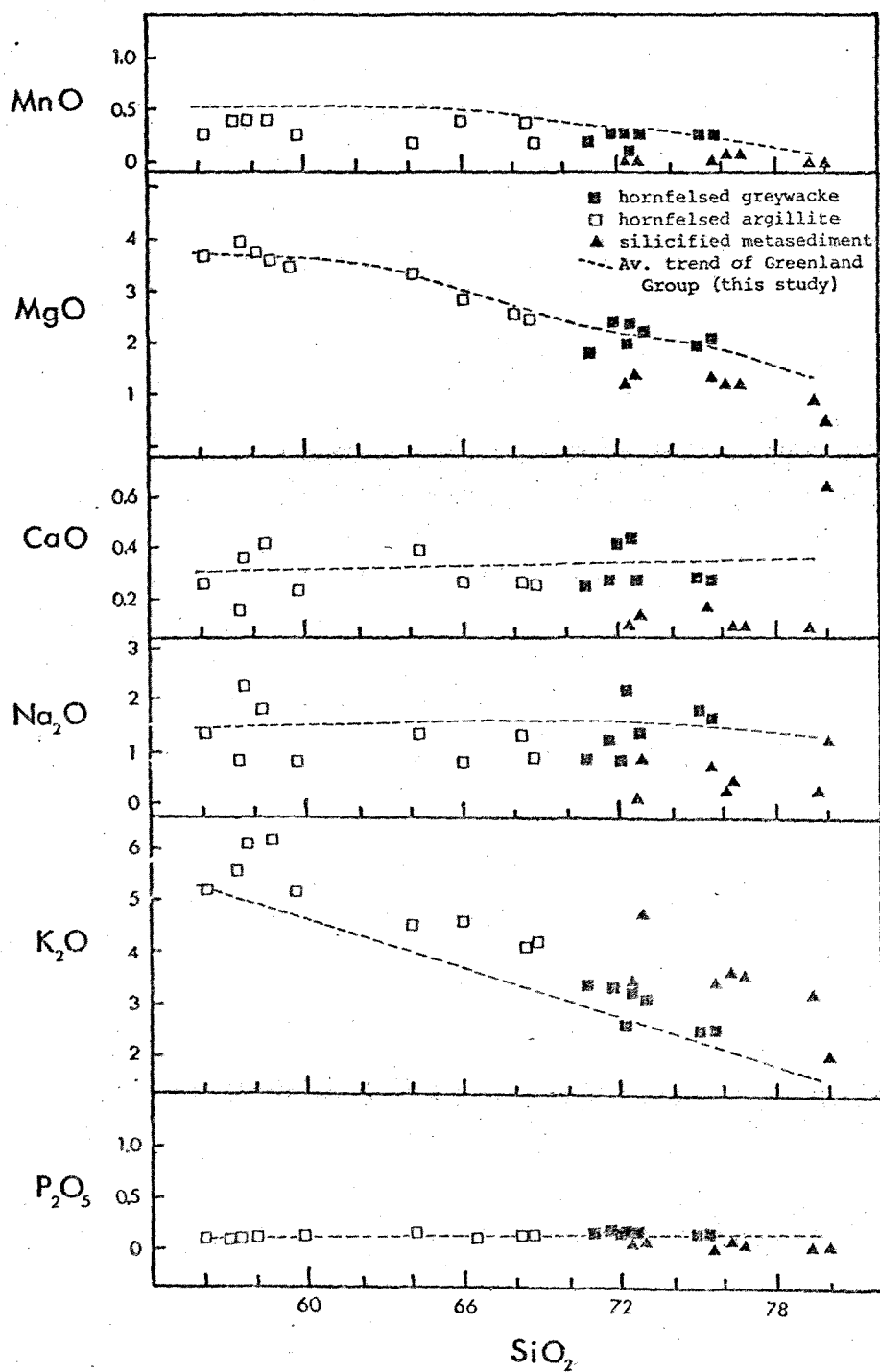
Fig. 4-4: Variation diagrams for analyses of hornfels zones I, II and III.
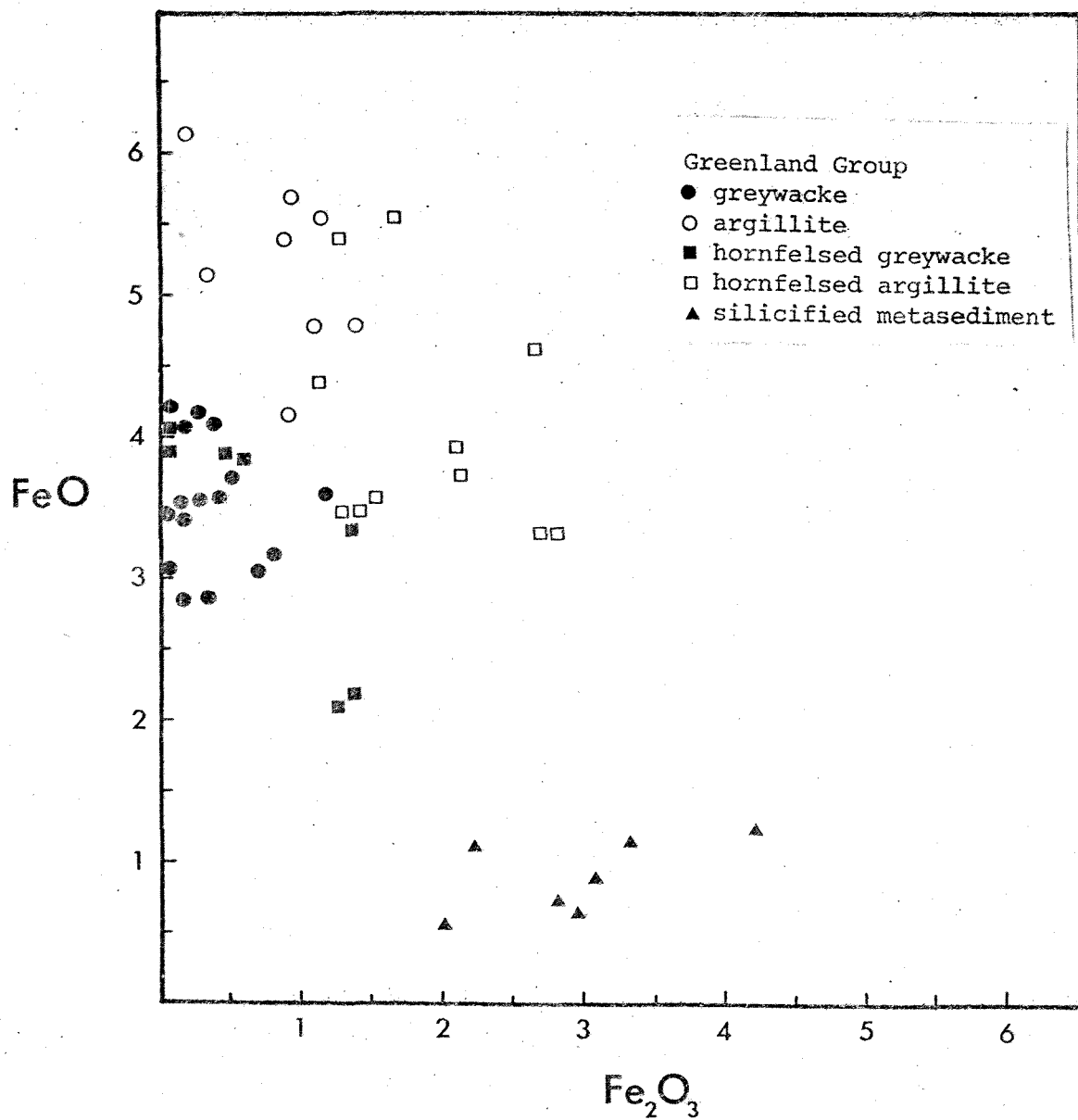
Fig. 4-5: FeO versus Fe_2O_3 plot for argillite alteration
sequence, Bald Hill.

argillite matrix by a quartz-sericite-pyrite assemblage.
Because of this matrix alteration within zone III, the
silicified sediments occupy a significantly different field
on ACF and AFM diagrams (Fig. 4-3).

Trace element values for the Bald Hill suite (Table 4-1)
compare closely to trace element values for other Greenland
rocks published by Nathan, (1976). Barium content from
331 to 412 ppm (Nathan: 347 to 492 ppm) in the greywackes
and 593 to 740 ppm (Nathan: 564 to 930 ppm) in the argillites
indicates that most of the barium is held in the clay matrix.
A similar trend in rubidium values of 40 to 126 ppm in the
greywackes and 125 to 268 ppm in the argillites, low
strontium abundances of 20 to 70 ppm with K/Rb ratios
average of 179 (Greenland Group average of 170, Nathan,
1976) show that the Bald Hill suite also has the distinctive
trace element composition of the Ordovician Greenland suite.
Barium and rubidium show a strong inverse relationship to
silica content (Fig. 4-6) while zirconium shows a systematic
increase with increasing silica content. Other trace
elements do not appear to be directly related to the silica
content of the rocks.

General trends for major and trace element constituents
during hydrothermal alteration of the metasediments can be
more clearly observed from plots of average major and trace
element bulk composition of each zone (Fig. 4-7). Silica
shows a continual enrichment during alteration with a marked
increase into zone III type alteration. Alumina increases
into zone I, and then decreases through the biotite zone
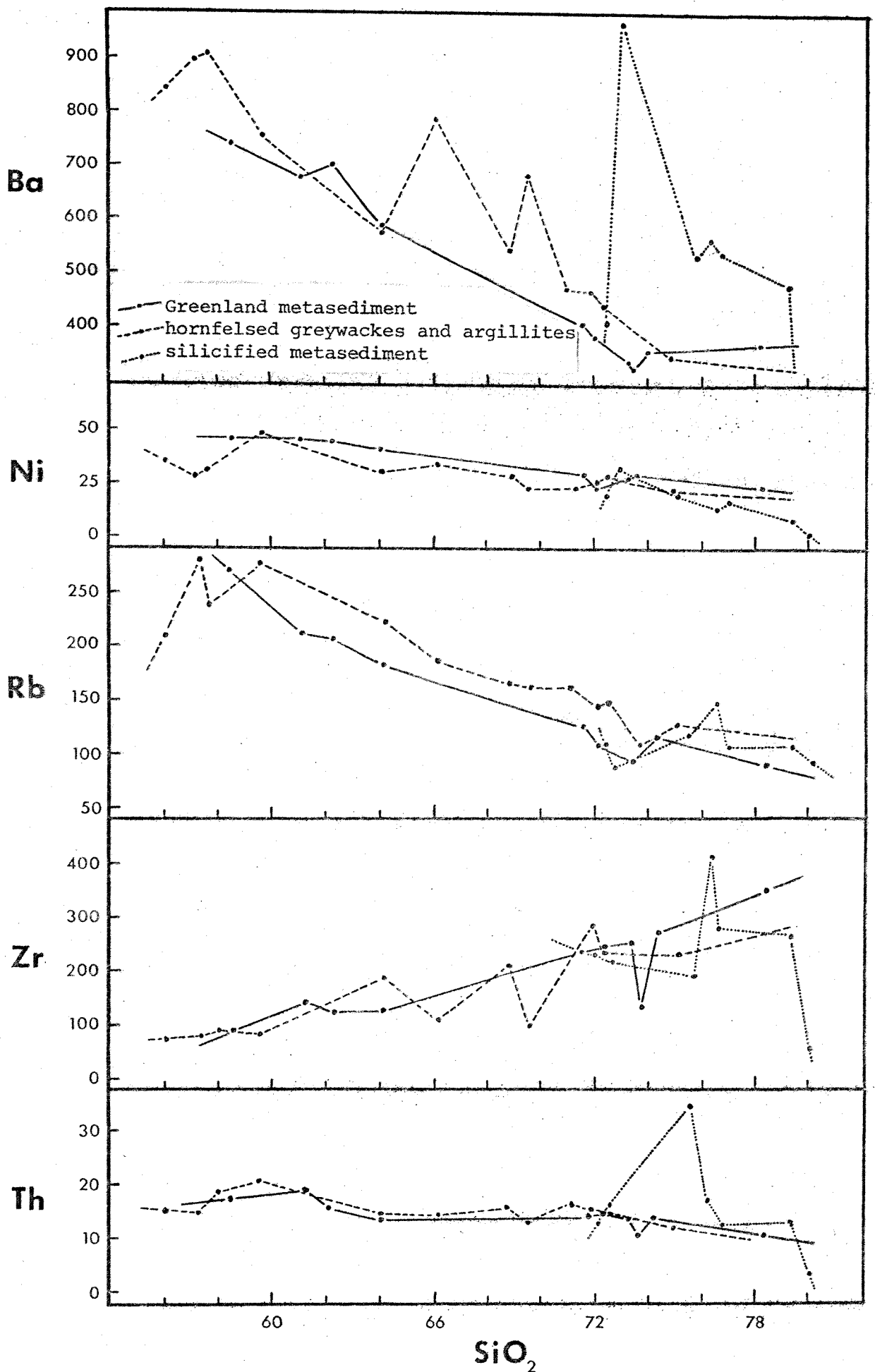
Fig. 4-6: Variation plots of selected trace elements to illustrate
the linear relationship between some trace elements and
silica content of the Greenland Group rocks.
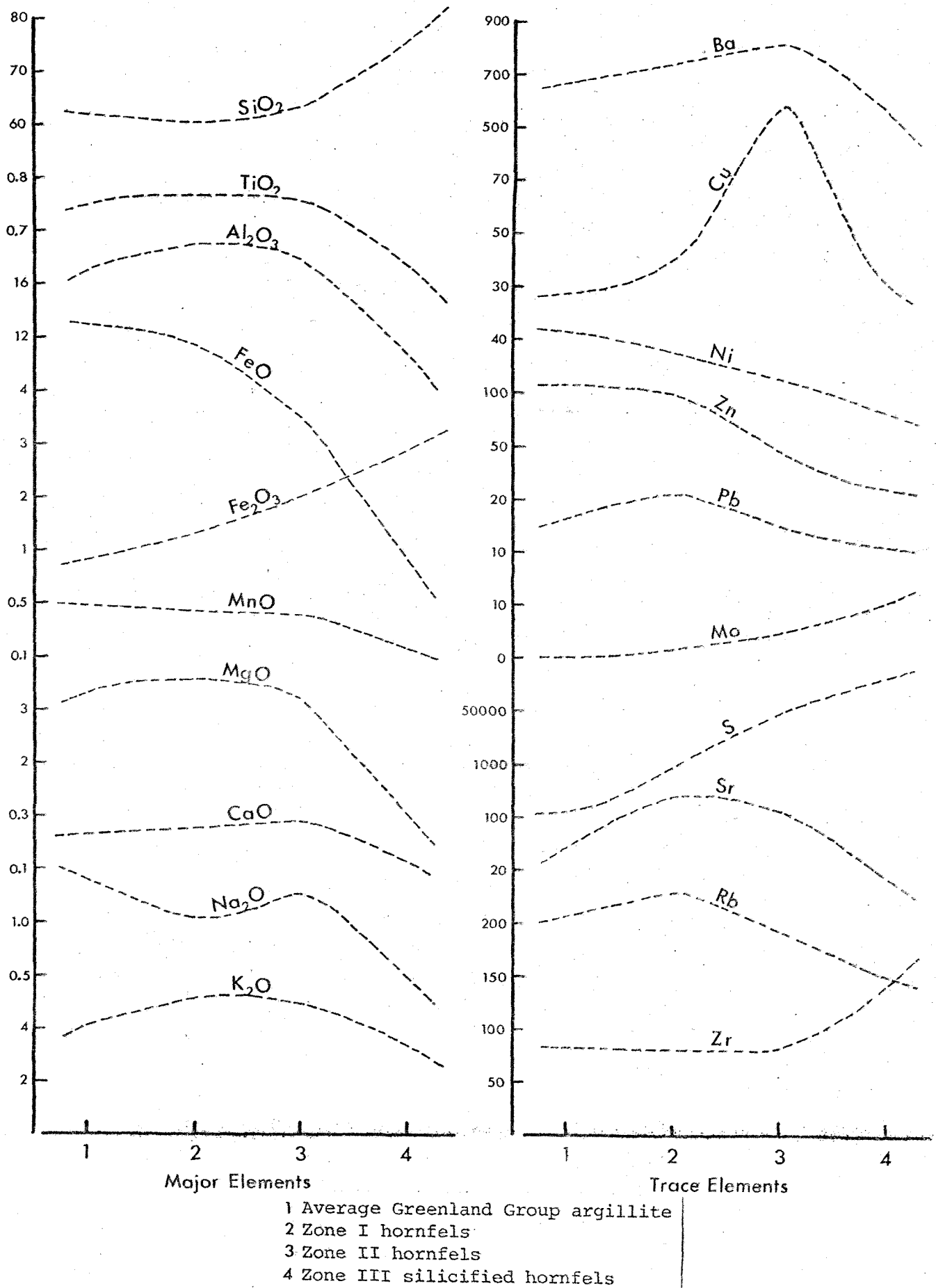
Fig. 4-7: Major and trace element variations during hydrothermal alteration of the Greenland Group rocks.

to the silicified zone. TiO_2 and ferrous iron decrease
systematically through the sequence while ferric iron shows
a consistent increase with more intense alteration. Magnesium
shows a sharp decrease into zone III type alteration. Calcium,
phosphorous, manganese and sodium levels show little syste-
matic alteration, although Na_2O and CaO are depleted in
zone III. Potassium increases into zone I and II type
alteration.

Trace element abundances possibly show more systematic
variation with alteration. A significant increase in copper,
molybdenum, sulphur and zirconium occur, with the exception
of copper being strongly depleted in zone III (ie: where
highest Mo values occur). Barium abundances show a slight
increase into zone II (possibly due to albite?) and decrease
into the siliceous zone III with nickel, zinc and lead
generally decreasing with increased alteration. Strontium
and rubidium values initially increase into zone I and then
decrease to zone III.

Discussion:

The major and trace element composition of the Greenland
metasediments at Bald Hill are comparable with all other
published data for the Greenland Group. The distinction
between greywacke and argillite was based on field
identification, and has been confirmed by the geochemistry.
The especially low calcium values probably reflect the lack
of calcic-plagioclase or calcium-bearing ferromagnesium

minerals, similarly, the low sodic nature of the sediments reflects the lack of plagioclase and/or volcanic rock fragments. The strong linear relationships between silica and alumina, magnesium, potassium, iron and some trace elements (eg: Ba, Rb and Zr), indicate the composition of the Greenland sediments to be a result of the different proportions of quartz and clay matrix, with little other detrital material, in contrast with Torlesse sediments which show a considerable scatter on a Al_2O_3/SiO_2 plot (Kawachi, 1974; Fig. 12, p.194). Major element compositions of the quartz-intermediate Torlesse greywacke-argillite suite (volcanic arc type) consistently lie outside the fields defined by Nathan's quartz-rich Greenland suite (non-volcanic trough type) and the Greenland metasedimentary suite at Bald Hill.

Nathan (1976) concluded that these (mature?) quartz-rich sediments probably had a polycyclic origin with any volcanic rock fragments and feldspar from the ultimate source being removed by physical and chemical weathering, and along with Cooper (1975), suggested the Ordovician quartz-rich metasediments in New Zealand show very similar characteristics to Ordovician sediments in Southeastern Australia and the Robertson Bay Group in Antarctica. Cooper concludes "there are no major objections to directly matching the major sedimentary belts of Victoria (Australia) with their counterparts in New Zealand, leading to the possibility that corresponding belts of the two regions were actually

continuous in the early Paleozoic", and indicated there is a similar sequence of sedimentary, igneous and tectonic activity in New Zealand and Central Victoria consistent with the suggestion that they were close together in early Paleozoic times.

Hydrothermal alteration of these metasediments surrounding intrusive porphyries and stockwork quartz veins shows systematic trends in most major and trace element abundances, especially silica, ferric and ferrous iron, alumina, magnesium, copper, molybdenum, sulphur and zirconium values.

Granitic Rocks of the Bald Hill Area:

The major and trace element chemistry of the granitic rocks were determined to:

1) Geochemically characterise the various granitic rocks distinguished in hand specimen, and by petrographic and modal techniques.

2) Observe any chemical similarities between the various granitic rocks (i.e. recognition of petrogenic provinces).

3) Relate geochemical characteristics of the plutonic rocks to their K-Ar age.

4) Compare the chemistry of the Mo-bearing granitic intrusives in West Nelson to Mo-bearing granitic intrusives in Southeastern Australia.

I: <u>Bald Hill Granites</u>

Major and trace element analyses of the Bald Hill Granites and CIPW Norms are given in Table 4-6. The suite is composed of gneissic leucogranites (LG), pink microgranites (PM) and biotite-granites (BG). Major element chemistry of this soda-poor, quartz-rich, potash-alkali series is illustrated by oxide variation diagrams in Fig. 4-8. The granites contain 72 to 76% SiO_2 with no apparent differentiation with respect to silica content, and no significant differences in major element chemistry between the differing granite types. Distinctive chemical characteristics of the suite are Al_2O_3 13 to 15%; total iron 0.5 to 2.0% (with Fe_2O_3 always <0.5%); MgO <0.6%; calcium <0.9%; K_2O >Na_2O, Na_2O <3.52% (K_2O/Na_2O ratios from LG 1.35 to BG 2.22) and total alkali values from 7.90 to 8.65%.

All the granites contain normative albite (an 100/(ab+an) range from 1.16 to 9.26) with >30% normative quartz and >3% normative corundum. The suite contains almost equal proportions of normative orthoclase and albite with a low anorthite component (i.e. up to 2.08%). Normative ilmenite values are <0.36% with apatite from 0.39 to 0.77%. Both the Differentiation Index (DI from 87.06 to 92.66) and the Solidification Index (SI from 0.77 to 5.53) show little, if any, systematic variation.

Trace element values are plotted against Differentiation Index (DI) in Fig. 4-9. The plots show no clearly defined trends. The granites do however, have closely similar trace

Table 4-6: Major and trace element analyses with CIPW Norms of the Bald Hill Granites

Type[1]	18891	18892	18911	18935	18959	18999	18901	18957	18977	18988	18988A	18988B	18992
	LG	LG	LG	LG	LG	LG	PM	PM	PM	PM	PM	PM	PM
SiO_2	74.28	73.42	74.44	73.71	74.22	74.01	72.39	72.57	75.51	72.88	72.51	73.42	73.21
TiO_2	0.13	0.09	0.12	0.17	0.12	0.12	0.18	0.18	0.10	0.15	0.18	0.18	0.16
Al_2O_3	14.38	14.36	14.27	14.36	14.34	14.35	14.91	14.90	13.28	14.86	14.97	14.74	14.63
Fe_2O_3	0.28	0.00	0.00	0.15	0.12	0.11	0.00	0.32	0.22	0.00	0.35	0.45	0.19
FeO	0.56	0.64	0.96	0.76	0.36	0.68	1.76	0.84	0.48	1.44	0.96	0.92	1.07
MnO	0.01	0.00	0.02	0.00	0.01	0.01	0.03	0.01	0.00	0.01	0.01	0.02	0.01
MgO	0.07	0.11	0.16	0.23	0.12	0.12	0.56	0.35	0.19	0.43	0.50	0.54	0.41
CaO	0.59	0.40	0.49	0.48	0.57	0.55	0.83	0.72	0.52	0.71	0.76	0.78	0.74
Na_2O	3.21	3.51	3.29	2.66	3.32	3.16	3.13	3.25	3.11	3.34	2.82	2.80	3.07
K_2O	4.98	4.75	4.64	5.93	4.93	5.05	5.01	5.40	5.07	4.70	5.51	5.28	5.16
P_2O_5	0.28	0.25	0.26	0.17	0.34	0.26	0.33	0.27	0.23	0.22	0.28	0.28	0.27
L.O.I.[2]	1.11	1.11	0.99	1.07	0.95	1.00	1.03	0.90	0.83	1.09	1.10	1.08	1.00
Total	99.89	98.64	99.65	99.69	99.39	99.43	100.17	99.72	99.55	99.84	99.96	100.50	99.94
Fe_2O_3[3]	0.90	0.71	1.07	1.00	0.52	0.84	1.96	1.25	0.75	1.60	1.42	1.47	1.41
Ba	85	19	23	158	35	64	173	149	110	212	234	219	183
Cu	12	8	14	4	10	10	11	8	4	25	43	54	30
Ni	3	3	4	5	4	4	9	4	5	5	6	5	5
Zn	52	33	25	32	23	30	55	37	33	40	41	46	42
Pb	25	14	27	28	21	20	22	41	31	53	52	44	40
Mn	2	4	1	4	3	2	2	1	2	0	2	1	1
S	155	96	85	98	86	101	110	119	110	106	107	94	105
Sr	32	4	12	42	11	20	56	39	30	68	64	64	55
Rb	383	388	370	331	379	371	318	390	361	308	306	290	330
Zr	37	20	21	65	32	36	75	68	26	49	61	64	62
Th	11	7	8	11	10	9	7	15	8	7	7	5	8
Y	6	7	8	2	6	5	6	11	7	12	11	10	10

CIPW Norms (Weight percent)

	18891	18892	18911	18935	18959	18999	18901	18957	18977	18988	18988A	18988B	18992
Q	35.71	34.05	36.27	34.21	35.44	35.09	31.98	31.25	37.03	32.83	32.90	34.77	33.49
C	3.31	3.32	3.57	3.10	3.32	3.30	3.62	3.05	2.28	3.51	3.66	3.67	3.31
or	29.43	28.07	27.42	35.04	29.13	29.84	29.61	31.91	29.96	27.77	32.56	31.20	30.49
ab	27.16	29.70	27.84	22.51	28.09	27.07	26.48	27.50	26.32	28.26	23.86	23.69	25.98
an	1.10	0.35	0.73	1.27	0.61	0.83	1.96	1.81	1.08	2.08	1.94	2.04	1.81
wo }Diop.	-	-	-	-	-	-	-	-	-	-	-	-	-
fs }Diop.	-	-	-	-	-	-	-	-	-	-	-	-	-
en }Diop.	-	-	-	-	-	-	-	-	-	-	-	-	-
fs }hyp.	0.58	1.01	1.58	0.97	0.36	0.90	2.97	1.00	0.51	2.39	1.17	1.04	1.52
en }hyp.	0.17	0.27	0.40	0.57	0.30	0.35	1.39	0.87	0.47	1.07	1.24	1.35	1.07
fo }ol.	-	-	-	-	-	-	-	-	-	-	-	-	-
fa }ol.	-	-	-	-	-	-	-	-	-	-	-	-	-
mt	0.41	-	-	0.22	0.17	0.16	-	0.46	0.32	-	0.51	0.65	0.32
hm	-	-	-	-	-	-	-	-	-	-	-	-	-
ilm	0.25	0.17	0.23	0.32	0.23	0.25	0.34	0.34	0.19	0.28	0.34	0.34	0.30
cc	-	-	-	-	-	-	-	-	-	-	-	-	-
ap	0.65	0.58	0.60	0.39	0.79	0.60	0.77	0.63	0.54	0.51	0.65	0.65	0.63
An 100/(ab+an)	3.88	1.16	2.56	5.34	2.11	2.98	6.87	6.17	3.93	6.87	7.52	7.93	6.51
D.I.[4]	92.30	91.82	91.53	91.76	92.66	92.01	88.07	90.66	93.31	88.87	89.32	89.66	89.96
S.I.[5]	0.77	1.22	1.77	2.36	1.36	1.53	5.35	3.44	2.09	4.34	4.93	5.40	4.32

(1) LG: Leucogranite
     PM: Pink-microgranite
     BG: Biotite-granite
(2) Loss on ignition
(3) Total iron as Fe_2O_3
(4) Differentiation Index after Thornton and Tuttle (1960)
(5) Solidification Index after Kuno et al., (1957).

Table 4-6: continued

	18958	18958/2	18987	18987A	18987B	18993
Type [1]	BG	BG	BG	BG	BG	BG
SiO_2	72.48	72.66	72.09	72.55	72.33	72.42
TiO_2	0.19	0.19	0.18	0.16	0.17	0.18
Al_2O_3	14.88	14.86	14.70	14.73	14.75	14.75
Fe_2O_3	0.10	0.03	0.00	0.43	0.00	0.10
FeO	1.44	1.44	1.48	0.88	2.16	1.50
MnO	0.02	0.02	0.01	0.00	0.01	0.01
MgO	0.57	0.47	0.49	0.42	0.48	0.51
CaO	0.72	0.74	0.86	0.69	0.83	0.77
Na_2O	3.02	2.84	2.86	2.85	2.65	2.84
K_2O	5.27	5.24	5.04	5.32	5.33	5.24
P_2O_5	0.32	0.31	0.30	0.28	0.28	0.30
L.O.I. [2]	1.16	1.16	1.06	1.11	1.06	1.15
Total	100.08	99.97	99.08	99.47	100.07	99.78
Fe_2O_3 [3]	1.60	1.63	1.65	1.41	2.40	1.74
Ba	198		189	187	180	188
Cu	9		16	14	14	13
Ni	8		9	8	7	8
Zn	50		51	45	50	49
Pb	37		44	35	34	37
Mo	3		0	1	4	2
S	110		141	116	178	136
Sr	60		56	59	54	60
Rb	294		320	279	299	301
Zr	69		63	58	58	61
Th	13		5	6	14	9
Y	12		15	10	10	11

CIPW Norms (Weight percent)

	18958	18958/2	18987	18987A	18987B	18993
Q	32.19	33.62	33.34	33.85	33.15	33.25
C	3.66	3.91	3.69	3.74	3.78	3.76
or	31.14	30.96	29.78	31.44	31.50	30.96
ab	25.55	24.03	24.20	24.12	22.42	24.03
an	1.48	1.65	2.31	1.59	2.29	1.86
wo } Diop.	-	-	-	-	-	-
fs } Diop.	-	-	-	-	-	-
en } Diop.	-	-	-	-	-	-
fs } hyp.	2.35	2.32	2.42	0.97	3.66	2.34
en } hyp.	1.42	1.17	1.22	1.05	1.19	1.22
fo } ol.	-	-	-	-	-	-
fa } ol.	-	-	-	-	-	-
mt	-	0.04	-	0.62	-	0.14
hm	-	-	-	-	-	-
ilm.	0.36	0.36	0.34	0.30	0.32	0.34
cc	-	-	-	-	-	-
ap	0.74	0.72	0.69	0.65	0.65	0.69
An 100/(ab+an)	5.48	6.41	8.70	6.20	9.26	7.18
D.I. [4]	88.88	88.61	87.32	89.41	87.06	88.25
S.I. [5]	5.53	4.61	4.96	4.24	4.52	4.83

(1) LG: Leucogranite
     PM: Pink-microgranite
     BG: Biotite-granite
(2) Loss on ignition
(3) Total iron as Fe_2O_3
(4) Differentiation Index after Thornton and Tuttle (1960)
(5) Solidification Index after Kuno et al., (1957)
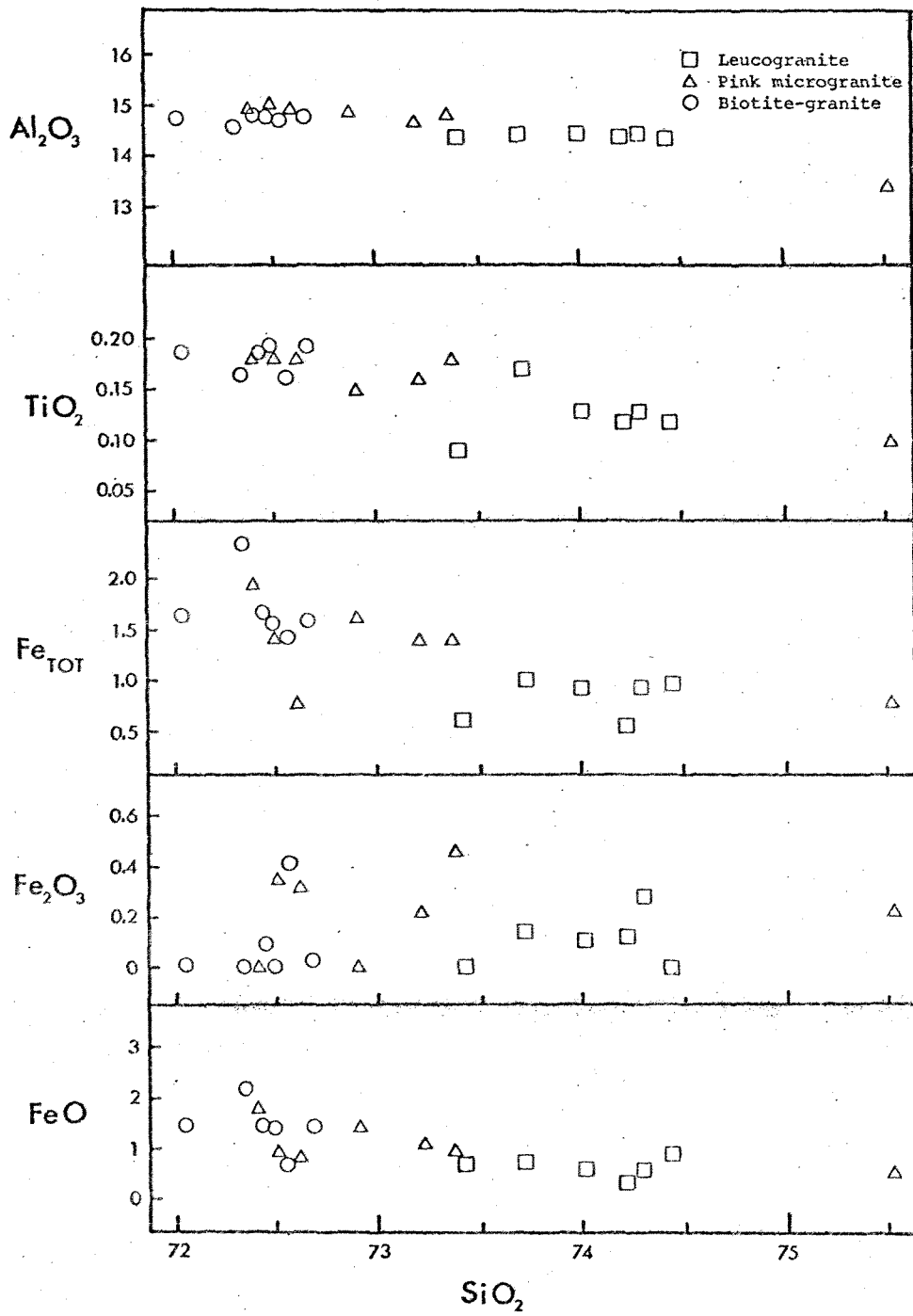
Fig. 4-8: Variation diagrams for Bald Hill Granites.
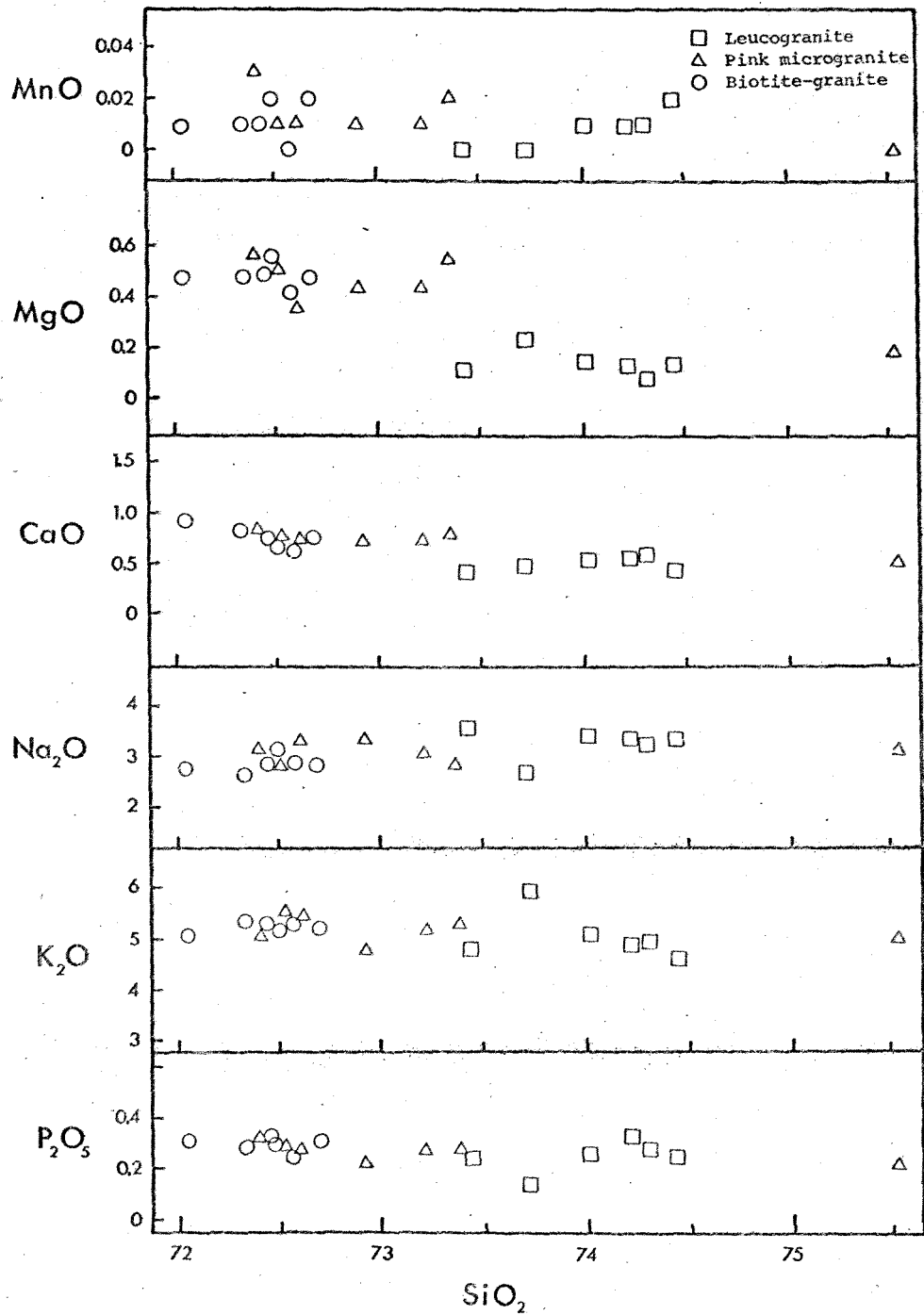
Fig. 4-8: Variation diagrams for Bald Hill Granites.
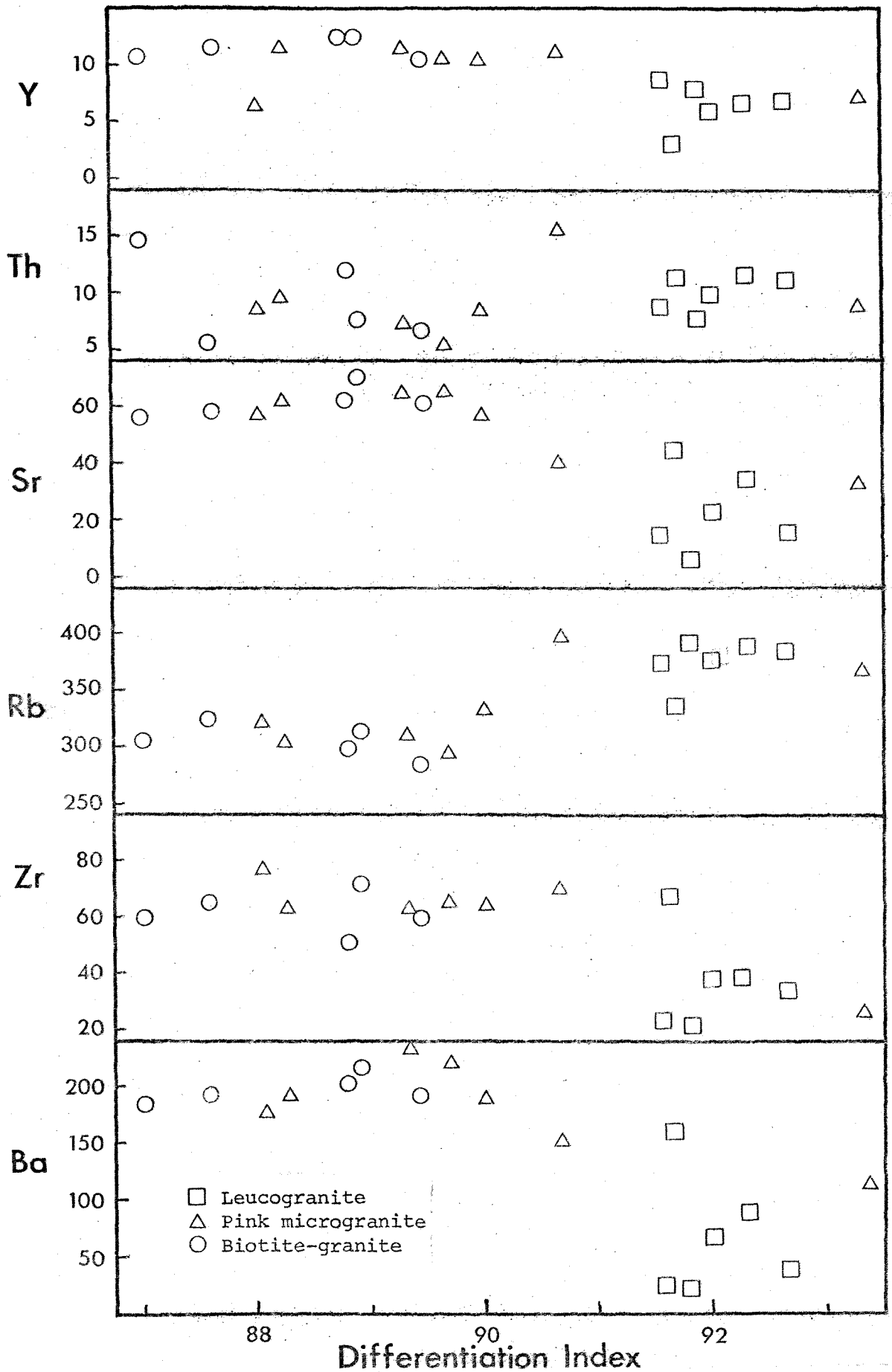
Fig. 4-9: Selected trace elements versus Differentiation Index (DI) for Bald Hill Granites.

element composition. Barium content ranges from 19 to
234 ppm, zirconium 20 to 80 ppm, thorium 5 to 15 ppm,
yttrium 2 to 15 ppm with rubidium always greater than
strontium. Rubidium ranges from 279 to 390 ppm and strontium
from 4 to 64 ppm, Rb/Sr ratios always 4.5 (max. 97).
Copper, nickel, molybdenum and sulphur abundances
(Cu: 4 to 54 ppm, Ni: 3 to 9 ppm, Mo: 0 to 4 ppm and
S: 85 to 178 ppm) are generally low, especially when
compared to the Lyell Porphyry granitic rocks (see below).
Zinc and lead values (Zn: 25 to 55 ppm, Pb: 20 to 53 ppm)
show little variation with Pb being higher than in the
Lyell Porphyry.

II: Lyell Porphyry

The Lyell Porphyry is composed of a series of soda-
rich calc-alkaline quartz trondhjemite porphyries (TP),
granodiorites (GD), quartz diorites (DI), lamprophyres (LD)
and quartz gabbroporphyries (GP). Major and trace element
analyses with CIPW Norms are given in Table 4-7. Major
element chemistry is illustrated by oxide variation diagrams
in Fig. 4-10. The Lyell Porphyry rocks are shown to have a
range of SiO_2 content from 46% in GP to 70% in TP, with
titanium, total iron, ferrous iron, manganese, magnesium,
calcium and sodium oxides suggesting that the suite is
petrologically related. These elements generally show
systematic trends with respect to silica.

Table 4-7: Major and trace element analyses with CIPW Norms of the Lyell Porphyries.

Type [1]	18960 TP	18970 TP	18971 TP	18971A TP	18973 TP	18975 TP	18975/2 TP	18955 GD	18956 GD	18963 GD	18963/2 GD	18995 GD
SiO_2	69.27	67.78	65.56	67.36	68.01	68.32	68.16	68.95	63.68	67.46	67.33	66.85
TiO_2	0.55	0.44	0.41	0.41	0.40	0.44	0.45	0.33	0.45	0.40	0.40	0.40
Al_2O_3	15.90	15.57	14.61	15.45	15.60	15.96	16.05	16.29	18.07	16.53	16.60	16.87
Fe_2O_3	0.41	1.87	2.77	2.33	2.00	1.85	1.89	1.00	1.23	0.34	0.37	0.73
FeO	1.48	1.29	1.32	1.44	1.56	0.92	0.92	1.36	1.88	2.40	2.40	2.01
MnO	0.00	0.01	0.02	0.01	0.01	0.01	0.02	0.04	0.04	0.05	0.04	0.04
MgO	2.09	1.58	1.51	1.53	1.43	1.43	1.41	1.09	1.66	1.50	1.49	1.43
CaO	2.52	2.66	2.44	2.72	2.28	2.96	3.02	2.60	4.06	3.01	3.01	3.17
Na_2O	4.71	4.88	3.84	4.63	5.45	5.59	5.83	4.47	4.87	4.78	4.65	4.69
K_2O	1.48	1.55	2.22	1.32	1.16	1.16	1.23	2.88	2.28	2.37	2.35	2.47
P_2O_5	0.18	0.19	0.20	0.21	0.16	0.20	0.22	0.14	0.20	0.17	0.17	0.17
L.O.I. [2]	1.66		4.66	2.87	2.51	1.85	1.85	0.94	1.20	0.92	0.92	1.05
Total	100.24	100.77	99.71	100.44	100.74	100.88	101.16	100.09	99.64	99.94	99.72	99.90
Fe_2O_3 [3]	2.05	3.28	4.24	3.93	3.73	2.87	2.91	2.51	3.32	3.01	3.04	2.96
Ba	496	–	399	468	444	513	460	643	596	609		618
Cu	8	10	109	86	361	473	178	8	6	7		7
Ni	12	9	7	10	8	7	9	8	9	8		8
Zn	23	19	24	21	21	23	20	71	82	77		77
Pb	10	14	17	17	13	17	15	25	21	27		22
Mo	8	1	22	48	5	2	14	1	2	0		1
S	2150	10370	11740	11330	10450	5455	8580	125	276	121		174
Sr	782	817	415	699	719	910	724	720	1037	788		850
Rb	52	50	118	60	48	45	60	114	111	109		109
Zr	125	124	86	96	95	118	108	85	112	104		98
Th	7	9	3	4	5	8	6	8	7	7		8
Y	18	17	13	14	14	19	16	12	16	18		15

CIPW Norms (Weight percent)

	18960	18970	18971	18971A	18973	18975	18975/2	18955	18956	18963	18963/2	18995
Q	27.73	25.70	27.81	27.86	25.30	23.32	21.59	24.59	15.24	20.77	21.51	20.55
C	2.40	1.03	1.93	1.96	1.62	0.60	0.16	1.43	0.69	1.04	1.34	1.12
or	8.75	8.45	13.12	7.80	6.85	6.85	7.28	17.02	13.47	14.01	13.89	14.60
ab	39.85	42.32	32.49	39.17	46.12	47.30	49.33	37.82	41.21	40.45	39.35	39.69
an	11.33	11.95	10.80	12.12	10.27	13.38	13.54	11.98	18.84	13.82	13.82	14.62
wo } Diop.	–	–	–	–	–	–	–	–	–	–	–	–
fs } Diop.	–	–	–	–	–	–	–	–	–	–	–	–
en } Diop.	–	–	–	–	–	–	–	–	–	–	–	–
fs } hyp.	1.04	–	–	–	–	–	–	1.18	1.71	3.54	3.49	2.46
en } hyp.	5.21	3.93	3.76	3.81	3.56	3.79	3.51	2.71	4.13	3.74	3.71	3.56
fo } ol.	–	–	–	–	–	–	–	–	–	–	–	–
fa } ol.	–	–	–	–	–	–	–	–	–	–	–	–
mt	0.59	–	–	–	0.11	–	–	1.45	1.78	0.49	0.54	1.06
hm	–	1.87	2.77	2.33	1.92	1.85	1.89	–	–	–	–	–
ilm	1.04	0.69	0.07	0.39	0.76	0.69	0.71	0.63	0.85	0.76	0.76	0.76
cc	–	–	–	–	–	–	–	–	–	–	–	–
ap	0.42	0.44	0.46	0.49	0.37	0.46	0.51	0.32	0.46	0.39	0.39	0.39
rt	–	0.08	0.38	0.21	–	0.08	0.08	–	–	–	–	–
An100/(ab+an)	22.13	22.03	24.94	23.63	18.21	22.05	21.54	24.06	31.37	25.47	26.00	26.92
D.I. [4]	76.33	76.46	73.43	74.84	78.27	77.48	78.19	79.43	69.92	75.22	74.74	74.83
S.I. [5]	20.55	14.17	12.95	13.60	12.33	13.76	12.50	10.09	13.93	13.17	13.23	12.62

(1) TP: Quartz trondhjemite porphyry
    GD: Granodiorite porphyry
    LD: Lamprophyre dykes
    DI: Quartz-diorite
    GP: Quartz-gabbroporphyry
(2) Loss on ignition
(3) Total iron as Fe_2O_3
(4) Differentiation Index after Thornton and Tuttle (1960)
(5) Solidification Index after Kuno et al., (1957).

Table 4-7: continued

Type[2]	18929 LD	18934 LD	18934/2 LD	18941 LD	18946 LD	18983 LD	18983/2 LD	18983/3 LD	18989 LD	18989/2 LD	18997 LD
SiO_2	54.22	52.02	52.32	53.51	52.38	52.60	53.53	53.67	53.57	53.47	53.13
TiO_2	1.02	1.12	1.10	1.10	1.06	1.09	1.05	1.06	1.07	1.08	1.07
Al_2O_3	16.23	16.46	16.57	16.69	16.17	17.09	16.11	16.35	16.28	16.33	16.43
Fe_2O_3	2.95	2.19	2.39	2.95	2.51	2.58	2.72	2.72	2.25	2.15	2.54
FeO	4.52	4.56	4.56	4.48	4.80	4.72	4.72	4.72	5.12	5.12	4.73
MnO	0.09	0.08	0.07	0.09	0.09	0.10	0.07	0.09	0.09	0.10	0.09
MgO	5.02	4.11	4.10	5.08	4.96	5.37	5.06	5.22	5.62	5.56	5.01
CaO	5.64	5.20	5.16	6.07	5.78	6.66	6.44	6.48	6.16	6.18	5.98
Na_2O	4.30	3.60	3.52	3.66	3.76	4.19	3.73	3.74	3.75	3.90	3.78
K_2O	2.03	2.69	2.70	1.13	2.05	0.90	0.84	0.85	1.63	1.62	1.67
P_2O_5	0.31	0.36	0.37	0.34	0.32	0.40	0.37	0.36	0.32	0.32	0.32
L.O.I.[2]	2.93	5.72	5.72	3.93	4.88	4.59	4.59	4.59	3.81	3.81	4.50
Total	99.26	98.47	98.57	99.02	98.77	100.30	99.23	99.84	99.68	99.65	99.33
Fe_2O_3	7.97	7.26	7.46	7.93	7.84	7.82	7.96	7.96	7.94	7.84	7.80
Ba	595	766		372	676	300			570		550
Cu	45	54		25	30	26			27		34
Ni	72	48		75	78	81			69		70
Zn	97	91		111	106	115			107		100
Pb	12	13		20	18	18			16		12
Mo	4	4		0	7	0			3		4
S	758	711		141	530	436			156		456
Sr	765	723		827	781	775			826		672
Rb	60	113		41	66	32			54		59
Zr	164	171		166	162	176			167		167
Th	5	6		5	6	7			3		5
Y	23	35		28	21	25			24		26

CIPW Norms (Weight percent)

	18929	18934	18934/2	18941	18946	18983	18983/2	18983/3	18989	18989/2	18997
Q	2.34	2.95	3.68	6.87	2.65	2.57	7.20	6.81	3.39	2.59	4.14
C	–	–		– –	–	–	–	–	–	–	–
or	11.99	15.89	15.95	6.68	12.11	5.32	4.96	5.02	9.63	9.57	9.69
ab	36.39	30.46	29.78	30.97	31.87	35.45	31.56	31.65	31.73	33.00	32.24
an	18.99	20.81	21.44	25.77	21.19	25.16	24.73	25.31	22.77	22.27	22.88
wo ｝Diop.	2.91	1.10	0.73	0.88	2.25	2.20	2.00	1.87	2.38	2.63	1.88
fs ｝Diop.	0.67	0.33	0.21	0.20	0.61	0.54	0.51	0.46	0.66	0.74	0.49
en	2.00	0.71	0.47	0.61	1.48	1.49	1.35	1.26	1.56	1.71	1.25
fs ｝hyp.	3.53	4.39	4.36	3.90	4.45	4.30	4.23	4.29	5.25	5.25	4.39
en ｝hyp.	10.50	9.53	9.74	12.04	10.87	11.89	11.26	11.74	12.44	12.14	11.23
fo ｝ol.	–	–	–	–	–	–	–	–	–	–	–
fa ｝ol.	–	–	–	–	–	–	–	–	–	–	–
mt	4.28	3.17	3.46	4.27	3.64	3.74	3.94	3.94	3.26	3.12	3.68
hm	–	–	–	–	–	–	–	–	–	–	–
ilm	1.94	2.13	2.09	2.09	2.01	2.07	1.99	2.01	2.03	2.05	2.03
cc	–	–	–	–	–	–	–	–	–	–	–
ap	0.72	0.83	0.86	0.79	0.74	0.93	0.86	0.83	0.74	0.74	0.81
rt	–	–	–	–	–	–	–	–	–	–	–
An100/(ab+an)	34.29	40.58	41.85	45.42	39.97	41.51	43.93	44.44	41.78	40.29	41.51
D.I.[4]	50.72	49.31	49.42	44.51	46.58	43.34	43.73	43.48	44.75	45.16	46.07
S.I.[5]	26.67	23.96	23.74	29.36	27.43	30.24	29.64	30.26	30.59	30.30	28.26

(1) TP: Quartz trondhjemite porphyry
GD: Granodiorite porphyry
LD: Lamprophyre dykes
DI: Quartz-diorite
GP: Quartz-gabbroporphyry
(2) Loss on ignition
(3) Total iron as Fe_2O_3
(4) Differentiation Index after Thornton and Tuttle (1960)
(5) Solidification Index after Kuno et al., (1957)

Table 4-7: continued

Type[1]	18980	18981	18996		18908	18910	18910/2	18962	18998
	DI	DI	DI		GP	GP	GP	GP	GP
SiO_2	54.45	53.17	54.01		46.80	46.98	47.28	53.11	48.90
TiO_2	0.85	1.19	1.12		1.92	1.51	1.52	2.23	1.78
Al_2O_3	18.80	19.63	19.31		12.66	17.73	17.76	15.97	17.40
Fe_2O_3	1.71	2.24	1.97		2.67	1.99	1.86	3.36	2.48
FeO	4.64	4.20	3.89		7.24	7.60	7.60	6.24	7.29
MnO	0.11	0.14	0.15		0.17	0.16	0.18	0.15	0.16
MgO	3.19	3.82	3.51		8.18	8.63	8.64	5.06	7.74
CaO	7.15	7.26	7.20		8.54	9.27	9.06	6.88	8.44
Na_2O	4.02	3.88	3.96		2.50	2.64	2.00	3.05	2.55
K_2O	1.23	1.51	1.37		1.95	1.29	1.27	1.12	1.41
P_2O_5	0.36	0.37	0.36		0.36	0.28	0.25	0.49	0.34
L.O.I. [2]	1.37	1.97	1.35		1.81	1.84	1.84	1.60	1.78
Total	97.88	99.36	98.44		99.80	99.93	99.25	99.26	99.71
Fe_2O_3 [3]	6.87	6.91	6.88		10.72	10.44	10.31	10.29	10.44
Ba	414	376	390		185	108		183	160
Cu	61	48	56		76	35		161	86
Ni	11	14	12		80	107		43	76
Zn	104	118	110		121	88		98	105
Pb	19	17	17		11	11		13	11
Mo	0	2	2		2	0		1	2
S	2515	386	1500		1550	550		2850	1650
Sr	1311	1175	1250		424	423		383	410
Rb	75	87	86		112	70		70	84
Zr	223	100	201		135	97		264	170
Th	7	4	5		0	1		7	3
Y	30	27	28		35	29		56	40

CIPW Norms (Weight percent)

	18980	18981	18996		18908	18910	18910/2	18962	18998
Q	5.60	3.20	4.37		--	--	--	--	--
C	--	--	--		--	--	--	--	--
or	7.27	8.92	8.10		11.52	7.62	7.50	8.98	8.33
ab	34.02	32.83	33.42		21.15	22.34	16.92	6.62	21.58
an	29.62	31.69	30.64		31.21	32.72	35.73	25.81	31.54
wo	1.46	0.80	1.16		3.68	4.78	3.16	26.58	3.39
fs }Diop.	0.56	0.22	0.38		0.66	1.42	0.95	1.82	0.95
en	0.83	0.52	0.71		2.67	3.05	2.01	0.46	2.21
fs }hyp.	4.83	3.85	4.35		0.85	0.16	4.81	1.22	4.89
en	7.11	8.94	8.03		3.42	0.33	10.20	4.25	11.41
fo }ol.	--	--	--		10.00	12.69	6.52	11.38	3.76
fa	--	--	--		2.73	6.52	3.39	--	1.78
mt	2.48	3.25	2.86		3.87	2.88	2.69	4.87	3.58
hm	--	--	--		--	--	--	--	--
ilm	1.61	2.26	1.94		3.65	2.87	2.89	4.23	3.40
cc	--	--	--		--	--	--	--	--
ap	0.83	0.86	0.83		0.83	0.65	0.58	1.14	0.79
rt	--	--	--		--	--	--	--	--
An100/(ab+an)	46.54	49.11	47.82		59.60	59.42	67.86	50.73	59.38
D.I. [4]	46.88	44.96	45.89		32.67	29.96	24.42	41.40	29.91
S.I. [5]	21.57	24.31	23.06		36.29	38.96	40.43	26.87	35.91

(1) TP: Quartz trondhjemite porphyry
    GD: Granodiorite porphyry
    LD: Lamprophyre dykes
    DI: Quartz-diorite
    GP: Quartz-gabbroporphyry
(2) Loss on ignition
(3) Total iron as Fe_2O_3
(4) Differentiation Index after Thornton and Tuttle (1960)
(5) Solidification Index after Kuno et al., (1957)
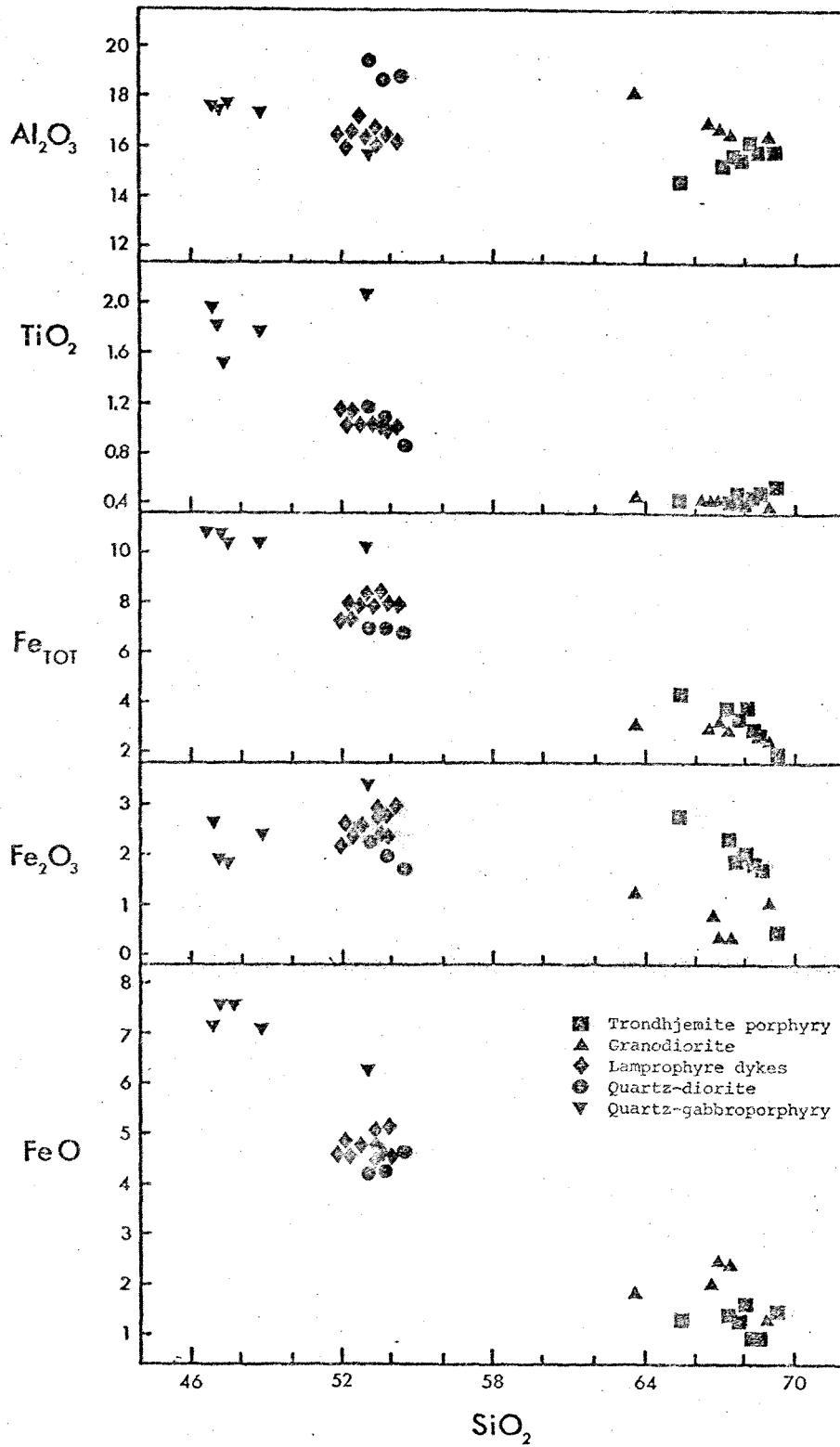
Fig. 4-10: Variation diagrams for Lyell Porphyry suite.
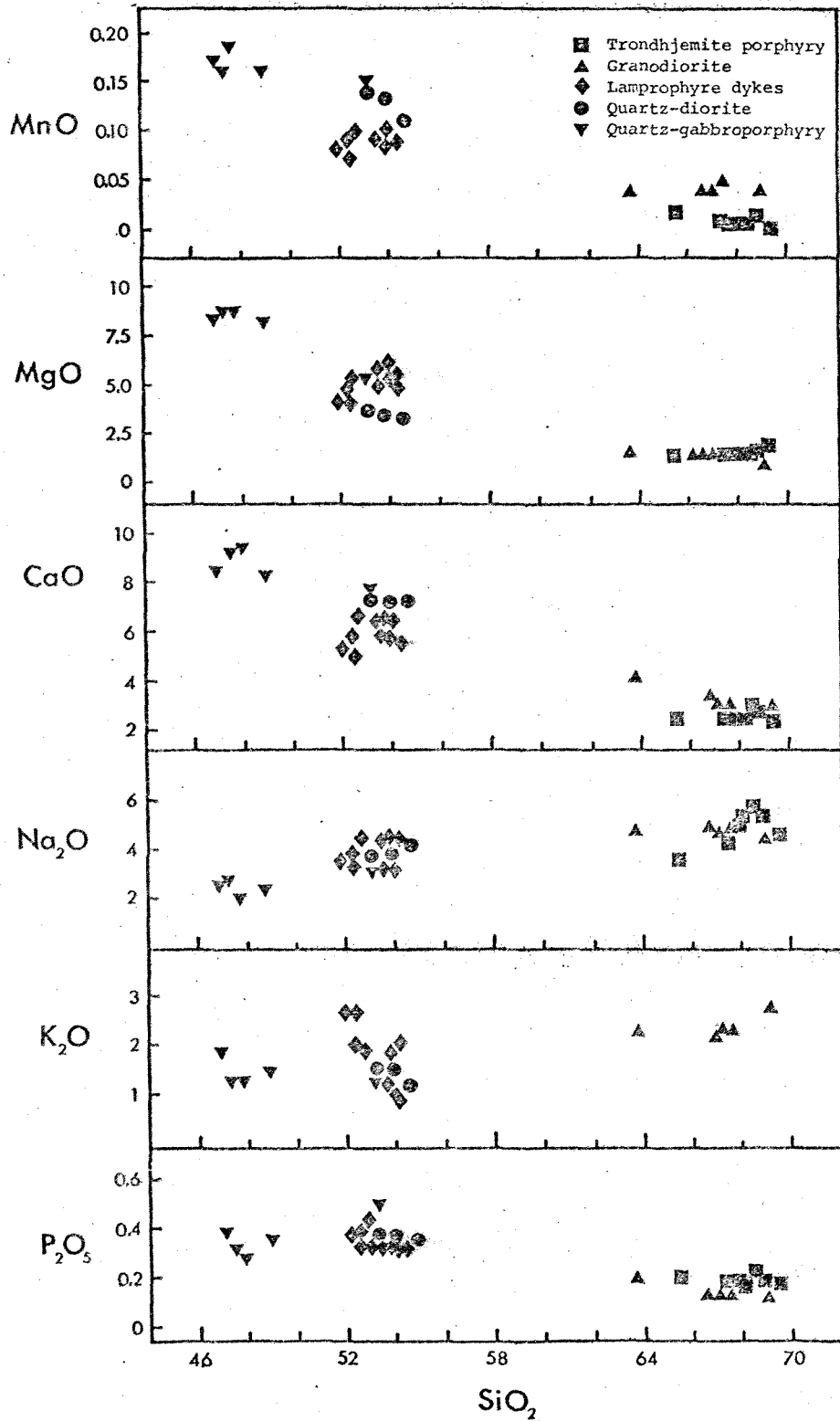
Fig. 4-10: Variation diagrams for Lyell Porphyry suite.

Distinctive chemical characteristics of the "porphyry" suite are high alumina content (14.61 to 19.63%), total iron always >2% (range 2% (TP) to 10.72% (GP)) (with Fe_2O_3 always >0.9%), MgO content >1.0%, high calcium content (range from 2.28% (TP) to 9.27% (GP)) with K_2O always <Na_2O (K_2O/Na_2O ratios from 0.21 (TP) to 0.78 (GP)) with total alkali values always <7.35% ranging from a maximum of 7.35% in GD to a minimum of 3.27% in GP. However, part of the chemical variation in LD and GP may be a consequence of later metasomatic alteration of these rocks (see Chapter 3).

The normative mineralogy of these granitic rocks also suggests a related series with normative plagioclase composition ranging through oligoclase (An_{18-25}) in TP, low-soda oligoclase-andesine (An_{24-31}) in GD, andesine (An_{34-45}) in LD, calcic andesine (An_{46-49}) in DI to calcic labradorite (An_{59-67}) in the olivine bearing GP. The series contains progressively less normative quartz (max. in TP: 28% to min. in GP: 0%) and always less than 2.4% normative corundum. All the rocks contain normative orthoclase (Or), albite (Ab) and anorthite (An) with Or generally being subordinate to the more soda and calcic components (Ab and An). Normative diopside and hypersthene are present in the more basic lamprophyres, diorites and gabbro-porphyries with minor hypersthene also present in the granodiorite. Normative ilmenite ranges from a minimum of 0.07% in TP to a maximum of 4.23% in GP and apatite from a maximum of 1.14 in GP to a minimum of 0.07 in TP. The quartz trondhjemite contains up to 0.78% normative rutile.

Differentiation Index (D.I.) and Solidification Index (S.I.)
increase and decrease respectively from the gabbroporphyry
(DI 24.42, SI 40.43) to the quartz trondhjemite (DI 78.27,
SI 12.50).

The calc-alkaline rocks have a distinctive trace element
composition further demonstrating the consanguinity of these
rocks, although, when plotted against DI in Fig. 4-11,
systematic trends with differentiation are not clear. Barium
content ranges from a minimum of 108 ppm in GP to a maximum
of 766 ppm in LD; zirconium 264 ppm (GP) to 85 ppm (GD);
thorium 0 to 9 ppm; yttrium increases from 12 (GD) to
56 ppm (GP); rubidium is always less than strontium with
Rb/Sr ratios 0.28 (min. 0.04). Absolute values of Rb are
low (32 to 118 ppm) with strontium values high (383 to
1311 ppm). Copper, nickel, molybdenum and sulphur values
show a considerable range in values (Cu: 6 to 473 ppm,
Ni: 7 to 107 ppm, Mo: 1 to 48 ppm and S: 121 to >10,000 ppm),
generally higher than the Bald Hill Granite values. Zinc
abundances tend to increase from the TP to the GP (min.
19 ppm TP to max. 121 ppm GP) with low lead values (11 to
27 ppm) being ubiquitous.

The trace element composition of the plutonic rocks
is closely related to the constituent mineral phases,
especially alkali feldspars; Sr and Y substitute for Ca
in plagioclases; Zr for Fe^{2+} in Ca-amphiboles and Th for
Zr in amphiboles and zircon minerals (Taylor, 1965). These
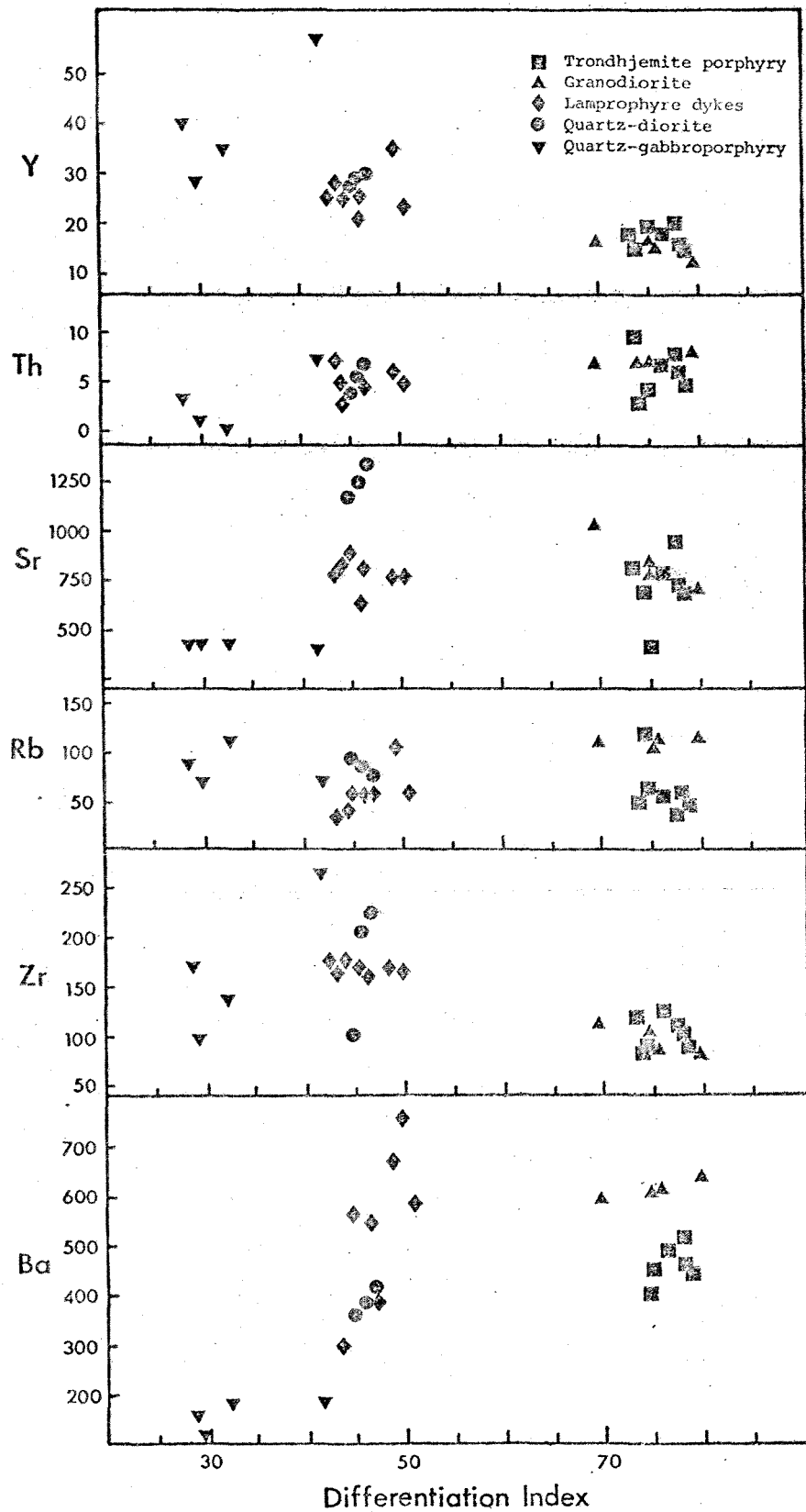
Fig. 4-11: Selected trace elements versus Differentiation Index
(DI) for Lyell Porphyry suite.

substitutions are shown by the low Sr and high Rb abundances
in the K-feldspar-albite bearing Bald Hill Granites; and
the high Sr and low Rb abundances in the calcic-plagioclase-
amphibole bearing Lyell Porphyry rocks. However, as
indicated in Figs. 4-12a and b, not all of the trace element
variation can be explained simply by changes in mineralogy
(see Table 3-1).

Increases in Rb relative to K (ie: reduction in the
K/Rb ratio) in a sequence of granites can be interpreted
as indicating the order of intrusion due to progressive
enrichment of Rb in residual magmas (Taylor, 1965). However
when K/Rb ratios of the Bald Hill plutonic rocks are plotted
against DI (Fig. 4-12a) they show no clear intrusive sequence,
especially from the Lyell Porphyry to the Bald Hill Granites.
Thus the following factors 1) the abundance of heavy metals
(Cu, Ni, Zn, Pb and Mo) and sulphur, 2) the K/Rb ratios and
3) the Ba/Sr and Ba/Rb ratios (Fig. 4-12b) suggest that the
Bald Hill Granites and Lyell Porphyry rocks belong to
separate petrogenic suites and, as with the individual Lyell
Porphyry rocks, are not the products of differentiation of
a common source magma.

I-type and S-type Granites:

Field relationships (Chapter 1), K-Ar evidence
(Chapter 2), petrographic and modal classification (Chapter 3)
and the geochemical data (this chapter) show that there are
two petrogenically contrasting granitic rock suites in the
Bald Hill area:
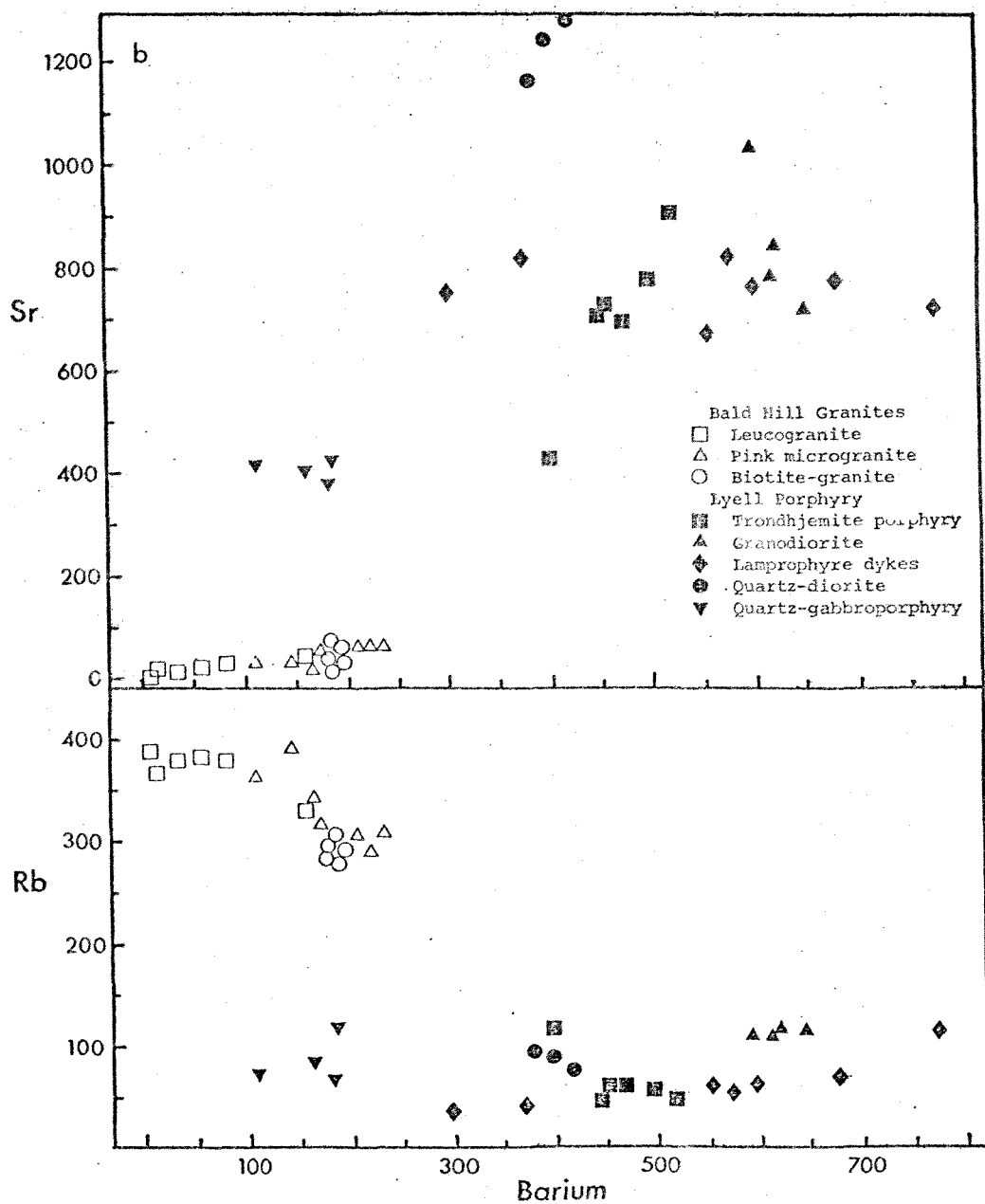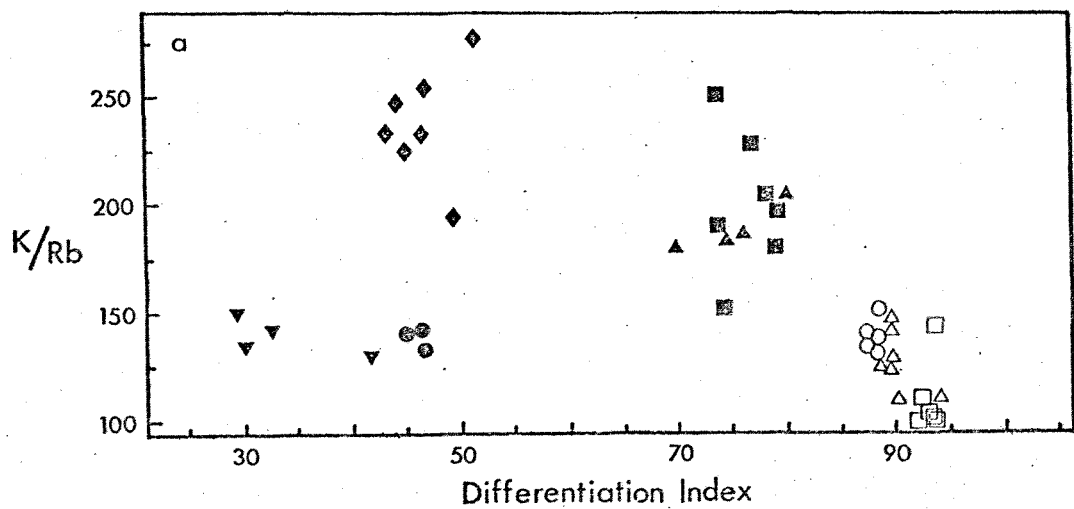
Fig. 4-12a and b: K/Rb ratios versus Differentiation Index,
Ba/Sr and Ba/Rb diagrams for all Bald Hill
plutonic rocks.

1) Bald Hill Granites. Medium to coarse-grained low-soda
   quartz rich potash-alkali granites with high Rb/Sr
   ratios of probable Tuhuan age. These granites are
   generally unmineralized, contain little sulphur, and
   form the western margin of a major batholith.

2) Lyell Porphyry rocks. Porphyritic soda-rich calc-
   alkaline series with low Rb/Sr ratios of Cretaceous age.
   These rocks form minor intrusive stocks and dykes, contain
   relatively high sulphur abundances when compared with the
   'batholith' granites, and are closely associated with
   molybdenum mineralization.

From their studies of the Lachlan Fold zone of South-
eastern Australia, Chappell and White (1974) used chemical,
mineralogical and field criteria listed in Table 4-8 below to
recognise two contrasting granitoid types called I-type and
S-type, I-types being derived from igneous source material

Table 4-8: Criteria to distinguish I-type and S-type granites from
Chappell and White (1974)

I-types	S-types
Relatively high sodium, Na_2O normally $> 3.2\%$ in felsic varieties, decreasing to $> 2.2\%$ in more mafic types	Relatively low sodium, Na_2O normally $< 3.2\%$ in rocks with approx. 5% K_2O, decreasing to $< 2.2\%$ in rocks with approx. 2% K_2O
Mol $Al_2O_3/(Na_2O + K_2O + CaO) < 1.1$	Mol $Al_2O_3/(Na_2O + K_2O + CaO) > 1.1$
C.I.P.W. normative diopside or $< 1\%$ normative corundum	$> 1\%$ C.I.P.W. normative corundum
Broad spectrum of compositions from felsic to mafic	Relatively restricted in composition to high SiO_2 types
Regular inter-element variations within plutons; linear or near-linear variation diagrams	Variation diagrams more irregular

(ie: crystallized largely from a silicate melt) and S-type derived from sedimentary source material (ie: metamorphism of sediments).

The Bald Hill Granites have been shown to be soda-poor (<3.51% Na_2O) and have Mol. $Al_2O_3/(Na_2O+K_2O+CaO)$ ratios of 1.16 to 1.26 (ie: always >1.1). The chemistry and modes show the granites to have high silica content with a restricted range and always >1% normative corundum. Variation diagrams are irregular, showing no well-defined linear trends. These granites thus conform to the "S" type as defined by Chappell and White (1974).

The porphyritic calc-alkaline granitic rocks are a soda rich series with >3.84% Na_2O in the felsic quartz trondhjemite to >2.00% Na_2O in the most mafic gabbroporphyry. Mol. $Al_2O_3/(Na_2O+K_2O+CaO)$ ratios of the calc-alkaline rocks range from 1.08 to 0.53 (with one exception of a TP at 1.15), always being less than 1.1. The lamprophyre, diorites and gabbroporphyry contain normative diopside while the quartz trondhjemite and granodiorite contain up to 2.40% normative corundum. The porphyritic series have a wide range of compositions from the basic gabbroporphyry to the quartz rich trondhjemite porphyry with a tendency towards linear inter-element relationships on variation diagrams. The Lyell Porphyry, with the exception of the normative corundum content in the quartz trondhjemite and granodiorite, conform to Chappell and White's criteria for "I"-type granites.

Other petrographic features and field relationships used by White and Chappell (1977) to distinguish the two

types of granites are also shown to be characteristic of the Bald Hill and Lyell Porphyry suites. These include 1) hornblende in I-type and muscovite in S-type, 2) needle-like apatite inclusions common in biotite and hornblende of I-type, whereas, it occurs as larger discrete crystals in S-types, 3) I-type contain hornblende-bearing xenoliths of igneous appearance and in S-type, metasedimentary xenoliths are common and, 4) when both types occur together in composite batholiths, the S-type with strong foliation are intruded by later I-type usually of massive igneous appearance, thus further confirming the distinction between I-type and S-type granites in the Bald Hill area.

The I-type granites are particularly soda-rich in character, as shown by their low K ratios (K_2O/K_2O+Na_2O) which range from average of 0.16 in TP to average of 0.27 in GP (compared to 0.51 to 0.55 in the S-type granites). The major element data for the Lyell Porphyry and the Bald Hill Granites have been plotted on an alkali plot of K_2O versus Na_2O (Fig. 4-13), AFM (Fig. 4-14a), CKN (Fig. 4-14b), normative Q-Ab-Or (Fig. 4-15) and An-Or-Ab (Fig. 4-16) diagrams and in each diagram two separate fields for I-type and S-type granites are distinguished.

On the AFM diagram (Fig. 4-14a) the Lyell Porphyry series show a trend from the GP to TP similar to the curve for the granitic series from the Lower California batholith (Carmichael et al., 1974), suggesting the porphyries crystallized from the differentiation of a single silicate melt. The Bald Hill Granites appear to be a (quartz-rich)
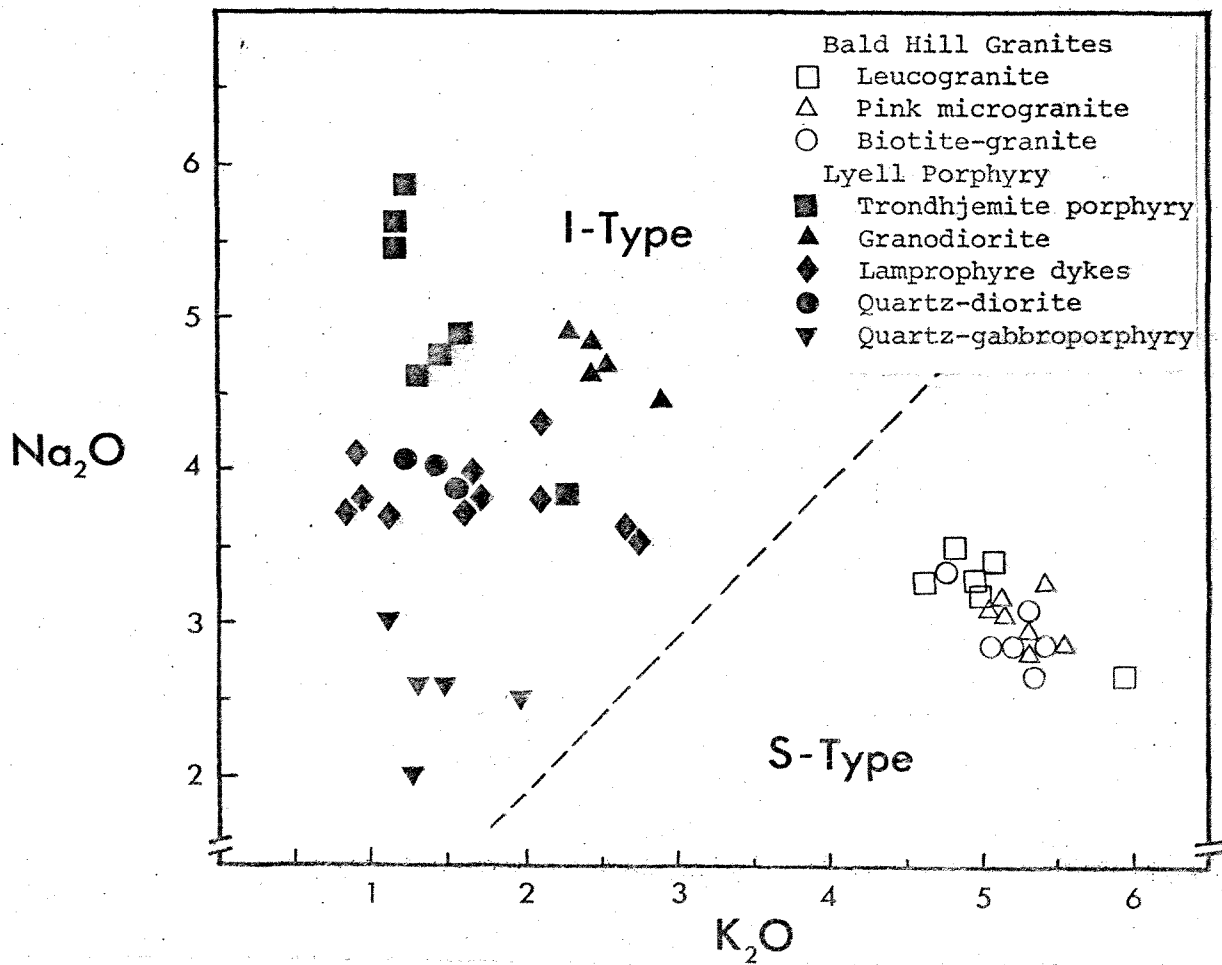
Fig. 4-13: Alkali diagram (K_2O vs. Na_2O) for Bald Hill Granites and Lyell Porphyry suite.
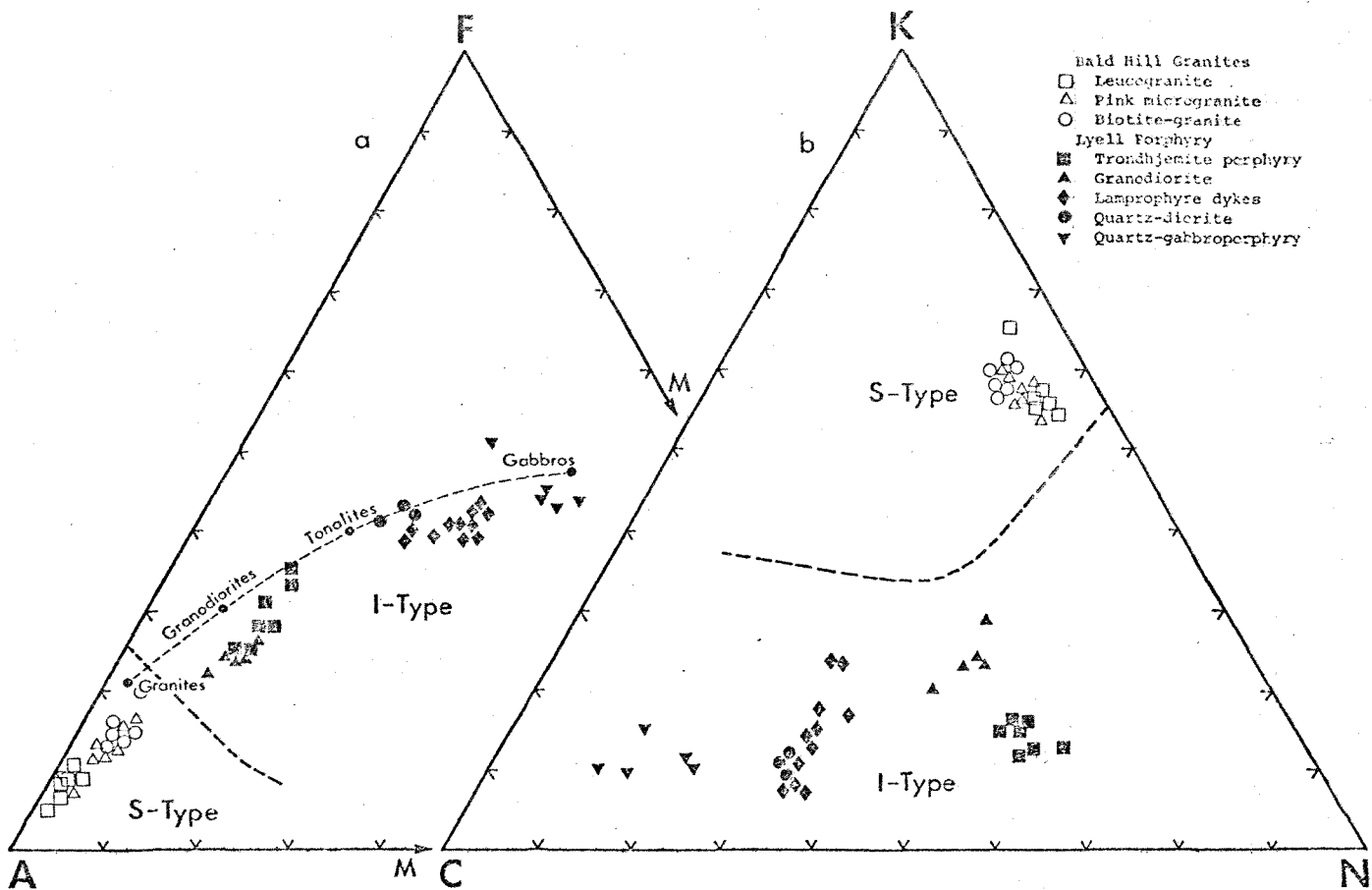
Fig. 4-14a and b: AFM and CKN plots of Bald Hill Granites and Lyell Porphyry rocks.
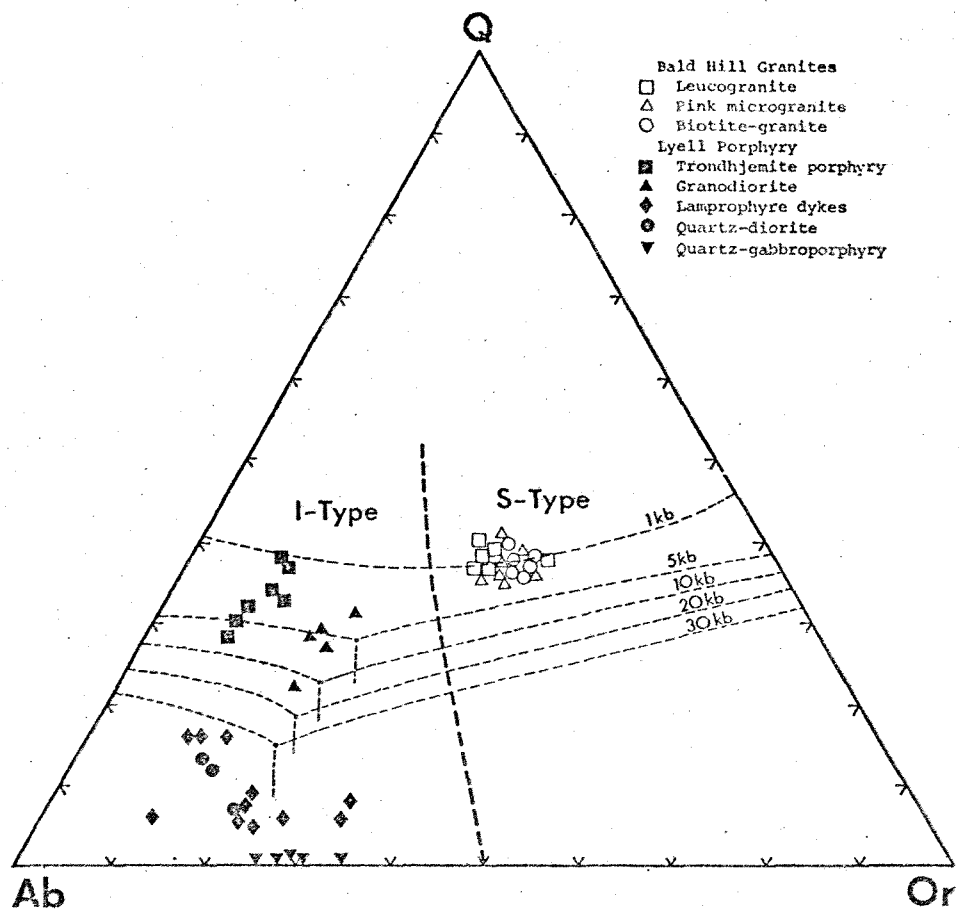
Fig. 4-15: Normative Q-Ab-Or diagram with P_{H_2O} isoboric eutectics for all Bald Hill plutonic rocks.
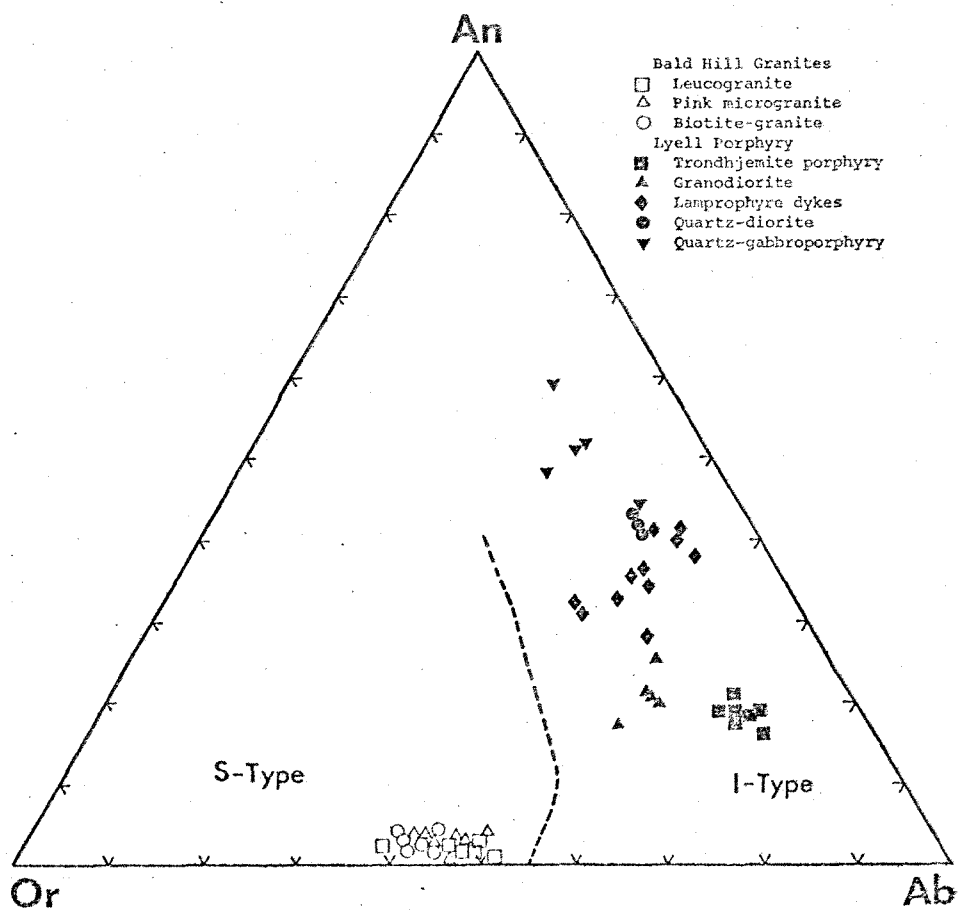
Fig. 4-16: Normative An-Or-Ab diagram for all Bald Hill plutonic rocks.

extension of this differentiated series, although the CKN,

normative Q-Ab-Or and Or-Ab-An plots and trace element

composition do not support this.

The 1 Kb, 5 Kb, 10 Kb, 20 Kb and 30 Kb P_{H_2O} eutectic

curves have been plotted on the Q-Ab-Or diagram (Fig. 4-15)

(after Tuttle and Bowen, 1958; Coats, 1968; Wyllie, 1977).

The Bald Hill Granites all plot around the 1 Kb eutectic

(equivalent to depth of origin approximately 4 km), whereas

the Lyell Porphyry sequence all plot below the 1 Kb eutectic

(ie: TP $\approx$3 Kb, GD $\approx$5 Kb, with LD, DI and GP >10 Kb). The

TP P_{H_2O} is approximately equal to 10 km, GD to 15 km and

more mafic rocks to >30 km depth of origin.

Unpublished major and trace element analyses for the

minor Mo-bearing granitic intrusives from the Karamea Bend,

Eliot Creek and Taipo Spur molybdenum occurrences and

Karamea batholith granites (Luna Granite) from Taipo Spur

are given in Table 4-9 (source: Rabone, 1977). Table 4-10

presents previously published and unpublished major element

data for minor Mo-bearing granitoid intrusives associated

with the Cascade Creek (Berlins Porphyry: Nathan, 1974),

Copperstain Creek (source: Wodzicki, 1972), and Canaan

(source: Peters, 1974) molybdenum occurrences. All other

available major element analyses for Karamea batholith

granites and Separation Point Granites are given in Table 4-11

(source: Challis, 1971). CIPW norms have been calculated.

The analyses have been plotted on Na_2O/K_2O (Fig. 4-17),

ternary AFM (Fig. 4-18a), CKN (Fig. 4-18b) and normative

Q-Ab-Or (Fig. 4-19) and An-Or-Ab (Fig. 4-20) diagrams and

Table 4-9: Unpublished major and trace element analyses for Karamea Bend, Eliot Creek and Taipo Spur (source: Rabone, 1977), with calculated CIPW Norms.

	26895	26796	26797	26725	26726	26727	26728	26823	26825	26827	26842	26843
Type [1]	KB	KB	KB	EC	EC	EC	EC	TG	TG	TG	LG	LG
SiO_2	70.16	70.57	69.48	72.50	70.30	69.60	70.30	74.65	70.91	71.00	71.26	61.29
TiO_2	0.31	0.27	0.37	0.26	0.27	0.23	0.23	0.08	0.32	0.27	0.48	0.96
Al_2O_3	16.53	16.91	16.75	16.04	16.25	15.95	16.20	14.29	15.10	15.30	14.47	16.69
Fe_2O_3	1.40	0.77	0.58	0.64	0.93	0.64	0.74	0.63	1.29	1.58	1.68	2.38
FeO	0.30	0.30	1.70	0.74	0.56	0.71	0.59	0.40	0.50	0.60	1.30	3.70
MnO	0.04	0.02	0.03	0.04	0.04	0.05	0.04	0.05	0.03	0.04	0.07	0.16
MgO	0.33	0.22	0.32	0.40	0.50	0.40	0.51	0.17	0.50	0.52	1.52	2.11
CaO	0.53	0.86	1.03	1.48	1.52	1.87	1.50	1.28	1.61	2.39	1.67	2.58
Na_2O	6.50	5.50	4.47	5.65	6.15	6.65	5.85	5.12	4.92	5.12	3.30	2.55
K_2O	3.60	4.41	3.11	2.82	2.80	2.94	2.85	3.66	3.59	2.96	3.26	5.19
P_2O_5	0.11	0.09	0.12	0.14	0.22	0.15	0.15	0.05	0.13	0.16	0.34	0.38
L.O.I. [2]	0.60	0.68	0.66	0.19	0.44	0.52	1.02	0.42	0.70	0.20	1.20	1.74
Total	100.41	100.60	98.62	100.90	99.98	99.35	99.98	100.80	99.60	100.14	100.55	99.73
Fe_2O_3 [3]	1.73	1.10	2.47	1.46	1.55	1.43	1.40	1.07	1.85	2.25	3.12	6.49
Ba	1210	1390	740	750	980	980	770	1120	1870	1770	390	510
Cu	100	75	80	80	105	50	80	43	94	70	55	40
Zn	71	49	165	172	148	66	126	30	21	23	-	103
Pb	11	27	7	69	16	8	30	30	13	16	23	10
Mo	5	5	5	3	4	6	6	5	8	4	6	2
S	790	1400	10	40	15	60	60	10	4680	3460	870	360
Sr	1127	1005	1192	955	1105	937	945	608	952	1158	245	180
Rb	103	109	90	110	108	118	102	172	91	63	118	169
Zr	457	434	510	436	418	380	370	254	394	424	236	319
Th	20	14	22	15	21	17	19	31	22	23	22	16

CIPW Norms (Weight percent)

	26895	26796	26797	26725	26726	26727	26728	26823	26825	26827	26842	26843
Q	17.26	19.78	28.28	41.03	20.43	15.98	21.74	28.10	24.72	24.62	34.55	17.38
C	1.24	1.74	4.44	0.98	0.86	-	1.12	-	0.50	-	3.29	3.10
or	21.27	26.06	18.38	0.83	16.54	17.37	16.84	21.63	21.21	17.49	19.26	30.67
ab	55.00	46.54	37.82	23.86	52.04	56.27	49.50	43.32	41.63	43.32	27.92	21.57
an	1.91	3.68	4.33	28.03	6.10	4.99	6.46	5.20	7.14	10.02	6.06	10.32
wo }Diop.	-	-	-	-	-	1.38	-	0.34	-	0.33	-	-
fs }Diop.	-	-	-	-	-	0.43	-	0.09	-	-	-	-
en	-	-	-	-	-	0.87	-	0.23	-	0.28	-	-
fs }hyp.	-	-	2.09	0.47	-	0.06	0.17	0.08	-	-	0.34	3.54
en }hyp.	0.82	0.55	0.80	3.69	1.24	0.13	1.27	0.20	1.24	1.01	3.79	5.26
fo }ol.	-	-	-	-	-	-	-	-	-	-	-	-
fa }ol.	-	-	-	-	-	-	-	-	-	-	-	-
mt	0.20	0.25	0.84	0.93	1.15	0.93	1.07	0.91	0.78	1.28	2.43	3.45
hm	1.26	0.60	-	-	0.13	-	-	-	0.75	0.70	-	-
ilm	0.59	0.51	0.70	0.49	0.51	0.44	0.44	0.15	0.61	0.51	0.91	1.82
cc	-	-	-	-	-	-	-	-	-	-	-	-
ap	0.25	0.21	0.28	-	0.51	0.35	0.35	0.12	0.30	0.37	0.79	0.88
An100/(ab+an)	3.36	7.32	10.26	54.01	10.50	8.14	11.55	10.71	14.63	18.78	17.84	32.35
D.I. [4]	93.53	92.38	84.48	65.72	89.02	89.62	88.01	93.06	87.57	85.43	81.74	69.63
S.I. [5]	2.72	1.96	3.14	25.43	4.57	3.53	4.84	1.70	4.63	4.82	13.74	13.24

(1) KB: Karamea Bend Mo-bearing Intrusive
EC: Eliot Creek Mo-bearing Intrusive
TG: Taipo granite Mo-bearing Intrusive
LG: Luna granite (Karamea phase) from Taipo Spur
(2) Loss on ignition
(3) Total iron as Fe_2O_3
(4) Differentiation Index after Thornton and Tuttle (1960)
(5) Solidification Index after Kuno et al.(1957)

Table 4-10: Published and unpublished major element analyses for Berlins Porphyry, Copperstain Creek and Canaan granites with calculated CIPW Norms.

	UC5192	P38077	P38728	P38651	P38738	31470	23241	23242	23244	23246	23247	32366	23272
Type [1]	BP	BP	BP	BP	BP	CS	CA	CA	CA	CA	CA	CA	CA
SiO_2	70.20	68.50	64.90	69.50	68.70	64.47	71.00	70.30	69.40	70.70	70.70	68.90	72.30
TiO_2	0.32	0.33	0.78	0.38	0.39	0.51	0.30	0.30	0.30	0.20	0.20	0.30	0.20
Al_2O_3	15.00	15.60	15.90	15.60	16.00	16.63	13.60	13.10	14.00	14.20	15.00	14.60	13.60
Fe_2O_3	1.20	0.59	1.67	0.91	0.77	4.75	2.60	2.60	4.60	0.80	0.80	1.00	1.00
FeO	1.60	2.31	3.01	1.91	1.80	-	0.90	0.90	0.90	1.20	0.90	1.40	0.60
MnO	0.04	0.04	0.00	0.04	0.04	0.00	0.02	0.01	0.05	0.18	0.02	0.01	0.01
MgO	1.60	1.37	2.76	1.13	1.39	2.31	0.20	0.30	0.30	0.10	0.65	1.30	0.40
CaO	1.60	2.23	3.27	1.60	1.50	3.81	1.50	1.50	2.30	2.00	2.50	1.80	0.60
Na_2O	3.90	3.83	3.30	3.78	3.78	3.45	4.50	5.00	3.60	6.00	6.40	4.00	4.20
K_2O	3.40	3.60	3.17	3.27	3.56	2.31	4.50	4.50	3.30	4.00	2.50	4.00	4.50
P_2O_5	0.14	0.16	0.23	0.14	0.16	-	0.20	0.10	0.10	0.05	0.05	0.15	0.15
L.O.I. [2]	1.40	0.80	0.90	0.80	0.85	-	0.10	0.80	1.00	0.28	0.20	2.00	2.00
Total	100.80	99.40	100.20	99.10	98.90	99.24	99.42	99.41	99.85	99.71	99.92	99.46	99.56
Fe_2O_3 [3]	2.98	3.16	5.01	3.03	2.77	5.08	3.60	3.60	5.60	2.13	1.80	2.56	1.67

CIPW Norms (Weight percent)

Q	28.41	24.58	21.80	29.28	27.30	23.76	25.19	22.08	30.74	17.57	18.97	24.37	29.19
C	2.33	1.73	1.64	3.27	3.58	1.79	-	-	0.56	-	-	0.78	1.09
or	20.09	21.27	18.73	19.32	21.07	13.65	26.59	26.59	19.50	23.64	14.77	23.64	26.59
ab	33.00	32.41	27.92	31.98	31.98	29.19	38.08	42.31	30.46	50.77	54.15	33.85	35.54
an	7.02	10.01	14.72	7.02	6.40	18.18	3.62	0.01	10.76	-	4.82	7.95	2.00
wo } Diop.	-	-	-	-	-	-	0.58	0.86	-	1.65	2.49	-	-
fs } Diop.	-	-	-	-	-	-	-	-	-	1.55	0.70	-	-
en	-	-	-	-	-	-	0.50	0.75	-	0.25	1.62	-	-
fs } hyp.	1.49	3.28	2.86	2.20	2.10	3.29	0.47	1.96	-	2.36	0.54	1.27	-
en } hyp.	3.99	3.41	6.87	2.82	3.46	5.75	-	-	0.75	-	-	3.24	1.00
fo } ol.	-	-	-	-	-	-	-	-	-	-	-	-	-
fa } ol.	-	-	-	-	-	-	-	-	-	-	-	-	-
mt	1.74	0.85	2.42	1.32	1.12	2.54	2.10	2.06	2.19	1.16	1.16	1.45	1.39
hm	-	-	-	-	-	-	1.15	1.17	3.09	-	-	-	0.04
ilm	0.61	0.63	1.48	0.72	0.74	0.97	0.57	0.57	0.57	0.38	0.38	0.57	0.38
cc	-	-	-	-	-	-	-	-	-	-	-	-	-
ap	0.32	0.37	0.53	0.32	0.37	0.25	0.46	0.23	0.23	0.12	0.12	0.35	0.35
An100/(ab+an)	17.55	23.61	34.52	18.00	16.66	38.38	8.68	0.02	26.09	0.00	8.17	19.02	5.32
D.I. [4]	81.50	78.26	68.45	80.59	80.32	66.61	89.87	90.98	80.70	91.97	87.90	81.86	91.32
S.I. [5]	13.67	11.71	19.84	10.27	12.30	18.02	1.57	2.26	2.36	0.83	5.78	11.11	3.74

(1) BP: Berlins Porphyry microgranodiorite (Nathan, 1974)
    CS: Copperstain Creek granodiorite (Wodzicki, 1972)
    CA: Canaan Separation Point granites (Peters, 1974)
(2) Loss on ignition
(3) Total iron as Fe_2O_3
(4) Differentiation Index after Thornton and Tuttle (1960)
(5) Solidification Index after Kuno et al., (1957)

Table 4-11: Published major element analyses for Karamea and Separation Point
Granites (Challis, 1971) with calculated CIPW Norms.

Bull. No.	1	5	10	11	15	17	22	25	26	20	23	24
Type [1]	SP	SP	SP	SP	SP	SP	SP	SP	SP	KA	KA	KA
SiO_2	78.04	74.75	73.00	72.97	71.51	71.30	67.78	66.71	66.61	71.04	67.71	67.20
TiO_2	0.27	0.12	0.09	0.07	0.17	0.42	0.37	0.44	0.33	0.48	0.59	0.69
Al_2O_3	12.54	13.39	15.32	15.06	15.47	15.79	16.53	16.74	17.70	14.50	14.93	15.38
Fe_2O_3	0.10	0.57	0.30	0.54	0.88	0.47	1.18	1.27	1.16	0.63	0.58	1.09
FeO	0.12	0.46	0.35	0.34	0.43	0.71	1.10	2.08	0.95	1.98	3.08	3.16
MnO	0.00	0.02	0.04	0.02	0.04	0.05	0.05	0.09	0.04	0.02	0.06	0.05
MgO	0.32	0.23	0.15	0.14	0.28	0.40	0.76	0.91	0.64	0.99	1.25	1.34
CaO	1.57	0.78	1.53	1.71	1.92	1.89	2.82	3.06	3.05	1.31	2.24	2.64
Na_2O	6.02	4.18	5.46	5.20	5.09	4.90	5.14	5.54	6.33	3.12	2.83	3.01
K_2O	0.38	4.66	2.88	3.17	3.36	3.76	3.43	1.88	1.95	4.30	5.51	3.25
P_2O_5	0.03	0.08	0.10	0.04	0.06	0.12	0.15	0.25	0.17	0.24	0.20	0.23
L.O.I. [2]	0.35	0.30	0.43	0.47	0.35	0.63	0.32	0.70	0.42	1.26	0.94	1.52
Total	99.74	99.87	99.95	100.19	99.93	100.36	99.97	100.02	99.89	100.23	100.19	100.17
Fe_2O_3 [3]	0.23	1.08	0.69	0.92	1.36	1.26	2.40	3.58	2.22	2.83	4.00	4.60

CIPW Norms (Weight percent)

	1	5	10	11	15	17	22	25	26	20	23	24
Q	38.14	33.01	26.85	26.91	24.68	23.96	18.00	19.08	15.17	31.76	22.10	28.49
C	--	0.89	0.68	0.68	0.11	0.51	-	0.63	0.04	2.91	0.72	2.66
or	2.25	23.99	17.02	17.02	19.85	22.22	20.27	11.11	11.52	25.41	32.56	19.20
ab	50.94	35.37	46.20	46.20	43.07	41.46	43.49	46.88	53.56	26.40	23.95	25.47
an	6.07	3.35	6.94	6.94	9.13	8.59	11.90	13.55	14.02	4.93	9.81	11.59
wo }Diop.	0.44	-	-	-	-	-	0.46	-	-	-	-	-
fs }Diop.	-	-	-	-	-	-	0.09	-	-	-	-	-
en	0.38	-	-	-	-	-	0.33	-	-	-	-	-
fs }hyp.	-	0.21	0.32	0.14	-	0.31	0.43	2.21	0.32	2.36	4.31	3.86
en }hyp.	0.42	0.57	0.37	0.37	0.70	1.00	1.56	2.27	1.59	2.47	3.11	3.34
fo }ol	-	-	-	-	-	-	-	-	-	-	-	-
fa }ol	-	-	-	-	-	-	-	-	-	-	-	-
mt	-	0.83	0.44	0.78	1.02	0.68	1.71	1.84	1.68	0.91	0.84	1.58
hm	0.10	-	-	-	0.17	-	-	-	-	-	-	-
ilm	0.25	0.23	0.17	0.13	0.32	0.80	0.70	0.84	0.63	0.91	1.12	1.31
cc	-	-	-	-	-	-	-	-	-	-	-	-
ap	0.07	0.19	0.23	0.23	0.14	0.28	0.35	0.58	0.39	0.56	0.46	0.53
An 100/(ab+an)	10.65	8.65	13.05	13.05	17.49	17.16	21.48	22.42	20.75	15.74	29.05	31.28
D.I. [4]	91.33	92.37	90.07	90.13	87.61	87.64	81.76	77.06	80.26	83.57	78.60	73.17
S.I. [5]	4.61	2.42	1.64	1.60	2.79	3.91	6.54	7.79	5.80	8.98	9.43	11.31

(1) SP: Separation Point Granite
    KA: Karamea phase Granite
(2) Loss on ignition
(3) Total iron as Fe_2O_3
(4) Differentiation Index after Thornton and Tuttle (1960)
(5) Solidification Index after Kuno et al., (1957)
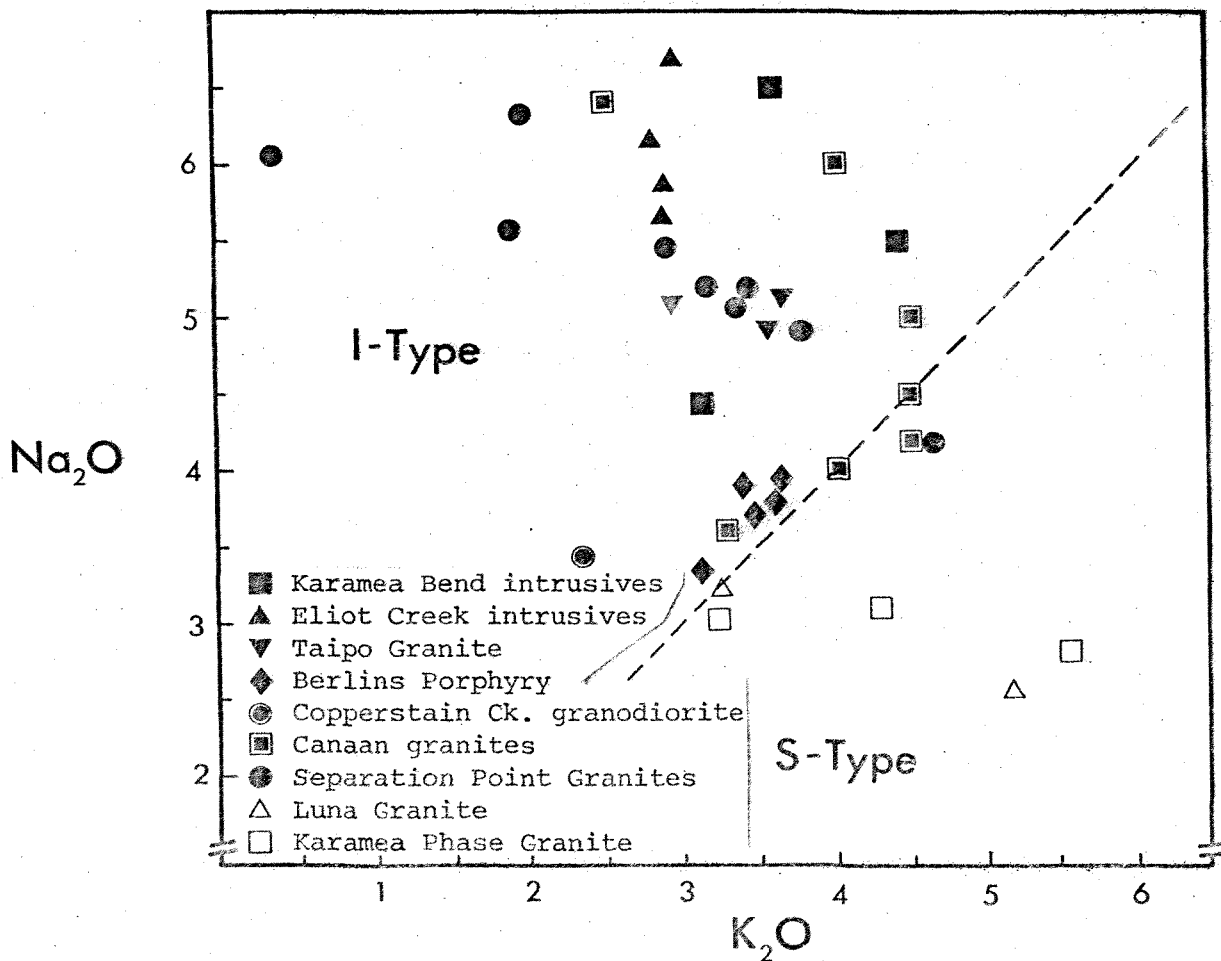
Fig. 4-17: Alkali diagram (K$_2$O vs. Na$_2$O) for other minor intrusive and 'batholith' granites of West Nelson.
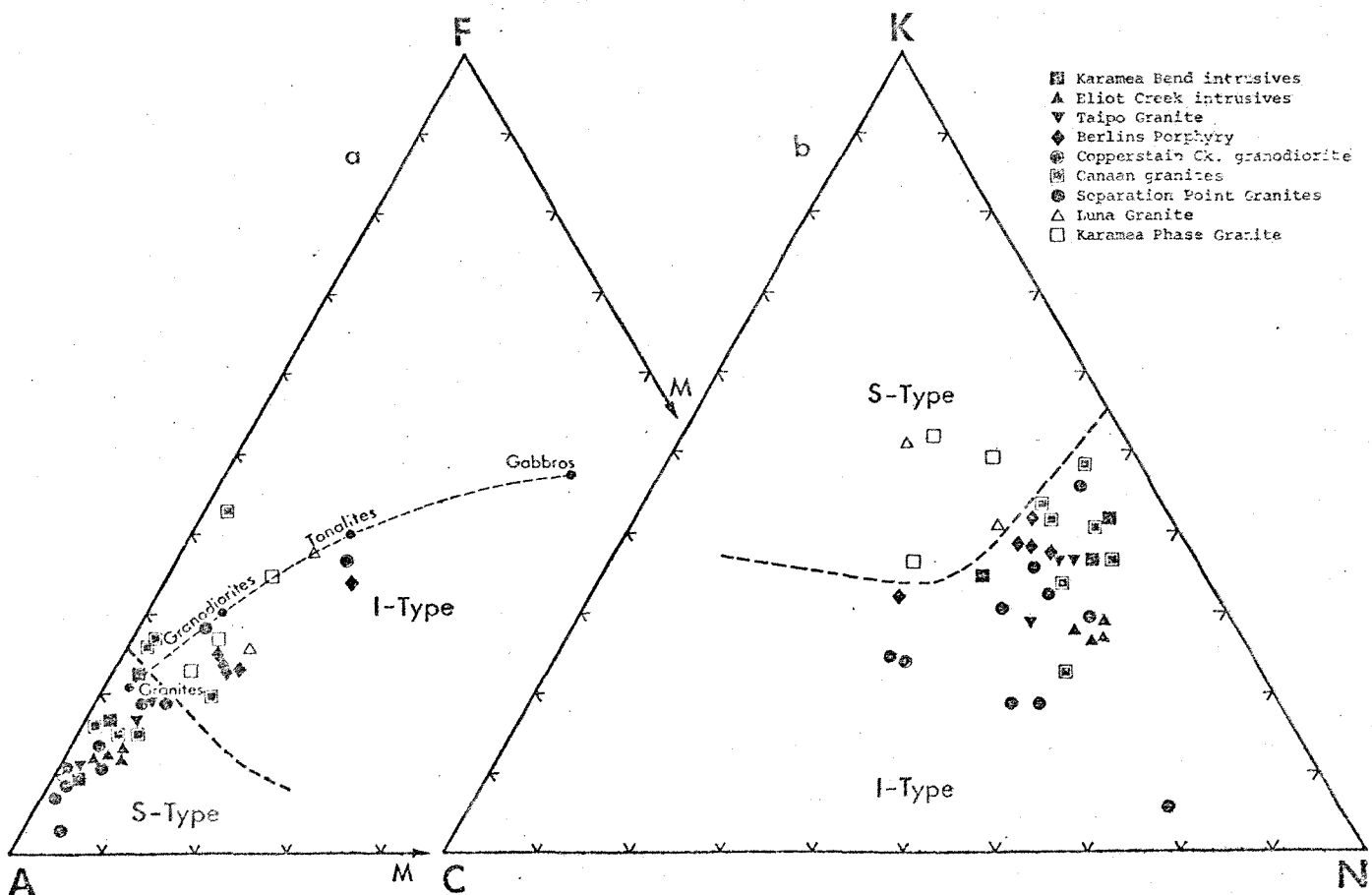
Fig. 4-18a and b: AFM and CKN plots of other minor intrusive and 'batholith' granites of West Nelson.
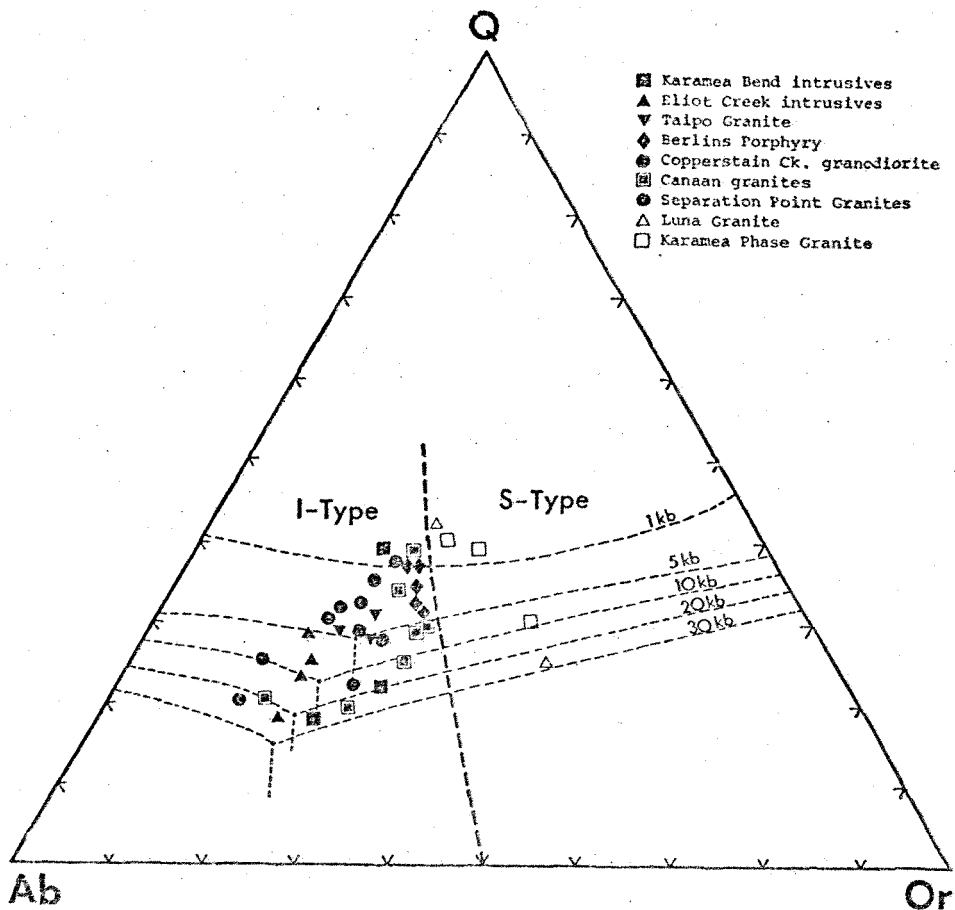
Fig. 4-19: Normative Q-Ab-Or diagram with P_{H_2O} isobaric eutectics for other minor intrusive and 'batholith' granites of West Nelson.
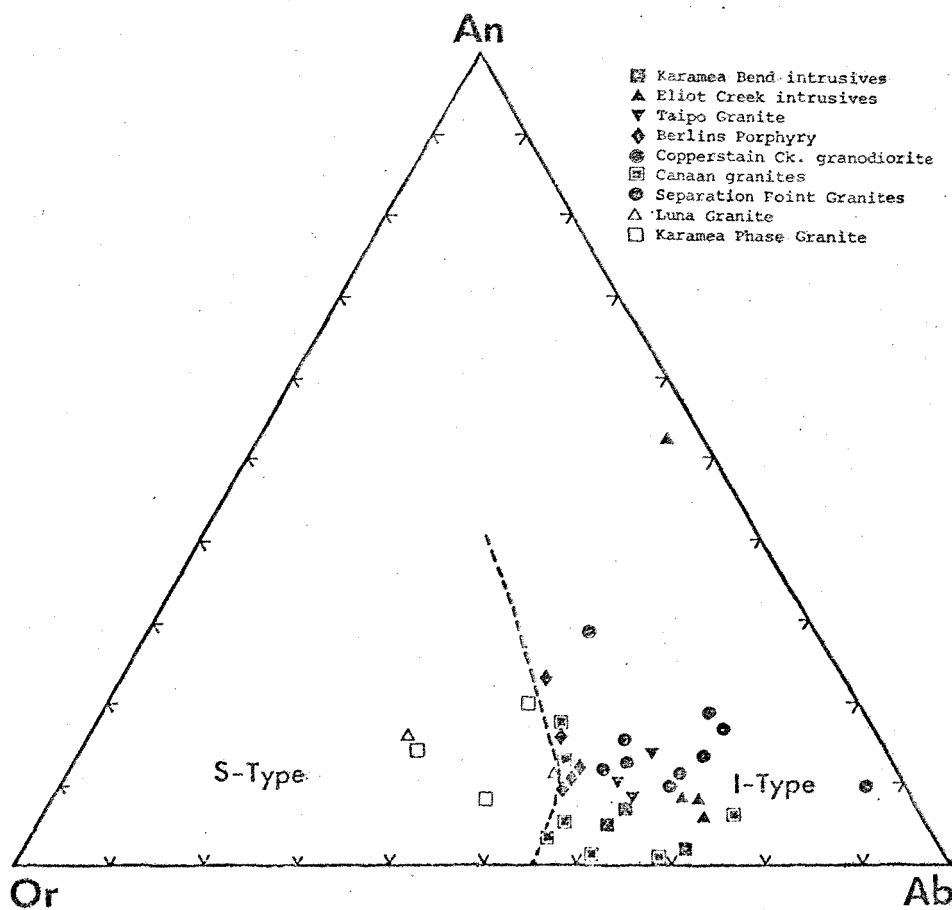
Fig. 4-20: Normative An-Or-Ab diagram for other minor intrusive and 'batholith' granites of West Nelson.

compared with fields for I-type and S-type granites based
on the Bald Hill suite of plutonic rocks. Minor intrusive
granitic rocks from all the molybdenum occurrences for which
major element data is available display a typical calc-
alkaline chemistry and conform to the I-type criteria of
Chappell and White (Table 4-8). The Mol. $Al_2O_3/(Na_2O+K_2O+CaO)$
ratios for some Karamea intrusives (sample 26797) and the
Berlins Porphyry (samples UC 5192, P38651 and P38738) are
>1.1 and the geochemistry of these rocks appears to be
somewhat transitional from I-type to S-type granites. All
of the Separation Point data (16 analyses) conforms to
I-type classification. The Luna Granite (from Taipo Spur)
and Karamea batholith granites are shown to be S-types.
The normative Q-Ab-Or diagram (Fig. 4-19) shows that the
transitional type granites have originated under lower P_{H_2O}
conditions (ie: shallower) than other Mo-bearing intrusives.
All other I-type intrusive rocks (ie: Canaan, Eliot Creek,
Taipo Spur, Karamea Bend, Copperstain Creek, and Separation
Point intrusives) are shown to have originated under similar
P_{H_2O} conditions to the Lyell Porphyry.

Petrogenesis of I-type and S-type Granites:

The terms "ultrametamorphism" and "granitoid magma"
are used in the following sense in the discussion on the
origin of I-type and S-type granites:

Ultrametamorphism is metamorphism within the earth's
crust where temperatures have been high enough for rocks
to begin to melt. White and Chappell (1977) reason that,

for melting to occur with geologically reasonable amounts
of water within the crust, there must be temperatures of
>750°C and pressures of <10 Kb (or <15 Kb if granitic rocks
are to be produced in regions of crustal thickening).

Granitoid magma implies a mixture of melt and solid
material (residue = restite). The restite in the granitoid
magma has not necessarily crystallized from melt (ie: can
be relict source material) and large bodies of granite
crystallized from pure melts are considered to be rare (White
and Chappell, 1977). The bulk composition of the granitoid
magma will reflect its source.

The I-type and S-type classification is essentially
based on geochemistry and the two granitic rock types are
considered to be derived by:

1) S-type: Geochemical characteristics of S-type granites
   are consistent with products of ultrametamorphism of
   sediments within the crust (White and Chappell, 1977:
   Wyllie, 1977). Weathering and depositional processes
   of sediments release Na and Ca which are removed in
   solution and give rise to clays which absorb K during
   sedimentation and diagenesis. S-type granites derived
   from the ultrametamorphism of these sedimentary rocks
   have the same chemical characteristics (eg: Bald Hill
   Granites and Karamea 'batholith' granites). White and
   Chappell (1977) also state "during the processes of
   weathering and deposition, pelitic rocks are enriched
   in Rb relative to Sr...." and therefore high Rb/Sr
   ratios in the S-type granites are characteristic of

granites derived from a pelitic source. The lack of linear trends on the variation diagrams when compared to I-type granitic rocks are probably due to metasedimentary sources being more heterogeneous in original composition.

2) I-type: The geochemistry of these granitoids indicate two possible sources: (a) partial anatexis of crustal material, with I-type granites crystallizing from the separated melt. Melts formed by the ultrametamorphism of shales and greywackes have been experimentally shown to be of granitoid composition (eg: Kilinc, 1972), granitoid magma being the minimum melt of any system containing feldspar and quartz (White and Chappell, 1977; White et al., 1974; Wyllie, 1977), or (b) by partial anatexis of rocks of primary igneous origin within the earth's crust (White and Chappell, 1977). High Na/K and high total alkali plus calcium relative to alumina are characteristic of igneous rocks that have not been through a weathering cycle and these characteristics are retained during the production of an I-type granitoid magma. The linear relationships on variation diagrams result from a more homogeneous (igneous) source.

The geochemical characteristics of a particular granite reflect 1) the nature of parental material; 2) the degree of partial melting of that material; and 3) the ratio in which the partial melt and the residuum left after partial

melting (restite) are mixed together (or unmixed from
each other) (White and Chappell, 1977; Price and Taylor,
1977).

At the source, the two products of partial melting are
melt and solid residual forming a granitoid magma, the
proportion of which depends on the degree of partial melting
which in turn is dependent on source rock composition,
temperature, pressure and volatile content. Restite can
be recognised as xenoliths, clots or xenocrysts and the
habit of apatite in I-type granites, and xenocrysts of
biotite, cordierite and/or garnets in S-type granites.
Tiny needles of rutile scattered throughout various minerals,
particularly biotite in the quartz trondhjemite (see
Fig. 3-12), needle-like apatite in more basic porphyry
rocks and clots of biotite in the gneissic granites, would
represent restite in the Bald Hill rocks.

White and Chappell (1977) consider the amount of melt
need not be high at the source (probably <50%). The
products of partial melting can move upwards to form
granitoid plutons or volcanic rocks. Due to the high
viscosity of a granitoid magma, the mass can diapirically
move upwards, the melt progressively freeing itself from
its residue. White and Chappell (1977) consider that the
criteria for rocks consisting largely of residue, include
the complete absence of complexly zoned plagioclases, and the
presence of cordierite and elements such as Mg and Ni near
zero and SiO_2 near 76% (ie: av. Bald Hill Granite, Table 4-12
and (R) Fig. 4-21). If a rock has these criteria it will be

Table 4-12: Approximations to the average bulk chemistry of the
Bald Hill Granites, Lyell Porphyry and possible source
rock, Greenland metasediments.

	B.H.G. [1]	G.M. [2]	L.P. [3]
SiO_2	73.01	70.54	58.01
TiO_2	0.16	0.67	0.94
Al_2O_3	14.58	14.04	17.10
Fe_2O_3	0.15	0.67	1.92
FeO	1.07	3.83	3.94
MnO	0.01	0.04	0.84
MgO	0.35	2.34	3.85
CaO	0.66	0.31	5.49
Na_2O	3.03	1.59	4.00
K_2O	5.15	2.83	2.38
P_2O_5	0.27	0.16	0.28
Ba	145	370	436
Cu	15	20	72
Ni	6	31	35
Zn	41	78	83
Pb	33	25	17
Mo	2	2	4
S	110	300	2000
Sr	40	42	786
Rb	320	152	75
Zr	50	180	140
Th	8	12	5
Y	10	30	25

(1) Av. Bald Hill Granite

(2) Av. Greenland metasediment (4 gke + 1 arg)

(3) Av. Lyell Porphyry
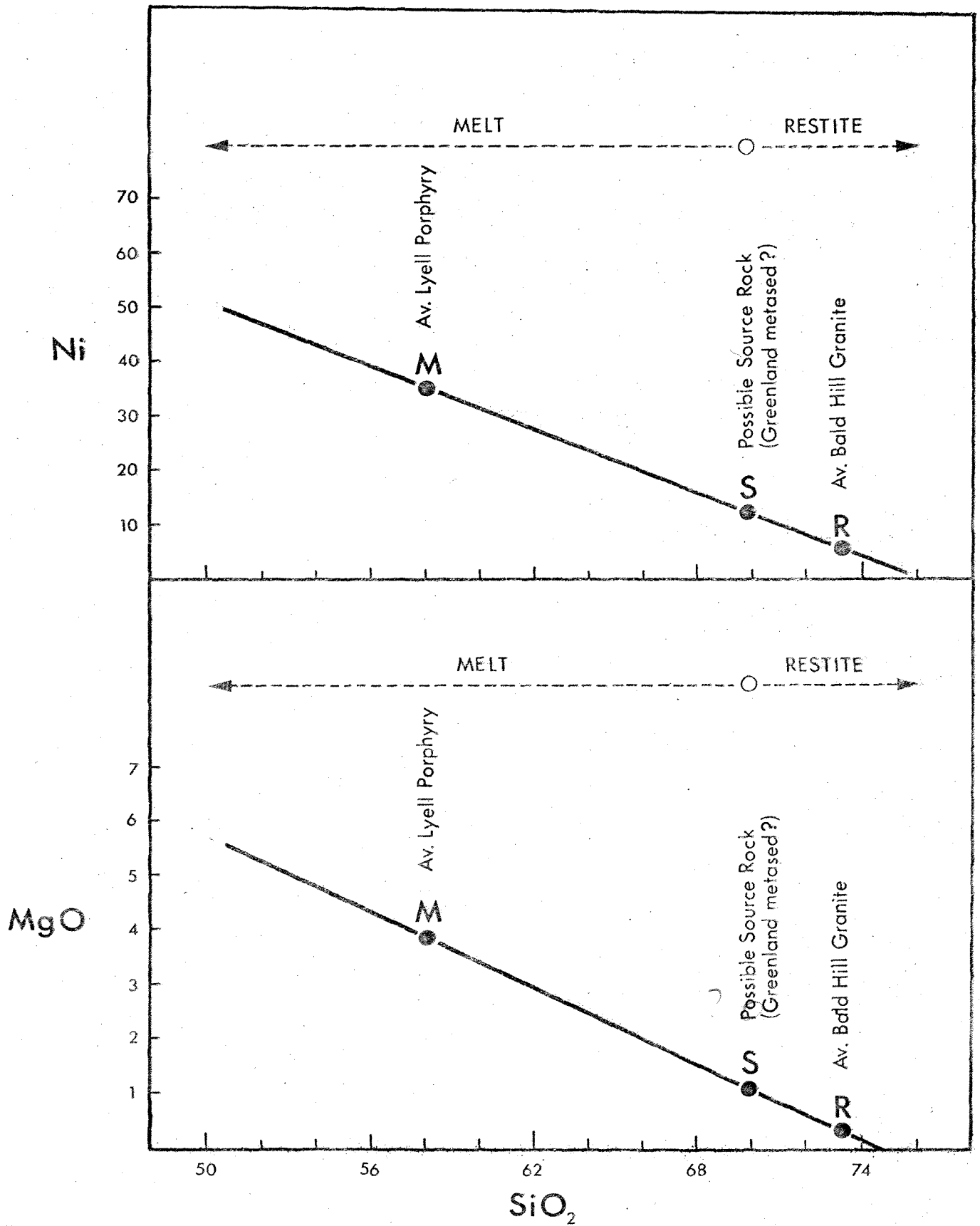
Fig. 4-21: MgO-SiO$_2$ and Ni-SiO$_2$ variation diagrams for 'average' Bald Hill Granites, Lyell Porphyry and Greenland Group metasediments.

an S-type granite. The same fusion event will produce a granitoid magma where melt is >restite, and will lie along the "unmixing line" (ie: line of progressive separation of melt from restite) at M in Fig. 4-21 (ie: av. Lyell Porphyry, Table 4-12), and correspond to an I-type granite. The source rock, S (see Fig. 4-21), will have an intermediate composition of elements which would enter a minimum melt (ie: SiO_2, MgO, K_2O, Ni, S and Rb). An approximation to the original bulk geochemical composition of the Greenland metasediments (ie: ≈4 greywacke plus ≈1 argillite, see Table 4-12) show these rocks to be possible source material, plotting approximately at S in Fig. 4-21 (NB: 4 gke plus 1 arg are estimated proportions of greywacke and argillite comprising the Greenland Group metasediments from field evidence.)

White et al. (1974), showed that the presence of primary muscovite in the S-type granites limits its crystallization conditions to the region below the muscovite breakdown curve and above the water-saturated granite solidus (White et al., Fig. 4, p.165) which is equivalent to a pressure of 4-5 Kb and a temperature of 650° to 750°C. Water-saturated muscovite bearing granites (ie: restite) cannot move upwards to lower pressure regimes without passing through their own solidus and hence crystallizing. They could not therefore form co-magmatic volcanic rocks. The H_2O-undersaturated melt produced by such an event however, can intrude the overlying sediments, forming subvolcanic intrusions of I-type granites and possibly reach the surface to form alkalic

tuffs (eg: Stitts Tuff at base of the Ohika Beds), both
of which have since been eroded off.

Brown and Fyfe (1970) from experimental studies
proposed that: if homogeneous crustal material is progressively
buried and heated, a series of liquids would be produced
starting from granitic fractions and moving towards more
basic types with increasing pressure and temperature" and
suggested that, due to the high viscosity of the overlying
crust, only large volumes of liquid would be capable of rising
fast enough to avoid cooling and crystallization. Hence
small volumes of H_2O-undersaturated liquid would soon
crystallize in the overlying granites, unless some structural
weakness, i.e. vertical to near vertical dipping faults, are
present, enabling more rapid rise of the melt. Brown and
Fyfe (1970) state: "There is also no reason why melting at
more than one level should not be virtually synchronous"
and suggest that the situation within many continental
margin batholiths where younger granites intrude older
granite masses supports this model of synchronous melting
at various depths.

Initial $^{87}Sr/^{86}Sr$ ratios; oxygen and hydrogen isotope
compositions have also been used to characterise I-type and
S-type granite suites (eg: Chappell and White, 1974; O'Neil
and Chappell, 1977; O'Neil et al., 1977). Granitic rocks
with low initial $^{87}Sr/^{86}Sr$ (<0.706) and δO^{18} (7.7-9.9) values
preclude all but insignificant contribution of old crustal
material to the formation of calc-alkaline magmas (ie: I-type)
while high $^{87}Sr/^{86}Sr$ (>0.706) and δO^{18} (10.4-12.5) values

are characteristic of a sedimentary source. However, as shown by Flood and Shaw (1977), low initial $^{87}Sr/^{86}Sr$ ratios of 0.706 for two S-type granitic suites from the New England Batholith in N.S.W. reflect the volcanoclastic nature and young age of the sedimentary source for these granites at the time of melting. Thus, variations in the composition of source material at the site of melt generation and/or later contamination of a primary magma by crustal sediments could produce granites transitional from S-type and I-type such as the 'transitional-type' granites from Karamea Bend (sample 26797) and the Berlins Porphyry (samples UC5192, P38651 and P38738) in West Nelson.

In summary, the S-type granites in West Nelson forming the Karamea Granite batholith were probably formed by ultra-metamorphism of sedimentary material with similar bulk chemistry to the Ordovician Greenland sediments. The H_2O-saturated S-type granites were formed at pressures of approximately 4-5 Kb and temperatures of about 700° to 750°C and formed virtually in place with little upward movement. Any H_2O-undersaturated melts produced would have intruded the overlying metasediments and since been eroded off. The Mo-bearing I-type granites represent the H_2O-undersaturated melt phase of granitoid magmas (residual probably granulites, Brown & Fyfe and others) produced by increasing pressure and temperature with increasing depth of burial, which have intruded the overlying S-type granites and adjacent metasediments, the emplacement being controlled by near vertical dipping faults. These I-type granites were formed

at pressures of >5 Kb and temperatures >800°C (H_2O-undersaturated melts are generally considered to form well above the granite liquidus), the range in composition a result of synchronous melting at various depths in the crust. The more basic I-types have a deeper origin, possibly melting of pre-existing basement rocks underlying the S-type granites.

CHAPTER FIVE

SULPHIDE MINERALIZATION

Introduction:

Several paragenetically distinct phases of quartz-vein and quartz-sulphide-oxide vein type mineralization cross-cut the hornfels metasediments and some of the porphyritic intrusive rocks (e.g. trondhjemitic porphyry and gabbroporphyry). Exposure of mineralized veins in outcrop is insufficient to determine the exact paragenetic sequence of veining. Minor disseminated mineralization occurs in the porphyritic intrusives and the hornfelsed metasediments.

Thirty representative polished mounts were examined to identify sulphide and oxide mineral phases and to establish equilibrium mineral assemblages for sulphur isotope analyses (Chapter 6). X-Ray Diffraction (XRD) techniques were used to identify silicate and oxide mineral phases. Vickers hardness numbers (VHN) were measured on a Leitz automatic micro-hardness tester following procedures given by Uytenbogaardt and Burke (1971).

I: Quartz veining:

Quartz veins (generally 1-2 cm thick) have no apparent systematic orientation, and appear to be fracture and joint controlled, forming a weak "stockwork type" deposit. Four paragenetically distinct phases of quartz veining at Bald Hill are:
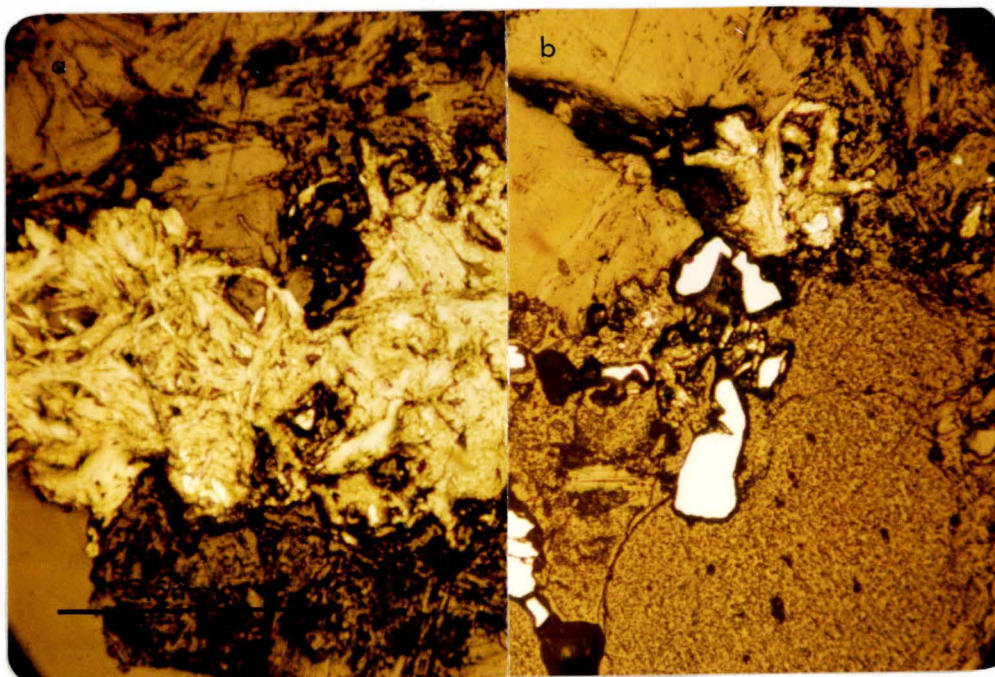
Fig. 5-1a and b: Interleaved molybdenite (pale yellow) and muscovite
and pyrite (white) in quartz vein in biotite hornfels
(18939).
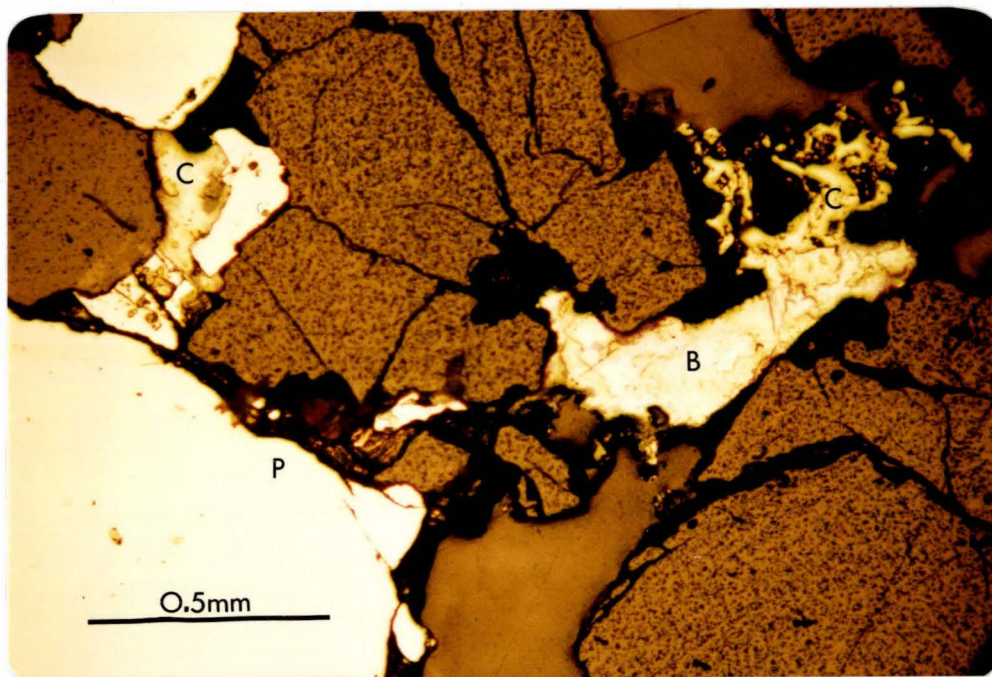
Fig. 5-2:   Chalcopyrite (C) inclusions in pyrite (P) and disseminated
chalcopyrite associated with bismuth (B) mineralization
(18976).

i) Barren quartz veins

ii) Quartz-muscovite±albite veining

iii) Quartz-muscovite-albite-pyrite-chalcopyrite-
molybdenite±magnetite veins

iv) Quartz-muscovite-albite-pyrite-chalcopyrite-
molybdenite-bismuth-bismuthinite±magnetite veins.

Microscopically the pale brown-whitish molybdenite (VHN_{10}:40)
is usually associated with coarse grained pyrite±chalcopyrite
and grey granular magnetite in quartz veins. Molybdenite
often forms interleaved rosette-shaped aggregates with blades
of muscovite (Fig. 5-1a and b) along the rock-quartz vein
interface, with the vein consisting of gangue quartz,
muscovite and albite. Brassy yellow chalcopyrite (VHN_{50}:230)
often forms minor inclusions within the pale yellow pyrite
(VHN_{400}:1080) crystals (Fig. 5-2) and occurs as disseminated
sulphide associated with rare bismuth mineralization.

Strongly anisotropic creamy-white to yellow bismuth
(VHN_{10}:18) is present in some quartz veins. The bismuth
metal (Bi) always shows exsolution replacement by bluish-grey
anisotropic bismuthinite (Bi_2S_3) (VHN_{50}:130) (Fig. 5-3a and b)
and is closely associated with olive green-yellow chalcopyrite.
Bismuth-bismuthinite mineralization is rare and only noted
in sample 18976.

Abundant quartz-sulphide veining is associated with
brecciated and silicified hornfels (zone III) rocks. Coarse
pyrite cubes form 'vugs' of sulphide up to ≈1 cm across.
However, only minor molybdenite and chalcopyrite have been
noted in breccia samples.
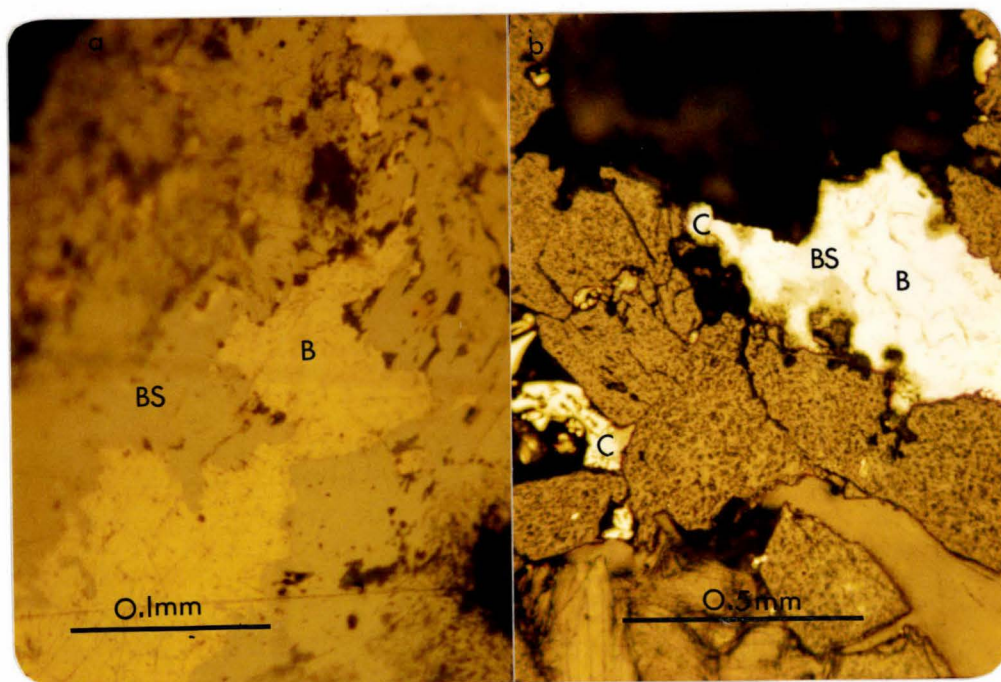
Fig. 5-3a and b: Bismuth (B) pseudomorphed and replaced by
                  bismuthinite (BS) and associated chalcopyrite (C)
                  (18976).
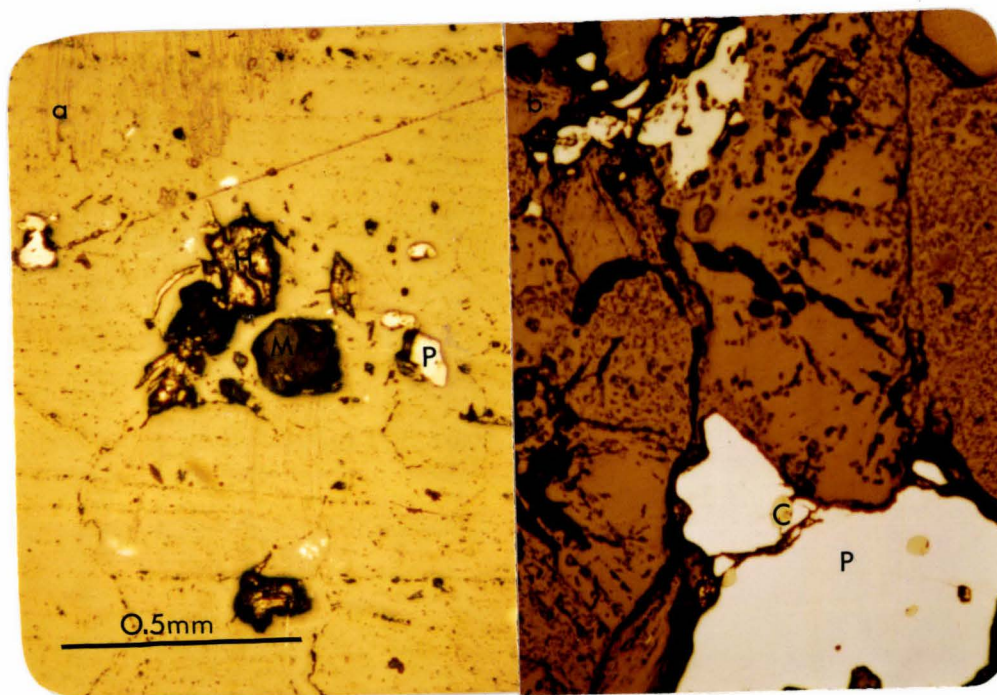
Fig. 5-4: a: Disseminated pyrite (P), magnetite (M) and hematite (H)
              in biotite hornfels (18939).
           b: Disseminated pyrite (P) with chalcopyrite inclusions (C)
              in trondhjemite porphyry (18971).
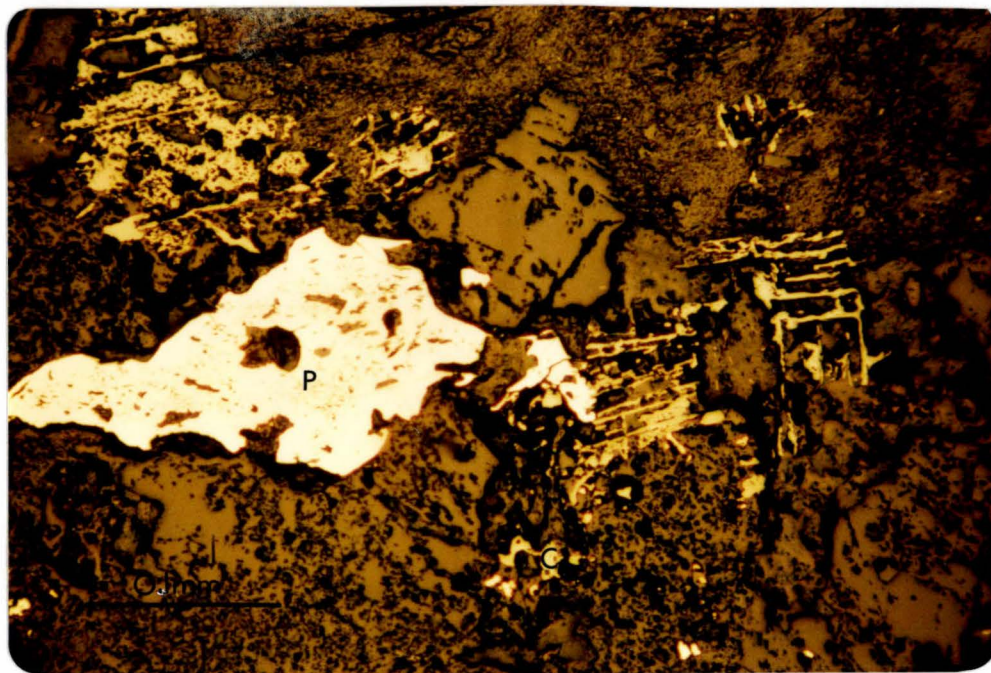
Fig. 5-5: Disseminated pyrite (P), chalcopyrite (C) and magnetite,
           ilmenite and rutile(?) replacing ferromagnesium minerals
           in gabbroporphyry (18908).
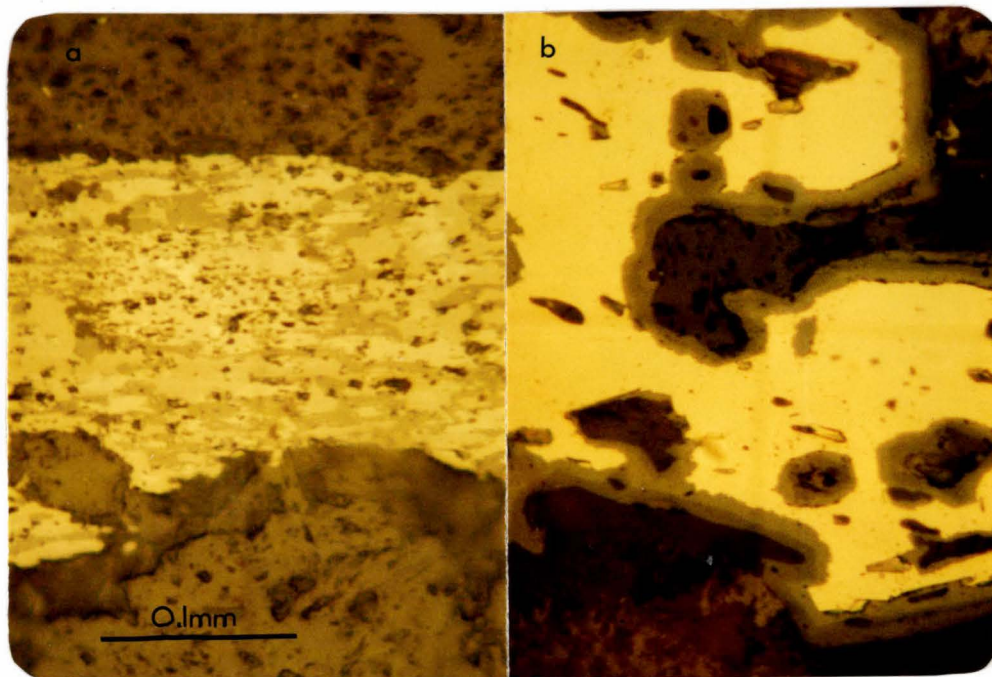
Fig. 5-6: a: Fine magnetite, ilmenite and rutile forming a saccharoidal
              replacement texture in gabbroporphyry (18910).
           b: Pyrite pseudomorphed and replaced by magnetite (±ilmenite)
              (18962).

II: Disseminated mineralization

Disseminated mineralization is present in the calc-alkaline intrusive porphyries, zone II and zone III hornfelsed greywackes and argillites. Cubic pale yellow pyrite±magnetite and pale bluish anisotropic hematite (VHN_{100}:792) (with strong reddish internal reflections) are associated with the pervasive hydrothermal alteration of the metasediments (Fig. 5-4a). Hematite is most abundant in the silicified breccia.

Trondhjemite porphyry intrusive contains abundant disseminated pyrite (up to 8%) and granular hematite, both usually associated with large biotite crystals. Chalcopyrite inclusions are common within the larger, cubic pyrite crystals (Fig. 5-4b).

Disseminated pyrite plus minor chalcopyrite are present in the gabbroporphyry with magnetite, ilmenite and very fine rutile(?) often exsolved along crystallographic planes of the ferromagnesium minerals (Fig. 5-5) (see also Fig. 3-18a and b). Pinkish, strongly anisotropic ilmenite (VHN_{100}:534) is replaced by very finely intergrown grey isotropic magnetite (VHN_{50}:440) and pale whitish-grey rutile (VHN_{200}:965). Rutile has abundant yellowish to reddish brown internal reflections and with magnetite and ilmenite forms a saccharoidal replacement texture (Fig. 5-6a). Some very fine bismuth may be present with the rutile. Occasionally large pyrite crystals are pseudomorphed and replaced by magnetite (and possibly minor ilmenite) in the gabbroporphyry (Fig. 5-6b).

Minor pyrite,chalcopyrite, magnetite and hematite are disseminated in the granodiorites, quartz diorites and lamprophyre dykes.

CHAPTER SIX

SULPHUR ISOTOPE STUDY OF MOLYBDENITE MINERALIZATION

Introduction:

Sulphur isotope ($\delta^{34}S_{CDT}$) values have been determined for sulphide mineral phases from the Bald Hill, Cascade Creek, Mount Radiant, Taipo Spur, Karamea Bend, Roaring Lion River, Burgoo Stream, Eliot Creek, Copperstain Creek and Canaan molybdenum occurrences in West Nelson. (For location of these deposits see Fig. 2-4).

Sulphur isotope analyses of these sulphides were undertaken to estimate the probable origin of sulphur in the sulphides and the temperature of the ore-bearing fluids. These two prerequisites are necessary to formulate any model of the metallogenesis of molybdenum-base metal deposits in West Nelson.

The theory and use of sulphur isotope geothermometry and ore genesis has been discussed in several excellent papers and reviews [eg: Ohmoto (1972), Rye and Ohmoto (1974) and Robinson (1974)].

Analytical Techniques:

Mineralized samples from each molybdenum occurrence were lightly crushed and various sulphide minerals separated by hand picking. All samples were purified and $\delta^{34}S_{CDT}$ values measured at the Institute of Nuclear Sciences (INS), Lower Hutt. Methods of preparation of sulphur dioxide (SO_2)

for mass spectrometric analyses used at INS are given in Robinson and Kusakabe (1975), and are only briefly described here.

The pyrite, chalcopyrite and molybdenite samples were finely ground in an agate mortar with excess Cu_2O and directly roasted in a ceramic boat to 1000°C for 10 minutes to obtain the SO_2 gas. However, poor percentage yields of SO_2 for molybdenite samples were obtained by this direct method and most samples were treated chemically. Impure MoS_2 samples were digested in aqua regia, taken up in 1/5HCl and filtered to remove any residues. The sulphate was precipitated as $BaSO_4$ and converted to Ag_2S by graphite reduction. Sphalerite and galena samples were chemically converted to Ag_2S. All Ag_2S samples were roasted with excess Cu_2O at 900°C to form SO_2 gas. Some CO_2 is produced with the SO_2 and virtually all is extracted by distilling from an n-pentane-liquid nitrogen cold trap.

Accuracy and precision of the sample preparation method and spectrometric analyses were checked by the analysis of a secondary Ag_2S standard (R2268) approximately every eight to ten samples, and the mass spectrometer calibrated against its accepted value of +3.2‰ (Robinson and Kusakabe, 1975).

Results:

Fifty sulphide samples were analysed for their isotopic composition and results are reported in per mil (‰) deviation from Cañon Diablo Troilite (CDT) sulphur

standard. Sample details and $\delta^{34}S_{CDT}$ values are listed in
Table 6-1 and calculated temperature data in Table 6-2.

Both experimental and theoretical data place the
sulphide minerals in the following order of $\delta^{34}S$ enrichment
under _equilibrium_ exchange conditions at temperatures below
about 500°C:

$$Mo > Py > Sph > Cpy > Gl$$
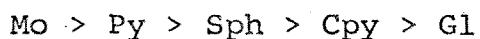
It can therefore be assumed that if $\delta^{34}S$ values do
not follow this order of enrichment, one or more of the
sulphide phases is out of equilibrium. Several experimental
and theoretical calibration curves for the temperature
dependence of sulphur isotope fractionation between coexisting
mineral pairs have been published. Limited experimental work
has been completed on the molybdenite and other sulphide
mineral pairs and the only published calibration curves are
those of Suvorova (1974). Suvorova has experimentally
determined calibration curves for Mo-Gl and Mo-Sph mineral
pairs and theoretically calculated the Mo-Py and Mo-Cpy
calibration curves in the temperature range 400°-750° (see
Appendix IV). Suvorova's calibrations have been used in
this study, and molybdenite-sulphide temperatures were
compared to other sulphide mineral pair temperatures where
possible, using Kajiwara and Krouse's (1971) and Czamanske
and Rye's (1974) calibration curves. In general, results
show good agreement between differing mineral pairs.

Table 6-1: Sample description and Sulphur Isotope $\delta^{34}S‰$ values of sulphides for West Nelson molybdenum occurrences.

BALD HILL

Sample	Description	Mineral	$\delta^{34}S_{CDT}$ (‰) *
1	Samples 1 & 2 from Mo-Py	Pyrite	0.8
2	bearing quartz vein (19000)	Molybdenite	1.1
3	Samples 3 & 4 from Mo-Py	Pyrite	0.9
4	albite bearing quartz vein (18984)	Molybdenite	0.9
5	Quartz trondhjemite intrusive (18970)	Pyrite	1.0
6	Quartz trondhjemite intrusive (18971)	Pyrite	1.0†
7	Silicified breccia (18894)	Pyrite	1.2†
8	Silicified breccia (18932)	Pyrite	2.2†
38	Pyrite bearing quartz vein (18882)	Pyrite	0.0

CASCADE CREEK

Sample	Description	Mineral	$\delta^{34}S_{CDT}$ (‰) *
13	Granodiorite intrusive (4003)	Pyrite	2.2
14	Samples 14 & 15 from Mo-Py	Pyrite	0.9
15	bearing quartz vein (4049)	Molybdenite	1.0

MOUNT RADIANT

Sample	Description	Mineral	$\delta^{34}S_{CDT}$ (‰) *
16	Samples 16, 16(a), 17, 17(a) and 39	Molybdenite	-4.7
16(a)	from Mo-Cpy-Py bearing quartz vein	Molybdenite	-4.9
17	from the Mt Radiant lode	Chalcopyrite	-7.5†
17(a)		Chalcopyrite	-8.0†
39		Pyrite	-4.2
18	Samples 18 & 19 from Mo-Cpy	Molybdenite	-4.4
19	bearing quartz vein Anaconda Reef	Chalcopyrite	-5.0

TAIPO SPUR

Sample	Description	Mineral	$\delta^{34}S_{CDT}$ (‰) *
23	Samples 23, 23(a) and 24 from	Pyrite	-0.9
23(a)	quartz veins with Mo-Py	Pyrite	-0.7
24	minerals	Molybdenite	-1.2

Table 6-1 (contd.)

KARAMEA BEND

28	Quartz vein containing Py-Mo-	Pyrite	-6.0
28(a)	orthoclase mineralization. Samples	Pyrite	-5.4
29	28, 28(a), 29 and 29(a)	Molybdenite	0.7
29(a)		Molybdenite	0.5†

ROARING LION RIVER

32	Samples 32, 32(a), 33 and 33(a)	Pyrite	6.0
32(a)	from Mo-Py bearing quartz vein on	Pyrite	5.7
33	Cobra Face prospect	Molybdenite	5.5
33(a)		Molybdenite	4.8
35	Samples 35 & 36 from Mo-Py	Pyrite	6.0
36	bearing quartz vein. Discovery Creek.	Molybdenite	6.1

BURGOO STREAM

30	Quartz-pyrite-molybdenite vein	Pyrite	5.9
31	in Granite. Samples 30 & 31	Molybdenite	6.1

ELIOT CREEK

20	Molybdenite-pyrite-sphalerite	Pyrite	4.2
20(a)	bearing quartz vein in Granite	Pyrite	4.3
21	Samples 20, 20(a), 21, 21(a) and 22	Molybdenite	2.7
21(a)		Molybdenite	2.9
22		Sphalerite	4.6

COPPERSTAIN CREEK

25	Dissem. Py from calc-silicate zone	Pyrite	2.8
26	Quartz vein containing Mo-Py	Pyrite	2.1
26(a)	mineralization, vein cutting	Pyrite	2.3
27	calc-alk. greenschist. All samples	Molybdenite	2.2
27(a)	26, 26(a), 27, 27(a) and 40	Molybdenite	2.2
40		Pyrite	2.0

CANAAN

9	All samples from single quartz	Galena	-3.2
10	reef, striking N-S, on S.W.	Sphalerite	-2.0
11	slope of Mt Pisgah. Reef	Pyrite	-1.6
12	contains Mo-Py-Gl-Sph-Cpy	Molybdenite	-0.7
37	and scheelite with tr. Sn & Bi	Sphalerite	-2.0

*Errors are ±0.1‰ except where indicated (†: ±0.2‰).

Table 6-2:   Indicated temperatures from Sulphur Isotope fractionations
             of coexisting sulphide mineral pairs.

BALD HILL

**Mineral pair	$\Delta^{34}S$	Temperature $^\circ C$	*Reference
Mo-Py	0.0	520±50	1
Mo-Py	0.3	400±30	1

CASCADE

Mo-Py	0.1	480±40	1

MOUNT RADIANT

Mo-Py	-0.5	>750?	1
Mo-Py	-0.7	>750?	1
Mo-Cpy	0.6	470±30	1
(Py-Cpy	0.8	480±50	2)
(Mo-Cpy	0.1	680±50	1)
(Mo-Cpy	0.3	570±40	1)

TAIPO SPUR

Mo-Py	-0.3	750±90	1
Mo-Py	-0.5	>750?	1

KARAMEA BEND

Mo out of equilibrium.

ROARING LION RIVER

Mo-Py	-0.5	>750?	1
Mo-Py	-0.2	660±60	1
Mo-Py	0.1	480±30	1
Mo-Py	0.4	380±20	1

BURGOO STREAM

Mo-Py	0.2	440±30	1

ELIOT CREEK

Sulphide minerals out of equilibrium.

COPPERSTAIN CREEK

Mo-Py	0.2	440±30	1
Mo-Py	0.1	480±40	1
Mo-Py	-0.1	590±60	1

Table 6-2 (contd.)

Mineral pair	$\Delta^{34}S$	Temperature °C	*Reference
		CANAAN	
Mo-Py	1.5	<300?	1
Mo-Sph	1.8	330±20?	1
Mo-Gl	3.3	290±20?	1
Sph-Gl	1.3	460±30	3
Sph-Gl	1.2	490±30	3
Sph-Gl	1.3	510±30	2
Sph-Gl	1.2	540±30	2
Py -Gl	1.6	560±30	2
Py-Sph	0.4	590±100	2
Py-Sph	0.4	590±100	2

* References

1. Suvorova (1974)

2. Kajiwara and Krouse (1971)

3. Czamanske and Rye (1974)

** Mo: molybdenite

   Py: pyrite

   Cpy: chalcopyrite

   Sph: sphalerite

   Gl: galena

Mineralization and Geothermometry:

Bald Hill

Disseminated pyrite-molybdenite mineralization occurs within an intrusive quartz trondhjemite porphyry and in stockwork type pyrite-molybdenite bearing quartz veins in the porphyry and the surrounding biotitic hornfels. Some mineralized breccia pipes(?) also occur. Pyrite-molybdenite-rare chalcopyrite-bismuth-bismhite sulphide assemblages with hematite and magnetite occur in the veins with gangue quartz, muscovite and albite. The bismuth mineralization is however, not widespread.

Molybdenite-pyrite (Mo-Py) mineral pairs from quartz veins in the hornfels indicate temperatures of $520° \pm 50°C$ and $400° \pm 30°C$. The $\delta^{34}S$ values for the disseminated sulphide in the porphyry and the silicified breccia (1.0‰ and 1.2‰ to 2.2‰ respectively) show no significant fractionation from the quartz vein sulphides (av. 1.0‰). A narrow range of $\delta^{34}S$ values, from 0.0‰ to 2.2‰, is shown for the nine $\delta^{34}S$ determinations from Bald Hill.

Cascade Creek

The mineralization occurs as quartz-sulphide veins and disseminated sulphides within granites and metasediments. The most abundant sulphide, pyrite, occurs with molybdenite and chalcopyrite sulphides in quartz veins with magnetite and hematite. Gangue minerals include albite and muscovite. Hematite does not appear to coexist with molybdenite.

A molybdenite-pyrite pair from a quartz vein in the granodiorite gave an indicated temperature of 480°±40°C Disseminated pyrite from the intrusive had a $\delta^{34}S$ value of 2.2‰. As at Bald Hill, the spread of $\delta^{34}S$ values from 0.9‰ to 2.2‰ is narrow.

Mount Radiant

Fracture controlled quartz-sulphide vein type mineralization forming reefs at Mount Radiant occurs with minor disseminated mineralization within the granites. The quartz reefs contain molybdenite-pyrite-chalcopyrite-bornite-tetrahedrite and bismuth mineral assemblages with gangue quartz, orthoclase and muscovite. The Anaconda Reef, 5 km to the north, has similar mineralization although chalcopyrite is more abundant and molybdenite less so.

Two molybdenite-pyrite temperatures of >750°C were determined for the Mount Radiant mineralization. The chalcopyrite $\delta^{34}S$ values of -7.5‰ and -8.0‰ are strongly negative when compared to the molybdenite and pyrite values of -4.8‰ and -4.2‰. This would indicate the chalcopyrite to be in disequilibrium with the other two sulphide mineral phases. The molybdenite-chalcopyrite pair from Anaconda Reef indicate a more geologically reasonable temperature of 470°±30°C. The value of -5.0 per mil for the chalcopyrite at Anaconda Reef would indicate that the chalcopyrite is in near equilibrium with the molybdenite, which has a similar value to the Mount Radiant molybdenite (-4.4‰ and av. -4.8‰ respectively). If the chalcopyrite for Anaconda

Reef is used with the pyrite value from the Radiant Reef, a pyrite-chalcopyrite temperature of 480°±50°C is indicated (using Kajiwara and Krouses' calibration), in excellent agreement with the Mo-Cpy temperature of 470°±30°C (using Suvorova's calibration).

Assuming that the Radiant Reef chalcopyrite is out of equilibrium and using the Anaconda Reef value for chalcopyrite (-5.0‰, assumed to be near equilibrium), temperatures of 570°±40°C and 680°±50°C are indicated for the Radiant Reef Mo-Cpy mineral pairs, which are more reasonable than the Mo-Py temperatures of >750°C. This would tend to suggest that the molybdenite in the Radiant Reef is slightly out of equilibrium, possibly fractionally re-equilibrated as the reef cooled.

The $\delta^{34}S$ values of the sulphides are all negative (i.e. light) at Mount Radiant with a wider spread of 3.8‰ (from -4.2‰ to -8.0‰).

Taipo Spur

Mineralization occurs in random quartz veins and along shears with minor disseminated sulphides within the porphyritic granite intrusive. Sulphide and oxide mineral assemblages of molybdenite-pyrite occur with minor magnetite-rutile-chalco-pyrite and rare cubanite, along with gangue quartz, coarse muscovite and albite.

Molybdenite-pyrite mineral pairs indicate temperatures of 750°±90°C and >750°C for the mineralization. These temperatures suggest that the mineral pair may be slightly

out of equilibrium. $\delta^{34}S$ values are slightly negative with a narrow spread from -0.7 per mil to -1.2 per mil.

Karamea Bend

Quartz-sulphide veins occur in metasediments in contact with microgranodiorite and micromonzonite stocks which contain minor disseminated sulphide. Pyrite-molybdenite-magnetite with rare lead-zinc and bismuth bearing mineral assemblages occur in quartz veins with gangue orthoclase, muscovite, sericite and rare carbonate.

Pyrite $\delta^{34}S$ values from the quartz veins are strongly negative at -6.0‰ and -5.4‰. Two $\delta^{34}S$ values of 0.7‰ and 0.5‰ for molybdenite indicates the mineral pair to be out of equilibrium and consequently a temperature for the mineralization could not be determined.

Roaring Lion River

Stockwork type molybdenite and pyrite bearing quartz veins occur in metasediments, and some disseminated sulphide occurs in the intrusive diorites and granodiorites. Pyrite-molybdenite-chalcopyrite and occasional pyrrhotite-rare galena and sphalerite-magnetite mineral assemblages are present with gangue of quartz, potassium feldspars and sericite. Some pegmatitic veins occur in the granites.

Four temperatures ranging from 380°±20°C to >800°±150°C were calculated from Mo-Py mineral pairs. However, one of the $\delta^{34}S$ values for molybdenite at Cobra Face is possibly slightly out of equilibrium and therefore

the Mo-Py temperature of 660°±60°C from Cobra Face and 480°±30°C for Discovery Creek are probably the most meaningful. $\delta^{34}S$ values are positive with a total range of 1.3‰ (4.8 to 6.1‰).

Burgoo Stream

Quartz and aplite veins cut both intrusive granite and granodiorite stocks and the surrounding metasediments. Molybdenite and pyrite with rare chalcopyrite occur in the quartz veins with gangue of albite and muscovite(?).

A pyrite-molybdenite mineral pair indicate a high temperature of 440°±30°C for the mineralization. The $\delta^{34}S$ values of 5.9‰ to 6.1‰ are similar to the nearby Roaring Lion River sulphides and are again positive with a narrow spread.

Eliot Creek

Quartz veins up to approximately a metre thick, sometimes accompanied by pegmatitic veins, occur within a greisen granite intrusive and hornfelsed metasediments. Molybdenite-pyrite-native bismuth with occasional galena and sphalerite in quartz veins with gangue muscovite and albite mineral assemblages are present. Disseminated molybdenite mineralization is found in the margins of some of the intrusive adamellites.

The positive $\delta^{34}S$ values have a spread of 1.9‰ (2.7‰ to 4.6‰). The sulphide values however, indicate that the pyrite, molybdenite and sphalerite are out of

equilibrium with each other. Therefore, meaningful temperatures for the mineralization could not be determined.

Copperstain Creek

A skarn type deposit has been developed along with quartz sulphide veining. Pyrite and molybdenite occur along with sphalerite-galena-magnetite sulphide and oxide minerals in quartz veins with gangue muscovite-sericite and albite. Some disseminated mineralization occurs in the granodioritic intrusives and the surrounding calc-silicate skarn and amphibole schists.

Three Mo-Py mineral temperatures of $440°±30°C$, $480°±40°C$ and $590°±60°C$ indicate a reasonably high temperature for the mineralization. $\delta^{34}S$ values of 2.0‰ to 2.8‰ are slightly positive with a small range. The pyrite value of 2.8‰ from the calc-silicate zone indicates little, or no fractionation from the pyrite in quartz veins (av. 2.1‰).

Canaan

Quartz reefs, up to 2 metres in width and several metres in length, containing sulphides, outcrop along the contact between the older diorites (Rameka Intrusives) and the Separation Point Granites. The reefs contain scheelite-molybdenite-sphalerite-chalcopyrite-pyrite-galena sulphide mineralization with accessory magnetite and stolzite in gangue quartz and muscovite.

Sulphur isotope values were determined for galena, sphalerite, pyrite and molybdenite. The $\delta^{34}S$ values are all negative although the molybdenite value of -0.7‰ would suggest molybdenite to be slightly out of equilibrium with the other sulphide minerals. The calculated temperatures using molybdenite paired with the pyrite, sphalerite and galena would tend to support this, the temperatures all being low when compared to the various other mineral pairs. Sph-Gl, Py-Gl and Py-Sph mineral pairs give seven temperatures from 460°±30°C to 590°±100°C, indicating a high temperature of mineralization, probably at about 500°C as indicated by the Sph-Gl pair using the well accepted and tested calibration of Czamanske and Rye (1974).

The $\delta^{34}S$ values are slightly negative with a slightly wider spread of $\delta^{34}S$ values of 3.1 per ml (-0.1 to -3.2), although if the molybdenite is out of equilibrium, a narrow spread of 1.6‰ occurs.

Discussion:

The sulphide geothermometry for Bald Hill, Cascade Creek, Burgoo Stream, Copperstain Creek, and Canaan all indicate temperatures in the range 380°C to 590°C for the molybdenite-pyrite-sulphide mineralization, with a strong tendency to suggest 380°C to 480°C to be the temperature of mineralization. Mount Radiant, Roaring Lion River and Taipo Spur have sulphide temperatures in the range 380°C to ~750°C which would seem to indicate a slightly wider range for these occurrences. However, the

higher temperatures indicated by the Mo-Py mineral pairs

(ie: >700°C) in these deposits are geologically unreasonable

and are possibly due to 1) a lack of equilibrium for Mo-Py

mineral pairs, or 2) Suvorova's (1974) theoretically

calculated temperature curve for Mo-Py fractionations at

higher temperatures being incorrect. Therefore, most of

the Mount Radiant and Roaring Lion River data (ie: Mount

Radiant, 470°C to 680°C; Roaring Lion, 380°C to 660°C)

suggest temperatures in the range 380°C to ≈660°C for the

molybdenum mineralization. Temperatures for Karamea Bend

and Eliot Creek could not be calculated owing to the lack

of equilibrated mineral pairs.

The sulphur isotope geothermometry is generally in

agreement with other temperature determinations for these

molybdenum-bearing deposits in West Nelson (Table 6-3).

Rabone (1977) estimated temperatures of Mo-mineralization

for Canaan, Eliot Creek, Karamea Bend, Taipo Spur and Mount

Radiant from studies of fluid inclusions. From the chemistry

of the fluids, Rabone estimated that the inclusions contained

5-15 wt % NaCl equivalent and that they formed at 1100 to

1800 bars pressure (Rabone; Table 23, pp.205). Potter (1977)

has shown that corrections for fluid inclusion homogenization

temperatures of approximately +100°C are required for

inclusions containing 10-15 wt % NaCl equivalent at 1000 bars

(see also Lemmlein and Klevtsov, 1961). The Mount Radiant

and Canaan sulphide data agree with the pressure corrected

fluid inclusion geothermometry of Rabone (1977)

(ie: ≈460°C-470°C). The corrected fluid inclusion data also

Table 6-3:   Comparison of other Temperature Data with Sulphur
Isotope Geothermometry

	$\delta^{34}S$ Temps.	Other Data	*Corrected Data
CANAAN	460°-590°C	365°-370°C[1]	465°-470°C
COPPERSTAIN	440°-590°C	500°C[2]	
ELIOT CREEK		325°-400°C[1]	425°-500°C
BURGOO STREAM	440°C		
ROARING LION RIVER	380°-660°C		
KARAMEA BEND		395°-410°C[1]	495°-510°C
TAIPO SPUR	750°C?	380°-450°C[1]	480°-550°C
MT RADIANT	470°-680°C	360°-375°C[1]	460°-475°C
CASCADE CREEK	480°C		
BALD HILL	400°-520°C		

1. Rabone (1977). Fluid inclusion data.

2. Wodzicki (1972). Mineralogy and sulphur isotopes

* Fluid inclusion temperatures corrected for pressure
   (Potter, 1977; for explanation see text).

indicate temperatures of 425°C to 550°C for Eliot Creek,

Karamea Bend and Taipo Spur. Wodzicki (1972) concluded from

mineralogical evidence, that the temperature of mineralization

at Copperstain Creek was approximately 500°C.   (A Py-Sph

sulphur isotope pair gives a temperature of 500°C).

Small fractionation values between coexisting

sulphides could be caused by a lack of sulphur in the

mineralizing fluids, thus all the sulphides being precipitated

at once over a very short period (with little or no fraction-

ation taking place) or the sulphides are very high temperature

in origin (where there is no significant fractionation between

sulphide pairs). With the exception of the Karamea Bend data,

the constancy of isotopic fractionation in these deposits, between coexisting pyrite, molybdenite and chalcopyrite, indicates attainment of isotopic equilibrium at an almost uniformly high temperature (see Fig. 6-1).

The narrow spread of $\delta^{34}S$ values for each deposit (av. 1.1‰ ; max. Bald Hill 2.2‰ ; min. Burgoo Stream 0.2‰) for the sulphide minerals considered to be in equilibrium, and a range of values about zero per mil (from -6.1‰ to +6.1‰) (see Fig. 6-2), indicate that the source of sulphur in these occurrences is possibly of magmatic origin (Rye and Ohmoto, 1974; Coleman, 1977). Rye and Ohmoto suggest that $\delta^{34}S$ values near zero per mil, and the association of acid igneous rocks indicates the sulphur is derived from igneous sources. This includes sulphur released from silicate melts. They concluded that igneous sulphur must be derived either from the upper mantle or from the homogenization of large volumes of deeply buried or subducted crustal material.

Chappell and White (1974) have classified Paleozoic granitoids in Southeastern Australia on the basis of field, mineralogical and chemical evidence into sedimentary ("S"-type) and igneous ("I"-type) type granites, derived from sedimentary and igneous sources respectively. This distinction has also been confirmed by oxygen and hydrogen isotope evidence (O'Neil and Chappell, 1977). The minor molybdenum-bearing granites in West Nelson, using the above criteria, have been shown to be of 'igneous' origin (see Chapter 4).
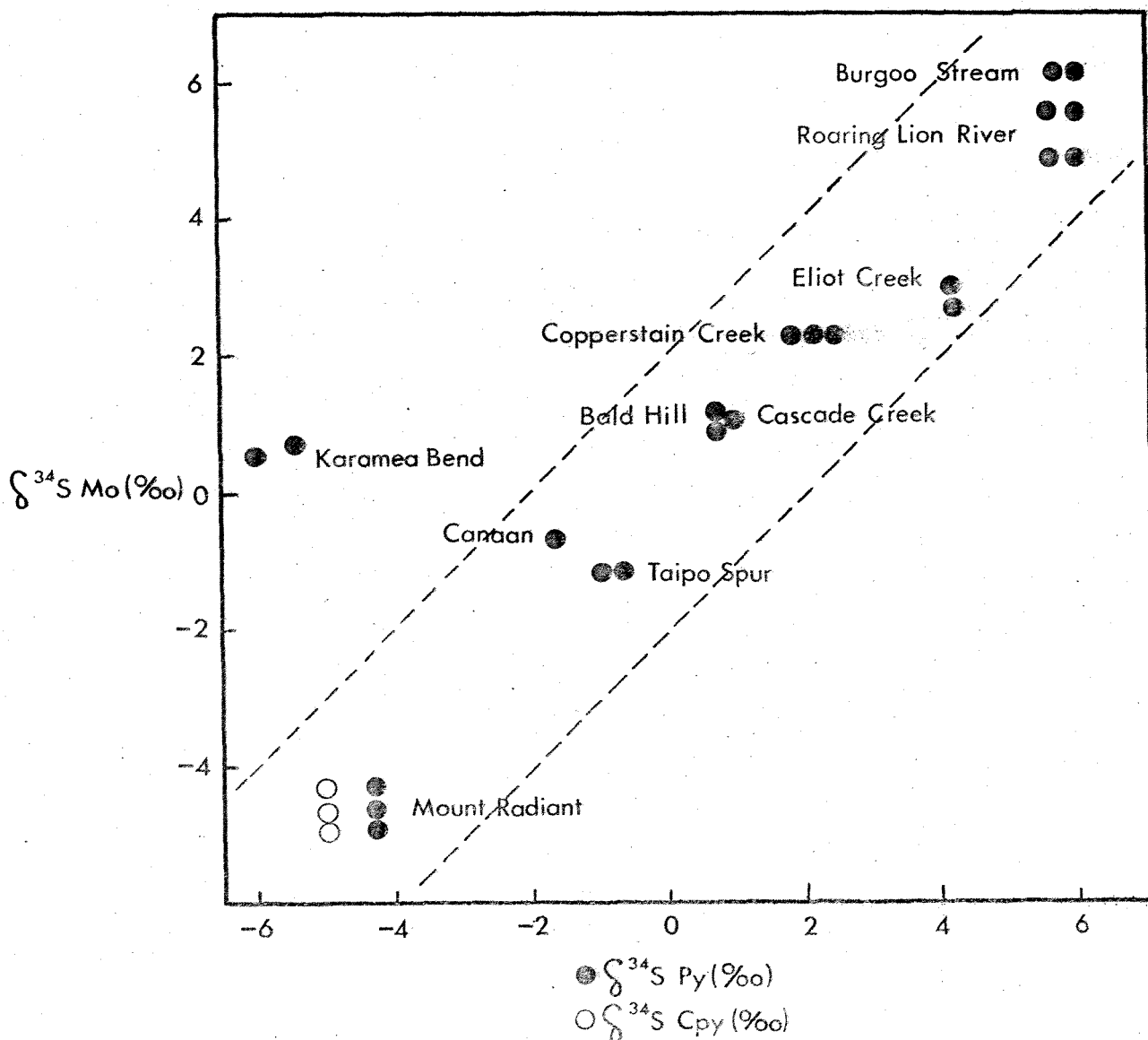
Fig. 6-1: Plot of δ^{34}S values for pyrite and chalcopyrite versus coexisting molybdenite for ten West Nelson molybdenum occurrences. Dashed lines represent $\pm 2.0\%$ difference in δ^{34}S isotope values.

Work by Shaw (pers. comm., 1976: in Coleman 1977) showed "I-type" granites to have δ^{34}S values, for total sulphur sulphate and sulphide combined, from -3.6‰ to +5.0‰ while "S-types" give -9.4‰ to +7.6‰ and with only one exception, do not give values from -5.0‰ to +5.0‰. The West Nelson molybdenum-bearing granites have a slightly wider spread for sulphides (-8‰ to +6‰). However, if the Karamea Bend, Roaring Lion River and Burgoo Stream granitic rocks are excluded, where possibly some assimilation and/or contamination of sulphur has occurred, all of the δ^{34}S
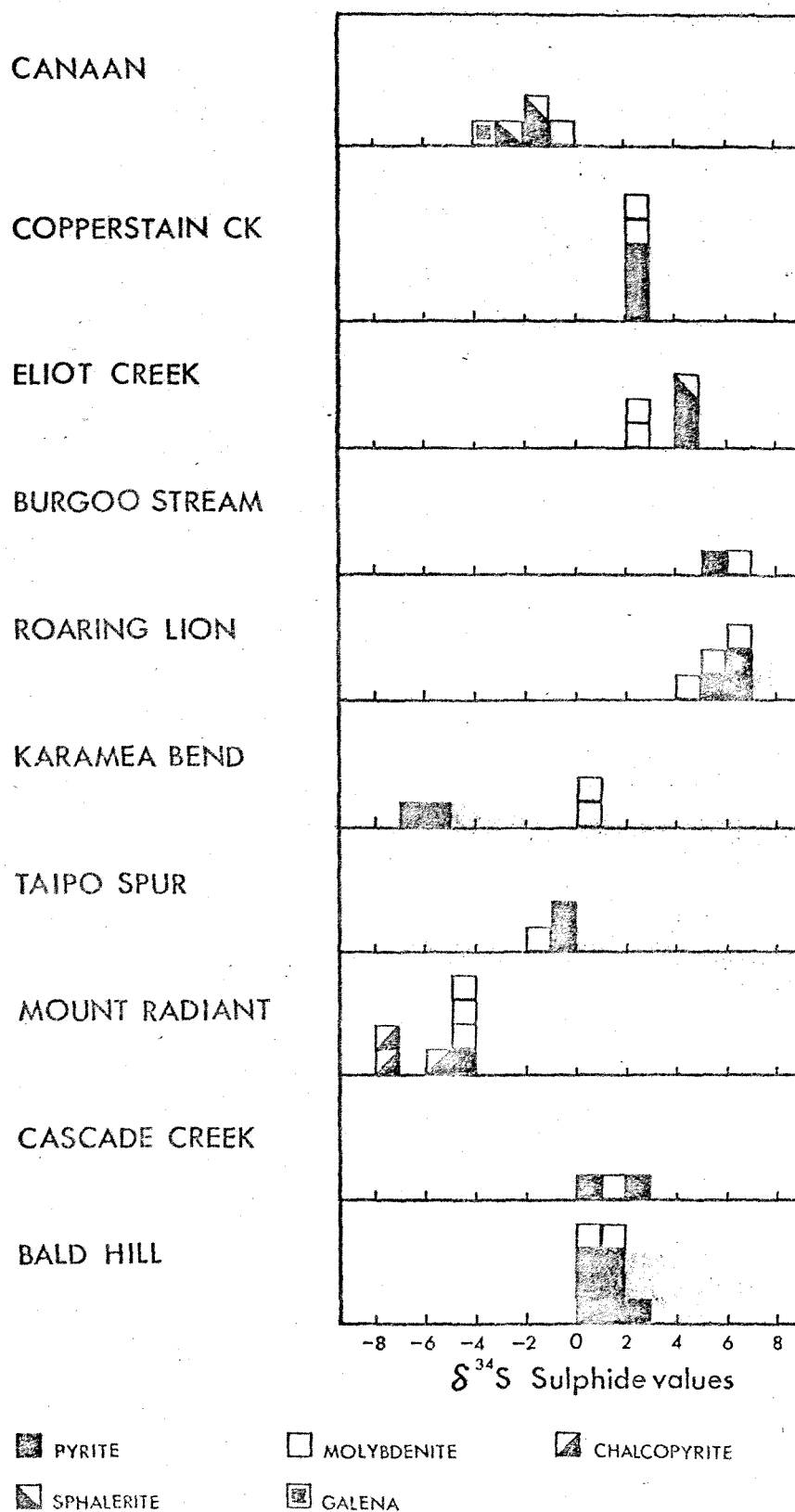
Fig. 6-2: Histograms showing frequency of $\delta^{34}S_{(CDT)}$ values of sulphide minerals in West Nelson molybdenum occurrences.

values also plot between -5.0‰ and +5‰ (Fig. 6-2)
(av. $\delta^{34}S$ values for basic igneous rocks, basalts and
volcanic material 0‰ , Coleman, 1977).

If the primary source material in the deposits is
crustal magmatic sulphur (ie: $\Sigma\delta^{34}S = 0$‰) then the variation
in sulphide values between -8‰ and +6‰ could be a consequence
of;

1) The intrusive rocks and contained sulphur, mixing with
   and being contaminated by connate or seawater sulphate
   (eg: evaporites, limestones or meteoric groundwater)
   to produce isotopically light sulphides. As discussed
   by Coleman (1977), the first formed product, in this
   case the sulphide, is enriched in the light isotope and
   the remaining sulphate depleted in the light isotope in
   a complementary way

   eg: magmatic H_2S ($\Sigma S = 0$‰) + [†]S.W.S. $SO_4^=$ ($\Sigma S = 20$‰)

   → H_2S -6‰ + $SO_4^=$ 26‰ .

   [†](av. seawater sulphate (S.W.S.) value +20‰,
   Coleman, 1977).

   Assimilation of crustal sulphide material, itself rich
   in the heavy isotope (eg: deeply buried sediments or
   granites) could produce sulphides similarly enriched.

   eg: 2 magmatic H_2S ($\Sigma S = 0$‰) + 1 crustal H_2S ($\Sigma S = 20$‰)

   → $3H_2S$ + 7‰ .

2) Changes in the chemistry of the ore bearing fluid
   precipitating the sulphide minerals. At a temperature
   of 500°C, the sulphur isotopic fractionation between

	$\delta^{34}S$		
H_2S	$SO_4^=$	MoS_2	FeS
-18.8	-6.8	-18.9	-18.8
-6.0	+6.0	-6.1	-6.0
6.8	18.8	6.9	6.8

$H_2S \quad SO_4^=$

0.1   0.9

$\Sigma S = 0‰$

0.5   0.5

0.9   0.1
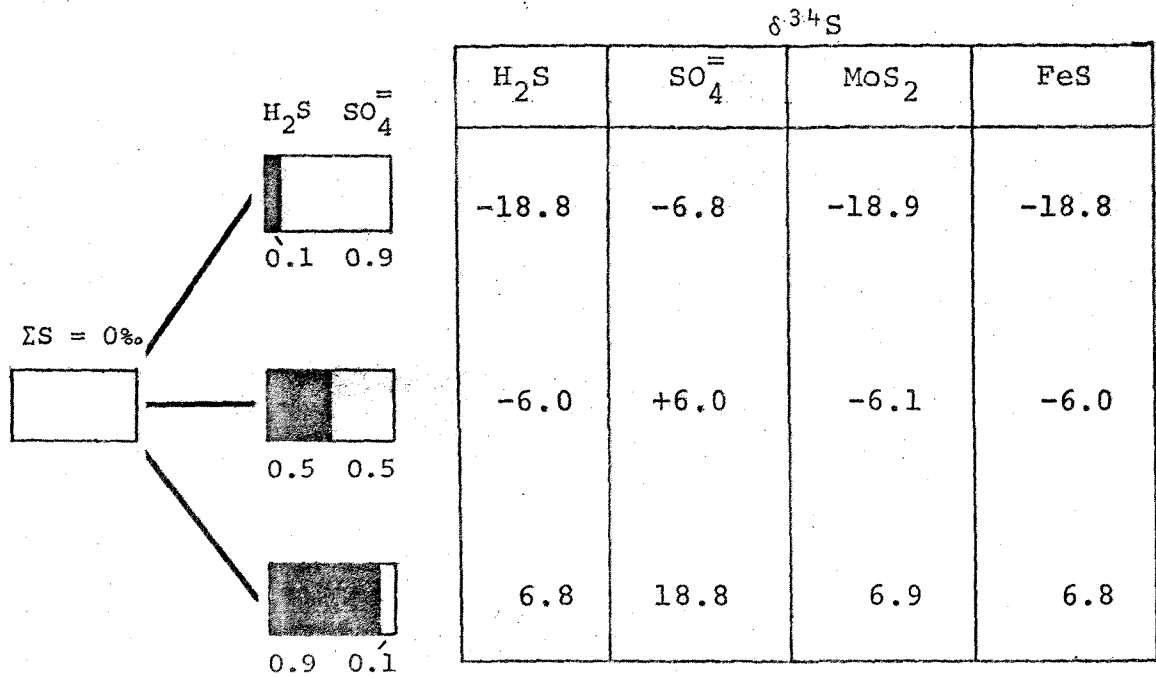
Fig. 6-3. Variation of $\delta^{34}S$ of sulphate and sulphide minerals with variation in $H_2S/SO_4^=$ ratio of the hydrothermal solution at $T = 500°C$, $\delta^{34}S\Sigma = 0$ per mil.

$SO_4^=$ and H_2S is about 12 per mil (Rye and Ohomoto, 1974). Assuming that the primary total sulphur is 0‰, Fig. 6-3 shows the complete variation in all deposits can be explained by changes in the chemistry of the ore fluid precipitating the sulphide mineral phases. The fractionation of $\delta^{34}S$ is due to the proportion of sulphur species ($H_2S/SO_4^=$) in the hydrothermal fluid. Light isotope values (eg: Mount Radiant and Karamea Bend) have been precipitated from ore fluids with $H_2S/SO_4^=$ ratios of 1, values about zero per mil (eg: Bald Hill, Cascade Creek, Taipo Spur and Canaan) from ore fluids with $H_2S/SO_4^=$ ratios of ≈2.5 and the isotopically heavy sulphides (eg: Copperstain Creek, Eliot Creek, Burgoo

Stream and Roaring Lion River) from ore fluids with $H_2S/SO_4^=$ ratios nearer to 9.

In summary, the sulphur isotope geothermometry for the molybdenum mineralization in West Nelson indicates reasonably high temperatures for the precipitation of the sulphide phases. These temperatures from 380°C to >700°C, are in agreement with fluid inclusion geothermometry. The isotope data is also consistent with a crustal magmatic source for the sulphur. The range in sulphur isotopes is a consequence of variations in the $H_2S/SO_4^=$ ratios of the ore-bearing fluids with possibly minor contamination and/or assimilation of the magmatic sulphur-bearing solutions by meteoric waters, seawater sulphate or crustal sulphide material.

CHAPTER SEVEN

SUMMARY AND CONCLUSIONS

All the molybdenite occurrences in West Nelson, including the Bald Hill prospect, emphasise the consistent association of molybdenum mineralization with minor mid-Cretaceous calc-alkaline plutonic activity. This activity appears to have occurred close to the contacts of the major granite batholiths and lower Paleozoic country rocks. The main geologic features of the molybdenite occurrences are summarised in Table 7-1.

The relationship of the molybdenite mineralization (and associated minor granites) to adjacent coarse granites and adamellites of the Karamea and Separation Point batholiths is not clear, and the age relationships are complicated by the protracted cooling histories of these deep-seated rocks. Rb/Sr total-rock age studies would be required to establish their original time of emplacement. However, the mineral age data discussed in this study and also data reported by Aronson (1965, 1968), Wodzicki (1972), Smale (1976), Adams and Nathan (1978) indicate that uplift, cooling, and substantial erosion of these granites occurred in the interval 80-120 Ma ago (Upper Cretaceous). It appears that the molybdenite mineralization is completely absent from areas of known Tuhuan-age (280-370 Ma) granites, although these occupy large areas of the two batholiths and extensively

Table 7-1: Geologic features associated with main South Island molybdenum prospects.

Prospect	Location	Rock Types Intrusives and Country	Age (Ma)	Associated Minerals	Tectonic Control and Distribution
Bald Hill	Headwaters of Lyell Stream, Upper Buller Gorge	Intrusive trondhjemite porphyry, granodiorites diorites & basic dykes into gneissic granites & greywackes & argillites	113-116	Molybdenite Pyrite Chalcopyrite Bismuth Bisminite Quartz	NW structural trend NE faulting Stockwork-veins, quartz veinlets, disseminated.
Cascade Creek	Rochfort and Cascade Creeks, Lower Buller Gorge	Dacite-granodiorite intruded into granites, greywackes and argillites	107-112	Molybdenite Pyrite Chalcopyrite Pyrrhotite Bornite Quartz	N-S structural trend N to NW faulting. Quartz veinlets and disseminated
Mount Radiant	Mt Radiant, Little Wanganui River area, N.W. Nelson	Porphyritic granites and granodiorites intrude hornfels, schists, gneisses and coarse grained granites	*116*	Molybdenite Chalcopyrite Pyrite Bornite Tetrahedrite Bismuth Quartz	N to NW foliation, shearing and faulting. Quartz reef and vein type mineralization
Taipo Spur	Headwaters of Karamea River N.W.Nelson	Trondhjemitic grano-diorite intruding porphyritic gneissic granites	106-116	Molybdenite Pyrite Rutile Chalcopyrite Cubanite Bismuth Quartz	NW trending granites ENE trending dykes & regional faulting. Disseminated and shear controlled mineralization.
Roaring Lion River	Roaring Lion River tributary of Karamea River, N.W. Nelson	Granodiorite & porphyritic quartz diorite intrude coarse grained granites and pelitic schists and quartzites	112*	Molybdenite Chalcopyrite Pyrite Pyrrhotite Galena Sphalerite Quartz	N-S trending faults and folding. Stockwork type quartz-sulphide veins.
Karamea Bend	Karamea River N.W. Nelson	Microgranodiorites & quartz monzonites intrude coarse potash granites and schists, phyllites & shales	112	Molybdenite Pyrite Galena Sphalerite Bismuth Quartz	ENE trending series of stocks. Faulting fracture, disseminated, shear and stockwork type minerali-zation.
Burgoo Stream	Headwaters of the Aorere River, N.W. Nelson	Granodiorites and adamellites intruding hornfels and mica schists	?	Molybdenite Pyrite Quartz	N to NW trending intrusives and contacts. Faults. Aplite and quartz-sulphide veins on or near contacts.
Eliot Creek	Aorere River N.W. Nelson	Granodiorites and adamellites intrude Palaeozoic sandstones and pelitic schists	104-107	Molybdenite Pyrite Bismuth Galena Sphalerite Quartz	Fault controlled NNW trending stocks. Disseminated, breccia and shear-controlled minerali-zation.
Copperstain Creek	Pariwhakaoho Stream, Takaka, Nelson	Granodioritic intrusives in pelitic schists and calc-silicate rocks.	108	Molybdenite Pyrite Sphalerite Chalcopyrite Galena Quartz	NW & NE intersecting faults with intrusives forming a skarn type deposit. Disseminated and quartz veinlets.
Canaan Valley	Canaan Valley, Takaka Hill, Nelson	Granites-granodiorites have intruded older amphibolites, diorites and marbles	95-112	Scheelite Molybdenite Pyrite Chalcopyrite Sphalerite Galena Quartz	N to NW trending contacts. Quartz reefs along contacts.
Knuckle Hill	N.W. Nelson	Granites intruding hornfels	99	Molybdenite Pyrite Quartz	Satellite stock of granites. Stockwork mineralization?

Table 7-1: continued

McConnochie Creek	Victoria Range, Westland	Quartz porphyry intruding a series of potash granites	102-112	Molybdenite Pyrite Chalcopyrite Quartz Argentite (Acanthite)	Quartz reef and veinlet type mineralization.
Dusky Sound Area	Head of Dusky Sound Fiordland	Quartzites, gneisses, schists & metagrey-wackes with intrusive granites	?	Molybdenite Pyrite Chalcopyrite Pyrrhotite	N-S striking bands with N to NW trending shears. Quartz veinlets and disseminated.
Bravo Island	Stewart Island	Granitic environment	99-115	Molybdenite Pyrite Chalcopyrite Quartz	N-W trending structure. Quartz reef.

*Ages by inference; actual mineralization undated.

intrude lower Paleozoic sediments.

The porphyritic calc-alkaline plutonic suite associated with the molybdenite mineralization at Bald Hill, and all other Mo-bearing deposits in West Nelson, conform to Chappell and Whites' I-type granites, while the Karamea 'batholith granites', including the Bald Hill Granites, appear to be S-type. Although the tin mineralization is apparently absent from the Karamea Granites in West Nelson, the tungsten, copper and molybdenum mineralization seems to be associated with the I-type granites.

This association of minerals and granite types is similar to Eastern Australia. Chappell and White (1974) also state of granites in Eastern Australia: "Tin mineralization appears to be confined to highly silicic S-type granites whereas tungsten and porphyry-type copper and molybdenum deposits are associated with the I-types."

The petrographic and geochemical data presented for the granitic rocks in West Nelson are consistent with the hypothesis that these granites are derived by partial melting of two different types of source material - igneous and sedimentary. Wyllie et al. (1976) conclude from experimental work that (i) primary granite magmas cannot be derived from the mantle or subducted ocean crust, (ii) granite magmas with low H_2O content are generated within the crust and (iii) batholiths are produced from crustal rocks as a normal consequence of regional metamorphism, with the formation of H_2O-undersaturated granite liquid and mobilized migmatites.

This crustal anatexis mode of formation for both the H_2O-undersaturated 'I-type' magmas and the H_2O-saturated 'S-type' granite magmas is consistent with the crustal magmatic source for sulphur in the molybdenum deposits indicated by sulphur isotope studies. However, strontium, oxygen and hydrogen isotope studies of the various plutonic rocks in West Nelson would be required to make a more positive statement on their petrogenesis.

The deformation and contact-aureole zone in the Greenland Group metasediments associated with the Karamea Granite batholith is very limited in the Bald Hill area. No sedimentary structures directly attributable to 'batholith' emplacement (and only rare schists) are evident. Apparently unaltered Greenland Group slates and metagreywackes have been mapped to the metasediment-granite contacts. As shown by White et al. (1974) for similar xenolith-bearing granites, in the Lachlan Fold Belt of southeastern Australia, the evidence is consistent with diapiric emplacement (similar to salt-dome intrusion) for the H_2O-saturated S-type granites, with intrusion speed and/or viscosity sufficiently high to prevent xenoliths from sinking. The I-type calc-alkaline magma melts are generated at greater depths in the crust and, due to their lower viscosities, begin to rise. These H_2O-undersaturated magmas and hydrothermal fluids, with their contained metals and sulphur, intrude upwards into the upper crust under lithostatic pressure. When these intrusive melts reach the large scale fractures caused by

the diapiric intrusion of the more viscous S-type granites (possibly circular shaped features up to 40 km across (see Appendix VI) a sudden drop in pressure would result (ie: change from lithostatic to hydrostatic P_{H_2O}). This sudden drop in pressure would cause the sulphide-bearing hydrothermal solutions to boil, precipitating the sulphide phases.

At least in the case of the Berlins Porphyry, it is likely that the minor hypabyssal granitic intrusions (and indirectly the molybdenite mineralization) were related to volcanic activity in the mid-Cretaceous. However, a more general statement of the relations between Rangitata orogenic plutonism, volcanism, and mineralization must await further geological study and radiometric dating.

Although the geologic setting, age, geochemical characteristics of the 'batholith' granites and Mo-bearing minor intrusives and temperature of mineralization have not been determined in all cases the following features seem apparent:

1) All of the molybdenum mineralization occurs in geological situations at or near the margins of the major granite batholiths (Karamea and Separation Point Granites), within or close to hornfelsed Lower Paleozoic country rocks.

2) The scattered ages for the Ordovician Greenland Group argillites in the Lyell Stream area are the result of partial argon loss within a thermal aureole surrounding the minor mineralized granitic intrusives.

3) Molybdenite mineralization at Bald Hill is associated with Lower Paleozoic Greenland Group metasediments which have been later hornfelsed and brecciated. These hornfels yield K-Ar total-rock ages of 103-120 Ma, synchronous with the intrusion of the Lyell Porphyry, also mineralized and dated at 112-116 Ma (Albian).

4) The Bald Hill Granites, to the east of the Lyell Porphyry, at the west margin of the Karamea batholith yield biotite and muscovite ages of 102-110 Ma, which probably reflect the time of uplift and cooling rather than intrusion.

5) The Bald Hill age data emphasises the consistent association of molybdenite mineralization with minor granitic-trondhjemitic hypabyssal stocks or dyke-like intrusions, or within their metamorphic aureoles, in West Nelson. These intrusions, where radiometrically dated, consistently give maximum mineral ages in the range 95-116 Ma (mid-Cretaceous) which is probably the time of intrusion.

6) I-type and S-type granites can be recognised in the Karamea and Separation Point batholiths of the South Island, and the molybdenum mineralization is invariably associated with minor I-type intrusives.

7) Field relationships, petrographic, geochemical and isotopic data are all compatible with a crustal origin for the granitic rocks, the plutonic rocks derived by ultrametamorphism of crustal sedimentary material with I-type and S-type granites having igneous and sedimentary source material respectively.

8) Sulphur isotope geothermometry for seven of the molybdenum occurrences, including Bald Hill, give minimum temperatures from 380°C to 480°C for the sulphide mineralization. This isotope geothermometry is in agreement with fluid inclusion temperature data which indicates minimum temperatures of mineralization for three other molybdenum deposits in the range 425°C to 495°C.

9) The narrow spread of sulphur isotope values about zero per mil for all the molybdenum occurrences is consistent with a crustal magmatic source for sulphur.

10) Finally, the data presented in this study of the Bald Hill and other molybdenum occurrences in West Nelson confirm the presence of a molybdenum metallogenic province. The various deposits appear to be structurally, mineralogically, chronologically and petrogenically related.

APPENDIX I: Rock sample location and V.U.W. Geology
             Department rock numbers

Table Al-1: V.U.W. Geology Department rock numbers for
             thesis samples.

Thesis No.	V.U.W. No.	Description
18812	12980	Gabbroporphyry. Lyell Porphyry.
840	981	Quartz trondhjemite. Lyell Porphyry.
842	982	Quartz trondhjemite. Lyell Porphyry.
849	983	Muscovite-biotite schist. Metasediment.
882	984	Quartz-sulphide vein from hornfels.
885	985	Greywacke metasediment. Greenland Group.
886	986	Argillite metasediment. Greenland Group.
887	987	Greywacke metasediment. Greenland Group.
888	988	Greywacke metasediment. Greenland Group.
890	989	Greywacke metasediment. Greenland Group.
18891	12990	Leucogranite. Bald Hill Granite.
892	991	Leucogranite. Bald Hill Granite.
893	992	Greywacke metasediment. Greenland Group.
894	993	Silicified hornfels. Altered metasediment.
895	994	Zone I argillite. Altered metasediment.
896	995	Biotite-hornfels. Altered metasediment.
897	996	Zone I greywacke. Altered metasediment.
901	997	Pink microgranite. Bald Hill Granite.
903	998	Biotite-hornfels. Altered metasediment.
904	999	Biotite-hornfels. Altered metasediment.
18905	13000	Silicified hornfels. Altered metasediments.
906	001	Silicified hornfels. Altered metasediments.
907	002	Argillite metasediment. Greenland Group.
908	003	Gabbroporphyry. Lyell Porphyry.
910	004	Gabbroporphyry. Lyell Porphyry.
911	005	Leucogranite. Bald Hill Granite.
916	007	Zone I greywacke. Altered metasediment.
918	008	Greywacke metasediment. Greenland Group.

Thesis No.	V.U.W. No.	Description
919	009	Zone I argillite. Altered metasediment.
18920	13010	Zone I greywacke. Altered metasediment.
922	011	Greywacke metasediment. Greenland Group.
925	012	Greywacke metasediment. Greenland Group.
926	013	Greywacke metasediment. Greenland Group.
927	014	Argillite metasediment. Greenland Group.
928	015	Greywacke metasediment. Greenland Group.
929	016	Lamprophyre dyke rock. Lyell Porphyry.
931	017	Biotite-hornfels. Altered metasediment.
932	018	Silicified hornfels. Altered metasediments.
933	019	Biotite-hornfels. Altered metasediments.
18934	13020	Lamprophyre dyke rock. Lyell Porphyry.
935	021	Leucogranite. Bald Hill Granite.
939	022	Biotite-hornfels. Altered metasediment.
941	023	Lamprophyre dyke rock. Lyell Porphyry.
942	024	Greywacke metasediment. Greenland Group.
945	025	Silicified hornfels. Altered metasediment.
946	026	Lamprophyre dyke rock. Lyell Porphyry.
947	027	Argillite metasediment. Greenland Group.
949	028	Argillite metasediment. Greenland Group.
950	029	Biotite-hornfels. Altered metasediment.
18952	13030	Zone I argillite. Altered metasediment.
955	031	Granodiorite. Lyell Porphyry.
956	032	Granodiorite. Lyell Porphyry.
957	033	Pink microgranite. Bald Hill Granite.
958	034	Biotite-granite. Bald Hill Granite.
959	035	Leucogranite. Bald Hill Granite.
960	036	Quartz trondhjemite. Lyell Porphyry.
962	037	Gabbroporphyry. Lyell Porphyry.
963	038	Granodiorite. Lyell Porphyry.
970	039	Quartz trondhjemite. Lyell Porphyry.
18971	13040	Quartz trondhjemite. Lyell Porphyry.
973	041	Quartz trondhjemite. Lyell Porphyry.
975	042	Quartz trondhjemite. Lyell Porphyry.
976	043	Silicified hornfels. Altered metasediment.

Thesis No.	V.U.W. No.	Description
977	044	Pink microgranite. Bald Hill Granite.
978	045	Biotite-hornfels. Altered metasediment.
979	046	Argillite metasediment. Greenland Group.
980	047	Quartz diorite. Lyell Porphyry.
981	048	Quartz diorite. Lyell Porphyry.
982	049	Zone I greywacke. Altered metasediment.
18983	13050	Lamprophyre dyke rock. Lyell Porphyry.
984	051	Biotite-hornfels. Altered metasediment.
987	052	Biotite-granite. Bald Hill Granite.
988	053	Pink microgranite. Bald Hill Granite.
989	054	Lamprophyre dyke rock. Lyell Porphyry.
991	055	Greywacke metasediment. Greenland Group.
992	056	Pink microgranite. Bald Hill Granite.
993	057	Biotite-granite. Bald Hill Granite.
995	058	Granodiorite. Lyell Porphyry.
996	059	Quartz diorite. Lyell Porphyry.
18997	13060	Lamprophyre dyke rock. Lyell Porphyry.
998	061	Gabbroporphyry. Lyell Porphyry.
999	062	Leucogranite. Bald Hill Granite.
19000	063	Quartz-sulphide vein from hornfels.
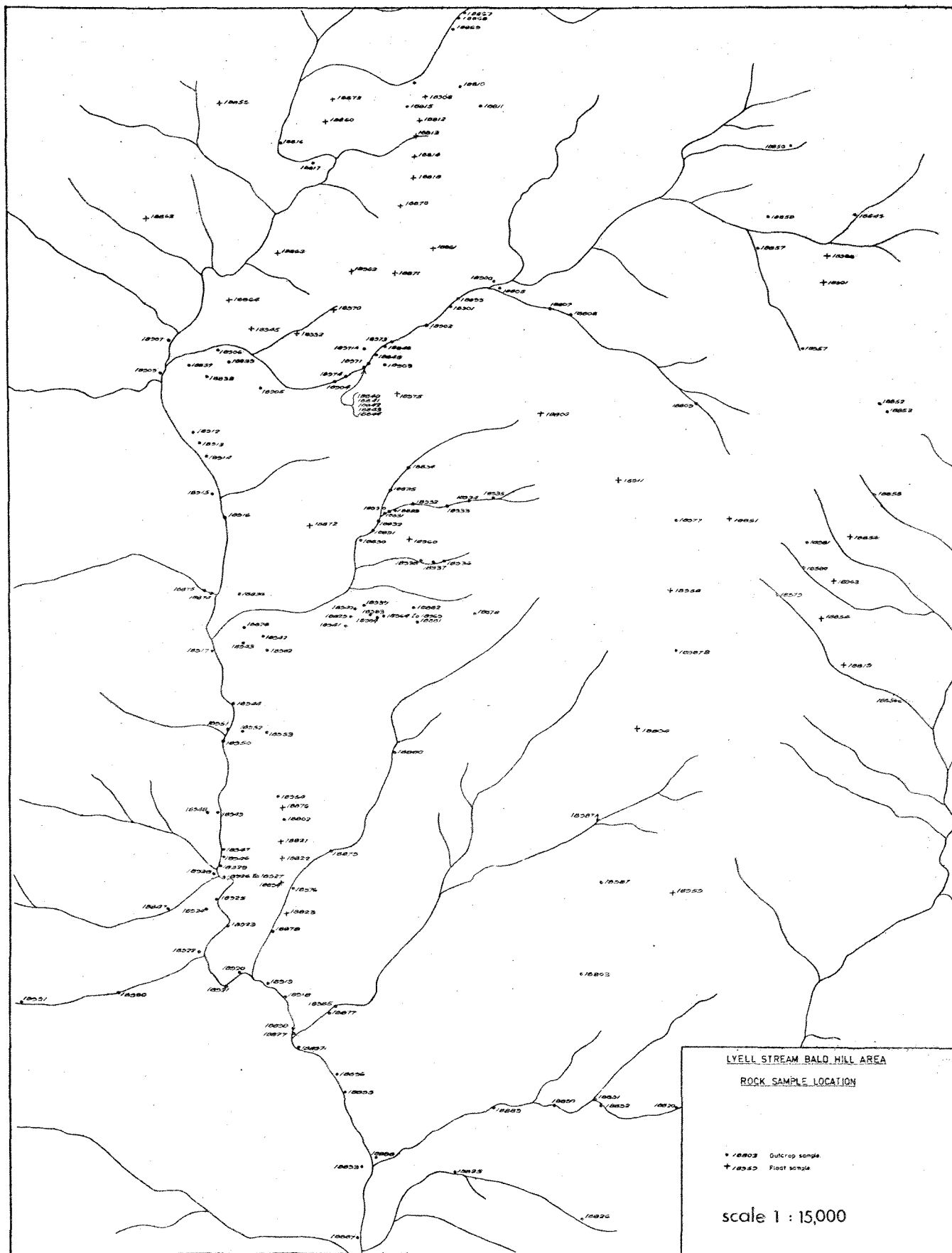
Fig. A1-1: Rock sample locations for Bald Hill molybdenum occurrence.

APPENDIX II: Theory of potassium argon dating technique

for rocks and minerals

K-Ar dating is based on the decay of ^{40}K atoms to two radiogenic daughter atoms ($^{40}Ar_{(rad)}$ and $^{40}Ca_{(rad)}$) and their accumulation within the mineral lattice. i.e.

$$^{40}K \quad \overset{\sim 11.2\%}{\underset{\sim 88.8\%}{\diagup \diagdown}} \quad \begin{matrix} ^{40}Ar \text{ radiogenic} \\ \\ ^{40}Ca \text{ radiogenic} \end{matrix}$$
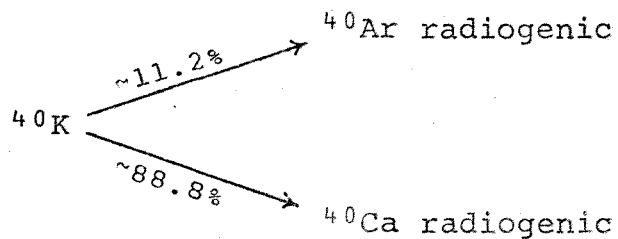
Argon content is determined by Stable Isotope Dilution for a whole rock or mineral. In this method a precisely known quantity of "spike" of different isotope composition (in this instance ^{38}Ar) to the natural element is mixed with the sample being analysed. The ratio of known spike (^{38}Ar) to unknown (^{40}Ar) is measured and total argon ($^{40}Ar_{(TOT)}$) calculated. All ^{40}Ar in the rock or mineral is radiogenic ($^{40}Ar_{(rad)}$) and/or atmospheric ($^{40}Ar_{(atm)}$). The degree of contamination by $^{40}Ar_{(atm)}$ is determined by measuring a third stable isotope of argon, ^{36}Ar. All ^{36}Ar in the sample will be atmospheric. The ratio of $^{36}Ar_{(atm)}$ to $^{40}Ar_{(atm)}$ for the atmosphere is precisely known, therefore by measuring ^{36}Ar, the amount of $^{40}Ar_{(atm)}$ contamination in the sample can be calculated. $^{40}Ar_{(atm)}$ is then subtracted from $^{40}Ar_{(TOT)}$ to get $^{40}Ar_{(rad)}$.

The $\%^{40}K$ and $\%^{40}Ar_{(rad)}$ for a rock or mineral sample are determined, decay constants applied and the age calculated.

There are then, essentially two processes in K-Ar dating a rock or mineral, 1) ^{40}K measurement and 2) ^{40}Ar measurement.

APPENDIX III: Analytical techniques. Major and trace
element analyses

Thirty to forty grams of selected rock sample was
crushed for one minute in a tungsten carbide 'tema' mill
and homogenised. Major, minor and trace element analyses
of bulk samples of rocks were determined by X-Ray
Fluorescence (XRF) carried out on the Siemens SRS-1
spectrometer at Victoria University. Operating conditions
for the spectrometer are given in Tables A3-1 and A3-2.

Major element silicate analyses were carried out on
glass fusion discs following the preparation and correction
procedures given by Norrish and Hutton (1969). Oxide
concentrations were determined by reference to a synthetic
standard, calibrated against international rock standards.
Up to eight unknowns were analysed at one time, with at
least one synthetic background disc and one rock standard
being included with each run to check on accuracy and
precision (Tables A3-3 and A3-4). Comparison with
international rock standards was shown to be excellent and
repeated XRF analysis of a single disc (JG-1) indicates
high standard of analytical precision.

Trace element analyses of copper, nickel, zinc, lead,
thorium, yttrium, zirconium, strontium and rubidium were
carried out on pressed powder pellets and barium determinations
were completed on glass fusion discs. Trace element concen-
trations were also determined by reference to a synthetic

Table A3-1: Operating conditions of XRF: Major elements

Oxide	Tube	Kv	mA	Crystal	Collimator	Count time	cs/%
SiO_2	Cr	45	50	PET	0.4	100	136
TiO_2	Cr	45	50	LiF(200)	0.15	40	7000
Al_2O_3	Cr	45	50	PET	0.4	100	130
Fe_2O_3	Cr	45	50	LiF(200)	0.4	40	1180
MnO	Cr	45	50	LiF(110)	0.15	40	223
MgO	Cr	45	50	ThAP	0.4	100	47
CaO	Cr	45	50	LiF(200)	0.15	40	2900
Na_2O	Cr	45	50	ThAP	0.4	200	17
K_2O	Cr	45	50	PET	0.4	40	3800
P_2O_5	Cr	45	50	PET	0.4	100	180

Table A3-2: Operating conditions of XRF: Trace elements

Element	Tube	Kv	mA	Crystal	Collimator	Line	X-Ray Path	Count time Pk.	Bk.
Ba	Cr	55	40	LiF(200)	0.15	Lα	Vac	100	40
Cu	Au	43	55	LiF(200)	0.15	Kα	Air	40	40
Ni	Au	43	55	LiF(200)	0.15	Kα	Air	40	40
Zn	Au	43	55	LiF(200)	0.15	Kα	Air	40	40
Rb	Mo	43	55	LiF(110)	0.15	Kα	Air	40	40
Th	Mo	43	55	LiF(110)	0.15	Lα	Air	40	40
Y	Mo	43	55	LiF(110)	0.15	Kα	Air	40	40
Pb	Mo	43	55	LiF(110)	0.15	Lβ	Air	40	40
Zr	Au	43	55	LiF(110)	0.15	Kα	Air	40	40
Sr	Au	43	55	LiF(110)	0.15	Kα	Air	40	40
Mo	Au	43	55	LiF(110)	0.15	Kα	Air	40	40
S	Cr	55	40	PET	0.4	Kα	Vac	40	—

Table A3-3: XRF analyses of USGS standard rocks (Accuracy)

	AGV-1		BCR		GSP-1		G2		DTS		JG-1	
	(1)	(2)	(1)	(2)	(1)	(2)	(1)	(2)	(1)	(2)	(1)	(2)
SiO_2	58.95	59.00	53.76	54.50	67.40	67.38	69.12	69.11	40.20	40.50	72.23	72.24
TiO_2	1.04	1.04	2.23	2.20	0.66	0.66	0.48	0.50	0.00	0.01	0.26	0.26
Al_2O_3	17.41	17.25	13.60	13.61	15.38	15.25	15.61	15.40	0.41	0.24	14.28	14.21
Fe_2O_3*	6.75	6.56	13.54	13.40	4.24	4.33	2.67	2.65	9.24	8.64	2.09	2.02
MnO	0.11	0.10	0.20	0.18	0.05	0.04	0.07	0.03	0.14	0.11	0.06	0.06
MgO	1.58	1.53	3.57	3.46	1.03	0.96	0.78	0.76	49.31	49.80	0.75	0.73
CaO	4.89	4.90	6.90	6.92	1.99	2.02	1.92	1.94	0.14	0.15	2.16	2.18
Na_2O	4.37	4.26	3.16	3.27	2.86	2.80	4.09	4.07	0.00	0.01	3.37	3.39
K_2O	2.94	2.89	1.71	1.70	5.55	5.53	4.52	4.51	0.00	0.00	4.01	3.96
P_2O_5	0.50	0.49	0.37	0.36	0.27	0.28	0.13	0.14	0.00	0.00	0.09	0.10

(1)   XRF analyses, Victoria University Analytical Facility.

(2)   Average values from Flanagan (1973; 1976).

*   All Fe as Fe_2O_3.

Table A3-4: XRF analyses of USGS standard rock JG-1 (Analytical
precision

	$\bar{x}$	θ	n	Sample
SiO_2	72.20	0.16	19	JG-1
TiO_2	0.26	0.01	19	"
Al_2O_3	14.24	0.06	19	"
Fe_2O_3*	2.10	0.02	19	"
MnO	0.06	0.01	19	"
MgO	0.71	0.06	19	"
CaO	2.16	0.01	19	"
Na_2O	3.36	0.05	19	"
K_2O	4.01	0.01	19	"
P_2O_5	0.10	0.01	19	"

$\bar{x}$: Mean value.

θ: One standard deviation.

n: Number of determinations.

* All Fe as Fe_2O_3.

standard and calibrated against international rock standards, with a synthetic background pellet and one rock standard being included in each run. Accuracy (Table A3-5) is shown to be good along with analytical precision (Table A3-6). Ba, Cu, Ni, Zn, Sr and Zr were all analysed in duplicate and average values presented.

Molybdenum and sulphur values were determined on powder mounts by XRF. For molybdenum, a synthetic standard was used for reference and concentrations calibrated against two international rock standards (JG-1 and JB-1) and six USGS geochemical exploration reference samples, with mean values given by Allcott and Lakin (1974). Analytical precision is excellent, although comparison analyses of standards appear not to be as good as for other trace elements (Tables A3-7 and A3-8).

The method used for sulphur determinations was to convert intensity of counts per second (I c/s) to parts per million (ppm) by using a normal regression curve, i.e.

$$S_{ppm} = -257 \times 3.219 \; c/s_{(sulphur)}.$$

The curve was calculated by counting five USGS rock standards (25 determinations) of known sulphur concentration (Leake, B. E. et al. 1970) and calculating the best fit relationship by the least squares method. Precision and accuracy for sulphur (Tables A3-9 and A3-10) were poor owing to 1) the lack of suitable international standards for calibration and 2) the method not allowing for background interference or mass absorption of other elements. The

Table A3-5: XRF trace element analyses of international standard rocks (ppm)

	AGV		BCR		GSP-1		G2		JG-1		JB-1		BR	
	(1)	(2)	(1)	(2)	(1)	(2)	(1)	(2)	(1)	(2)	(1)	(2)	(1)	(2)
Ba	–	–	–	–	–	–	–	–	–	–	–	–	1054	1050
Cu	65	60	17	18	32	33	–	–	5	3	56	52	76	70
Ni	18	18	15	16	7	12	–	–	5	10	119	139	249	270
Zn	88	84	122	120	108	98	–	–	45	36	84	83	141	160
Rb	78	67	–	–	253	254	170	168	–	–	46	41	52	45
Th	10	6	–	–	101	104	26	24	–	–	9	9	–	–
Y	24	21	–	–	29	30	13	12	–	–	26	–	31	27
Pb	43	35	–	–	53	51	33	31	–	–	13	14	–	–
Zr	226	225	167	190	493	500	301	300	87	160	123	300	259	240
Sr	678	657	321	330	233	233	479	479	182	184	460	438	1328	1350

(1)   XRF analyses, Victoria University Analytical Facility.

(2)   Average values from Flanagan (1973; 1976).

Table A3-6:   XRF trace element analyses of USGS standard rock
BR (Analytical precision)

	$\bar{x}$	θ	n	Sample
Ba	1054	14	20	BR
Cu	76	2	22	"
Ni	249	3	23	"
Zn	141	2	24	"
Rb	52	1	13	"
Th	10	3	12	"
Y	31	1	13	"
Pb	8	1	13	"
Zr	259	6	21	"
Sr	1328	7	21	"

$\bar{x}$:   Mean value.

θ: One standard deviation.

n: Number of determinations.

Table A3-7: XRF molybdenum determinations of international standard rocks and synthetic standard.

	(1)	(2)		(3)	(4)
GXR1	19	30	JB-1	28	25
GXR2	4	12			
GXR3	2	14	JG-1	1	2
GXR4	332	301			
GXR5	40	31	SYN STD.	1148	*1150
GXR6	3	10			

(1) Victoria University analytical facility.

(2) Mean values for Allcott, G. and Lakin, H. 1974.

(3) Victoria University analytical facility.

(4) Mean values from Ando, A. et al. 1974

* Calculated value of synthetic standard.

Table A3-8: XRF molybdenum determinations for JB-1, G-2 standards and synthetic standard.

	$\bar{x}$	θ	n	Sample
Mo	28	3	13	JB-1
Mo	191	7	11	G-2
Mo	1148	9	13	Synthetic standard

$\bar{x}$: Mean value.

θ: One standard deviation.

n: Number of determinations.

Table A3-9: XRF sulphur counts per second (c/s) for five
USGS rock standards

Rock standard	c/s		*Sulphur ppm
G.1	113.94		
	105.14		124
	119.17		
G.2	140.57	138.35	161
	139.30	136.32	
	139.75	135.50	
	139.92	141.05	
	138.27	144.00	
	137.55	140.32	
GSP-1	168.31		289
	171.04		
BR	208.73		414
	206.70		
	213.85		
BCR	232.11		482
	231.49		
	241.04		

Regression curve: $S_{ppm} = -257.57 + 3.219 \times c/s$.

* S_{ppm} mean values from Leake, B. E. et al. 1970.

Table A3-10: XRF sulphur determinations of USGS standard rocks

| AGV		GSP-1		BCR		G-1		G-2		BR	
(1)	(2)	(1)	(2)	(1)	(2)	(1)	(2)	(1)	(2)	(1)	(2)
110	56	289	289	499	482	106	124	191	161	418	414

(1) Analytical facility Victoria University.

(2) Mean values from Leake, B.E. et al. 1970.

values do however, demonstrate sulphur ratios from unmineralized to mineralized samples.

Ferrous iron (Fe^{2+}) was determined by titration using the method as outlined by Shapiro and Brannock (1962) using V.U.W. basalt as the internal standard. Ignition loss (L.O.I.) was determined by heating one gram of sample to 1000°C for one hour.

APPENDIX IV: Experimental and calculated sulphur isotope temperature calibration curves for molybdenite-sulphide mineral pairs from Suvorova (1974).

GEOLOGICAL SURVEY

PROFESSIONAL PAPER 440-KK   FIGURE 49
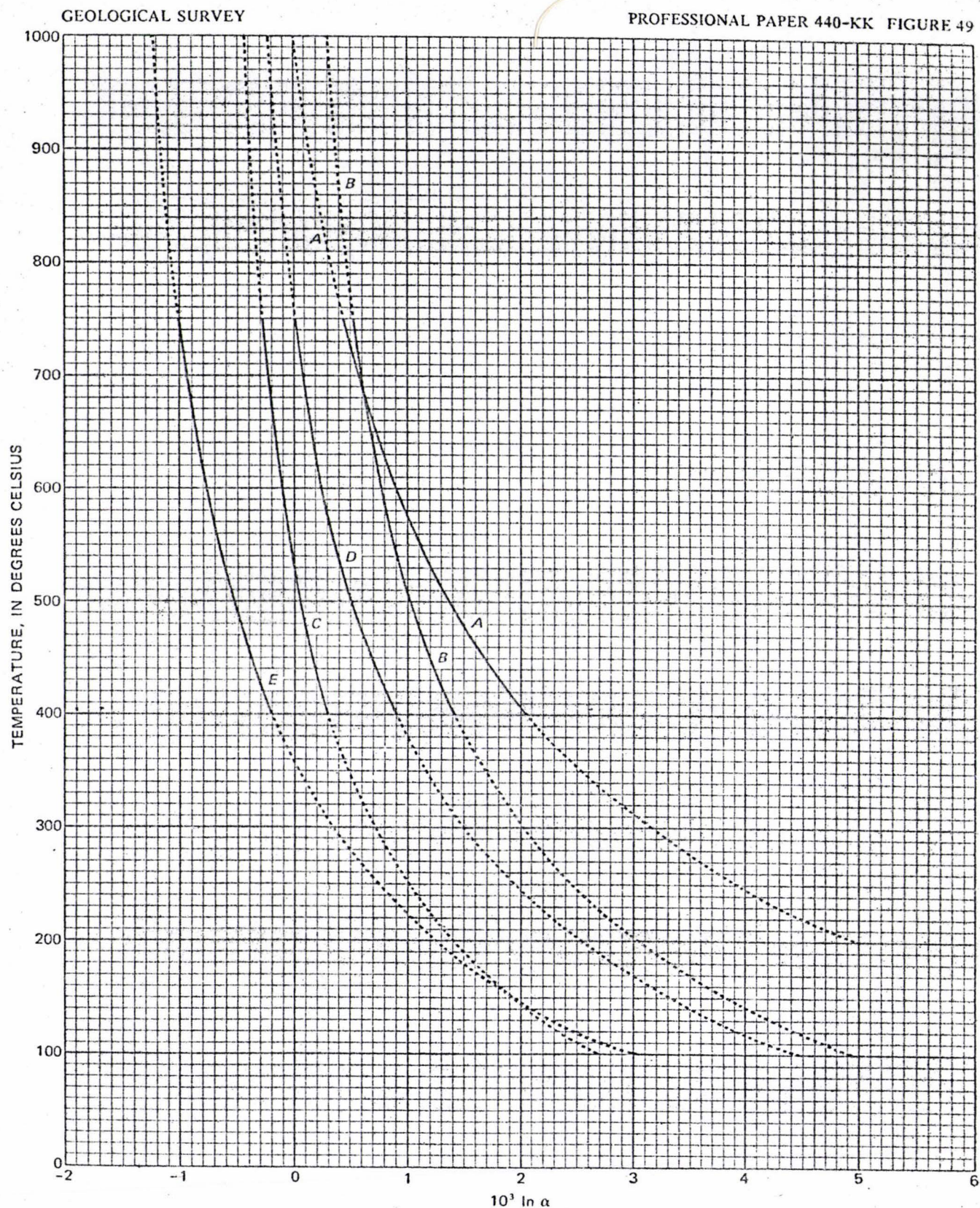
MOLYBDENITE-SPHALERITE, -GALENA, -CHALCOPYRITE, -PYRITE, AND -PYRRHOTITE

Fig. A4-1:   Molybdenite-sulphide temperature calibration curves.

Published in Friedman and O'Neil, 1977.

APPENDIX V: 'Open file' Mines Department Reports
               (Unpublished).

Ballantyne, G. H.; Smale, D.; Turbott, M. J. 1971,
    Progress Report. New Zealand Molybdenum
    Reconnaissance. Big Bend examination.
    For: Kennecott Explorations (Aust) Pty. Ltd.

Dodds, L. R. 1969, Eliot Creek molybdenum prospect,
    Nelson, New Zealand.
    For: Asarco Developments (New Zealand) Ltd.

Foster, J. T. 1971, Progress Report. New Zealand
    Molybdenum. Roaring Lion examinations.
    For: Kennecott Explorations (Aust) Pty. Ltd.

Maxwell, M. G. 1974, Taipo prospect. Geological Report.
    For: New Zealand-Cities Service Inc.

_____ 1975, Petrographic reports on drill core
    from Taipo P.L. 31155. (Two reports).
    For: New Zealand-Cities Service Inc.

_____ 1975, Drilling Results. Taipo prospect.
    For: New Zealand-Cities Service Inc.

Turbott, M. J. 1968, Final Report. Eliot Creek examination.
    For: Kennecott Explorations (Aust) Pty. Ltd.

_____ 1972, Final Report on M.P.W.s 14861 & 14862.
    Roaring Lion River.
    For: Kennecott Explorations (Aust) Pty. Ltd.

_____ 1972, Final Report on M.P.W.s 14958 & 14959.
    Planet Creek Area, Karamea River.

_____ 1972, Final Report on M.P.W. 14770 Roaring
    Lion River Area.
    For: Kennecott Exploration (Aust) Pty. Ltd.

Smale, D. 1974, Report on the examination of Copperstain
    Creek copper prospect, Northwest Nelson.
    For: Kennecott Exploration (Aust) Pty. Ltd.

APPENDIX VI: Large scale circular features in West Nelson
and North Westland; Possible structural
control for porphyry molybdenum-copper
mineralization?

The 1:500,000 Landsat photograph of the northern
half of the South Island, New Zealand (Figs.A6-1 and A6-3)
shows many, previously mapped lineations, faults and
drainage patterns. In addition, the most interesting
features noted were previously unobserved circular
structures (generally from 8 km to 40 km in diameter).
They occur at least partially, if not completely in the
320 Ma to 100 Ma granite terranes (Eggers and Adams, 1978)
of West Nelson and North Westland. The circles appear
to place extraordinary control on ore mineralization,
especially "stock-work or reef-type" molybdenum mineralization
closely associated with minor calc-alkaline intrusive stocks
(Eggers, 1978).

In western Nelson fifteen of the most clearly
definable circular features have been plotted to the same
scale in Figs.A6-2 and A6-4 and the location of all significant
porphyry molybdenum-copper prospects (Eggers and Adams, 1978)
have been superimposed. All these prospects plot on, or very
near to the rims of the features.

The present topographic expression of the features is
enhanced by rivers and streams which have preferentially
eroded the more fractured and sheared rock along the rims
of the features subsequently exposed by erosion. The circles
are of a similar size, near perfect in outline, and although

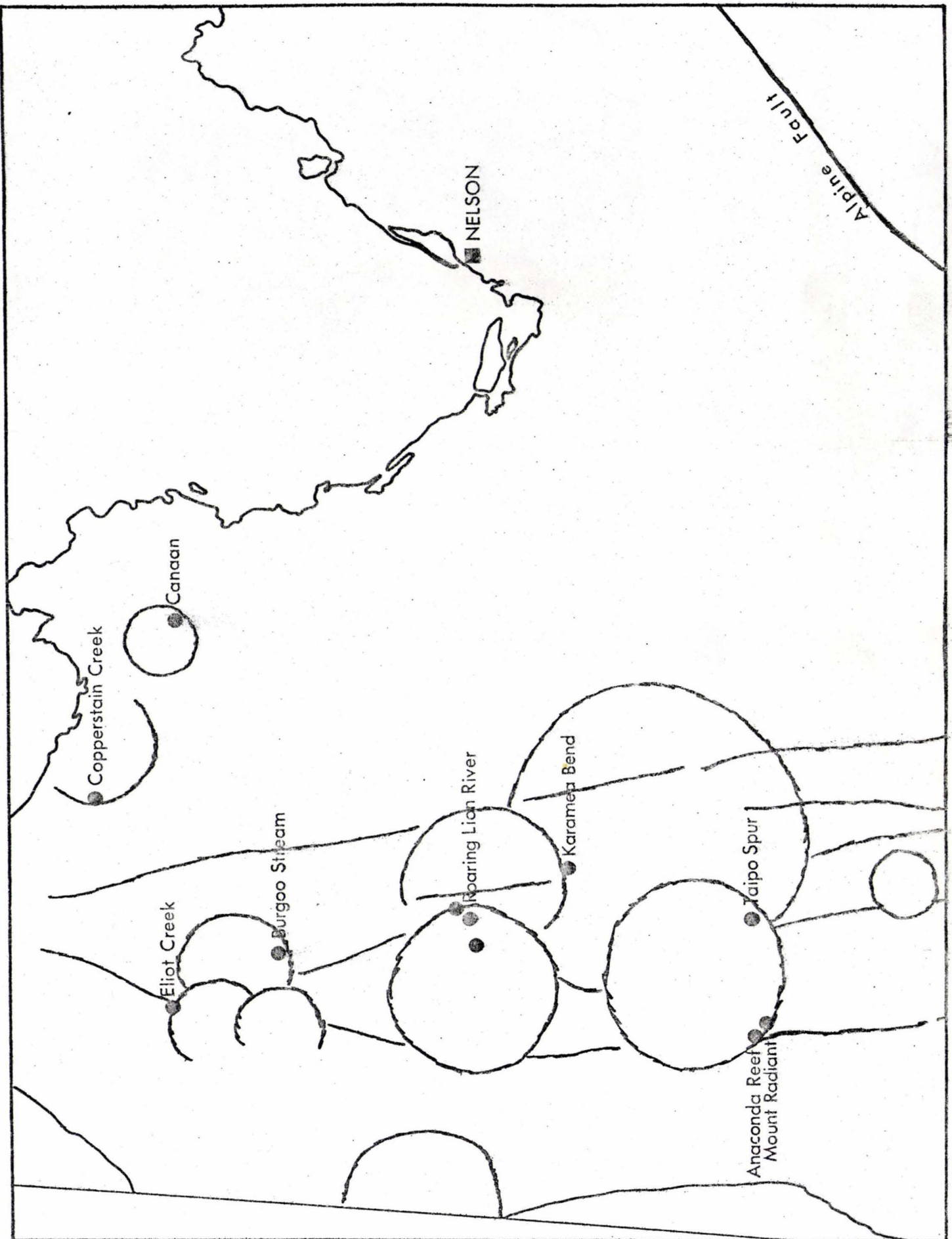Fig. A6-1: Landsat photograph of Northwest Nelson

(1:500,000)

Fig. A6-2: Circles and location of molybdenum-copper prospects for the area of Fig. A6-1
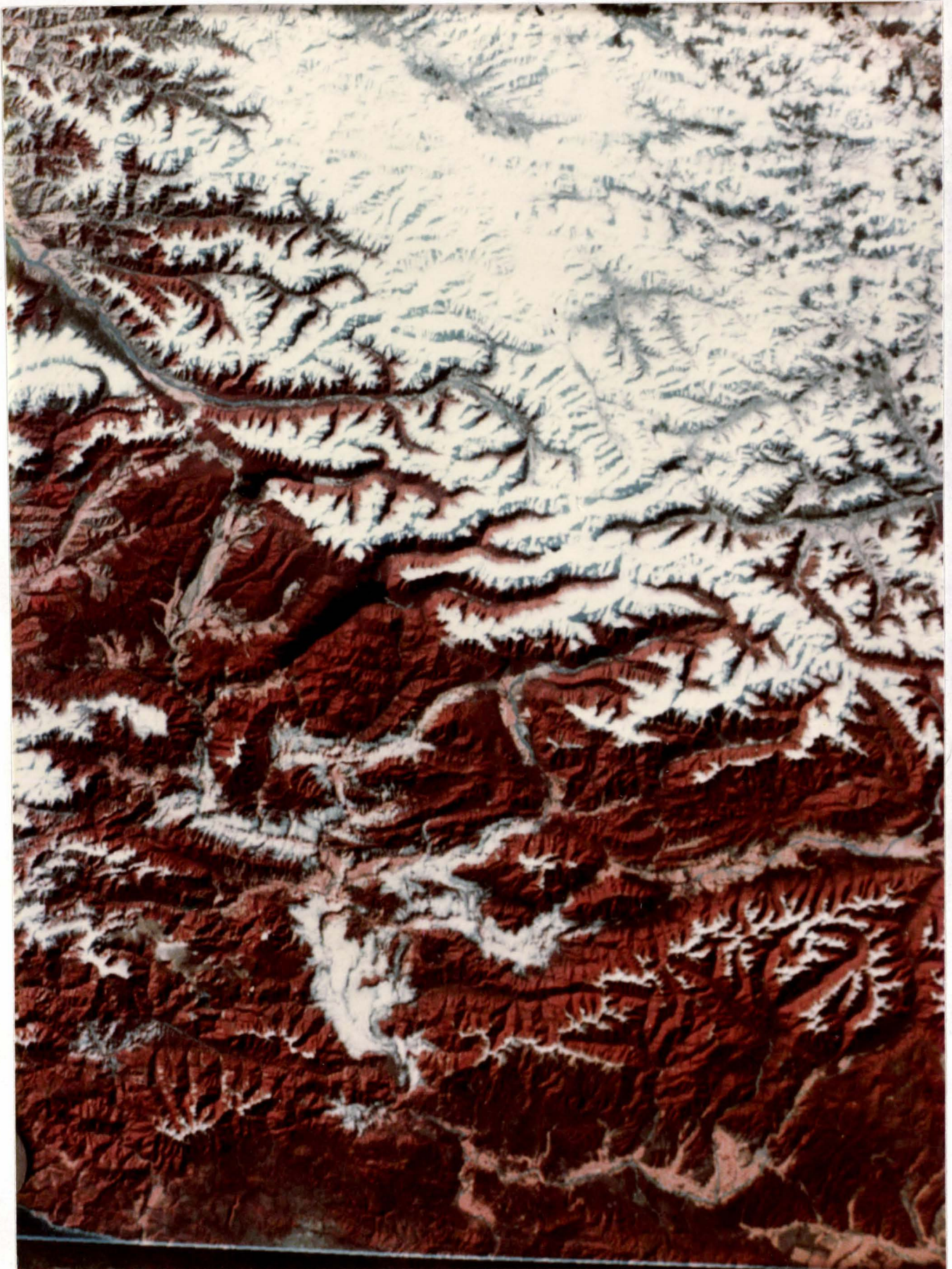
Fig. A6-3: Landsat photograph of North Westland - Buller District
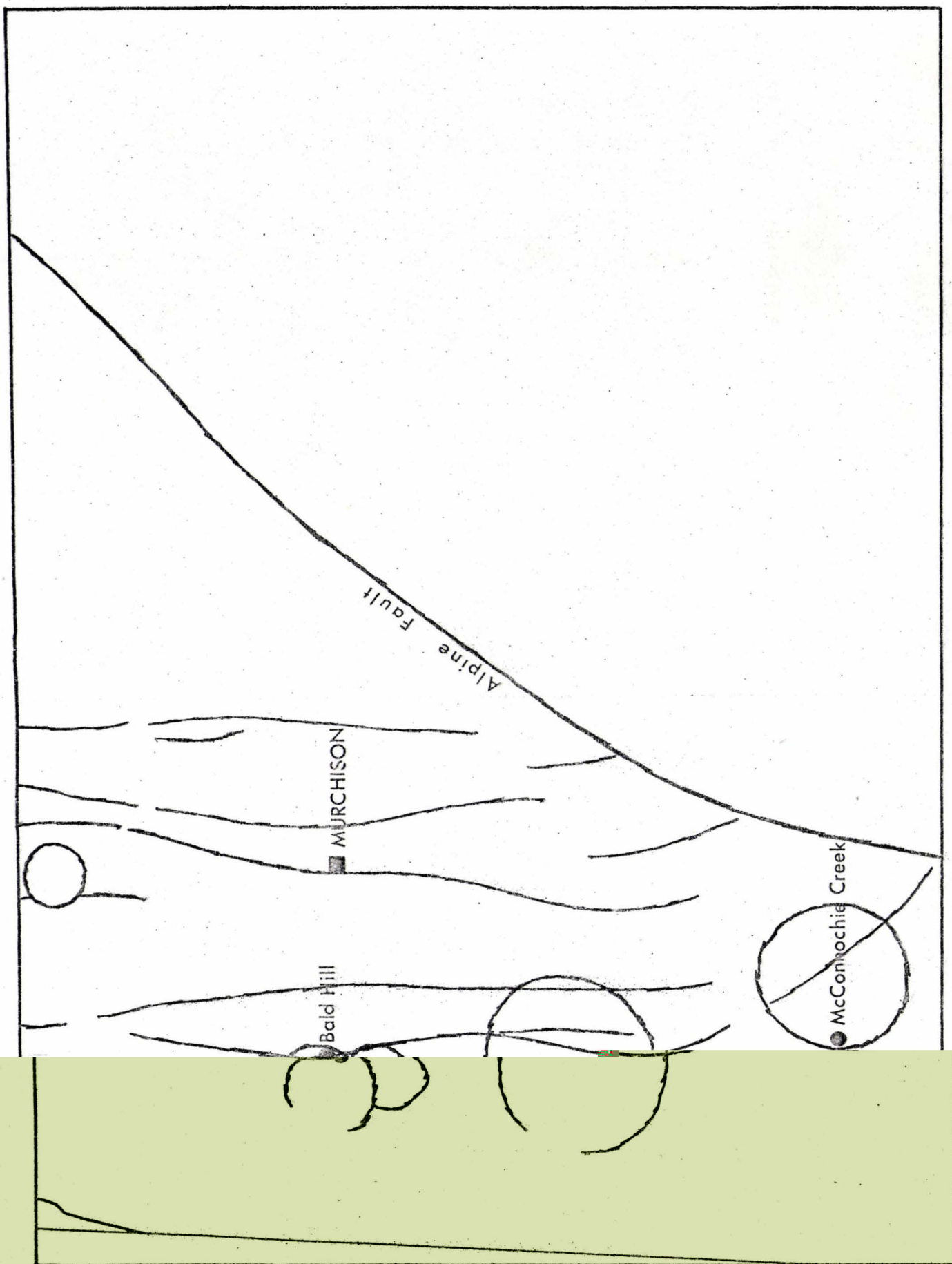
(1 : 500,000)

Fig. A6-4: Circles and location of molybdenum-copper
prospects for the area of Fig. A6-3

mostly outlined by topographic lows, sections of some circles are outlined by topographic highs. Intersection of these circles and the north-south linear structures and faults in western Nelson do not appear to have any particular spatial control on the location of molybdenum mineralization. This would indicate these linear features are post porphyry emplacement and did not exert any significant control on porphyry intrusion.

Adams (1978), in a note submitted to the Geological Society of New Zealand Newsletter, noted four circular features (3 km to 7 km across) on Landsat photographs of the Lowery Peaks and Hurunui Ranges in Canterbury, New Zealand. These features occur in Torlesse Group sedimentary rocks and mineralization is unknown in these areas.

Saul (1978) has identified similar features in Arizona and comments that they have also been observed in the western United States, northernmost Mexico, the Appalachians, Alaska, the Yukon and probably in Madagascar and Corsica. He noted a similar relationship between circles and mineralization, especially the occurrence of molybdenum-copper porphyries. Also Saul (1978) makes reference to circular features being associated with the Butte molybdenum occurrence in Montana and the Bingham porphyry deposit in Utah.

As stated by Saul (1978) for comparable features in Arizona, "The correlation of mineralization with the circles stands on its own and does not depend on the acceptance of any particular theory as to how the circles came into existence."

Saul (1978) interpreted the circles in Arizona as
having been formed by the impacts of meteorites during the
most recent bombardment of the Earth, approximately 4,000 Ma
ago. The circular features have been propagated downwards
through the Earth's crust with time, the present structures
inherited from pre-existing structures in the overlying
older rocks long since eroded away.

Whether or not this hypothesis holds for Arizona,
it is believed to be an unlikely explanation in western
Nelson. For the meteorite impact mechanism to hold, a
stable continental shield-type situation must be invoked.
Geologic evidence for western Nelson shows the area to
have been an active continental margin-type situation with
any structures formed 4,000 Ma ago long since destroyed.
Consequently a "caldera-fracture" hypothesis is suggested
for the circular features in western Nelson. It is proposed
that the features have been generated from below by the large
scale diapiric intrusion of highly viscous H_2O-saturated
granite magmas (similar to salt dome intrusion, White et al.,
1974; Wyllie et al., 1976 and Wyllie, 1977). The updoming
of these 'diapir-like' bodies has formed large scale ring-
fractures and/or minor collapse in the overlying granites
and metasediments. The circular features formed, by tension
above the 'diapirs', would be the equivalent of the lower
half of large scale caldera-type structures (eg: Smith
and Bailey, 1968). Calc-alkaline molybdenum-copper bearing
porphyry melts generated at greater depths in the Earth's
crust (eg: White and Chappell, 1977; Wyllie, 1977) would

have much lower viscosities. The melts are able to move upwards, intruding the overlying silicic granites and meta-sediments, preferentially intruding into areas of reduced lithostatic pressure around the margins of the diapirically intruded silicic granites. Surface volcanic activity may have been coeval with the emplacement of the mineralized stocks (eg: Stitts Tuff, Adams and Nathan, 1978). The change from lithostatic to hydrostatic pressure in these fractures would cause ascending hydrothermal fluids to boil, thereby precipitating any sulphide phases. In a similar manner the "caldera-fracture" hypothesis also provides a mechanism whereby descending meteoric waters could infiltrate the upper crust and be heated by or mixed with, rising magma or hydrothermal fluids respectively.

Whatever the mode of formation, or significance of the circular features, they provide both possible mechanisms and structural control for the concentration of hydrothermal metalliferous deposits in West Nelson and North Westland.

REFERENCES

Adams, C.J.D. 1974, New Zealand Potassium-Argon age list-2; N.Z. Journal of Geology and Geophysics v.18(3); p.443-467.

Adams, C.J.D. 1975, Discovery of Precambrian rocks in New Zealand. Age relationships of the Greenland Group and Constant Gneiss, West Coast, South Island; Earth and Planetary Science Letters v. 28; p.98-104.

Adams, C.J.D.; Harper, C. T.; Laird, M. G. 1975, K-Ar ages of low grade metasediments of the Greenland and Waiuta Groups in Westland and Buller, New Zealand; N.Z. Journal of Geology and Geophysics v.18(1); p.39-48.

Adams, C.J.D.; Nathan, S. 1978, Cretaceous chronology of the Lower Buller Valley, South Island, New Zealand; N.Z. Journal of Geology and Geophysics v.21(3); p.42- .

Allcott, G. H.; Lakin, H. W. 1974, Statistical summary of geochemical data furnished by 85 laboratories for six geochemical exploration reference samples; United States Department of the Interior Geological Survey. Open File Report; pp 96.

Ando, A.;Kurasawa, H.; Ohmori, T.; Takeda, E. 1974, 1974 compilation of data on the GSJ geochemical reference samples JG-1 granodiorite and JB-1 basalt; Geochemical Journal v.8; p. 175-192.

Aronson, J. L. 1965, Reconnaissance rubidium-strontium geochronology of New Zealand plutonic and metamorphic rocks; N.Z. Journal of Geology and Geophysics v.8(3); p.401-423.

Aronson, J. L. 1968, Regional geochronology of New Zealand.

  Geochimica et. Cosmochimica Acta v.32; p.669-697.

Bailey, D. G. 1972, The geology and sulphide mineralization

  at Mount Radiant, North-West Nelson; Unpublished honours

  project held at Geology Department, Victoria University

  of Wellington.

Bailey, D. G. 1973, Geology and Geochemistry of the Rochfort

  Creek and Cascade Creek watersheds; Otter Minerals

  Internal Report; pp 19.

Bell, J. M.; Webb, E.J.H.; Clarke, E.; De, C. 1907, The

  Geology of the Parapara Subdivision; N.Z. Geological

  Survey Bulletin 3; pp 111.

Bowen, F. E. 1964, Sheet 15 Buller; Geological Map of

  New Zealand 1:250,000 (1st Ed.).

Brown, G. C.; Fyfe, W. S. 1970, The Production of Granitic

  Melts during Ultrametamorphism; Contrib. to Mineralogy

  and Petrology v.28; p.310-318.

Carmichael, I. S.; Turner, F. J.; Verhoogen, J. 1974,

  Igneous Petrology; McGraw-Hill Book Company; pp 739.

Chappell, B. W.; White, A.J.R. 1974, Two contrasting granite

  types; Pacific Geology v.8; p.173-174.

Coats, R. R. 1968, The Circle Creek Rhyolite, a volcanic

  complex in Northern Elko County, Nevada; Geological

  Society of America Memoir No.116; p.69-106.

Coleman, M. L. 1977, Sulphur isotopes in petrology;

  Journal of Geological Society of London; v.133;

  p.593-608.

Cooper, R. A. 1974, Age of the Greenland and Waiuta
Groups, South Island, New Zealand; N.Z. Journal of
Geology and Geophysics v.17(4); p.955-962.

Cooper, R. A. 1975, New Zealand and South-East Australia
in the Early Palaeozoic; N.Z. Journal of Geology and
Geophysics v.18(1); p.1-20.

Eggers, A. J.; Adams, C.J.D. 1978, Potassium-argon ages of
molybdenum mineralization and associated granites at
Bald Hill and correlation with other molybdenum
occurrences in the South Island, New Zealand; (In Press)
Economic Geology.

Flanagan, F. J. 1973, 1972 values for international
geochemical reference samples; Geochimica et. Cosmochimica
Acta, v.37; p.1189-1200.

Flanagan, F. J. 1976, Description and Analyses of eight new
USGS Rock Standards; U.S. Geological Survey Professional
Paper 840.

Flood, R. H.; Shaw, S. E. 1977, Two "S-type" granite suites
with low initial $^{87}Sr/^{86}Sr$ ratios from the New England
Batholith, Australia; Contrib. to Mineralogy and
Petrology v.61(2); p.163-173.

Friedman, I.; O'Neil, J. R. 1977, Data of Geochemistry
(6th Ed.). Chapter KK. Compilation of Stable Isotope
Fractionation Factors of Geochemical Interest;
Geological Survey Professional Paper 440-KK; pp 112.

Harper, C. T.; Russell, C. W.; Sherrer, G.; Stonebraker, J.D.; Kish, S. 1973, The Arvonia Slate: a useful standard for K-Ar dating; Geological Society of America, Abstracts with Programs, Annual General Meeting, South-East Section, Knoxville, Tennesse; pp 402.

Henderson, J. 1917, The geology and mineral resources of the Reefton Subdivision; N.Z. Geological Survey Bulletin 18: pp 232.

Henderson, S. M. 1975, Taipo Ridge Molybdenum Prospect. A comparative study; Unpublished B.Sc. Honours Project held at Geology Department, Victoria University of Wellington.

Hulston, J. R.; McCabe, W. J. 1972, New Zealand Potassium-Argon Age List-1; N.Z. Journal of Geology and Geophysics v.15(3); p.406-432.

Kawachi, Y. 1974, Geology and petrochemistry of weakly metamorphosed rocks in the Upper Wakatipu District, Southern New Zealand; N.Z. Journal of Geology and Geophysics v.17(1); p.169-208.

Kilinc, I. A. 1972, Experimental study of partial melting of crustal rocks and formation of migmatites; 24th Int. Geol. Congr., Montreal; Abstracts; p.47-48.

Kuno, H.; Yamasaki, K.; Iida, C.; Nagashima, K. 1957, Differentiation of Hawaiian magmas; Japan Journal of Geology and Geography v.28; p.179-218.

Lanphere, M. A.; Dalrymple, G. B. 1965, P-207, an inter-laboratory standard muscovite for argon and potassium analyses; Journal of Geophysical Research v.70; p.3497-3503.

Lanphere, M. A.; Dalrymple, G. B. 1967, K-Ar and Rb-Sr measurements on P-207, the U.S.G.S. interlaboratory standard muscovite; Geochimica et. Cosmochimica Acta v.31; p.1091-1094.

Leake, B. E.; Hendry, G. L.; Kemp, A.; Plant, A. G.; Harrey, P. K.; Wilson, J. R.; Coats, J. S.; Aucott, J. W.; Lünell, T.; Howarth, R. J. 1970, The chemical analysis of rock powders by automatic X-ray fluorescence; Chemical Geology v.5; p.7-86.

McBirney, R. A.; Aoki, K. 1968, Petrology of the Island of Tahiti; Geological Society of America, Memoir No. 116; p.523-556.

McDonald, G. A. 1968, Composition and origin of Hawaiian Lavas; Geological Society of America Memoir No.116; p.477-522.

Nathan, S. 1974, Petrology of the Berlins Porphyry: A study of crystallization of granitic magma; Journal of the Royal Society of New Zealand v.4(4); p.463-483.

Nathan, S. 1976, Geochemistry of the Greenland Group (Early Ordovician), New Zealand; N.Z. Journal of Geology and Geophysics v.19(5); p.683-706.

Nathan, S. 1978, Sheet S31 and part S32 Buller-Lyell. "Geological Map of New Zealand 1:63360"; N.Z. Department of Scientific and Industrial Research, Wellington.

Norrish, K.; Hutton, J. T. 1969, An accurate x-ray spectrographic method for the analysis of a wide range of geological samples; Geochimica et. Cosmochimica Acta v.33; p.431-453.

Odin, G. S. 1976, Le glauconite GL-O, etalon inter-
laboratories pour l'analyse radiochronometrique;
Analusis v. 4(6); p.287-291.

Ohmoto, H. 1972, Systematics of sulphur and carbon isotopes
in hydrothermal ore deposits; Economic Geology v.67;
p.551-578.

O'Neil, J. R.; Chappell, B. W. 1977, Stable isotope relations
in the Berridale Batholith, Southeastern Australia;
Journal of Geological Society of London v.133; p.559-572.

O'Neil, J. R.; Shaw, S. E.; Flood, R. H. 1977, Oxygen and
hydrogen isotope compositions as indicators of granite
genesis in the New England Batholith, Australia;
Contrib. to Mineralogy and Petrology v.62(3); p.313-328.

Ongley, M.; MacPherson, E. O. 1923, The geology and mineral
resources of the Collingwood Subdivision; N.Z. Geological
Survey Bulletin 25; pp 52.

Potter, R. W. 1977, Pressure corrections for fluid-inclusion
homogenization temperatures based on the volumetric
properties of the system $NaCl-H_2O$; Journal of Research
of the U.S. Geol. Survey v. 5(5); p. 603-607.

Price, R. C.; Taylor, S. R. 1977, The rare earth element
geochemistry of granite, gneiss, and migmatite from
the Western Metamorphic Belt of South-Eastern Australia.
Contrib. to Mineralogy and Petrology v.62(3); p.249- .

Rabone, S.D.C. 1977, Molybdenum-base metal-bismuth minerali-
zation at Eliot Creek, Karamea Bend, and Taipo Spur,
North-West Nelson, New Zealand; Unpublished Ph.D.
Thesis held at University of Auckland, N.Z.

Reed, J. J. 1957, Petrology of the Lower Mesozoic rocks
of the Wellington District. N.Z. Geological Survey
Bulletin 57; pp 60.

Reed, J. J. 1958, Granites and mineralization in New Zealand;
N.Z. Journal of Geology and Geophysics v.1(1); p.47-64.

Robinson, B. W. 1974, The origin of mineralization at the
Tui Mine, Te Aroha, New Zealand, in the light of stable
isotope studies. Economic Geology v.69(6); p.910-925.

Robinson, B. W.; Kusakabe, M. 1975, Quantitative preparation
of sulphur dioxide, for $^{34}S/^{32}S$ analyses, from sulphides
by combustion with cuprous oxide; Analytical Chemistry
v.47(7); p.1179-1181.

Rye, R. O.; Ohmoto, H. 1974, Sulphur and carbon isotopes
and ore genesis: A Review; Economic Geology v.69(6);
p.826-842.

Saul, J. M. 1978, Circular structures of large scale and
great age on the Earth's surface, Nature v.271; p.345-349.

Shapiro, L.; Brannock, W. W. 1962, Rapid analysis of silicate,
carbonate and phosphate rocks; U.S. Geol. Survey Bull.
1144-A.

Shima, M.; Gross, W. H.; Thode, H. G. 1963, Sulphur isotopic
abundances in basic sills, differentiated granites, and
meteorites; Journal of Geophysical Research v.68;
p.2835-2846.

Smale, D. 1976, Hydrothermal alteration around younger
intrusives near Karamea Bend, North-West Nelson, New
Zealand; Proceedings of the Australian Institute of
Mining and Metallurgy 260; p.53-59.

Smith, R. L.; Bailey, R. A. 1968, Resurgent Cauldrons;
In Studies in Volcanology; Coats, Hay, Anderson (Eds);
Geological Society of America Memoir 116; p.613-662.

Steiger, R. H.; Jager, E. 1977, Subcommission on geochronology:
Convention on the use of decay constants in geo- and
cosmochronology; Earth and Planetary Science Letters
v.36; p.359-362.

Streckeisen, A. L. 1967, Classification and Nomenclature
of Igneous Rocks; Neues Jahrbuch fur Mineralogie,
Abhandlungen v.107; p.144-240.

Streckeisen, A. L. 1973, IUGS Subcommission on the Systematics
of Igneous Rocks; Geotimes v.18(10); p.26-30.

Suvorova, V. A. 1974, Temperature dependence of the
distribution coefficient of sulphur isotopes between
equilibrium sulphides; National symposium on stable
isotope geochemistry. 5th Moscow Program. Pt. 1;
pp 128 (In Russian).

Taylor, S. R. 1965, The application of trace element data
to problems in petrology; Physics and Chemistry of
the Earth v.6; p.133-213.

Thornton, C. P.; Tuttle, O. F. 1960, Chemistry of igneous
rocks. I. Differentiation index; American Journal of
Science v.258; p.664-684.

Travis, R. B. 1955, Classification of rocks; Quarterly of
the Colorado School of Mines v.50(1); pp 98.

Tullock, A. 1977, pers. comm. K-Ar mineral ages of granites
in the Victoria Range, Westland, New Zealand.

Tuttle, O. F.; Bowen, N. L. 1958, Origin of granite in the light of experimental studies; Geological Society of America Memoir 74; pp 153.

Uytenbogaardt, W.; Burke, E.A.J. 1971, Tables for Microscopic Identification of Ore Minerals; Elsevier, London; pp 430.

van Hinte, J. E. 1976, A Cretaceous Time-Scale; Bulletin of the American Association of Petroleum Geologists v.60(4); p.498-516.

Webb, E.J.H. 1910, The geology of the Mount Radiant Subdivision; N.Z. Geological Survey Bulletin 11; pp 46.

White, A.J.R.; Beams, S.D.; Cramer, J. J. 1977, Granitoid types and mineralization with special reference to tin; In: Plutonism in Relation to Volcanism and Metamorphism. Papers presented at the 7th CPPP Meeting, Toyama; p.89-126.

White, A.J.R.; Chappell, B. W. 1977, Ultrametamorphism and Granitoid Genesis; Tectonophysics, v.43; p.7-22.

White, A.J.R.; Chappell, B. N.; Cleary, J. R. 1974, Geological setting and emplacement of some Australian Palaeozoic batholiths and implications for intrusive mechanisms; Pacific Geology 8; p.159-171.

White, A.J.R.: Williams, I. S.; Chappell, B. W. 1976, The Jindabyne Thrust and its tectonic physiographic and petrogenetic significance; Journal of Geological Society of Australia v.23; p.105-112.

Williams, G. J. 1974, Economic Geology of New Zealand (Second edition); The Australian Institute of Mining and Metallurgy, Parkville. Monograph Series 4; pp 490.

Williams, G. J.; Sanderson, F. L. 1959, Molybdenite-copper prospects, Mt Radiant, Western Nelson; Paper No.132. Fourth Triennial Mineral Conference, School of Mines and Metallurgy, University of Otago, Dunedin, New Zealand; pp 10.

Winkler, H.G.F. 1976, Petrogenesis of Metamorphic Rocks (fourth edition); Springer-Verlag, New York; pp 334.

Wodzicki, A. 1960, Geology and mineralization of the Mount Radiant Area, North-West Nelson, New Zealand; N.Z. Journal of Geology and Geophysics v.3(3); p.355-363.

Wodzicki, A. 1972, Mineralogy, geochemistry and origin of hydrothermal alteration and sulphide mineralization in the disseminated molybdenite and skarn type copper sulphides deposit at Copperstain Creek, Takaka, New Zealand; N.Z. Journal of Geology and Geophysics v.15(4); p.599-631.

Wyllie, P. J. 1977, Crustal Anatexis: An experimental review; Tectonophysics, v.43; p.41-71.

Wyllie, P. J.; Huang, W.; Stern, C. R.; Maaløe, S. 1976, Granitic magmas: possible and impossible sources, water contents, and crystallization sequences; Canadian Journal of Earth Sciences v.13(8); p.1007-1019.